# Structure and Properties of Molecular Crystals Composed of Tetracyanoquinodimethane-Type Electron Acceptors Fused with 1,2,5-Thiadiazole Rings

# 博士論文

Structure and Properties of Molecular Crystals Composed of Tetracyanoquinodimethane-Type Electron Acceptors Fused with 1,2,5-Thiadiazole Rings

(1,2,5-チアジアゾール環が縮合したテトラシアノキノジメタン型電子受容体を構成成分とする分子結晶の構造と性質)

福島孝典

平成11年

DOCTORAL DISSERTATION

# Structure and Properties of Molecular Crystals Composed of Tetracyanoquinodimethane-Type Electron Acceptors Fused with 1,2,5-Thiadiazole Rings

Takanori Fukushima

Department of Chemistry
Graduate School of Science
Tohoku University

1999

# *Contents*

**General Introduction** 1

**Chapter 1 Photochemistry of Charge-Transfer Complexes Composed of Bis[1,2,5]thiadiazolotetracyanoquinodimethane and Divinylbenzenes**

1-1. Introduction 9
1-2. Charge-Transfer Excitation Reaction of EDA Complexes 12
1-3. Charge-Transfer Excitation Reaction of CT Crystals 15
1-4. X-ray Structural Analyses of CT Crystals and Structure-Reactivity Relationships 19
1-5. Conclusion 35
Experimental Section 36
References and Notes 46

**Chapter 2 Asymmetric [2 + 2] Cycloaddition Reaction via Single Crystal-to-Single Crystal Transformation and Evaluation of Structure-Reactivity Relationship in the Solid State Reactions**

2-1. Introduction 49
2-2. Single Crystal-to-Single Crystal Photoreaction 51
2-3. Absolute Asymmetric Synthesis 55
2-4. Exploring for Other Systems 58
2-5. Conclusion 67
Experimental Section 68
References and Notes 75

**Chapter 3 Structure and Properties of Bi{4*H*,8*H*-4-(dicyanomethylene)benzo-[1,2,5]thiadiazol-7-ylidene}**

3-1. Introduction 77
3-2. Molecular Design and Preparation 79
3-3. Molecular and Crystal Structure 81

3-4. Estimation of Energy of S•••N Interactions 84
3-5. Redox Properties and Electrical Conductivities of Charge-Transfer Crystals and Anion Radical Salts 88
3-6. Attempted Preparation of Thiadiazolopyrazino-TCNQ 90
3-7. Conclusion 91
Experimental Section 92
References and Notes 96

**Chapter 4 New Entry into Overcrowded Ethylenes with High Electron Affinity: Structure and Properties of Bi{4*H*,8*H*-4-(dicyanomethylene)benzo-[1,2-*c*:4,5-*c*′]bis[1,2,5]thiadiazol-8-ylidene}**

4-1. Introduction 98
4-2. Preparation and Isolation of Two Conformers 101
4-3. X-ray Analyses of Two Conformers 102
4-4. Conformational Behavior in Solution 104
4-5. Conformational Behavior in the Solid State 109
4-6. Related Overcrowded Ethylene Fused with 1,2,5-Thidiazole Rings 113
4-7. Redox Properties 117
4-8. Conclusion 119
Experimental Section 120
References and Notes 123

**Acknowledgments** 125

**Appendix X-ray Diffraction Data** 127

# *Abbreviations*

| | |
|---|---|
| abs | absorbance |
| Az | azulene |
| BEDT-TTF | bis(ethylenedithio)tetrathiafulvalene |
| BTDA | bis[1,2,5]thiadiazolotetracyanoquinodimethane |
| Bu | butyl |
| CNVTD | cyanovinylthiadiazole |
| CT | charge transfer |
| CV | cyclic voltammetry |
| DMN | dimethylnaphthalene |
| oDV | *o*-divinylbenzene |
| mDV | *m*-divinylbenzene |
| pDV | *p*-divinylbenzene |
| DVs | divinylbenzenes |
| EDA | electron donor and acceptor |
| ee | enantiomeric excess |
| Et | ethyl |
| ET | electron transfer |
| HOMO | highest occupied molecular orbital |
| HPLC | high performance liquid chromatography |
| Ind | indene |
| LUMO | lowest unoccupied molecular orbital |
| oMA | *o*-methylanisole |
| pMA | *p*-methylanisole |
| Me | methyl |
| oMeST | *o*-methylstyrene |
| MO | molecular orbital |
| NMAc | *N*-methylacridinium |
| NMQ | *N*-methylquinolinium |
| OMe | methoxy |
| oOMeST | *o*-methoxystyrene |
| PET | photoinduced electron transfer |
| Ph | phenyl |
| RHF | restricted Hartree-Fock |
| SCE | saturated calomel electorode |
| ST | styrene |
| TCNDQ | tetracyanodiphenoquinodimethane |
| TCNQ | tetracyanoquinodimethane |
| TCNTP | tetracyanotetrahydropyrenoquinodimethane |
| TD | thiadiazole |
| TDA | 1,2,5-thiadiazolotetracyanoquinodimethane |
| THF | tetrahydrofuran |
| TMTSF | tetramethyltetraselenafulvalene |
| TSeT | tetraselenatetracene |
| TTF | tetrathiafulvalene |
| vdW | van der Waals |

# General Introduction

## Solid-State Supramolecular Architecture (Crystal Engineering)

Recently solid-state supramolecular architecture has been the focus of growing attention in organic chemistry due to the intrinsic scientific reasons as well as the practical applications in material sciences.[1] To develop organic crystals which exhibit physical properties (e.g., electrical conductivity, ferromagnetism, and nonlinear optics) or act as template for subsequent chemical transformations (e.g., solid-state reaction, molecular recognition, organic zeolites), it is indispensable to control both the molecular and crystal structures. Current synthetic technology has reached mature levels which make it possible to synthesize a wide variety of organic compounds with multiple properties, yet little is known about the generally successful approach to predicting and/or controlling crystal structures.[2] Thus, supramolecular synthesis in the solid state, that is, crystal engineering today is still at the early stage, in which the knowledge for rational design of organic solids is accumulated.

According to Desiraju, crystal engineering is defined as "understanding of intermolecular interactions in the context of crystal packing and in the utilization of such understanding in the design of new solid with desired physical and chemical properties".[3] Despite the absence of general strategy, two approaches for crystal engineering have been mainly considered as listed in Table 1. One approach is to take advantage of molecular shape of known structure to predict and/or control of molecular orientation in crystals. In the case of single component crystals, this approach is simply based on the idea of shape mimicry.[4] On the other hand, crystal engineering in multi-components crystals is carried out by doping of isomorphous molecule as an impurity into host lattices in the absence of predefined cavities.[5-8] Although the molecular shape approaches are powerful method in a certain case, they involve disadvantageous for generalization due to restriction of the molecular composition in crystals. Another approach is to utilize intermolecular interaction by incorporating interactive sites into a molecule that can limit the possible molecular arrangement in crystals. A large number of interesting structural patterns in various organic crystals have hitherto designed and

constructed.[9-10] In multi-components crystals, control of the orientation of constituent molecules can be achieved by virtue of host-guest complexation, where guest molecules are trapped in well-defined cavities formed between host molecules by intermolecular interactions.[11-14] Because organic compound with appropriate functional groups can be arbitrarily selected or prepared, the second approach seems to be far advantageous for broad application than molecular shape approach. As a consequence, many works in this area are now directed toward the understanding and the manipulation of intermolecular interactions for fabrication of desired supramolecular structure in organic crystals.

**Table 1**. Methods for Crystal Engineering

| Method | Crystal | |
|---|---|---|
| | Single component | Multi-components |
| Molecular shape | Shape mimicry | Doping of isomorphous molecules |
| Intermolecular interaction | Introduction of interactive sites into the molecules | Utilization of molecules having interactive sites as the components |

## Supramolecular Synthons in Crystal Engineering

Utilization of intermolecular interactions for rational design of molecular crystals has been a main subject in crystal engineering. The conventional O-H•••O and N-H•••O hydrogen bondings are the most attractive and common. These kinds of hydrogen bonds are strong and directional, which allow the prediction of crystal structures with a reasonable degree of accuracy. Hence these interactions have been extensively used for construction of various one-, two-, and three-dimensional structural motifs such as "tape", "sheet", and "cavity", respectively. In addition, weaker forces like C-H•••O and C-H•••N interactions are now included in hydrogen bonding, and their importance in determining molecular orientation in crystal has recently been recognized.[15-18]

For the purpose of the general use of such directional intermolecular interactions, Desiraju introduced the concept of supramolecular synthon which is defined as "structural

units within supramolecules which can be formed and/or assembled by known or conceivable synthetic operations involving intermolecular interactions".[19] Supramolecular synthon is not identical to the intermolecular interaction itself but derived from designed combinations of interactions. On the basis of the systematic studies on the relationships between molecular and crystal structure, a variety of supramolecular synthons was proposed and reviewed. Scheme 1 shows typical examples of synthons where the molecular fragments are connected each other by attractive and directional forces. However most of them are constituted with, more or less, some kinds of hydrogen bondings, and there exists a restricted number of synthons with other interactions.

**Scheme 1**

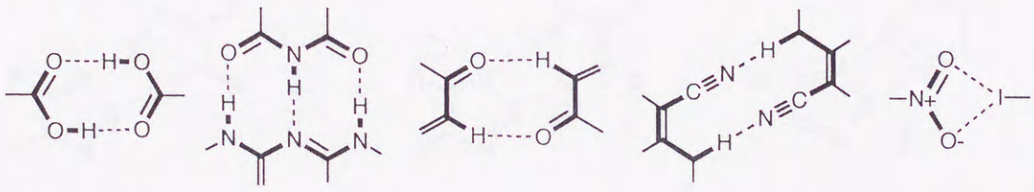


In order to advance this concept to more sophisticated levels, it is necessary not only to obtain the deep insight into the known interactions but also to seek novel interactive sites. From this point of view, the interaction between sulfur and nitrogen atoms (S•••N interaction) is of interest because these hetero atoms are often incorporated into the molecules which are good candidates for functional materials such as organic conductors.

### Supramolecular Synthon Based on S•••N Interaction

The short interatomic contacts between sulfur and nitrogen atoms in crystal were first suggested by Gieren et al. in their research on the series of heterocyclic aromatic compounds as represented by 1,2,5-thiadiazole ring.[20] They explained the nature of these contacts in terms of electrostatic interaction between $-N^{-}-S^{+}=N-$ dipoles and/or weak intermolecular bonding involving a partial rehybridization at sulfur with d-orbital participation (Scheme 2). This finding was later spread out by Suzuki and Yamashita, et al. through their intensive

investigations on development of organic conductors.[21-25] Along these lines, it was found that sulfur-cyano interaction (S•••N≡C interaction) can be operative when the dicyanovinyl groups are introduced into 1,2,5-thiadiazole systems.[21, 23] As shown in Scheme 3, large polarization of =N-S-N= linkage due to the delocalization of negative charge to the dicyanomethylene group would be responsible for this interaction. In addition, the S•••N≡C interaction was proven to be one of the dominant sources of directionality in determining the molecular packing in crystals. Thus, the molecular fragments containing 1,2,5-thiadiazole (**I**) as well as dicyanovinyl substituted 1,2,5-thiadiazole (**II**) now can be regarded as supramolecular synthons.

**Scheme 2**

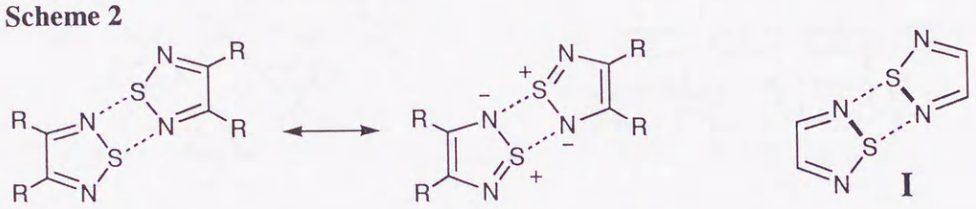

**Scheme 3**

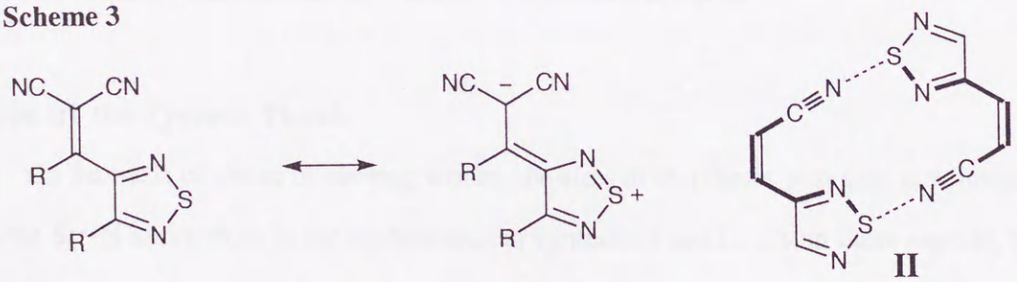

In this connection, bis[1,2,5]thiadiazolotetracyanoquinodimethane (BTDA, **1**)[21] is the typical molecule which possesses two pieces of synthon II. The electron acceptor **1** was designed and prepared as a novel component for organic conductors and actually gave an organic metal[26] and two dimensionally conducting anion radical salts.[27] Besides these physical properties, **1** is of interest from the standpoint of its crystal structure. In the crystal, **1** forms coplanar two dimensional "sheet" networks by S•••N≡C interaction (Figure 1).[28] Ab initio calculations of **1** and related compounds revealed the origin of this interaction to be the electrostatic nature between positively charged sulfur and negatively charged nitrogen atoms.

Furthermore, upon charge-transfer (CT) complexation of **1** with small aromatic hydrocarbons as electron donors, **1** forms inclusion cavities between ribbon-like networks, in which donor molecules was incorporated (Figure 2).[29] It is worth noting that the shape of host lattices varies with the geometry of guest molecules, resulting in the separation of isomeric disubstituted benzenes via highly selective complexation.

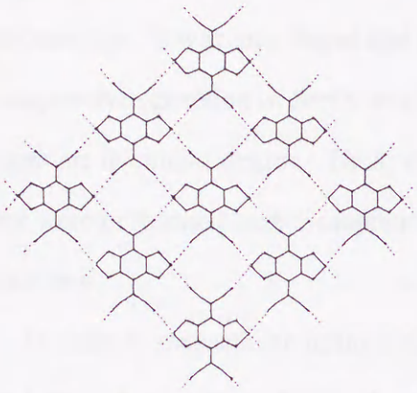

**Figure 1**. "Sheet"-like network in BTDA.

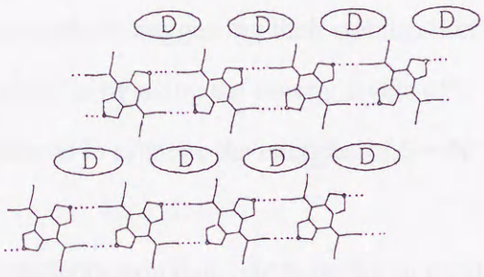


**Figure 2**. CT crystals of BTDA with aromatic hydrocarbons (D).

## Scope of the Present Thesis

On the basis of above pioneering works, the aims of this thesis is to gain new insight into the S•••N interactions in the supramolecular synthons I and II. From these aspects, the present work is concerned with the development of novel molecules containing those synthons as well as the utilization of the resulting structural motifs in exploring unique properties of organic molecular crystals.

First of all, the solid-state photoreaction of the CT crystals composed of BTDA and vinyl benzenes will be discussed in chapter 1. This work provides the first example of CT excitation reaction in the solid state and reveals that CT crystals can serve as novel photoreactive chemical species. The relationships between crystal structures and reactivities were investigated in detail by means of X-ray structural analyses.

Chapter 2 deals with an asymmetric [2+2] cycloaddition reaction via single-crystal-to-single crystal transformation in the photoreaction of o-divinylbenzen•**1** CT crystal. Because

both absolute asymmetric synthesis and single-crystal-to-single crystal reaction have been the special issue in the field of organic solid-state reaction, other related systems were also examined to evaluate the roles of intermolecular interaction in the context of this unique photoreactivity.

In the chapter 3, the preparation and properties of the first stable tetracyanodipheno-quinodimethane derivative (**11**) will be described. The novel electron acceptor **11** was designed as a component of organic conductors. The molecular structure was determined by X-ray analysis. It was also found that **11** forms two-dimensional coplanar sheet structure by the cooperative operation of S•••N and C-H•••N interactions, suggesting their stabilization energies are in similar degree. Thus, ab initio calculations by using the several levels of theory were performed here on supramolecular synthons to estimate the energies of S•••N interactions.

In order to evaluate the influences of S•••N interactions on dynamic behavior in crystal, were designed and prepared a novel overcrowded ethylene derivative (**20**) which can follow the interconversion between two conformers. The structure and conformational behavior of **20** will be discussed in the chapter 4. It was revealed that the S•••N interaction plays a significant role in the solid state conformational isomerism. In addition, **11** is the first interconvertible overcrowded ethylene which both conformers can be isolated and their geometries are determined by X-ray analyses. The electrochemical properties of **20** will be also described.

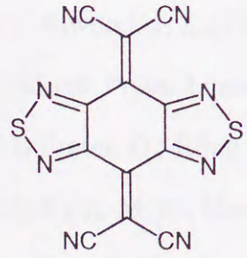


BTDA (**1**)

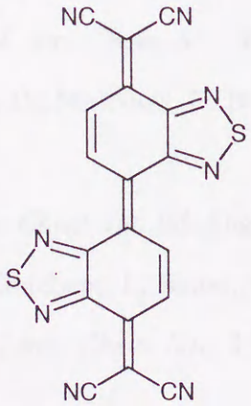


**11**

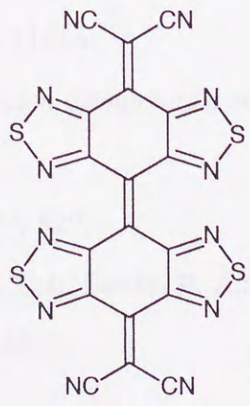


**20**

**References**

(1) Desiraju, G. R. In *Comprehensive Supramolecular Chemistry, vol. 6*; MacNicol, D. D.; Toda, F.; Bishop, R. Ed; Pergamon: Oxford, 1996.

(2) (a) Chin, D. N.; Palmore, G. T. R.; Whitesides, G. M. *J. Am. Chem. Soc.* **1999**, *121*, 2115. (b) Perlstein, J. *J. Am. Chem. Soc.* **1994**, *116*, 455. (c) Gavezzotti, A. *J. Am. Chem. Soc.* **1991**, *113*, 4622. (d) *idem, ibid.*, **1992**, *114*, 1955.

(3) Desiraju, G. R. *Crystal Engineering: The Design of Organic Solids*; Elsevier: New York, 1989.

(4) Whitesell, J. K.; Davis, R. E.; Wong, M.-S.; Chang, N.-L. *J. Am. Chem. Soc.* **1994**, *116*, 523.

(5) (a) Elgavi, A.; Green, B. S.; Schmidt, G. M. J. *J. Am. Chem. Soc.* **1973**, *95*, 2058.

(6) Green, B. S.; Lahav, M.; Rabinovich, D. *Acc. Chem. Res.* **1979**, *12*, 191.

(7) Vaida, M.; Shimon, L. J. W.; Van Mil, J.; Ernst-Babrera, K.; Addai, L.; Leiserowitz, L.; Lahav, M. *J. Am. Chem. Soc.* **1989**, *111*, 1029.

(8) (a) Sarma, J. A. R. P.; Desiraju, G. R. *J. Chem. Soc., Perkin Trans. 2* **1987**, 1187. (b) Sarma, J. A. R. P.; Desiraju, G. R. *J. Am. Chem. Soc.* **1986**, *108*, 2791.

(9) For recent reviews, see: (a) MacDonald, J. C.; Whitesides, G. M. *Chem. Rev.* **1994**, *94*, 2383. (b) Lawrence, D. S.; Jiang, T.; Levett, M. *Chem. Rev.* **1995**, *95*, 2229. (c) Bernstein, J.; Davis, R. E.; Shimoni, L.; Chang, N.-L. *Angew. Chem. Int. Ed. Engl.* **1995**, *34*, 1555.

(10) Palacin, S.; Chin, D. N.; Simanek, E. E.; MacDonald, J. C.; Whitesides, G. M.; McBride, M. T.; Palmore, T. R. *J. Am. Chem. Soc.* **1997**, *119*, 11816.

(11) Atwood, J. L.; Davies, J. E. D.; MacNicol, D. D., Ed. *Inclusion Compounds, vols. 1-3*; Academic Press: London, 1984.

(12) Ermer, O.; Eling, A. *Angew. Chem. Int. Ed. Engl.* **1988**, *27*, 829.

(13) Byrn, M. P.; Curtis, C. J.; Goldberg, I.; Hsiou, Yu.; Khan, S. I.; Sawin, P. A.; Tendlick, S. K.; Strouse, C. E. *J. Am. Chem. Soc.* **1991**, *113*, 6549.

(14) (a) Endo, K.; Sawaki, T.; Koyanagi, M.; Kobayashi, K.; Masuda, H.; Aoyama, Y. *J. Am. Chem. Soc.* **1995**, *117*, 8341. (b) Endo, K.; Ezuhara, T.; Koyanagi, M.; Masuda, H.Aoyama, Y. *J. Am. Chem. Soc.* **1997**, *119*, 499.

(15) Taylor, R.; Kennard, O. *J. Am. Chem. Soc.* **1982**, *104*, 5063.

(16) Berkovitch-Yellin, Z.; Leiserowitz. *Acta Crystallogr.* **1984**, *B40*, 159.

(17) (a) Desiraju, G. R. *Acc. Chem. Res.* **1996**, *26*, 441. (b) *idem, ibid.,* **1991**, *24*, 290.

(18) Suzuki, T.; Fujii, H.; Miyashi, T.; Yamashita, Y. *J. Org. Chem.* **1992**, *57*, 6744.

(19) Desiraju, G. R. *Angew. Chem. Int. Ed. Engl.* **1995**, *34*, 2311, and references cited therein.

(20) (a) Gieren. A.; Lamm, V.; Haddon, R. C.; Kaplan, M. L. *J. Am. Chem. Soc.* **1979**, *101*, 7277. (b) *idem, ibid.,* **1980**, *102*, 5070.

(21) Yamashita, Y.; Suzuki, T.; Mukai, T.; Saito, G. *J. Chem. Soc., Chem. Commun.* **1985**, 1044.

(22) Yamashita, Y.; Saito, K.; Suzuki, T.; Kabuto, C.; Mukai, T.; Miyashi, T. *Angew. Chem. Int. Ed. Engl.* **1988**, *27*, 434.

(23) Tsubata, Y.; Suzuki, T.; Yamashita, Y.; Mukai, T.; Miyashi, T. *Heterocycles*, **1992**, *33*, 337.

(24) Suzuki, T.; Okubo, T.; Okada, A.; Yamashita, Y.; Miyashi, T. *Heterocycles*, **1993**, *35*, 395.

(25) Yamashita, Y.; Ono, K.; Tomura, M.; Imaeda, K. *Chem. Commun.* **1997**, 1851.

(26) Ugawa, A.; Iwasaki, K.; Kawamoto, A.; Yakushi, K.; Yamashita, Y.; Suzuki, T. *Phys. Rev. B* **1991**, *43*, 14718.

(27) Suzuki, T.; Kabuto, C.; Yamashita, Y.; Mukai, T.; Miyashi, T. *Bull. Chem. Soc. Jpn.* **1988**, *61*, 483.

(28) Kabuto, C.; Suzuki, T.; Yamashita, Y.; Mukai, T. *Chem. Lett.* **1986**, 1433.

(29) Suzuki, T.; Yamashita, Y.; Kabuto, T.; Tanaka, S.; Harasawa, M.; Mukai, T.; Miyashi, T. *J. Am. Chem. Soc.* **1992**, *3034*, 1992.

# Chapter 1

## Photochemistry of Charge-Transfer Complexes Composed of Bis[1,2,5]thiadiazolotetracyanoquinodimethane and Divinylbenzenes

### 1-1. Introduction

Recently organic solid-state photoreactions have drawn considerable attention and a large number of reactions has been investigated to explore the intriguing facets of organic molecular crystals.[1] Because the physical restraints on the molecular movements prevent drastic conformational, translational, and rotational changes along the reaction coordinate and lead to alternate reaction pathways, the reactions in the solid state often differ from those in solution. In addition, the intrinsic reactivity of a molecule is frequently of secondary importance compared with the nature of molecular packing arrangement around the reactant. Therefore, most of these works highlight the structural and geometric requirements in determining reactivity.

On the basis of the detailed studies of [2+2] photodimerization of cinnamic acid derivatives[2] the topochemical principle was first formulated by Schmidt and co-workers, which states, "a solid-state reaction proceeds with minimum of atomic and molecular movement".[3] This concept was later generalized to include the idea of minimal distortion of the "reaction cavity".[4] The distinguished feature of the topochemical reactions is that the initial solid-state environment dictates both the possibility of reaction and the structure of its products. Thus, the topochemical principle refers to only the relation of the initial structure to reactivity and dose not involve other important facets of the mechanisms such as the structural and dynamic changes of the lattice during the reactions,[5-7] yet the concept is widely accepted in the studies of organic solid-state reactions.

On the other hand, in the recent research field of photochemistry, photoinduced electron-transfer (PET) reactions in solution have been extensively studied on a wide variety of organic compounds from both theoretical and experimental points of view.[8,9] One of the most

characteristic feature of PET reactions compared with conventional photoreactions in the excited state is the generation of radical ions which undergo the subsequent thermal reactions. Thus, PET reactions in solution have offer many interesting examples of organic reactions via radical ions,[9] however, little is known about PET reactions in the solid state.[10]

Since radical ions can be generated in solution by direct excitation of their charge-transfer (CT) bands of molecular complexes composed of electron donors and acceptors, *i.e.* EDA complexes, the photoexcitation of crystalline complexes, *i.e.* CT crystals, would provide a unique opportunity to investigate the reactions of radical ions included in the highly organized crystal lattices (Scheme 1). In this case, the ET process may be more efficient than in solution because of the preorganized face-to-face overlap of the donor and the acceptor in crystal. Furthermore, chemical reactions subsequent to ET would exhibit the intriguing behavior characteristic to both the PET reactions and the organic solid-state reactions. One of the aims of this work in Chapter 1 is to demonstrate that photochemistry of CT crystals can serve as a new motif to be exploited.

**Scheme 1**

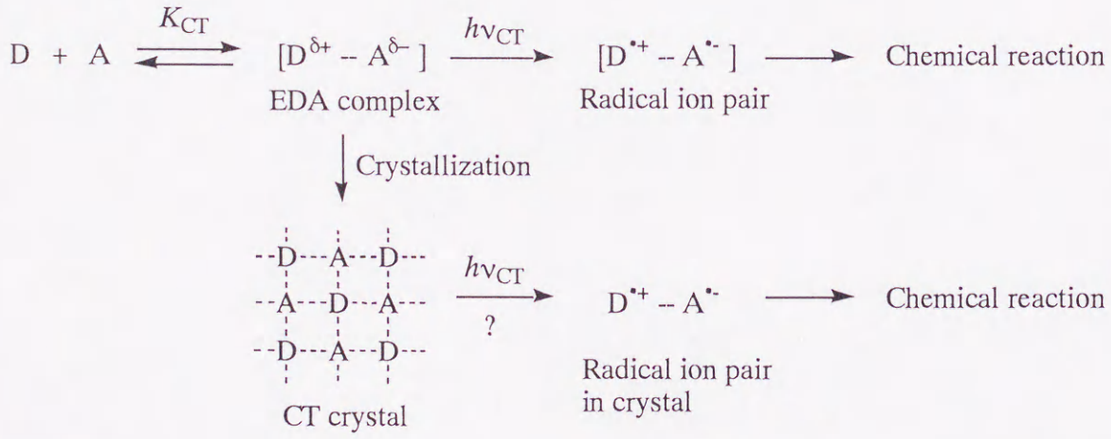


For the successful execution of solid-state reactions crystal engineering is of significant importance, which allows the prediction and the designing of molecular arrangements. From this point of view, BTDA (**1**) is a promising acceptor for this purpose, because **1** shows the electrostatic interaction between sulfur atoms and cyano groups (S•••N≡C interaction) in crystal and the interaction is one of the dominant sources of directionality in determining the

crystal structure.[11] Moreover, **1** forms inclusion cavities by S•••N≡C interaction in its CT crystals with small aromatic hydrocarbons as electron donors.[11b] Therefore, in the course of the solid-state reactions of **1** with appropriate donors via CT excitation, such inclusion cavities can be regarded as the unique reaction cavities. As the electron donors, were chosen styrene (ST) and three isomers of divinylbenzene (oDV, mDV, and pDV) because of the sufficient donating properties of benzene nuclei as well as the versatile reactivities at the vinyl group in their cation radicals.[12]

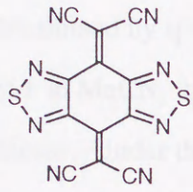

BTDA (**1**)

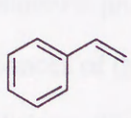
ST

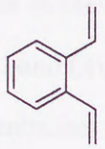
oDV

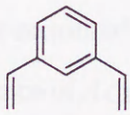
mDV

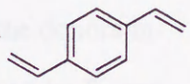
pDV

## 1-2. Charge-Transfer Excitation Reaction of EDA Complexes

In order to compare the photoreactivities in the solid state with those in solution, the CT excitation reaction of the corresponding EDA complexes were also examined.

When a yellow solution of **1** in MeCN was mixed with colorless arylolefins, the solution turned faint orange, red, or brown. The changes in color can be accounted for by the formation of EDA complexes and absorption spectra are shown in Figure 1 with that of uncomplexed **1**. Since **1** has no significant absorption above 450 nm, the newly appeared broad absorptions in the 450-600 nm region were assigned to the CT bands from HOMOs of arylolefins to LUMO of **1**. The association constants ($K_{CT}$) for the EDA complexes were determined by spectrophotomeric procedure in MeCN at 20 °C. Because of the low solubility of **1** in MeCN, the absorbances of the CT band ($A_{CT}$) were measured with the donors in excess. Under these conditions, the concentration dependence of $A_{CT}$ is given by Benesi-Hildebrand relationship (eq. 1).[13] In all cases, linear correlations were found, indicating a 1:1 molar ratio for the EDA complexes. The $K_{CT}$ values thus obtained are summarized in Table 1 with the oxidation potentials of donors measured by cyclic voltammetry (CV). These small values indicate the presence of weak CT interactions in the ground state.

$$\frac{[\mathbf{1}]}{A_{CT}} = \frac{1}{\varepsilon_{CT}} + \frac{1}{K_{CT}\varepsilon_{CT}[\text{donor}]} \qquad (1)$$

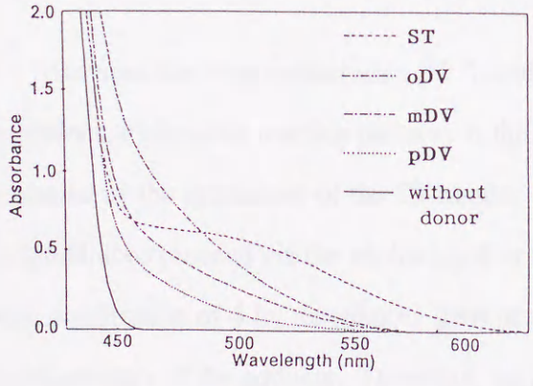


**Figure 1**. The CT absorption spectra in MeCN at 20 °C, [donor] = 0.05 M, [BTDA] = 0.01 M.

**Table 1** Oxidation Potentials ($E^{ox}$)[a] of Donors and Association Constants ($K_{CT}$)[b] for EDA Complexes

| donor | $E^{ox}$ / V | $K_{CT}$ / $M^{-1}$ |
|---|---|---|
| ST | +1.90 | 0.85 |
| oDV | +1.82 | 1.1 |
| mDV | +1.83 | 1.4 |
| pDV | +1.51 | 1.5 |

[a] $E$ / V vs SCE, 0.1 mol $dm^{-3}$ $Et_4NClO_4$ in MeCN. [b] Measured in MeCN at 20 °C.

Photolyses of the EDA complexes were performed by using the output of 2 kW xenon lamp passed through a glass cut-off filter. When a solution of **1** (0.01 mol $dm^{-3}$) and ST (0.05 mol $dm^{-3}$ ) in 10 mL of MeCN[14] was irradiated ($\lambda > 450$ nm) for 5 h at 20 °C, the [2+2]-type cycloaddition occurred between **1** and ST to give **2st** as a sole product in 4% yield. Photolyses of the EDA complexes of **1** and DVs (DVs-**1**) under similar conditions also gave [2+2]-type cycloadducts **2o** (9%), **2m** (11%), and **2p** (8%), respectively. These results are summarized in Table 2. Although the yield of **2p** increased up to 44% upon prolonged irradiation (20 h), the resulting reaction mixture became rather complicated presumably due to the formation of the oligomers of pDV. No attempt was made to identify the small amount of by-products. Thus, in spite of the different electron-donating properties of arylolefins or substituting positions of the vinyl groups, no distinct difference in the photoreactivities of the EDA complexes could be observed.

**Table 2.** CT Excitation Reaction of EDA Complexes[a]

| donor | yield of **2** / % | recovery[b] of **1** / % |
|---|---|---|
| ST | 4 | 78 |
| oDV | 9 | 63 |
| mDV | 11 | 51 |
| pDV | 8 | 64 |

[a] A 10 mL MeCN solution was irradiated by a 2 kW Xe lamp at 20 °C for 5 h. [donor] = 0.05 M, [BTDA] = 0.01 M. [b] Isolated yields.

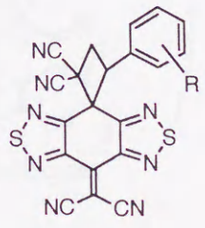


**2st** : R = H
**2o** : R = 2-vinyl
**2m** : R = 3-vinyl
**2p** : R = 4-vinyl

Because the local excited state ($^1$**1***) could not be accessible under the present irradiation conditions, a plausible reaction pathway is the stepwise bond making of radical ion pairs generated by the excitations of the CT bands. As shown in Scheme 2, it seems likely that the cycloadditions proceed via the zwitterion **4** or the corresponding biradicals by considering the large stabilization of **4** by resonance. This proposed reaction pathway is in accord with the regiochemistry of the adducts. Therefore, regioisomer **3** which may be formed via less stable intermediate **5** could not be observed in the reaction mixtures. Another possibility could be the participation of the triplet excited state of **1** ($^3$**1***) formed by the back electron-transfer from the triplet radical ion pair. However, the photolyses of EDA complex of **1** and mDV under

oxygen did not result in a decrease of the yield of **2m**, suggesting that the $^{3}\mathbf{1}^{*}$ is not involved in the photoreactions.

**Scheme 2**

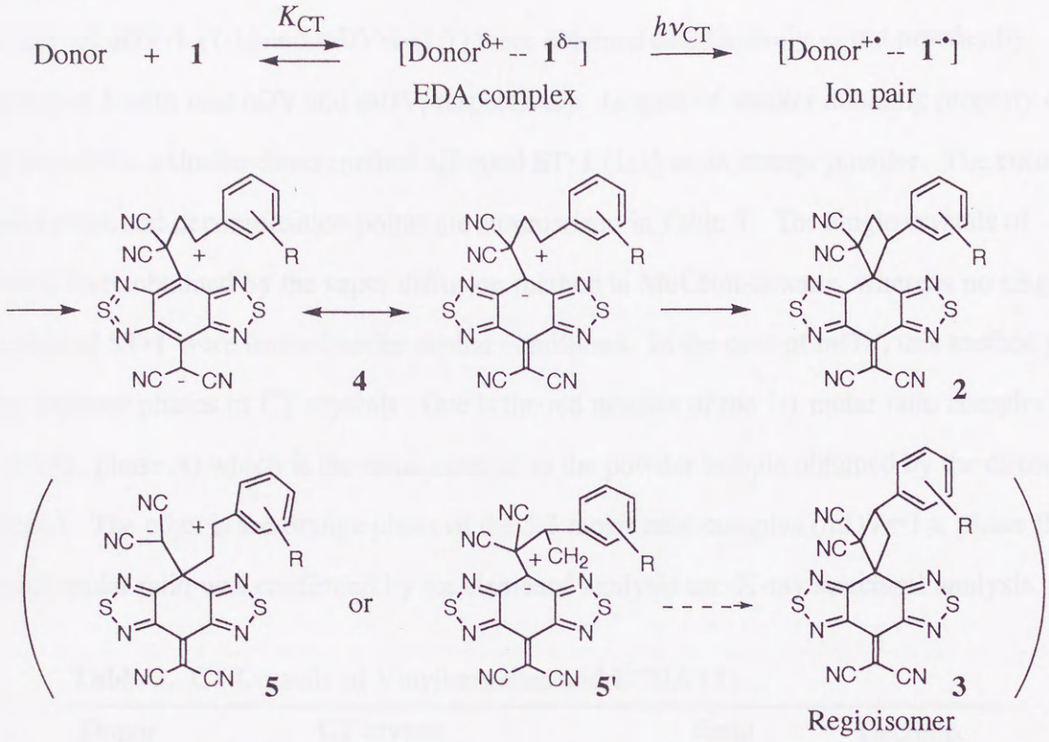

### 1-3. Charge-Transfer Excitation Reaction of CT Crystals

Recrystallization of **1** from MeCN containg excess pDV gave pDV•**1** (1:1) CT crystal as purple plates. A powder sample of pDV•**1** was obtained by mixing of **1** with pDV in small amount of $CH_2Cl_2$ followed by removal of solvent and excess pDV *in vacuo*. Powdered CT crystals of oDV•**1** (1:1) and mDV•**1** (1:1) were obtained quantitatively as red powder by mixing of **1** with neat oDV and mDV, respectively. In spite of weaker donating property of ST than DVs, a similar direct method afforded ST•**1** (1:1) as an orange powder. The color, molar ratio, and decomposition points are summarized in Table 3. The single crystals of oDV•**1** were obtained by the vapor diffusion method in MeCN/*n*-hexane, whereas no single crystals of ST•**1** were formed under similar conditions. In the case of mDV, this method gave two different phases of CT crystals. One is the red needles of the 1:1 molar ratio complex (mDV•**1**, phase A) which is the same material as the powder sample obtained by the direct method. The other is the orange plates of the 5:3 molar ratio complex ($mDV_5$•$\mathbf{1}_3$, phase B), whose molar ratio was confirmed by the elemental analysis and X-ray structural analysis.

**Table 3**. CT Crystals of Vinylbenzenes and BTDA (**1**)

| Donor | CT crystal | Ratio | Decomp. |
|---|---|---|---|
| ST | ST•**1** (orange powder) | 1:1 | 82 - 86 °C |
| oDV | oDV•**1** (red powder) | 1:1 | 95 - 98 °C |
| mDV | mDV•**1** (red powder) | 1:1 | 95 - 98 °C |
| pDV | pDV•**1** (violet powder) | 1:1 | 168 - 174 °C |

In accord with the small $K_{CT}$ values, the CT crystals dissociated into **1** and donors upon exposure in any organic solvents, hence the CT crystals were suspended in water and irradiated. Photoirradiation of the CT crystals was performed by using the output from a 2 kW xenon lamp passed through a glass cut filter. Because of the difficulty of distinguishing the CT bands from the local absorption of **1** in crystal, the longer-wavelength light than in solution was used for the selective excitation of the CT band. When a suspension of finely powdered ST•**1** in 10 mL of water was irradiated ($\lambda > 505$ nm) for 1 h at 15 °C, the regiospecific [2+2]-type cycloaddition was occurred to give **2st** as a sole product in 71% yield

(Table 4). It is worth noting that **2st** was obtained in high yield within a shorter irradiation time with longer-wavelengh light, suggesting the higher photoreactivity in the solid state. The reactivity is much more outstanding in the photoreaction of oDV•**1**. Upon irradiation ($\lambda > 540$ nm) of a water suspension of oDV•**1** for 15 min, adduct **2o** (84%) was formed with the rapid change of the color from red to yellow. The yield of **2o** was increased up to 91% upon prolonged irradiation (1 h) (Table 4). These results show that the cycloaddition via ET in the solid state actually occurs more efficiently than in solution probably due to the preorganized face-to-face overlaps.

**Table 4**. CT Excitation Reaction of CT Crystals (15 °C, 1 h)[a]

| CT crystal | Wavelength / nm | Product yield / % |
|---|---|---|
| ST•**1** | $\lambda > 505$ | **2st**: 71[b] |
| oDV•**1** | $\lambda > 540$ | **2o**: 91[b] |
| mDV•**1** | $\lambda > 540$ | **2m**: 15[c] |
| pDV•**1** | $\lambda > 540$ | **2p**: 8[c], **6**: 2[c] |

[a] A 10 mL water suspension was irradiated by a 2 kW Xe lamp. [b] Isolated yields. [c] Determined on the basis of $^1$H NMR spectra.

In contrast, photoirradiation ($\lambda > 540$ nm) of mDV•**1** (phase A) for 1 h gave **2m** in only 15% yield (Table 4). In this case, the time-dependence of the product yield was determined on the basis of $^1$H NMR analyses of as-prepared samples obtained by independent photolyses. As shown in Figure 2, upon prolonged irradiation the yield of **2m** increased with the consumption of mDV, and reached the maximum value (ca. 45%) after 5 h. The significant decrease of mDV on 10 h- and 20 h-irradiation may be due to the other reactions such as the dimerization or oligomerization between $mDV^{+\bullet}$ and mDV in crystal. In fact, the formation of mDV oligomer was confirmed in the preparative scale experiments. Moreover, no distinct decrease of mDV was observed in the control experiment (5 h-irradiation followed by stirring for 5 h in the dark). On the other hand, the photoirradiation of $mDV_5$•$\mathbf{1}_3$ (phase B) was also proven to give adduct **2m**, yet the reactivity was lower than that in mDV•**1** (phase A). When the red-orange plates of $mDV_5$•$\mathbf{1}_3$ sealed in a glass capillary were irradiated ($\lambda >$ 540 nm) at 15 °C, **2m** was formed as a sole product. The yield of **2m** (6% based on mDV)

and the recovery of mDV (92%) upon 1 h-irradiation were determined on the basis of the $^1$H NMR analyses. Upon 20 h-irradiation increased the yield of **2m** up to 24% with the recovery of mDV (68%).

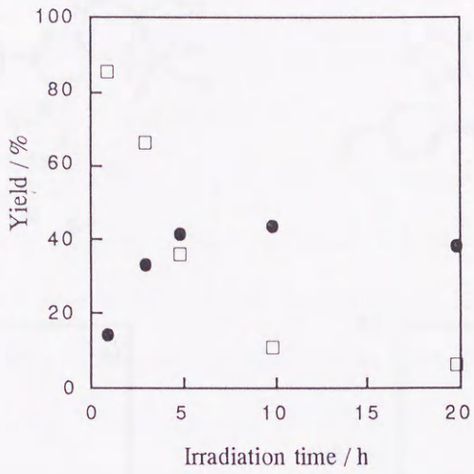


**Figure 2**. The time-course of the solid-state reaction of mDV•**1**. The yield of **2m** (filled circle) and recovery of mDV (open square) are plotted as a function of irradiation time.

More notable feature was observed in the photoreaction of pDV•**1**. Upon irradiation ($\lambda$ > 540 nm, 15 °C) of a water suspension of powdered pDV•**1** for 5 h, adduct **2p** (16% yield) was formed with a considerable amount of 1:2 adduct **6** (36% yield) and very small amount of 2:1 adduct **7** (3% yield). The latter two products were missing in the photolysis of the corresponding EDA complex in solution. The time-dependence of the combined yield of products (**2p** and **6**) and the recovery of pDV shows the presence of the induction period (*ca.* 30 min) in this reaction (Figure 3a). In addition, the time-dependence of the product distribution (**2p** and **6**) suggests that **6** was the secondary product from **2p** (Figure 3b). The formation of adduct **6** (22%) decreased in the photoreaction at longer wavelength ($\lambda$ > 580 nm, 5 h) and the yield of **2p** was up to 29%. Considering the existence of significant induction period, the reaction can be regarded as defects-accelerated type.[15]

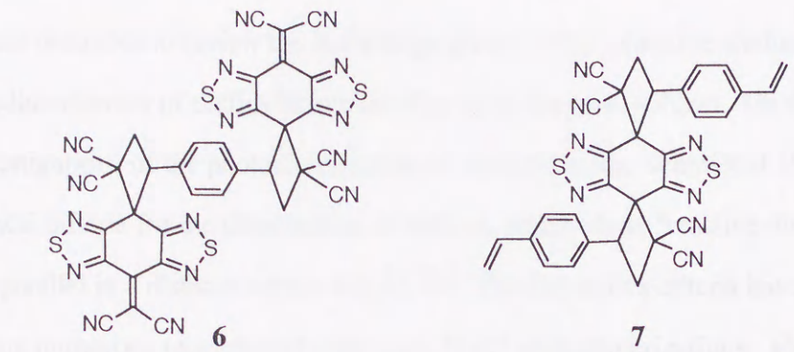


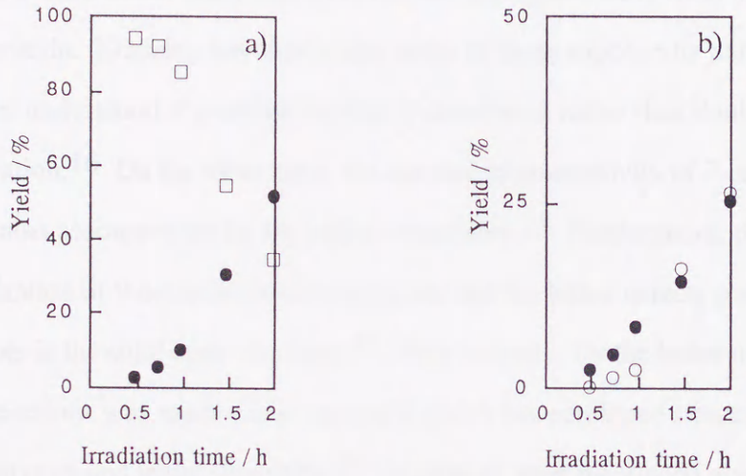


**Figure 3**. The time-course of the solid-state reaction of pDV•**1**. (a) The combined yield of adducts (**2p** and **6**) (filled circle) and recovery of pDV (open square) are plotted as a function of irradiation time. (b) Irradiation time dependence of the product distribution (**2p**, filled circle; **6**, open circle).

Accordingly, the [2+2]-type cycloaddition reactions of arylolefins•**1** by CT excitation showed the diversity in the reactivities compared with the similarity in those of the EDA complexes in solution. These solid-state photoreactivities would not depend on the intrinsic reactivites of the substrates and/or the radical ions, but on the molecular arrangements in crystal. Thus, the structure-reactivity relationship and the unique characteristics in the photoreactions of divinylbenzene•**1** CT crystals will be discussed in the next section through the examination of the X-ray crystal structural analyses.

## 1-4. X-ray Structural Analyses of CT Crystals and Structure-Reactivity Relationships

It seems desirable to review the knowledge given by the extensive studies of classical [2+2] photodimerization of olefins before moving on to the main subject. On the basis of the detailed investigations of the photodimerization of cinnanic acids, Schmidt et al. established the geometrical criteria for the dimerization of olefins, which state, "reactive double bonds are arranged in parallel in a distance within 4.2 Å".[2,3] The Schmidt's criteria have been used for understanding numerous examples of solid-state [2+2] photodimerizations. However, in the recent studies, there exists many examples that deviate significantly from the well-accepted Schmidt's criteria. Kearsley has shown that many of these supposedly anomalous situations may be better understood if p-orbital overlap is considered rather than double bond center-to-center separation.[16] On the other hand, the unusual photoreactivity of 7-methoxycoumarin in crystal was also accounted for by the lattice relaxability.[15] Furthermore, the studies on the photodimerization of 9-cyanoanthracene suggests that the lattice defects sometimes play an important role in the solid-state reactions.[17] Very recently, for the better understanding of solid-state reactions was made a new approach which has combined structural considerations with photophysics and lattice dynamics.[18] In view of what mentioned above, the detailed structure-reactivity relationship in the present reactions will be discussed.

### Molecular Arrangement in oDV•1 and Crystal-to-Crystal Transformation of oDV•1 into Adduct 2o.

X-ray structural analysis of oDV•**1** was performed on a reddish rod-like crystal obtained by the vapor diffusion method from MeCN/*n*-hexane. The crystallographic details are shown in Table 5. In the crystal, molecules of **1** are connected to each other by S•••N≡C interaction, and linear "ribbon"-like networks are formed along the *a* axis and repeated along the *b* axis (Figure 4). The distances of S•••N are 3.14 and 3.43 Å for S(1)•••N(7) and S(2)•••N(8), respectively. Molecules of oDV are incorporated in the cavities formed between the two "ribbons", thus the molecules in Figure 4 are arranged in a corrugated sheet on the *ab* plane (the interplanar distances and the dihedral angles between neighboring molecular planes are as

follows: 1.64 Å and 0° for A and B; 3.15 Å and 22.0° for A and E; 1.51 Å and 22.0° for B and E; 0.41 Å and 22.0° for C and E; 2.05 Å and 22.0° for D and E). These structural features are common in the CT crystals of **1** with small aromatic hydrocarbons.[11b] However, in this case, it is worth noting that the inclusion lattice is asymmetric because of the adoption of chiral space group ($P2_1$). As shown in Figure 5, perpendicularly to this molecular arrangement, one-dimensional columnar mixed stacks are formed along the *c* axis, and a column is related with the four neighbors by 2-fold screw axes along the [1 1 0] and [1 -1 0] directions.

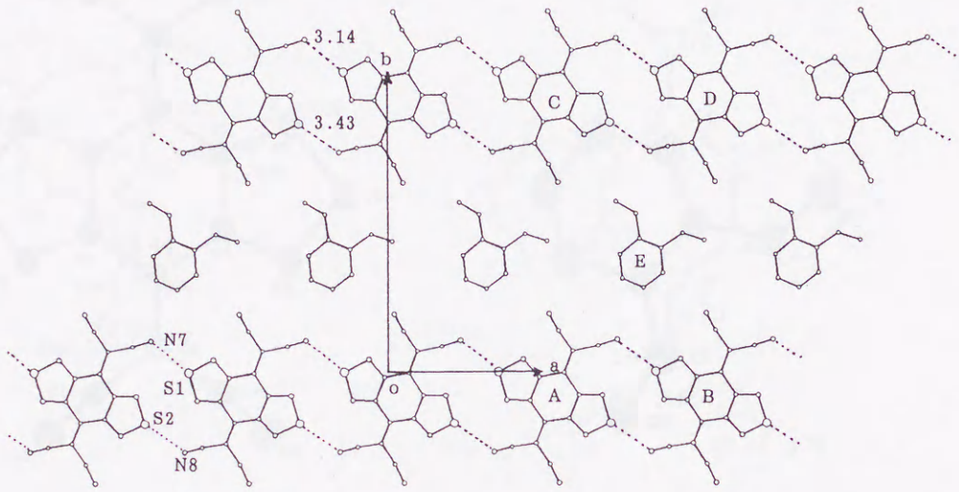


**Figure 4.** Molecular arrangement in oDV•**1** viewed along the *c* axis. The interatomic distances of S•••N≡C are shown by broken lines.

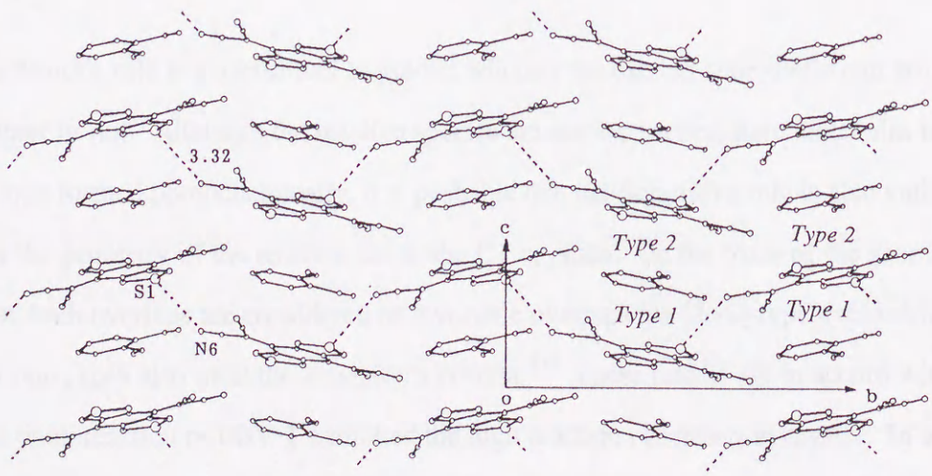


**Figure 5.** One-dimensional columnar stacks in oDV•**1** viewed along the *a* axis.

In the stacks, two different types of molecular overlaps between **1** and oDV (*Type 1* and *Type 2*) are repeated alternately. The molecular overlaps viewed along the molecular planes are shown in Figure 6. In both overlaps, two olefinic parts are aligned nearly in parallel with the distance of less than 4 Å [*Type 1*: 3.44 and 3.87 Å for C(5) - C(29) and C(7) - C(30), respectively; *Type 2*: 3.75 and 3.55 Å for C(5) - C(29) and C(7) - C(30), respectively].

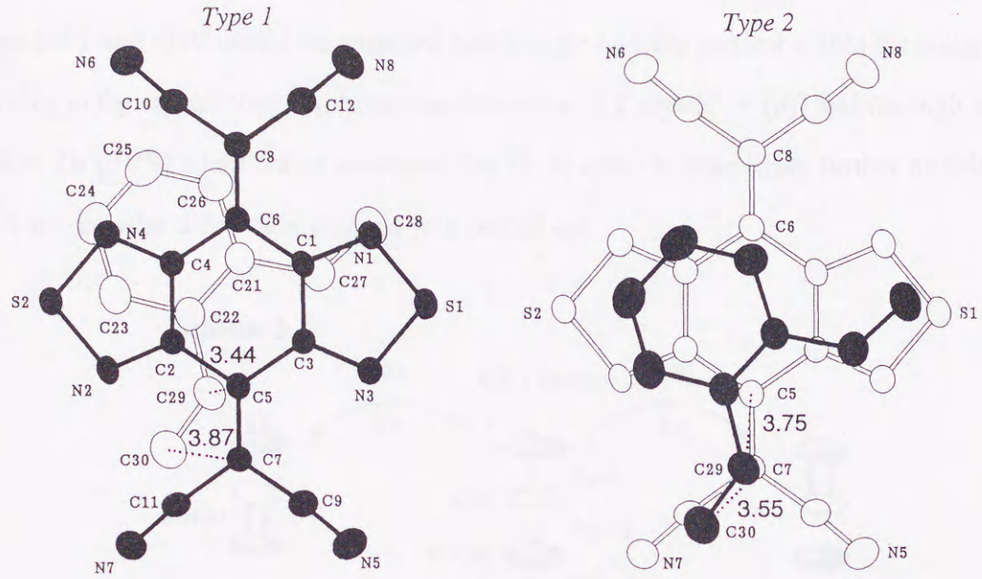


**Figure 6.** Two types of molecular overlaps in oDV•**1** (*Type 1* and *Type 2*). The interplanar distances and dihedral angles are 3.40 Å and 2.6° in *Type 1*, and 3.44 Å and 2.6° in *Type 2*, respectively.

Schmidt's rule is a useful tool to predict whether the excited-state olefin can afford the photodimer or not. Although the reactive species are not the excited-state molecules but the radical ions formed photochemically, it is probable that the Schmidt's rule is also valid to evaluate the geometry of the reactive site in the CT crystals. On the basis of the geometrical criterion, both overlaps are considered as favorable overlaps for [2+2]-type cycloaddition. Furthermore, they also meet the Kearsley's criteria.[19] These results are in accord with the fact that photoreaction of oDV•**1** exhibited the high reaction efficiency in crystal. In addition, the regiochemistry of adduct **2o** can be accounted for by these molecular overlaps. On the

other hand, in view of the CT interaction which may be related with the efficiency of ET, *Type 2* seems more favorable by considering the MO coefficients of HOMO of oDV and LUMO of **1**.[20] It is interesting to investigate if the reaction proceeds predominantly via one of the two overlaps.

As shown in Scheme 3, if one of the two overlaps is much more favorable for the reaction, the crystallinity would be maintained after the reaction because the addition would occur from the one side [CT crystal → (a)]. If this is not the case, a considerable amount of unreacted **1** and oDV would be remained between the adducts formed within the stack, resulting in the crystal-to-amorphous transformation [CT crystal → (b)] and the high isolated yield of **2o** (91%) could not be accounted for.[21] In order to investigate further on this point, the X-ray powder diffraction analysis was carried out .

**Scheme 3**

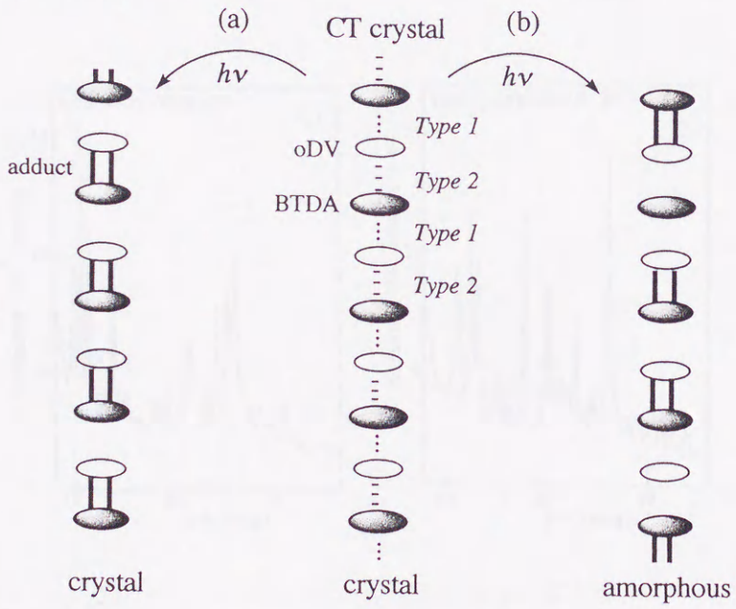


The continuous changes in the X-ray powder diffraction patterns on irradiation are shown in Figures 7a-c. The analyses indicated that the high crystallinity was maintained during entire course of the reaction; namely, this reaction proceeds through a crystal-to-crystal transformation. This result is consistent with the assumption that the reaction proceeds predominantly via one of the two overlaps. It is also noteworthy that the diffraction pattern of

as-prepared **2o** (Figure 7c) was quite dissimilar to that of recrystallized **2o** (Figure 7d), suggesting the significant differences in the crystal stuructre between them. These intriguing features in oDV•**1** will be further inspected in the following chapter.

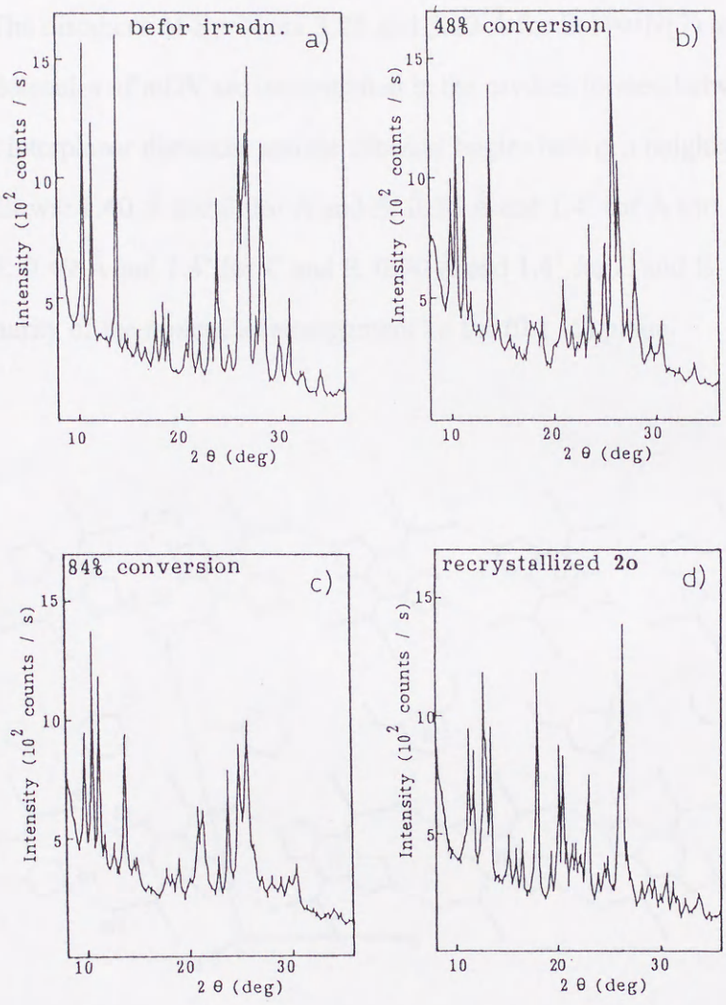


**Figure 7**. The continuous changes in the X-ray powder diffraction pattern (CuKα) on photoirradiation (λ > 540 nm) of oDV•**1**: a) before irradn.; b) 5 min irradn. (48% conversion); c) 15 min irradn. (84% conversion); d) adduct **2o** after recrystallization.

**Molecular Arrangement in mDV•1 and Crystal-to-Amorphous Transformation of mDV•1 into Adduct 2m**

A reddish needle-like crystal of mDV•**1** was obtained by the vapor diffusion method from MeCN/*n*-hexane. The X-ray crystallographic details are depicted in Table 5. As shown in Figure 8, linear "ribbon"-like networks are formed along the *a* axis by S•••N≡C interaction in the crystal. The distances of S•••N are 3.25 and 3.23 Å for S(1)•••N(7) and S(2)•••N(8), respectively. Molecules of mDV are incorporated in the cavities formed between the two "ribbons". The interplanar distances and the dihedral angles between neighboring molecular planes are as follows: 1.40 Å and 0° for A and B; 0.36 Å and 1.4° for A and E; 1.03 Å and 1.4° for B and E; 0.49 Å and 1.4° for C and E; 0.90 Å and 1.4° for D and E. These values show the coplanarity of the molecular arrangement on the (0 1 -1) plane.

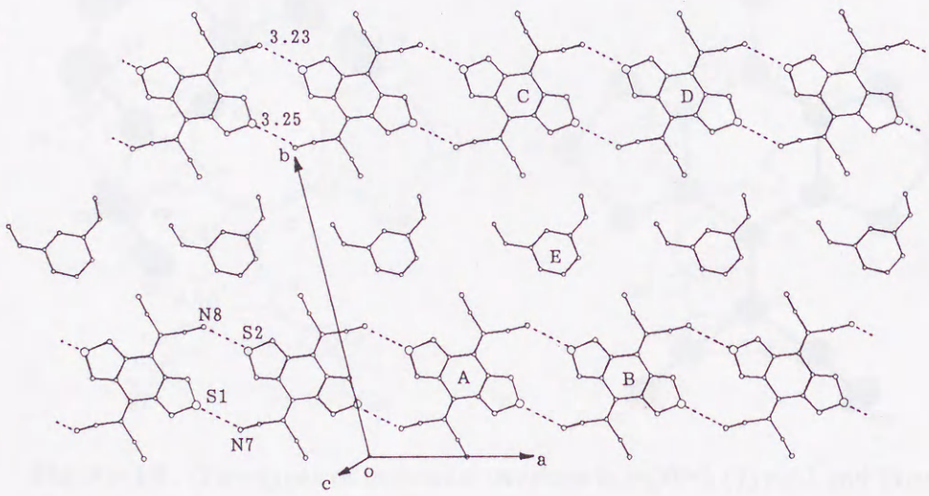


**Figure 8.** Molecular arrangement in mDV•**1**.

Perpendicularly to this molecular arrangement, one-dimensional columnar mixed stacks are formed along the *c* axis (Figure 9). In the stacks, two different types of molecular overlaps between **1** and mDV (*Type 1* and*Type 2*) are repeated alternately. In addition, dyad form of **1** by S•••N contacts (3.28 Å) are found.

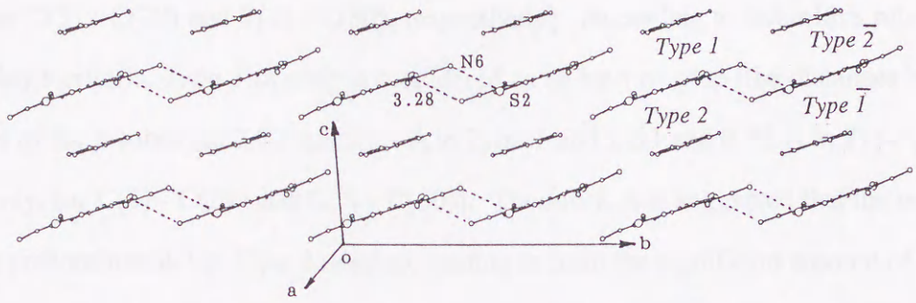


**Figure 9.** One-dimensional columnar stacks in mDV•**1** showing the dyad formayion of **1**.

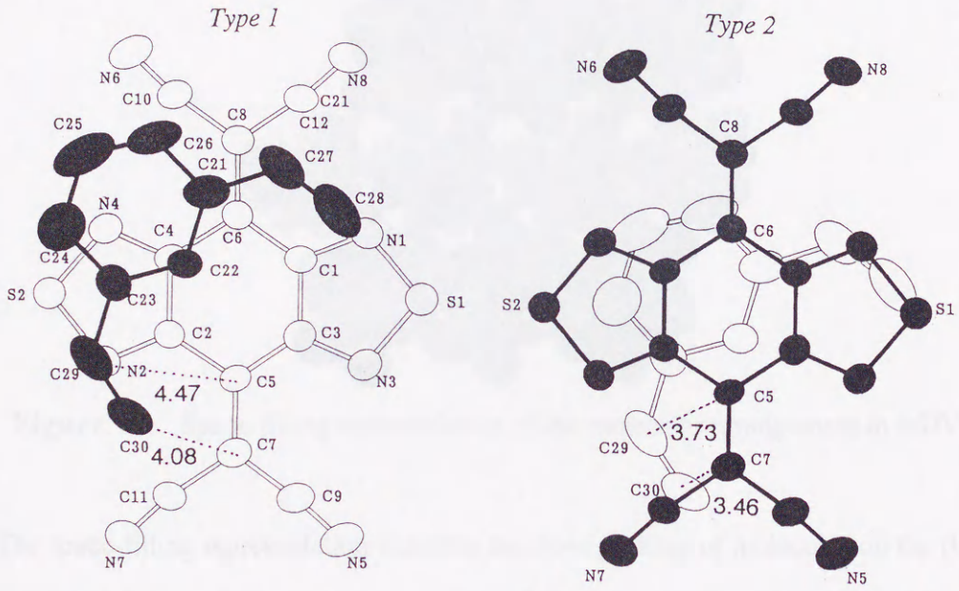


**Figure 10.** Two types of molecular overlaps in mDV•**1** (*Type 1* and *Type 2*). The interplanar distances and dihedral angles are 3.46 Å and 1.4° in *Type 1*, and 3.38 Å and 1.4° in Type 2, respectively.

Figure 10 shows the molecular overlaps viewed along the molecular planes. Both molecular overlaps appear to be favorable for the interaction between HOMO of mDV and LUMO of **1** in terms of the MO coefficients.[20] However, since the shorter interplanar distances are found in in Type 2 overlap (3.46 Å in *Type 1* and 3.38 Å in *Type 2*), *Type 2* seems more advantageous for CT interaction than *Type 1* overlap. Furthermore, taking the

geometry of reactive site into acount, *Type 2* seems by far favorable for the cycloaddition [*Type 1*: 4.47 and 4.08 Å for C(5) - C(29) and C(7) - C(30), respectively; *Type 2*: 3.73 and 3.46 Å for C(5) - C(29) and C(7) - C(30), respectively]. According to Schmidt's rule as well as Kearsley's criteria, *Type 1* overlap is considered as an inert overlap [the distances between the apices of the p-lobes are 2.87 and 2.29 Å in *Type 1* and 1.63 and 0.72 Å in *Type 2*, respectively, for C(5) - C(29) and C(7) - C(30)]. Therefore, it is suggested that the reaction proceeds predominantly via *Type 2* overlap, leading to form the significant amount of adduct. However, the reaction efficiency of mDV•**1** was lower than that of oDV•**1**. This can be explained by considering the other structural features in mDV•**1**.

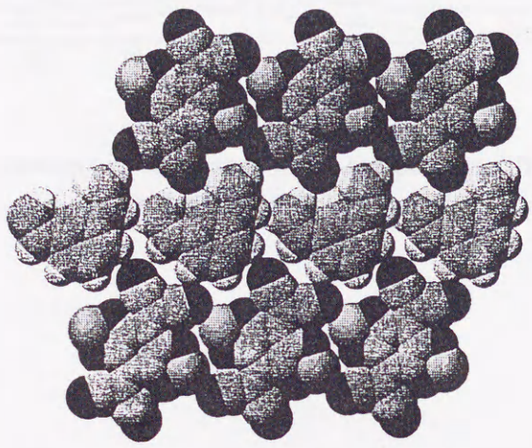

**Figure 11.** Space-filling representation of the molecular arrangement in mDV•**1**.

The space-filling representation indicates the close packing of molecules on the (0 1 -1) plane in mDV•**1** (Figure 11). During the course of the cycloaddition, the reactive sites had to move perpendicularly to this plane, and the movements accompanied the in-plane motion such as the translation and slight rotation of benzene nucleus of mDV. However, the close molecular packing would prevent such in-plane movements. Moreover, once **2m** is formed, the molecular arrangement would suffer the significant structural change which causes the disintegration of the crystal lattice. It seems likely that this environmental change makes the initially reactive *Type 2* overlap inert with the progress of the reaction. The continuous changes in the X-ray powder diffraction patterns on irradiation revealed that the initial crystalline phase was transformed into the amorphous phase with the progress of

cycloaddition (Figure 12), *i.e.* the crystal-to-amorphous transformation occurred. These results may be relevant to the low maximum yield of **2m** on irradiation.

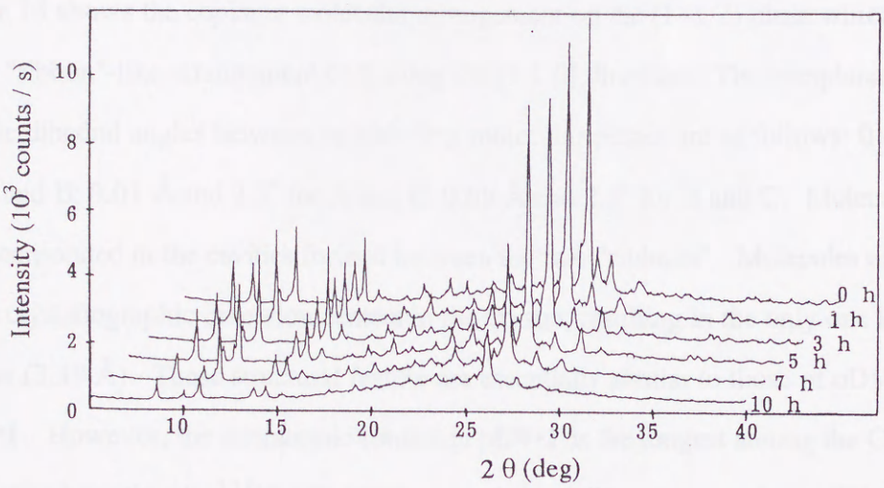


**Figure 12**. The continuous changes in the X-ray powder diffraction pattern (CuKα) on photoirradiation (λ > 540 nm) of mDV•**1**.

**Molecular Arrangement and the Photoreactivity of pDV•1**

A purple rod-like crystal of pDV•**1** was obtained by recrystallization of **1** from MeCN in the presence of excess pDV. X-ray crystallographic details of pDV•**1** are shown in Table 5. Figure 13 shows the coplanar molecular arrangement on the (1 -1 2) plane which involves the linear "ribbon"-like arrangement of **1** along the [1 1 0] direction. The interplanar distances and the dihedral angles between neighboring molecular planes are as follows: 0.67 Å and 0° for A and B; 0.01 Å and 2.3° for A and C; 0.68 Å and 2.3° for B and C. Molecules of pDV are incorporated in the cavities formed between the two "ribbons". Molecules of **1** and pDV lie on crystallographic inversion centers in the crystal, resulting in the only one kind of S•••N contact (3.49 Å). These structural feature are essentially similar to those of oDV•**1** and mDV•**1**. However, the interatomic contact in pDV•**1** is the longest among the CT crystals of **1** examined previously,[11b] leading to the very loose "ribbon" network in pDV•**1**. In addition, vinyl moieties are positionary disordered. These results suggest the presence of large voids around the vinyl moieties, which are well shown in the space-filling representation of this molecular arrangement (Figure 14).

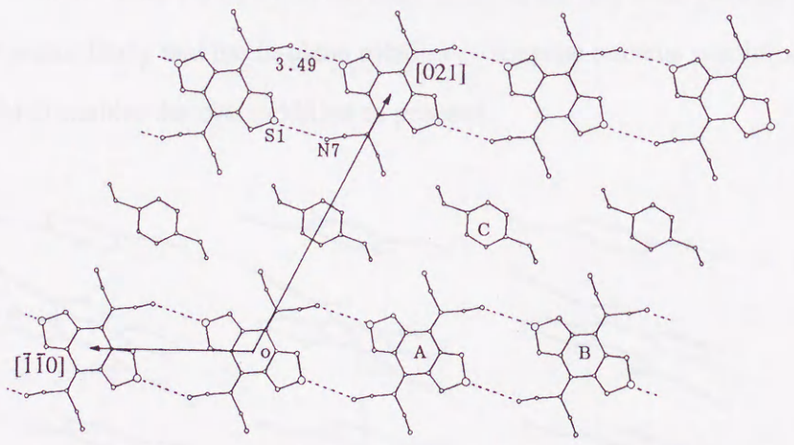


**Figure 13.** Molecular arrangement in pDV•**1**.

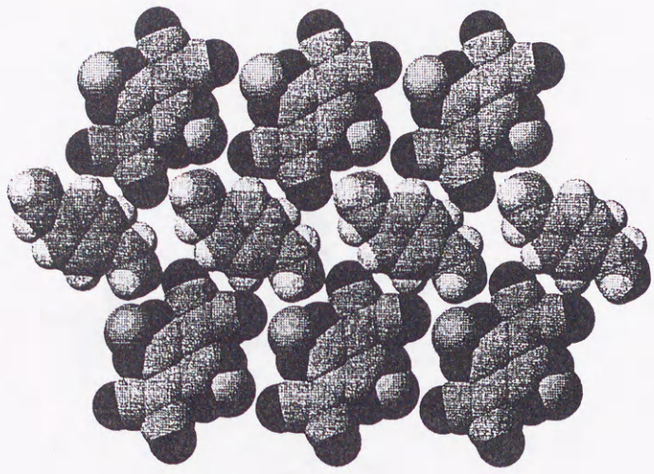

**Figure 14.** Space-filling representation of the molecular arrangement in pDV•**1**.

Perpendicularly to this coplanar arrangement, one-dimensional columnar mixed stacks are formed along the *c* axis (Figure 15). In this case, there exists only one kind of molecular overlap and repeated infinitely. As shown in Figure 16, the molecular overlap within the stack seems quite unfavorable for the cycloaddition. The photoinertness at the initial stage is consistent with the molecular arrangement. In spite of this unfavorable overlap, the cycloaddition occurred to give adducts. The time-dependence of the products yields exhibited the presence of significant induction period, suggesting that the reaction must be initiated at the lattice defects. On the other hand, when the large space in the inclusion cavities are considered, it seems likely that the in-plane rotation of benzene nucleus would be allowed in the crystal, which enables the cycloaddition to proceed.

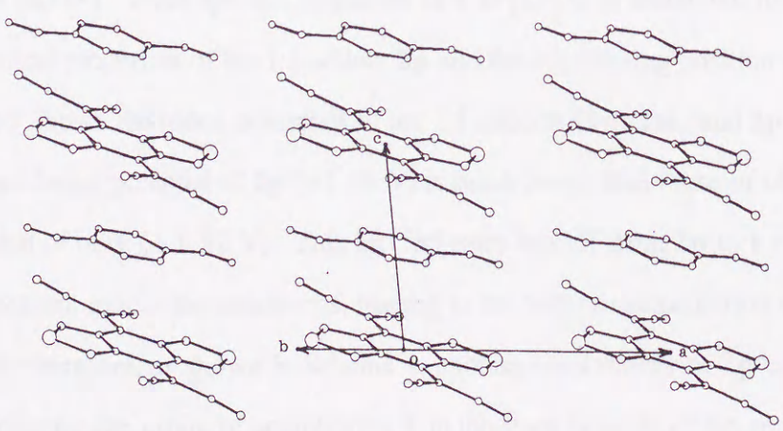


**Figure 15.** One-dimensional columnar stacks in pDV•**1**

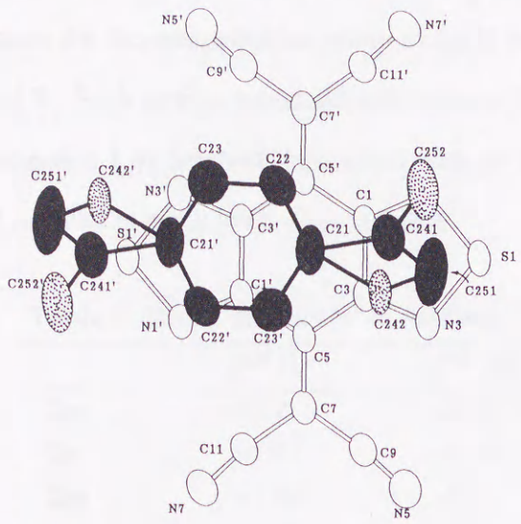


**Figure 16.** Molecular overlap in pDV•**1**. The interplanar distance and dihedral angles are 3.46 Å and 1.4°, respectively.

Thus, once adduct **2p** is formed, the molecular arrangement would suffer the significant structural changes which increase the lattice defects in order to accommodate the products in crystal, and the resulting lattice defects would accelerate the cycloaddition; namely, this reaction is regarded as "defect-accelerated" type.

Although no formation of the 1:2 adduct **6** observed in the photolysis of pDV-**1** EDA complex, the photoreaction of pDV•**1** afforded a considerable amount of **6**. This is due to the low concentration of **2p** in solution and also due to the intimate arrangement of adduct **2p** and **1** in crystal. On the other hand, this kind of product was also absent in the photoreactions of oDV•**1** and mDV•**1**. Such specific formation of **6** in pDV•**1** is accounted for by the electrochemical properties of the 1:1 adduct **2p** and the substituting position of vinyl group in **2p**. Table 5 shows the redox potentials of the 1:1 adducts (**2o**, **2m**, and **2p**) measured by CV. The oxidation potential of **2p** (+1.86 V) is much lower than those of other adducts and as low as that of oDV (+ 1.82 V). This fact indicates that ET from **2p** to **1** can be induced under the present irradiation conditions, leading to the further cycloaddition of **2p** with **1** to form **6**. Furthermore, as shown in Scheme 4, another vinyl moiety of **2p** can be accessible to the dicyanomethylene group of neighboring **1** in the stack because of the geometry of *para* substitution. The effective overlap of olefinic parts for further cycloaddition can not be

attained in other DVs•**1**. The formation of the 2:1 adduct **7** is also accounted for by the similar consideration. In this case, the dicyanomethylene group of **2p** is required to move toward pDV for the formation of **7**. Such motion seems difficult because of the large size of that group as well as the connection **1** by S•••N≡C interaction with the neighboring molecules of **1**. Thus, the yield of **7** resulted in much lower than that of **6**.

**Table 5**. Redox Potentials[a] of Adducts

| | $E^{ox}$ / V | $E^{red}$ / V |
|---|---|---|
| **2st** | > +2.2 | -0.33 |
| **2o** | +1.97 | -0.34 |
| **2m** | +1.95 | -0.31 |
| **2p** | +1.86 | -0.31 |
| oDV | +1.82 | - |

[a] $E$ / V vs SCE, 0.1 mol dm$^{-3}$ $Et_4NClO_4$ in MeCN.

**Scheme 4**

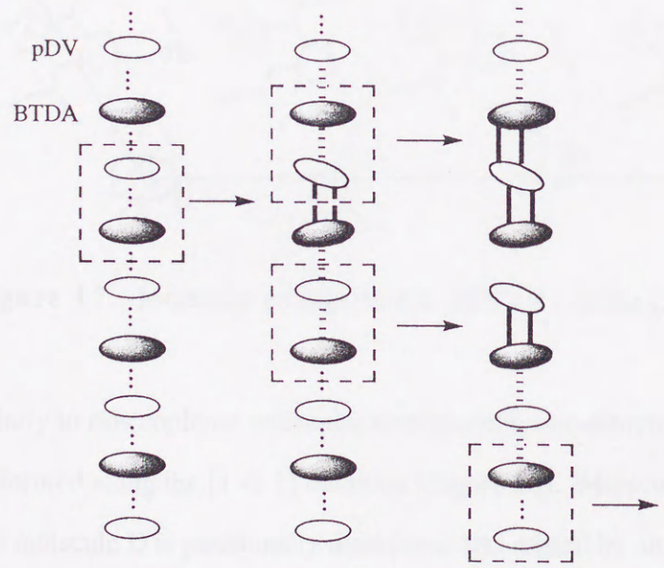

**Molecular Arrangement and the Photoreactivity of mDV5•1$_3$ (Phase B)**

The X-ray structural analysis of mDV5•**1**$_3$ was also carried out. The structural features were different from those of above described other CT crystals. In the crystal, there exist two crystallographically independent molecules of **1** (A and B) and three kinds of mDV (C, D, and E). As shown in Figure 17, molecules of A - D form coplanar sheet on the (2 -3 1) plane, whereas molecule E is arranged nearly perpendicularly to this plane between molecules A and B. There are no short S•••N contact of **1** in mDV5•**1**$_3$ and the absence of the linear "ribbon"-like networks of **1** is due to the intercalation of by molecule E.

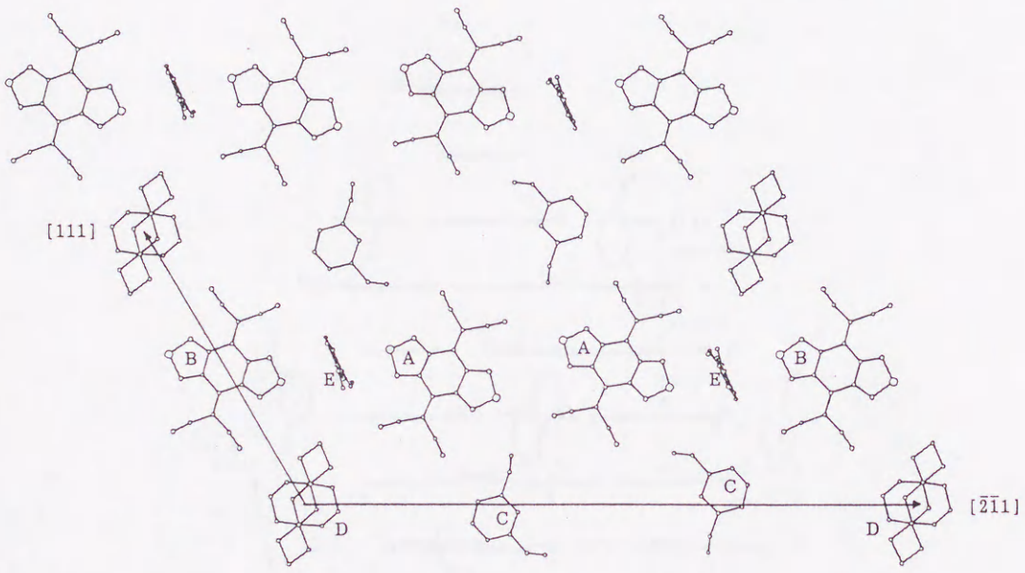


**Figure 17.** Molecular arrangement in mDV5•**1**$_3$ on the (2 -3 1) plane.

Perpendicularly to this coplanar molecular arrangement, one-dimensional columnar mixed stacks are formed along the [1 -1 1] direction (Figure 18). Molecule B lies on a center of symmetry, and molecule D is positionally disordered and related by an inversion center with molecule D'. In the stacks, there exist four different types of molecular overlaps (*Type 1* - *Type 4*) as well as their mirror images between **1** and mDV. These molecular overlaps are shown in Figure 19. Although the reactive sites in all the molecular overlaps meet the Schmidt's criteria for distance, *Type 3* and *Type 4* seem more favorable for the cycloaddition by considering the similarity to *Type 2* overlap in oDV•**1**. Furthermore, for the interaction

between HOMO of mDV and LUMO of **1**, *Type 3* and *Type 4* are more favorable than *Type 1* and *Type 2*.[20] These facts suggest that the reaction may proceed via *Type 3* and *Type 4* overlaps. This means that two kinds of mDV molecules (C and D) would not react in mDV5•**1**3, therefore, the number of mDV which can participate in the cycloaddition is only one fifth of the total. In fact, the yield of **2m** was only 24% (based on mDV) on 20-h irradiation with the recovery of 68% of mDV. In this case, it is difficult to discuss further the detailed structure-reactivity relationship because of the complicated molecular arrangement and the positional disorder of the reactive sites.

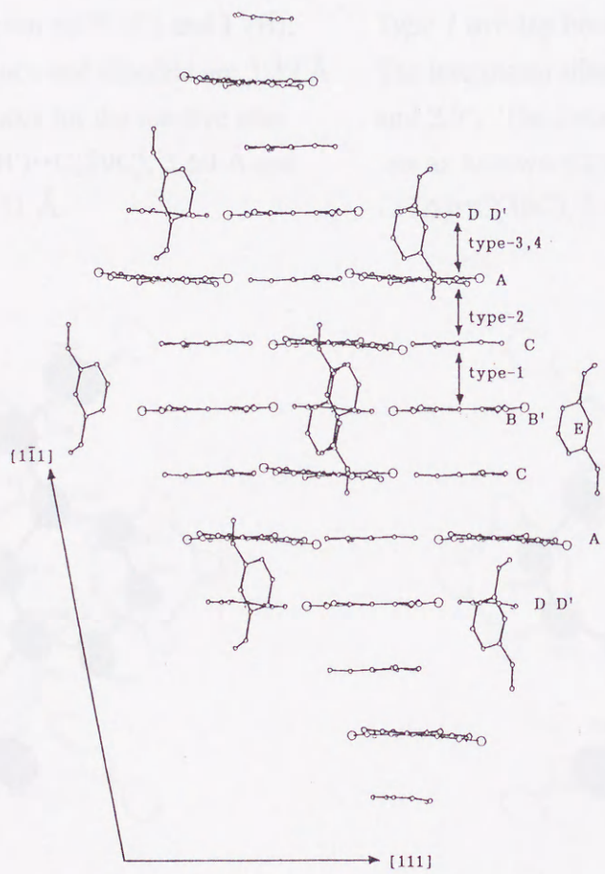


**Figure 18.** Molecular arrangement in mDV5•**1**3 showing the one-dimensional columnar stack along the [1 -1 1] direction.

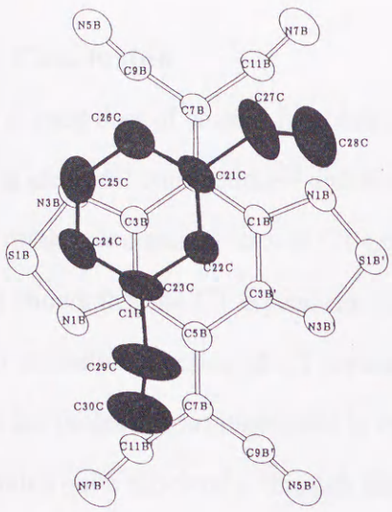


**Figure 19a.** Molecular overlap in mDV5•**1**3: *Type 1* overlap between mDV (C) and **1** (B). The interplanar distance and dihedral are 3.39 Å and 3.3°. The distances for the reactive sites are as follows: C(5B')••C(29C), 3.60 Å and C(7B')••C(30C), 3.51 Å.

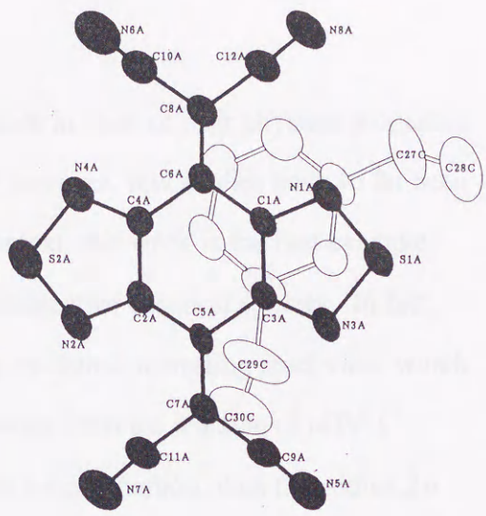


**Figure 19b.** Molecular overlap in mDV5•**1**3: *Type 1* overlap between mDV (C) and **1** (A). The interplanar distance and dihedral are 3.33 Å and 2.9°. The distances for the reactive sites are as follows: C(5A)••C(29C), 3.60 Å and C(7A)••C(30C), 3.46 Å.

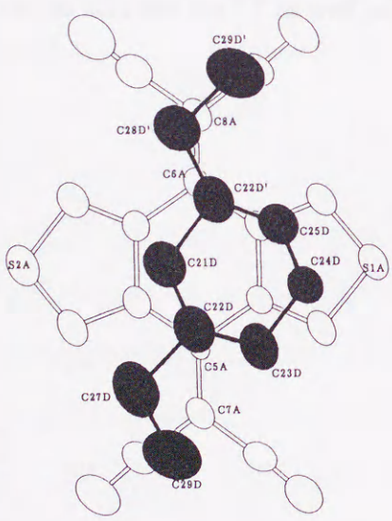


**Figure 19c.** Molecular overlap in mDV5•**1**3: *Type 3* overlap between mDV (D) and **1** (A). The interplanar distance and dihedral angle are 3.39 Å and 2.3°. The distances for the reactive sites are as follows: C(6A)••C(28D'), 3.62 Å and C(8A)••C(29D'C), 3.64 Å.

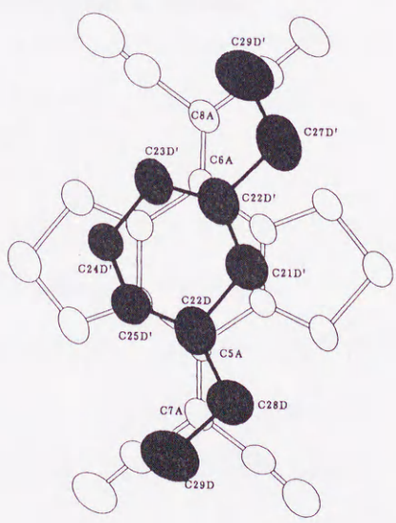


**Figure 19d.** Molecular overlap in mDV5•**1**3: *Type 4* overlap between mDV (D') and **1** (A). The interplanar distance and dihedral angle are 3.39 Å and 2.3°. The distances for the reactive sites are as follows: C(5A)••C(28D), 3.56 Å and C(7A)••C(29D), 3.54 Å.

## 1-5. Conclusion

A great deal of studies has been made on CT crystals in view of their physical properties such as electrical conduction[22] and ferromagnetism,[23] however, few studies have so far been made on the photoreactivities of CT crystals. In this context, this work is the first example which shows that the CT crystal can serve as novel photoreactive chemical species. In fact, the CT excitation reaction of CT crystals of **1** with DVs exhibited interesting reactivities which reflect the molecular arrangements in crystal. It was revealed that the reaction of oDV•**1** proceeded quite efficiently through the crystal-to-crystal transformation, thus the adduct **2o** can be obtained in high yield. In contrast, the crystal-to-amorphous transformation was observed in the case of mDV•**1** because of the large atomic and molecular motions in the crystal with the progress of the reaction. On the other hand, photoreaction of pDV•**1** can be considered as defect-accelerated type and afforded 1:2 adduct **6** besides 1:1 adduct **2p**. The formation of **6** was never attained by the photolysis of the corresponding EDA complex in solution. This result suggests that the importance of the preorganized face-to-face overlap of a donor and an acceptor for ET as well as much higher concentration in crystal.

## Experimental Section

**General.** All the melting points are reported uncorrected. Elemental analyses were performed at the Instrumental Analysis Center for Chemistry, Faculty of Science, Tohoku University. MS spectra were obtained in the EI mode at 70 eV. $^{1}H$ NMR spectra were recorded at 90 or 200 MHz. $^{13}C$ NMR spectra were recorded at 50 MHz. Preparative thick-layer chromatography (TLC) was performed on 0.5 mm x 20 cm x 20 cm silica gel plates.

**Materials.** BTDA (**1**) was prepared according to the reported procedure[24] in 72% yield. DVs were obtained by Wittig reactions[25] of the corresponding aldehydes in oDV 65% (oDV), 71% (mDV), and 92% (pDV), respectively. ST was commercially available and used as recieved. MeCN was dried over $CaH_2$ and distilled before each of use for photoreaction.

**Preparation of CT Crystals of BTDA (1) with Arylolefins.**

**ST•1.** Finely powdered **1** (128 mg, 0.40 mmol) and ST (104 mg, 1.0 mmol) were mixed at room temperature. The color changed gradually from yellow to orange. After allowing to stand for 12 h at -40 °C, the orange powder of ST•**1** (168 mg, yield 99%) was obtained by removal of excess ST in vacuo for 10 min at room temperature. Prolonged drying caused decomposition of the CT crystal to lose volatile ST: mp 82-86 °C dec; IR (KBr) 2220 $cm^{-1}$. Anal. Calcd for $C_{20}H_8N_8S_2$ (1:1): C, 56.59; H, 1.90; N, 26.40. Found: C, 56.04; H, 2.15; N, 26.00.

**oDV•1.** Finely powdered **1** (100 mg, 0.31 mmol) and oDV (82 mg, 0.63 mmol) were mixed at room temperature. The color of the solid gradually changed from yellow to red. After allowing to stand for 12 h at -40 °C, the red powder of oDV•**1** (141 mg, yield 100%) was obtained by removal of excess oDV in vacuo for 30 min at room temperature: mp 95-98 °C dec; IR (KBr) 2220 $cm^{-1}$. Anal. Calcd for $C_{22}H_{10}N_8S_2$ (1:1): C, 58.66; H, 2.24; N, 24.87. Found: C, 58.45; H, 2.36; N, 24.72.

**mDV•1 (phase A).** Finely powdered **1** (100 mg, 0.31 mmol) and mDV (82 mg, 0.63 mmol) were mixed. The color of the solid gradually changed from yellow to red. After allowing to stand for 12 h at -40 °C, the red powder of mDV•**1** (137 mg, yield 98%) was obtained by removal of excess mDV in vacuo for 30 min at room temperature: mp 95-98 °C

dec; IR (KBr) 2215 $cm^{-1}$. Anal. Calcd for $C_{22}H_{10}N_8S_2$ (1:1): C, 58.66; H, 2.24; N, 24.87. Found: C, 58.90; H, 2.49; N, 24.54.

**mDV$_5$•1$_3$ (phase B).** Single crystals of mDV$_5$•**1**$_3$ were obtained as orange plates by vapor diffusion method in MeCN/*n*-hexane accompanied with red needles of mDV•**1** (phase A): mp 96-102 °C dec; IR (KBr) 2215 $cm^{-1}$. Anal. Calcd for $C_{86}H_{50}N_{24}S_6$ (5:3): C, 64.08; H, 3.13; N, 20.86. Found: C, 63.36; H, 3.37; N, 20.94.

**pDV•1.** Finely powdered **1** (200 mg, 0.63 mmol) was suspended in 2 mL of $CH_2Cl_2$ containing pDV (164 mg, 1.26 mmol) and the mixture was concentrated with a stream of nitrogen until the color of suspension turned to brownish purple. After allowing to stand for 12 h at room temperature, pDV•**1** (283 mg, yield 100%) was obtained as a dark purple powder by removal of excess pDV in vacuo for 3 h at room temperature: mp 168-174 °C dec; IR (KBr) 2215 $cm^{-1}$. Anal. Calcd for $C_{22}H_{10}N_8S_2$ (1:1): C, 58.66; H, 2.24; N, 24.87. Found: C, 58.42; H, 2.35; N, 24.75.

**Measurement of Redox Potentials.** All the oxidation ($E^{ox}$) and reduction ($E^{red}$) potentials described here were measured under argon atomosphere by CV method in dry MeCN containing 0.1 mol $dm^{-3}$ $Et_4NClO_4$ as a supporting electrolyte. All the value are in *E*/V vs SCE, and Pt wire was used as the working electrode. In the case of irreversible waves, half-wave potentials were estimated from the peak potentials as $E^{ox} = E^{pa} - 0.03$ V or $E^{red} = E^{pa} + 0.03$ V.

**Determination of Association Constants ($K_{CT}$) of EDA Complexes [Arylolefins-BTDA (1)].** In the presence of a large excess of donor, $K_{CT}$ values for the EDA complexes of **1** were determined by spectrophotometric procedure based on the Benesi-Hildebrand relationship in MeCN at 20 °C. In all cases, linear correlations were observed ($\gamma$ = 0.998 - 0.999, n = 7 - 10), indicating a 1:1 molar ratio for the EDA complexes. Molar absorption coefficients ($\varepsilon$ / $dm^3$ $mol^{-1}cm^{-1}$) at 460 nm are as follows: pDV-**1**, 1400; mDV-**1**, 1800; oDV-**1**, 1400; ST-**1**, 1100.

**CT Excitation Reactions of EDA Complexes [Arylolefins-BTDA (1)].**

**ST-1.** A solution of ST (52 mg, 0.5 mmol) and **1** (32 mg, 0.1 mmol) in MeCN (10 mL) was irradiated by using a 2 kW xenon lamp through a Y-47 glass cutoff filter ($\lambda$ > 450 nm)

for 5 h at 20 °C under nitrogen. After the photolysis, the reaction mixture was concentrated in vacuo. The recovery of ST (24%) was determined on the basis of 90 MHz $^1$H NMR spectrum ($CCl_4$) by using 1,1,1,2-tetrachloroethane (δ 4.27 ppm) as an internal standard. After the addition of 2 mL of $CH_2Cl_2$ to the photolysate, unreacted **1** (25 mg, 78%) was recovered as a yellow powder by filtration of the separated precipitates followed by washing with $CH_2Cl_2$ (10 mL). The TLC separation on $SiO_2$ ($CH_2Cl_2$) of the filtrate afforded the adduct **2st** (Rf 0.43 - 0.36). The product was dissolved in *ca.*. 0.5 mL of $CDCl_3$ containing 1 mL of $CH_2Br_2$ (0.0144 mmol). The yield (1.6 mg, 4%) of 2st was determined on the basis of 200 MHz $^1$H NMR spectrum by using $CH_2Br_2$ (δ 4.95 ppm) as an internal standard.

**2st**: faintly yellow powder, mp 159-164 °C dec; IR (KBr) 2220 cm$^{-1}$; $^1$H NMR (200 MHz, $CDCl_3$) δ 7.14-7.17 (3 H, m), 6.72-6.76 (2 H, m), 5.41 (1 H, dd, *J* = 9.0, 12.0 Hz), 4.32 (1 H, dd, *J* = 12.0, 12.0 Hz), 3.38 (1 H, dd, *J* = 9.0, 12.0 Hz); UV (MeCN) λmax (ε) 370 sh (10200), 352 (13000), 324 (15200), 290 sh (14800), 280 (16100), 272 sh (15400), 230 (10100), 214 sh (14700) nm; MS *m/z* (relative intensity) 424 ($M^+$, 0.4), 347 ($M^+$ - $CH_2$=C(CN)$_2$ - 1, 100). Anal. Calcd for $C_{20}H_8N_8S_2$•1.25 $H_2O$: C, 53.74; H, 2.37; N, 25.07. Found: C, 53.83; H, 2.07; N, 24.77.

**oDV-1**. A solution of oDV (65 mg, 0.5 mmol) and **1** (32 mg, 0.1 mmol) in MeCN (10 mL) was irradiated by using a 2 kW xenon lamp through a Y-47 glass cutoff filter (λ > 450 nm) for 5 h at 20 °C under nitrogen. After the photolysis, the reaction mixture was concentrated in vacuo. The recovery of oDV (88%) was determined on the basis of 90 MHz $^1$H NMR spectrum ($CCl_4$) by using 1,1,1,2-tetrachloroethane as an internal standard. After addition of 2 mL of $CH_2Cl_2$ to the photolysate, unreacted **1** (20 mg, 63%) was recovered as a yellow powder by filtration of the separated precipitates followed by washing with $CH_2Cl_2$ (10 mL). The TLC separation on $SiO_2$ ($CH_2Cl_2$) of the filtrate afforded the adduct **2o** (Rf 0.40 - 0.27) in 9% yield. The weight (4.1 mg) of **2o** was determined on the basis of 200 MHz $^1$H NMR spectrum ($CDCl_3$) by using 1,1,1,2-tetrachloroethane (0.0095 mmol, δ 4.30 ppm) as an internal standard.

**2o**: pale yellow powder, mp 155-158 °C dec; IR (KBr) 2220 cm$^{-1}$; $^1$H NMR (200 MHz, $CDCl_3$) δ 7.04-7.28 (4 H, m), 5.88 (1 H, dd, *J* = 10.8, 17.2 Hz), 5.34 (1 H, dd, *J* = 8.8,

12.0 Hz), 4.87 (1 H, dd, $J$ = 1.2, 17.2 Hz), 4.56 (1 H, dd, $J$ = 1.2, 10.8 Hz), 4.43 (1 H, dd, $J$ = 12.0, 12.0 Hz), 3.41 (1 H, dd, $J$ = 8.8, 12.0 Hz); UV (MeCN) λmax (ε) 350 (12800), 324 (15600), 290 sh (14000), 274 (16400), 232 (18700) nm; MS *m/z* (relative intensity) 450 ($M^+$, 6), 372 ($M^+$ - $CH_2$=C(CN)$_2$, 98), 345 ($M^+$ - $CH_2$=C(CN)$_2$ - CN - 1, 100). Anal. Calcd for $C_{22}H_{10}N_8S_2$: C, 58.66; H, 2.24; N, 24.87. Found: C, 58.04; H, 2.47; N, 24.67.

**mDV-1.** A solution of mDV (65 mg, 0.5 mmol) and **1** (32 mg, 0.1 mmol) in MeCN (10 mL) was irradiated by using a 2 kW xenon lamp through a Y-47 glass cutoff filter (λ > 450 nm) for 5 h at 20 °C under nitrogen. After the photolysis, the reaction mixture was concentrated in vacuo. The recovery of mDV (84%) was determined on the basis of 90 MHz $^1$H NMR spectrum ($CDCl_3$) by using 1,1,1,2-tetrachloroethane as an internal standard. After addition of 2 mL of $CH_2Cl_2$ to the photolysate, unreacted **1** (16 mg, 50%) was recovered as a yellow powder by filtration of the separated precipitates followed by washing with $CH_2Cl_2$ (10 mL). The TLC separation on $SiO_2$ ($CH_2Cl_2$) of the filtrate afforded the adduct **2m** (Rf 0.68 - 0.58) in 11% yield. The weight (4.8 mg) of **2m** was determined on the basis of 200 MHz $^1$H NMR spectrum (acetone-$d_6$) by using 1,1,1,2-tetrachloroethane (0.0095 mmol, δ 4.65 ppm) as an internal standard.

**2m**: yellow powder, mp 157-162 °C dec; IR (KBr) 2215 cm$^{-1}$; $^1$H NMR (200 MHz, $CDCl_3$) δ 7.22 (1 H, d, $J$ = 7.8 Hz), 7.08 (1 H, dd, $J$ = 7.6, 7.8 Hz), 6.83 (1 H, s), 6.57 (1 H, d, $J$ = 7.6 Hz), 6.54 (1 H, dd, $J$ = 11.1, 17.6 Hz), 5.62 (1 H, dd, $J$ = 0.5, 17.6 Hz), 5.38 (1 H, dd, $J$ = 8.8, 12.4 Hz), 5.25 (1 H, dd, $J$ = 0.5, 11.1 Hz), 4.34 (1 H, dd, $J$ = 11.5, 12.4 Hz), 3.38 (1 H, dd, $J$ = 8.8, 11.5 Hz); UV (MeCN) λmax (ε) 368 sh (10500), 352 (13400), 324 (15600), 278 (18000), 250 (19000), 236 sh (18100), 214 (33900) nm; MS *m/z* (relative intensity) 372 ($M^+$ - $CH_2$=C(CN)$_2$, 73), 371 ($M^+$ - $CH_2$= C(CN)$_2$ - 1, 100), 346 ($M^+$ - $CH_2$=C(CN)$_2$ - CN, 15), 345 ($M^+$ -$CH_2$=C(CN)$_2$ - CN - 1, 35). Anal. Calcd for $C_{22}H_{10}N_8S_2$•0.5$H_2O$: C, 57.51; H, 2.41; N, 24.39. Found: C, 57.32; H, 2.50; N, 24.00.

**pDV-1.** A solution of pDV (65 mg, 0.5 mmol) and **1** (32 mg, 0.1 mmol) in MeCN (10 mL) was irradiated by using a 2 kW xenon lamp through a Y-47 glass cutoff filter (λ > 450 nm) for 5 h at 20 °C under nitrogen. After the photolysis, the reaction mixture was

concentrated in vacuo. The recovery of pDV (82%) was determined on the basis of 90 MHz $^1$H NMR spectrum ($CCl_4$) by using 1,1,1,2-tetrachloroethane as an internal standard. After addition of 2 mL of $CH_2Cl_2$ to the photolysate, unreacted **1** (21 mg, 67%) was recovered as a yellow powder from the separated precipitates by filtration followed by washing with $CH_2Cl_2$ (10 mL). The TLC separation on $SiO_2$ ($CH_2Cl_2$) of the filtrate afforded the adduct **2p** (Rf 0.81 - 0.74) in 8% yield. The weight (3.6 mg) of **2p** was determined on the basis of 200 MHz $^1$H NMR spectrum ($CDCl_3$) by using $CH_2Br_2$ (0.0144 mmol) as an internal standard. The photolysis for 20 h under the similar conditions gave the adduct **2p** (20 mg) in 44% yield. In this case, the recovery of pDV was only 25% ($^1$H NMR), and **1** could not be recovered from the photolysate. The TLC analysis of the photolysate showed the presence of many other products. However, no attempt was made to identify them because their quantities were very small.

**2p**: yellow powder, mp 124-130 °C dec; IR (KBr) 2215 cm$^{-1}$; $^1$H NMR (200 MHz, $CDCl_3$) δ 7.17 (2 H, AA'XX'), 6.71 (2 H, AA'XX'), 6.55 (1 H, dd, $J$ = 11.0, 17.6 Hz), 5.64 (1 H, dd, $J$ = 0.6, 17.6 Hz), 5.38 (1 H, dd, $J$ = 9.0, 12.0 Hz), 5.22 (1 H, dd, $J$ = 0.6, 11.0 Hz), 4.29 (1 H, dd, $J$ = 12.0, 12.0 Hz), 3.36 (1 H, dd, $J$ = 9.0, 12.0 Hz); $^{13}$C NMR (50 MHz, $CDCl_3$), δ 157.55, 155.87, 150.94, 150.10, 138.18, 137.78, 135.53, 133.11, 126.73, 126.51, 115.13, 112.89, 112.51, 112.46, 112.12, 84.56, 56.15, 49.24, 36.70, 33.92; UV (MeCN) λmax (ε) 350 (14000), 324 (17100), 280 sh (19200), 258 (26600), 236 sh (19100) nm; MS *m/z* (relative intensity) 372 ($M^+$ - $CH_2$=C(CN)$_2$, 69), 371 ($M^+$ - $CH_2$=C(CN)$_2$ - 1, 100), 346 ($M^+$ - $CH_2$=C(CN)$_2$ - CN, 15), 345 ($M^+$ - $CH_2$=C(CN)$_2$ - CN - 1, 23). Anal. Calcd for $C_{22}H_{10}N_8S_2$: C, 58.66; H, 2.24; N, 24.87. Found: C, 58.74; H, 2.63; N, 24.44.

**CT Excitation Reactions of CT Crystals of BTDA (1) with Arylolefins (Powder Sample).**

**ST•1.** A water suspension (10 mL) of ST•**1** (42 mg, 0.1 mmol) was irradiated by using a 2 kW xenon lamp through a Y-52 glass cutoff filter (λ > 505 nm) for 1 h at 15 °C. The orange powder gradually turned to yellow. Filtration of the resulting precipitates followed by the TLC separation ($CH_2Cl_2$) afforded 30 mg of **2st** (Rf 0.50 - 0.30) as a faintly yellow powder in 71% yield.

**oDV•1.** A water suspension (10 mL) of oDV•**1** (45 mg, 0.1 mmol) was irradiated by using a 2 kW xenon lamp through an O-57 glass cutoff filter ($\lambda > 540$ nm) for 1 h at 15 °C. The red powder gradually turned to yellow. Filtration of the resulting precipitate followed by the TLC separation ($CH_2Cl_2$) afforded 41 mg of **2o** (Rf 0.56 - 0.34) as a pale yellow powder in 91% yield. After the similar photolysis for 15 min, **2o** (38 mg) was obtained by the TLC separation in 84% yield.

**mDV•1.** A water suspension (10 mL) of mDV•**1** (45 mg, 0.1 mmol) was irradiated by using a 2 kW xenon lamp through an O-57 glass cutoff filter ($\lambda > 540$ nm) for 1 h at 15 °C. In this case, there was no obvious change in the color of the powder. Filtration of the resulting percipitates followed by the TLC separation ($CH_2Cl_2$) afforded **2m** as a pale yellow powder in 10% yield. The weight (4.5 mg) of **2m** was determined on the basis of 200 MHz $^1$H NMR spectrum ($CDCl_3$) by using $CH_2Br_2$ (0.0144 mmol) as an internal standard. After the similar photolysis for 3 h, **2m** (10 mg, Rf 0.50 - 0.39) was obtained by the TLC separation in 22% yield.

**pDV•1.** A water suspension (10 mL) of pDV•**1** (45 mg, 0.1 mmol) was irradiated by using a 2 kW xenon lamp through an O-57 glass cutoff filter ($\lambda > 540$ nm) for 5 h at 15 °C. The resulted precipitates were collected by filtration. After addition of 2 mL of $CH_2Cl_2$, separated precipitates were filtered and washed successively with $CH_2Cl_2$ (5 mL), acetone (2 mL) to afford **6** (14 mg) as a pale yellow powder in 36% yield based on **1**. The adducts **2p** (7 mg, Rf 0.49 - 0.36) and 7 (1 mg, Rf 0.75 - 0.69) were obtained from the filtrate by the TLC separation ($CH_2Cl_2$) in 16% and 3% yield, respectively. The wavelength-dependence of the photoreaction was also examined at $\lambda > 580$ nm. Water suspensions (5 mL) of pDV•**1** (23 mg, 0.05 mmol) were irradiated separately by using a 2 kW xenon lamp through an R-60 glass ($\lambda > 580$ nm) cutoff filter for 5 h at 15 °C. After filtration, the resulted percipitates were analysed by 200 MHz $^1$H NMR spectroscopy (DMSO-$d_6$) with 1,1,1,2-tetrachloroethane ($\delta$ 4.80 ppm) as an internal standard. The analysis showed that the yields of **2p** and **6** were formed in 29% and 22%, respectively, and pDV was recovered in 35% yield.

**6**: pale yellow powder, mp 115-130 °C dec; IR (KBr) 2215 cm$^{-1}$; $^1$H NMR (200 MHz, DMSO-$d_6$) $\delta$ 6.54 (4 H, s), 5.12 (2 H, dd, $J$ = 10.6, 11.9 Hz), 3.82 (2 H, dd, $J$ = 11.9,

11.9 Hz), 3.50 (2 H, dd, J = 10.6, 11.9 Hz); UV (MeCN) λmax (ε) 368 sh (18000), 350 (23600), 324 (28000), 290 sh (27100), 274 (31200), 222 (29600) nm; MS *m/z* (relative intensity) 614 ($M^+$ - $2CH_2$=$C(CN)_2$, 67), 613 ($M^+$ - $2CH_2$=$C(CN)_2$ - 1, 80), 588 ($M^+$ - $2CH_2$=$C(CN)_2$ - CN, 100); HRMS *m/z* 587.9673 ($M^+$ - $2CH_2$=$C(CN)_2$ - CN; calcd for $C_{25}H_6N_{11}S_4$, 587.9690). Anal. Calcd for $C_{34}H_{10}N_{16}S_4 \cdot 4H_2O$: C, 48.45; H, 2.15; N, 26.60. Found: C, 48.44; H, 1.45; N, 27.18.

**7**: colorless powder, mp 180-205 °C dec; IR (KBr) 2235 $cm^{-1}$; $^1H$ NMR (200 MHz, $CDCl_3$) δ 7.18 (4 H, AA'XX'), 6.72 (4 H, AA'XX'), 6.57 (2 H, dd, *J* = 11.0, 17.6 Hz), 5.65 (2 H, dd, *J* = 0.8, 17.6 Hz), 5.22 (2 H, dd, *J* = 0.8, 11.0 Hz), 5.15 (2 H, dd, *J* = 8.8, 12.4 Hz), 4.32 (2 H, dd, *J* = 11.4, 12.4 Hz), 3.27 (2 H, dd, *J* = 8.8, 11.4 Hz); HRMS *m/z* 580.1255 ($M^+$; calcd for $C_{32}H_{20}N_8S_2$, 580.1252), 502.1012 ($M^+$ - $CH_2$=$C(CN)_2$; calcd for $C_{28}H_{18}N_6S_2$, 502.1034), 424.0786 ($M^+$ - $2CH_2$=$C(CN)_2$; calcd for $C_{24}H_{16}N_4S_2$, 424.0816).

**CT Excitation Reaction of $mDV_5$•$\mathbf{1}_3$ CT Crystal.** Single crystals of $mDV_5$•$\mathbf{1}_3$ (17 mg, 0.011 mmol) were sealed in a glass capillary tube and were irradiated by using a 2 kW xenon lamp through an O-57 glass cutoff filter (λ > 540 nm) for 1 h at 15 °C. As the reaction proceeded, the surface of the crystals became opaque, and the crystalline samples disintegrated into powder. The resulting powder was analyzed by 200 MHz $^1H$ NMR spectroscopy (acetone-$d_6$) with $CH_2Br_2$ (0.0259 mmol, δ 5.30 ppm) as an internal standard. The analysis showed that adduct **2m** was formed in 6% yield (based on mDV) and mDV was recovered in 92% yield. The photolysis for 20 h under the similar conditions gave the adduct **2m** (10 mg) in 24% (based on mDV) yield with the recovery of mDV in 68% yield.

**The Time-Course of the CT Excitation Reaction of mDV•1.** Water suspensions (5 mL) of mDV•**1** (23 mg, 0.05 mmol) were irradiated (λ > 540 nm) separetely for 1 h, 3 h, 5 h, 10 h, and 20 h at 15 °C. After filtration, the resulted precipitates were analyzed by 200 MHz $^1H$ NMR spectroscopy (acetone-$d_6$) with 1,1,1,2-tetrachloroethane as an internal standard.

**The Time-Course of the CT Excitation Reaction of pDV•BTDA.** Water suspensions (5 mL) of pDV•**1** (23 mg, 0.05 mmol) were irradiated (λ > 540 nm) separetely

for 0.5 h, 0.75 h, 1 h, 1.5 h, and 2 h at 15 °C. After filtration, the resulted precipitates were analyzed by 200 MHz $^1$H NMR spectroscopy (DMSO-$d_6$) with 1,1,1,2-tetrachloroethane as an internal standard.

**X-ray Powder Diffraction Analyses.**

**oDV•1.** Water suspensions (10 mL) of oDV•**1** (120 mg, 0.27 mmol) were irradiated ($\lambda >$ 540 nm) separately for 5 min and 15 min at 15 °C. The resulted precipitates were collected and analyzed by XRD technique (CuK$\alpha$, 40 kV, 20 mA, 2 ° min$^{-1}$) along with oDV•**1** and *dl*-2o. After the TLC separation ($CH_2Cl_2$) of the photolysates, the conversions were determined to be 43% and 84%, respectivery.

**mDV•1.** Water suspensions (5 mL) of mDV•**1** (120 mg, 0.27 mmol) were irradiated ($\lambda >$ 540 nm) separately for 1 h, 3 h, 5 h, 7 h, and 10 h at 15 °C. The resulted precipitates were collected and analyzed by XRD technique (CuK$\alpha$, 40 kV, 50 mA, 2 ° min$^{-1}$) along with mDV•**1**. After the TLC separation ($CH_2Cl_2$) of the photolysates, the conversions were determined to be 6%, 16%, 20%, 28%, and 30%, respectively.

**X-ray Structural Analyses**

**oDV•1.** A reddish rod-like crystal with a dimension of 0.15 x 0.15 x 0.30 mm was obtained by the vapor diffusion method from MeCN/*n*-hexane and sealed in a glass capillary with oDV. A total of 2438 reflections was collected on an AFC-5R automated four-circle diffractometer with a rotating anode (200 mA, 45 kV) at 13 °C by using graphite monochromated MoK$\alpha$ radiation ($\lambda$ = 0.71049 Å) within $2\theta$ = 55°. The $\omega$ - $2\theta$ scan mode with a scan speed of 4° min$^{-1}$ was employed with the $\omega$ scan range of $(1.26 + 0.3 \tan \theta)°$. Crystal data are as follows: MF $C_{22}H_{10}N_8S_2$, MW 450.50, monoclinic, space group $P2_1$, $a$ = 8.866(2) Å, $b$ = 16.764(3) Å, $c$ = 7.006(3) Å, $\beta$ = 99.63(2)°, $V$ = 1026.6 (5) Å$^3$, $Z$ = 2, and $D_{calcd}$ = 1.457 g cm$^{-3}$. The structure was solved by the direct method using RANTAN 81 program with some modification, and was refined by the block-diagonal least-squares method with anisotropic temperature factors. All the hydrogen atoms were located in the difference Fourier map and included in the refinement with isotropic temperature factors. The final $R$ value is 4.22% for 1950 reflections with $|Fo| > 3\sigma|Fo|$.

**mDV•1.** A reddish needle-like crystal with a dimension of 0.30 x 0.10 x 0.10 mm was obtained, accompanied with phase B, by the vapor diffusion method from MeCN/*n*-hexane. It was sealed in a glass capillary with mDV and used for the data collection on an AFC-5R automated four-circle diffractometer with a rotating anode (200 mA, 45 kV) at 13 °C. The $\omega$ - $2\theta$ scan mode with a scan speed of 4° min$^{-1}$ was employed with the ω scan range of (1.155 + 0.3 tan $\theta$)°. A total of 4035 independent reflections was collected by using graphite monochromated MoKα radiation within $2\theta$ = 52°. Crystal data are as follows: MF $C_{22}H_{10}N_8S_2$, MW 450.50, triclinic, space group $P\bar{1}$, $a$ = 9.238(4) Å, $b$ = 17.264(6) Å, $c$ = 7.046(5) Å, $\alpha$ = 94.21 (4)°, $\beta$ = 104.65(4)°, $\gamma$ = 103.93(3)°, $V$ = 1044.4(9) Å$^3$, $Z$ = 2, and $D_{calcd}$ = 1.433 g cm$^{-3}$. The structure was solved by the direct method using RANTAN 81 program with some modification, and was refined by the block-diagonal least-squares method with anisotropic temperature factors. Most of hydrogen atoms were picked up from the difference Fourier map and others (H25, H26, H282, H302) were calculated geometrically. They were included in the refinement with isotropic temperature factors. The final $R$ value is 8.34% for 2045 reflections with $|Fo| > 3\sigma|Fo|$.

**pDV•1.** A purple rod-like crystal with a dimension of 0.20 x 0.10 x 0.05 mm was obtained by recrystallizing **1** from MeCN in the presence of excess pDV, and used for the data collection on an AFC-5R automated four-circle diffractometer with a rotating anode (120 mA, 50 kV) at 23 °C. The $\omega$ - $2\theta$ scan mode with a scan speed of 4° min$^{-1}$ was employed with the ω scan range of (1.26 + 0.5 tan $\theta$)°. A total of 2251 independent reflections was collected by using graphite monochromated MoKα radiation within $2\theta$ = 52°. Crystal data are as follows: MF $C_{22}H_{10}N_8S_2$, MW 450.50, triclinic, space group $P\bar{1}$, $a$ = 8.882(4) Å, $b$ = 9.418(4) Å, $c$ = 7.363(3) Å, $\alpha$ = 108.96(3)°, $\beta$ = 95.14(4)°, $\gamma$ = 111.91(3)°, $V$ = 524.6(4) Å$^3$, $Z$ = 1, and $D_{calcd}$ = 1.426 g cm$^{-3}$. The structure was solved by the direct method using RANTAN 81 program with some modification, and was refined by the block-diagonal least-squares method with anisotropic temperature factors. The final $R$ value is 6.62% for 1591 reflections with $|Fo| > 3\sigma|Fo|$. The refinement was not converged when the disordered vinyl atoms (C242 and C252) were not included.

**mDV5•13.** An orange plate-like crystal with a dimension of 0.20 x 0.30 x 0.15 mm was obtained by the vapor diffusion method from MeCN/*n*-hexane accompanied with red needles of phase A. The crystal was sealed in a glass capillary with mDV and used for the data collection on an AFC-5R automated four-circle diffractometer with a rotating anode (120 mA, 50 kV) at 23 °C. The $\omega$ - $2\theta$ scan mode with a scan speed of 6° min$^{-1}$ was employed with the $\omega$ scan range of $(1.16 + 0.5 \tan \theta)°$. A total of 7555 independent reflections was collected by using graphite monochromated MoK$\alpha$ radiation within $2\theta = 50°$. Crystal data are as follows: MF $C_{86}H_{50}N_{24}S_6$, MW 1611.86, triclinic, space group $P\bar{1}$, $a$ = 12.422(4) Å, $b$ = 15.141(3) Å, $c$ = 11.840(5) Å, $\alpha$ = 97.72(3)°, $\beta$ = 116.19(2)°, $\gamma$ = 88.24(3)°, $V$ = 1979.2(12) Å$^3$, $Z$ = 1, and $D_{calcd}$ = 1.352 g cm$^{-3}$. The structure was solved by the direct method using RANTAN 81 program with some modification, and was refined by the block-diagonal least-squares method with anisotropic temperature factors. The final $R$ value is 9.40% for 3942 reflections with $|Fo| > 3\sigma|Fo|$. Hydrogen atoms were not included in the refinement.

**References and Notes**

(1) (a) Ramamurthy, V.; Venkatesan, K. *Chem. Rev.* **1987**, *87*, 433. (b) Singh, N. B.; Singh, R. J.; Singh, N. P. *Tetrahedron* **1994**, *50*, 6441. (c) Ito, Y. *Synthesis*, **1998**, 1, and references cited therein.

(2) Cohen, M. D.; Schmidt, G. M. J. *J. Chem. Soc.* **1964**, 1996. Cohen, M. D.; Schmidt, G. M. J.; Sonntag, F. I. *J. Chem. Soc.* **1964**, 2000. Schmidt, G. M. J. *J. Chem. Soc.* **1964**, 2014.

(3) Schmidt, G. M. J. *Pure Appl. Chem.* **1971**, *27*, 647.

(4) Cohen, M. D. *Angew. Chem., Int. Ed. Engl.* **1975**, *14*, 386.

(5) For the purpose of further understanding of solid-state reactions, new approaches are made very recently; one is on the oligomerization of 2,5-distyrylpyrazine from the photophysical points of view (ref. 6) and the other is on the dimerization of cinnamic acid by using atomic force microscopy (ref. 7).

(6) Peachey, N. M.; Eckhardt, C. J. *J. Am. Chem. Soc.* 1993, *115*, 3519. Stezowski, J. J.; Peachey, N. M.; Goebel, P.; Eckhardt, C. J. *J. Am. Chem. Soc.* 1993, *115*, 6499.

(7) Kaupp, G. *Angew. Chem., Int. Ed. Engl.* 1992, *31*, 592.

(8) Foster, R. *Organic Charge-Transfer Complex*; Academic Press: London and New York, 1969.

(9) Fox, M. A.; Chanon, M. *Photoinduced Electron Transfer*; Elsevier: Amsterdam, 1988; Mattay, J. *Photoinduced Electron Transfer I*; Springer-Verlag: Berlin, 1990, and references cited therein.

(10) The photoreaction of the CT crystals of cinnamic acids having the electron donating and accepting substituent were examined by Desiraju, et al. They only pointed out that the CT interaction may be useful tool for crystal engineering. Sarma, J. A. R. P.; Desiraju, G. R. *J. Chem. Soc., Perkin Trans. II* 1985, 1905. Desiraju, G. R.; Sharma, C. V. K. M. *J. Chem. Soc., Chem. Commun.* **1991**, 1239. Very recently, several groups have reported on the photochemistry of CT crystals. Koshima, H.; Ding, K.; Chisaka, Y.; Matsuura, T.; Ohashi, Y.; Mukasa, M. *J. Org. Chem.* **1996**, *61*, 2352. Koshima, H.; Ding, K.; Chisaka, Y.; Matsuura, T. *J. Am. Chem. Soc.* **1996**, *118*, 12059. Ito, Y.; Endo, S. *J. Am. Chem. Soc.*

**1997**, *119*, 5974. Haga, N.; Nakajima, H.; Takayanagi, H.; Tokumaru, K. *J. Org. Chem.* **1998**, *63*, 5372.

(11) (a) Kabuto, C.; Suzuki, T.; Yamashita, Y.; Mukai, T. *Chem Lett.* **1986**, 1433. (b) Suzuki, T.; Fujii, H.; Yamashita, Y.; Kabuto, C.; Tanaka, S.; Harasawa, M.; Mukai, T.; Miyashi. T. *J. Am. Chem. Soc.* **1992**, *114*, 3034.

(12) For example, Miyashi, T.; Ikeda, I.; Konno, A.; Okitsu, O.; Takahashi, Y. *Pure Appl. Chem.* **1990**, *62*, 1531.

(13) Benesi, H. A.; Hildebrand, J. H. *J. Am. Chem. Soc.* **1949**, *71*, 2703.

(14) Other organic solvents can not be used for the photolyses of the EDA complexes because of the low solubility of **1**.

(15) Murthy, G. S.; Arjunan, P.; Venkatesan, K.; Ramamurthy, V. *Tetrahedron* **1987**, *43*, 1225. Another explanation for the initial inertness might be that the phase transformation would occur before the cycloaddition.

(16) If the point T is the apex of the p-orbital and T' is the corresponding point on the opposing pre-bonding atomic orbital, then the smaller the distance T-T', the more parallel and colinear is the alignment of the reacting p-orbitals.

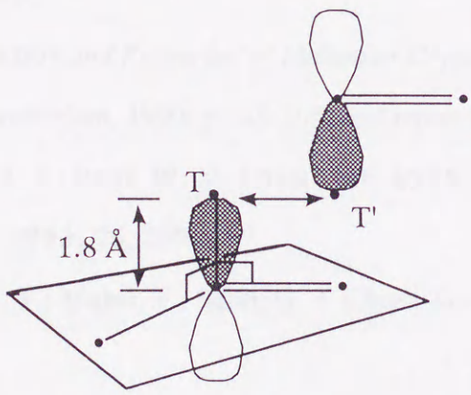


Sum of the distances for a set of double bonds would be less than 3.5 Å in reactive crystals. Kearsley, S. K. In *Organic Solid State Reactions: The Prediction of Chemical Reactivity within Organic Crystals using Geometrical Criteria;* Desiraju, G. R. Ed; Elsevier: Amsterdam, 1987; p 69-115.

(17) Sarti-Fantoni, P.; Teroni, R. *Mol. Cryst. Liq. Cryst.* **1970**, *6*, 431.

(18) Peachey, N. M.; Eckhardt, C. J. *J. Am. Chem. Soc.* **1993**, *115*, 3519. Stezowski, J. J.; Peachey, N. M.; Goebel, P.; Eckhardt, C. J. *J. Am. Chem. Soc.* **1993**, *115*, 6499.

(19) The distances for a set of double bonds are 1.00 and 1.93 Å in *Type 1*, and 1.32 and 1.08 Å in *Type 2*, respectively, for C(5) - C(29) and C(7) - C(30).

(20) The atomic orbitals of LUMO of **1**, and HOMOs of DVs obtained by simple HMO method are as follows.

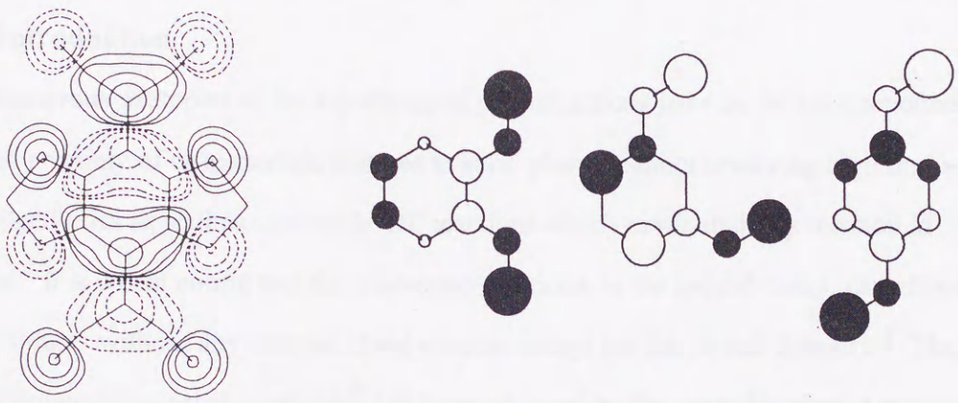

(21) In the idealized photodimerization model whose dimers are formed with a uniform probability among the pairs of neighboring monomers along an infinite one-dimensional stack, the theoretical maximum yield was reported to be 86.5%. Wernick, D. L.; Schochet, S. J. *J. Phys. Chem.* 1988, *92*, 6773.

(22) Bechgaard, K. In *Structure and Properties of Molecular Crystals: Organic Conductors*; Pierrot, M. Ed; Elsevier: Amsterdam, 1990; p 235-295, and references cited therein.

(23) Miller, J. S.; Epstein, A. J.; Reiff, W. M. *Chem. Rev.* **1988**, *88*, 201. Kollmac, C.; Kahn, O. *Acc. Chem. Res.* **1993**, *26*, 259.

(24) Yamashita, Y.; Suzuki, T.; Mukai, T.; Saito, G. *J. Chem. Soc., Chem. Commun.* **1985**, 1044.

(25) Wittig, G.; Eggera, H.; Duffner, P. *Liebigs Ann. Chem.* **1958**, *619*, 10.

# Chapter 2

## Asymmetric [2 + 2] Cycloaddition Reaction via Single Crystal-to-Single Crystal Transformation and Evaluation of Structure-Reactivity Relationship in the Solid State Reactions

### 2-1. Introduction

Numerous examples of the topochemical photoreactions have so far been reported and provided a variety of characteristic features in solid phase reaction involving high regio- and stereoselectivities as well as unprecedented reactions which never attain by reaction in solution. It is worth noting that the solid-state reactions, in the special cases, can afford the chiral products without any external chiral sources except for the crystal chirality.[1] The so-called absolute asymmetric synthesis[2] has been achieved by the crystallization of reactants in chiral space group and their subsequent topochemical reactions. The successful examples are rare, yet such asymmetric synthesis has attracted many researches in this area.

In order to elucidate the nature of solid-state reaction, it is of great importance to establish the detailed reaction pathway in each reaction. However, most of attempts result in only referring to a plausible reaction mechanism by the inspection of the initial solid-state environment. This arises due to the fact the initial crystal lattice of a reactant is disintegrated with the progress of reaction and the X-ray analysis of the as-prepared crystal can not be carried out. From this point of view, the reactions which undergo single crystal-to-single crystal transformation are very important for the deeper understanding of the reaction sequences. These examples are extremely rare,[3-12] but there have been reported some leading studies up to now. For instance, the photodimerization of 2-benzyl-5-benzylidene-cyclopentanone were documented crystallographic details and the comparisons of packing arrangements in monomer and its dimer crystal (eq. 1).[5] Furthermore, it was revealed recently that the well-studied photodimerization of *trans*-cinnamic acid also exhibits the single crystal-to-single crystal transformation upon irradiation of the absorption tail (eq. 2). This

landmark work pointed out the importance of the choice of a suitable wavelength to realize homogeneous photoreactions.[11]

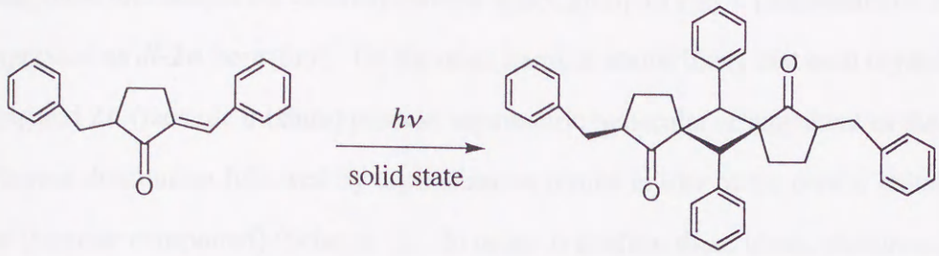


(eq. 1)

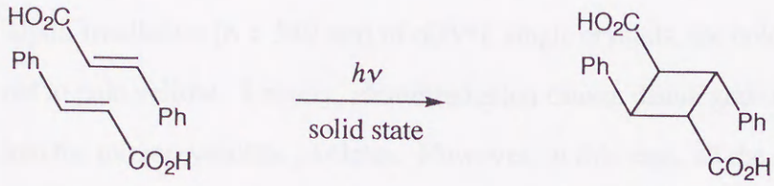


(eq. 2)

α-form α-truxinic acid

In this connection, the CT excitation reaction of CT crystals (oDV•**1**) composed of BTDA (**1**) and *o*-divinylbenzene (oDV) described in chapter 1 proven to proceed via crystal-to-crystal transformation with high regio- and stereoselectivity (eq. 3). In addition, the space group is chiral $P2_1$. These findings provides a good opportunity to examine this reaction in detail. In fact, it was found that the reaction undergoes in a single crystal-to-single crystal fashion to give the chiral adduct **2o** in high optical yield. These intriguing behaviors in the reaction of oDV•**1** as well as the exploration for other related systems will be described herein.

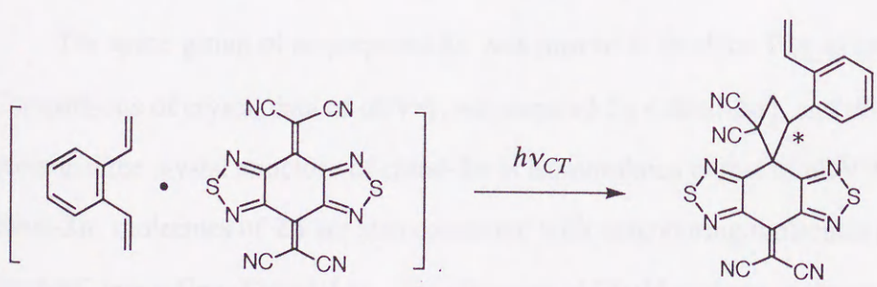


(eq. 3)

oDV•**1** CT crystal **2o**

## 2-2. Single Crystal-to-Single Crystal Photoreaction

The X-ray analysis of the recrystallized **2o** showed that the crystal is a racemic compound and adopts the centrosymmetric space group of $P2_1/n$ (recrystallized **2o** is expressed as *dl*-**2o** hereafter). On the other hand, it seems likely that each crystals of as-prepared **2o** (racemic mixture) possess asymmetric molecular arrangement as that of oDV•**1**, whereas dissolution followed by crystallization results in loss of the crystal chirality to give *dl*-**2o** (racemic compound) (Scheme 1). In order to confirm these ideas, photoreaction of oDV•**1** single crystals was examined.

Upon irradiation ($\lambda > 540$ nm) of oDV•**1** single crystals, the color changed gradually from red to pale yellow. Usually, photoirradiation causes disintegration of the single crystal form into the microcrystalline particles. However, in this case, all the samples kept the clear appearance and fortunately was obtained a single crystal of as-prepared **2o** which has an enough size for the X-ray analysis. Thus, the detailed reaction sequence could be visualized by X-ray analysis.

**Scheme 1**

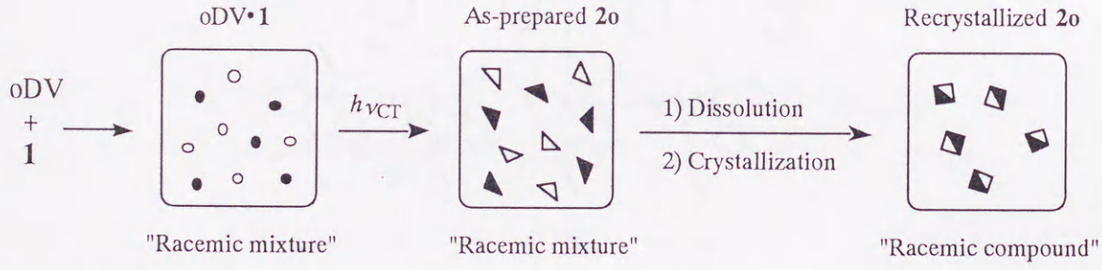


The space group of as-prepared **2o** was proven to be chiral $P2_1$ as expected. Comparisons of crystal data of oDV•**1**, as-prepared **2o** (chiral-**2o**), and *dl*-**2o** in Table 1 show that the crystal structure of chiral-**2o** is isomorphous to that of oDV•**1**. In the crystal of chiral-**2o**, molecules of **2o** are also connected with neighboring molecules along the *a* axis by S•••N≡C interaction (Figure 1b). The distances of S•••N contacts in the crystal are 3.35 and 3.25 Å for S(1) ••• N(7) and S(2) ••• N(8), respectively. The structural feature resembles that of oDV•**1** in this respect, and it is evident that the cycloaddition proceeds without significant structural changes (Figure 1).

**Table 1.** Crystal Data of oDV•**1**, as-prepared **2o**, and recrystallized **2o**

| | oDV•**1** | as-prepared **2o** | recrystallized **2o** |
|---|---|---|---|
| space group | $P2_1$ | $P2_1$ | $P2_1$ / n |
| crystal system | monoclinic | monoclinic | monoclinic |
| $a$, Å | 8.866 (2) | 9.120 (1) | 14.759 (1) |
| $b$, Å | 16.764 (3) | 16.394 (2) | 9.659 (1) |
| $c$, Å | 7.006 (3) | 7.181 (1) | 15.120 (1) |
| $\beta$, deg | 99.63 (2) | 106.27 (1) | 106.00 (1) |
| $V$, Å$^3$ | 1026.6 (5) | 1030.7 (3) | 2071.9 (3) |
| $Z$ | 2 | 2 | 4 |
| $D_{calcd}$, gcm$^{-3}$ | 1.457 | 1.452 | 1.444 |
| $R$,% | 4.22 | 8.21 | 7.72 |

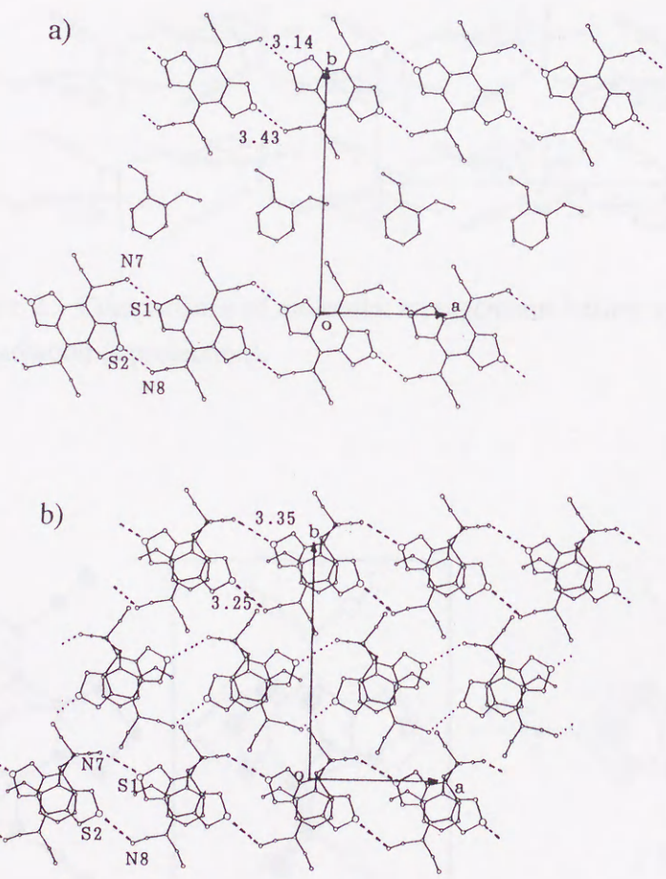


**Figure 1.** Comparisons of molecular arrangements before a) and after b) the irradiation ($c$ projection).

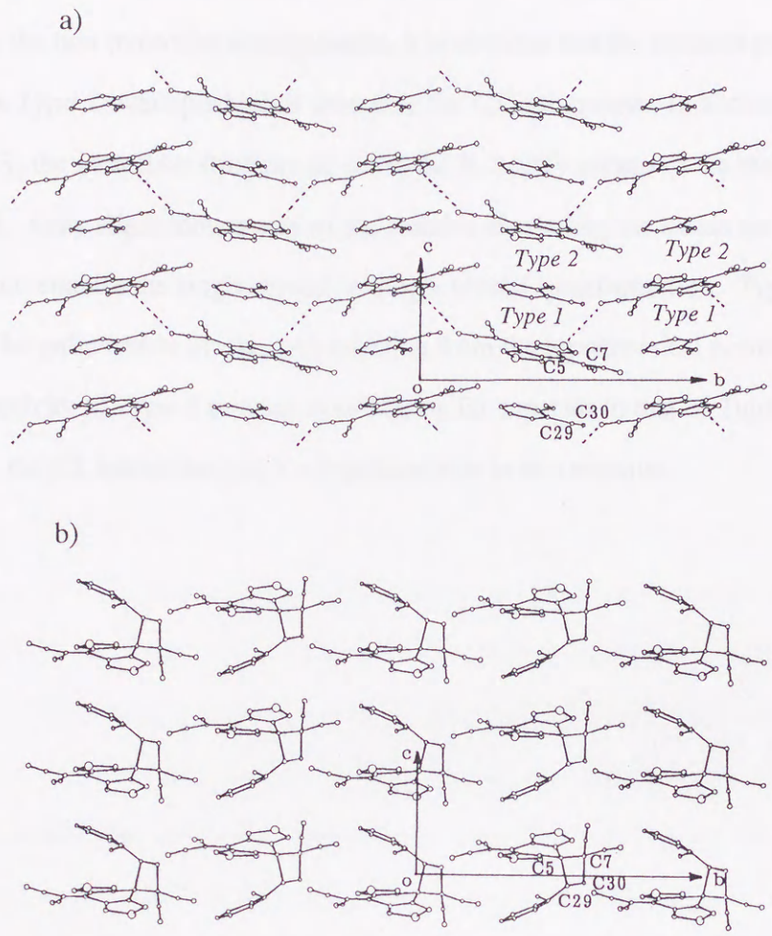


**Figure 2.** Comparisons of molecular arrangements before a) and after b) the irradiation (*a* projection).

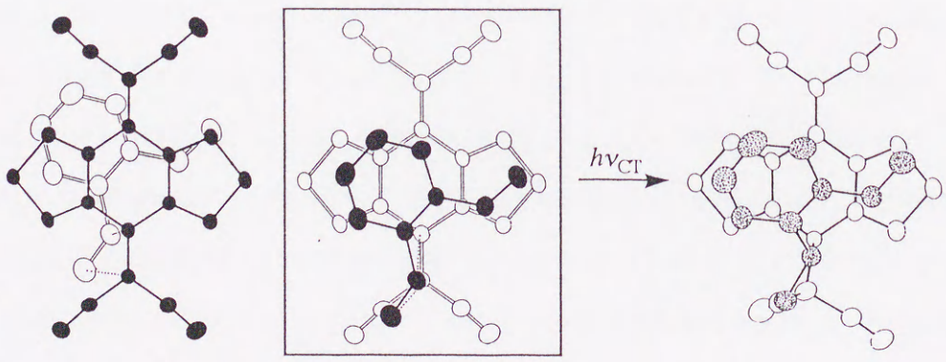


**Figure 3.** Schematic illustration of the formation of **2o** via *Type 2*.

Figure 2 shows the molecular arrangements of oDV•**1** and chiral-**2o** viewed along the *a* axis. Comparing the two molecular arrangements, it is obvious that the reaction proceeds predominantly via *Type 2* overlap which is favorable for CT interaction. In addition, as shown in Figure 3, the molecular structure of chiral-**2o** is closely related to the molecular overlap in *Type 2*. Only slight movements of the reactive sites along the *c* axis are enough to form adduct, which enables the single crystal-to-single crystal transformation. *Type 1* overlap does not seem to be unfavorable for the cycloaddition from the topochemical points of view. However, the reactivity of *Type 2* overlap wolud be by far superior to that of *Type 1*. This fact suggests that the CT interaction plays a important role in this reaction.

## 2-3. Absolute Asymmetric Synthesis

The topochemically controled stereospecific reaction of oDV•**1** allowed not only the single crystal-to-single crystal transformation but also the absolute asymmetric synthesis of **2o** by using the crystal chirality of oDV•**1** (space group $P2_1$). That is, the crystal chirality of oDV•**1** was transferred as the molecular chirality of **2o** by covalent bonds. Scheme 2 indicates the schematic representation of the absolute asymmetric synthesis in this system. For example, upon irradiation of a certain single crystal of oDV•**1** whose molecular overlaps are *Type 1* and *Type 2*, will give (*R*)-**2o** as a major enantiomer because of the highly stereoselective cycloaddition from *Type 2* as well as the absence of the mirror images of molecular overlaps of *Type 1* and *Type 2* within the same crystal. Another enantiomer, (*S*)-**2o**, will be obtained by photolysis of the single crystal whose molecular overlaps are the mirror images of *Type 1* and *Type 2*. In fact, when a single crystal of oDV•**1** was irradiated ($\lambda > 540$ nm) at 15 °C and analyzed by chiral HPLC, the resulting **2o** exhibited a high enantiomeric excess (*ca.* 70% *ee*). The value of enantiomeric excess was reproducible for the twelve specimens obtained by irradiation under similar conditions (av. 71% *ee*, $[\alpha]_D^{20}$ = 117°).[13] These optical yields reflect the relative reactivities between *Type 1* and *Type 2* overlaps, thus allowing the quantitative evaluation of the reactivities as *Type 1* : *Type 2* = 15 : 85 at 15 °C.

It is noteworthy that the values of *ee* exhibited interesting temperature dependence. Figure 4 shows the bargraph representation of the values obtained by photoirradiation of single crystals at four different temperatures (40, 15, -40, and -70 °C). The reproducible values of *ee* were obtained at each temperature. These values increased with lowering the reaction temperature, and the optical yields nearly reached the quantitative value (95% *ee*) at -70 °C. The relative reactivities of *Type 1* and *Type 2* overlaps were deduced from these values of *ee* and are shown in Table 2, which indicate the suppression of the reaction via *Type 1* and/or enhancement of the *Type 2* reactivity at lower temperature. If the reaction path in crystal is the same as that for the EDA complex described in chapter 1, the first bond making process should occur between C(7) of **1** and C(30) of oDV. Suppression of thermal motion at lower temperature

**Scheme 2**

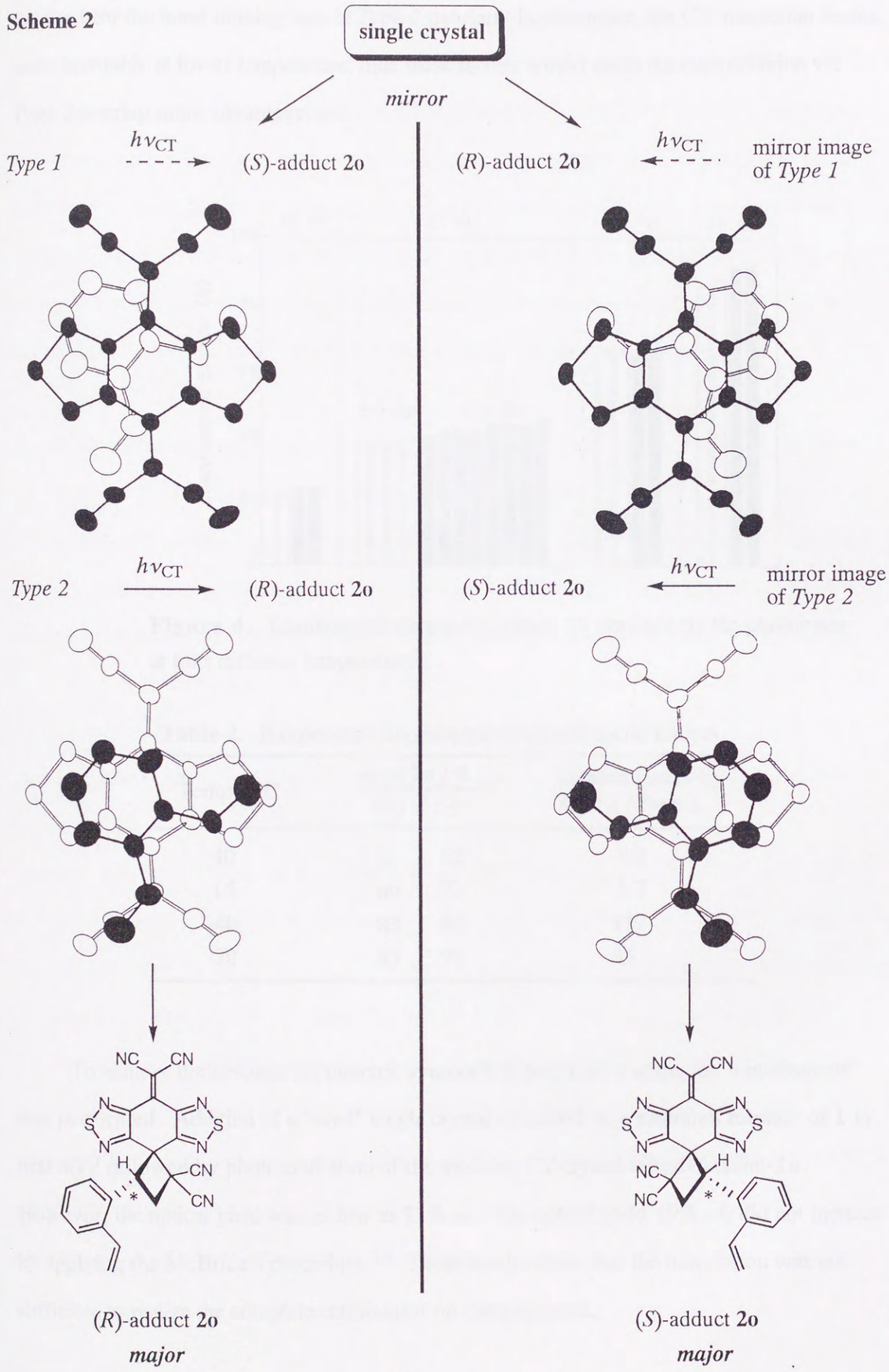
single crystal
mirror
Type 1
hνCT
(S)-adduct 2o
(R)-adduct 2o
hνCT
mirror image of Type 1
Type 2
hνCT
(R)-adduct 2o
(S)-adduct 2o
hνCT
mirror image of Type 2
NC
CN
N
S
H
CN
*
(R)-adduct 2o
major
(S)-adduct 2o
major

may retard the cycloaddition via *Type 1* overlap in which larger shifts of atomic positions are required for the bond making than in *Type 2* overlap. Furthermore, the CT interaction seems more favorable at lower temperature, thus these factors would make the cycloaddition via *Type 2* overlap more advantageous.

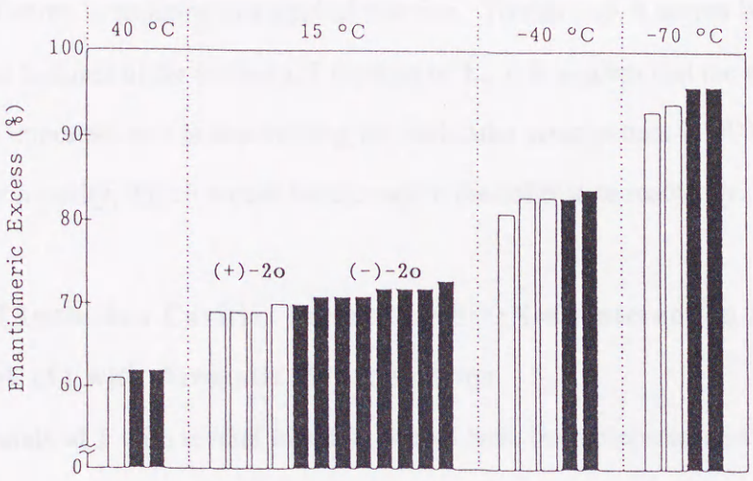


**Figure 4.** Enantiomeric excess for adduct **2o** obtained by the photolyses at four different temperatures.

**Table 2.** Temperature Dependence of Enantiomeric Excess

| Temp. / °C | *ee* of **2o** / % | | Relative reactivitiy *Type 2 / Type 1* |
|---|---|---|---|
| | (+) | (-) | |
| 40 | 61 | 62 | 4.3 |
| 15 | 69 | 71 | 5.7 |
| -40 | 83 | 83 | 11 |
| -70 | 93 | 96 | 35 |

To achieve the absolute asymmetric synthesis in preparative scale, the "entrainment" was performed. Addition of a "seed" single crystal of oDV•**1** to a saturated solution of **1** in neat oDV followed by photoirradiation of the resulting CT crystal afforded chiral-**2o**. However, the optical yield was as low as 11% *ee*. The optical yield (9% *ee*) did not increase by applying the McBride's procedure.[14] These results show that the inoculation was not sufficient to realize the complete entrainment on complexation.

## 2-4. Exploring for Other Systems

The above mentioned absolute asymmetric synthesis via single crystal-to-single crystal transformation is the first example in the field of photochemistry of organic molecular crystals. Furthermore, the sequences of the asymmetric induction was disclosed in detail. Encouraged by this intriguing finding, investigations on other related systems were carried out in order to seek the important factors in realizing this kind of reaction. To this end, it seems helpful to review the structural features of the known CT crystals of **1**. It is evident that the electron acceptor **1** plays an important role in determining the molecular arrangement in oDV•**1** and offers unique reaction cavity, which would be relevant to the solid-state reactivity.

### Classification of Inclusion Cavities Formed by S•••N≡C Interaction in the CT crystals of BTDA (1) with Aromatic Hydrocarbons

Many CT crystals of **1** with several kinds of donors have been prepared and examined in view of their properties such as electrical conduction and molecular recognition. On the basis of these studies, it was found that, in most cases where small aromatic hydrocarbons were used as an electron donor, **1** forms the ribbon-like networks by intermolecular S•••N≡C interactions as well as the inclusion cavities between the ribbons. These structural features are also common in the CT crystals of **1** with DVs and summarized in Table 3 with other five examples.

According to the center-to-center separation of **1** [*d* (**1**-**1**)] and the angle of S•••N≡C (∠S−N-C), the pattern of molecular arrangement can be classify into two distinct types (type A and type B) (Scheme 3). In the type A, molecules **1** are connected by the S•••N≡C interactions in the lateral direction with the distances [*d* (**1**-**1**) ~ 10.3 Å] and the angles (∠S−N-C ~ 150 - 175°), resulting in the formation of a "linear" ribbon-like network. Besides, the inclusion cavities formed between two ribbons are fractionated by the cyano groups of **1** and accommodate donor molecules. On the other hand, a "zigzag"-ribbon is formed in the type B arrangement where shorter distances [*d* (**1**-**1**) ~ 9.0 Å] and smaller angles (∠S−N-C ~ 120°) are found. In this case, inclusion cavities adopts continuous "tunnel"-like shape. Although it

**Table 3.** Some Structural Features in the CT crystals of BTDA (**1**) with Several Donors

| Donor | Space group | $Z$ | Position of Donor | Position of **1** | $d$ (**1**-**1**) / Å |
|---|---|---|---|---|---|
| 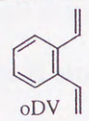 oDV | $P2_1$ (chiral) | 2 | general | general | 8.84 |
| 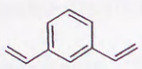 mDV | $P\bar{1}$ | 2 | general | general | 9.24 |
| 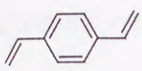 pDV | $P\bar{1}$ | 1 | inversion center | inversion center | 10.26 |
| 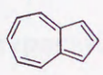 Az 1) | P1 (chiral) | 1 | general | general | 9.05 |
| 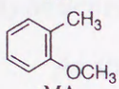 oMA 2) | $P\bar{1}$ | 2 | general | general | 9.24 |
| 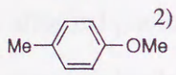 pMA 2) | $P\bar{1}$ | 1 | inversion center (disorder) | inversion center | 10.31 |
| 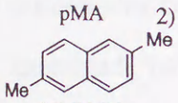 2,6-DMN 2) | $P\bar{1}$ | 1 | inversion center | inversion center | 10.27 |
| 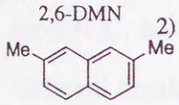 2,7-DMN 2) | $P\bar{1}$ | 2 | general | pseudo inversion center | 10.27 |

1) K. Iwasaki, Ph. D Thesis, Insutitute for Molecular Science (1992). 2) T. Suzuki, H. Fujii, Y. Yamashita, C. Kabuto, S. Tanaka, M. Harasawa, T. Mukai, and T. Miyashi, *J. Am. Chem. Soc.*, **114**, 3034 (1992).

**Scheme 3**

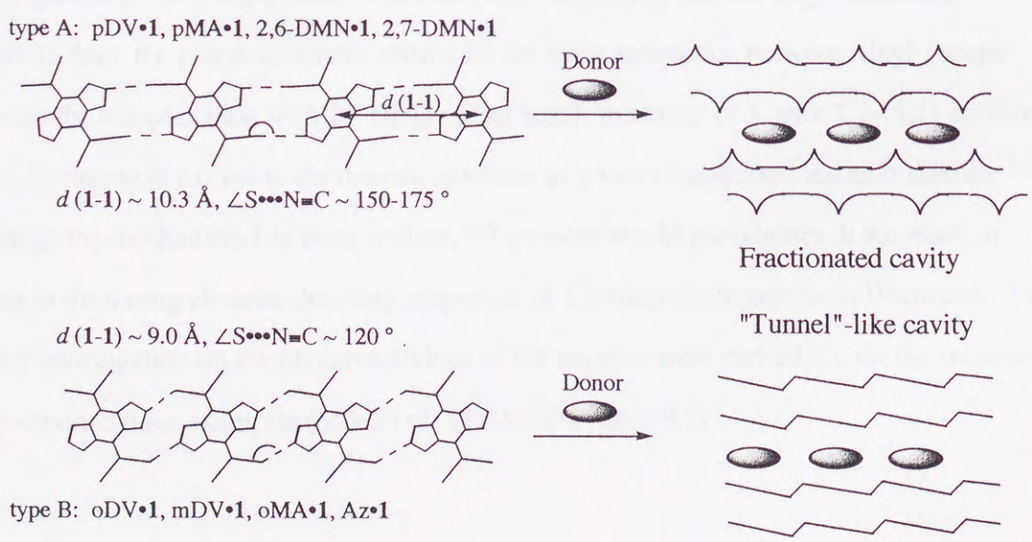

is difficult to predict crystal structures, it is likely that type A arrangement can be obtained by choosing a molecule having a long molecular axis as an electron donor, alternatively, relatively small aromatic hydrocarbons tend to give type B arrangement. It is worth noting here that the type B arrangement affords two chiral CT crystals in the eight examples (Table 3), suggesting *ortho*-disubstituted benzenes are one of the promising donors for the solid-state asymmetric synthesis. Thus, the preparation and photoirradiation of CT crystals composed of several structural types of *ortho*-disubstituted benzenes were performed.

**Preparation of the CT Crystals of BTDA (1) and Several Aromatic Hydrocarbons**

As shown in Table 4, *o*-methylstyrene (oMeST) and *o*-methoxystyrene (oOMeST) afforded photoreactive CT crystals with **1**, whereas *o*-chlorostyrene failed in the formation of the complex because of the lower electron-donating ability. The cyclic systems are also examined. Indene (Ind) was afforded a photoreactive CT crystal with a 3 : 2 stoichiometry ($Ind_3$•$\mathbf{1}_2$), however slight structural modification at the methylene moiety give rise to a different result. The photoirradiation of the successfully obtained CT crystal of 1,2-dihydronaphthalene did not show any reactions, presumably due to the ineffective overlap between the reactive double bonds in crystal. Attempts to prepared the CT crystals by using two kinds of $\alpha,\alpha'$-disubstituted divinylbenzene derivatives were failed. In the case of 1,2-bis(1-methylethenyl)benzene, no complexation was observed, suggesting that the large molecular distortion from the planar geometry caused by the steric interaction between vinyl groups prevents the complexation with **1**. On the other hand, treatment of **1** with 1,2-bis(1-methoxyethenyl)benzene at r.t. led to the thermal reactions to give a complicated reaction mixture.[15] Although the mechanism has been unclear, ET process would participates in the reaction owing to the strong electron-donating properties of 1,2-bis(1-methoxyethenyl)benzene. Thus, further investigation on the photoreactivities of CT crystals were carried out on the successfully obtained three examples (oMeST•**1**, oOMeST•**1**, $Ind_3$•$\mathbf{1}_2$).

Table 4. CT Crystals of BTDA (**1**) with Several *ortho*-Disubstituted Benzenes

| | $E^{ox}$ / V[a] | CT crystal | decomp. | Ratio (D : **1**) | Photoreactivity |
|---|---|---|---|---|---|
| 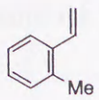 | +1.89 | red powder | 93 - 96 °C | 1 : 1 | **yes** |
| 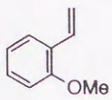 | +1.63 | violet powder | 103 - 113 °C | 1 : 1 | **yes** |
|  | +2.03 | no complexation | — | — | — |
|  | +1.58 | red powder | 73 - 79 °C | 3 : 2 | **yes** |
| 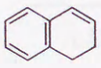 | +1.47 | brown powder | 96 - 98 °C | 1 : 1 | no |
| 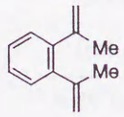 | n.d.[b] | no complexation | — | — | — |
| 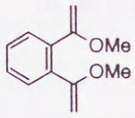 | n.d.[b] | no complexation | — | — | — |

[a] $E$ / V vs SCE, 0.1 mol dm$^{-3}$ $Et_4NClO_4$ in MeCN. [b] not determined.

**Charge-Transfer Excitation Reaction of oMeST•1, oOMeST•1, and Ind$_3$•1$_2$**

Photoirradiation of the CT crystals were performed by using the output from a 2 kW xenon lamp passed through a glass cut filter. When a suspension of finely powdered Ind$_3$•**1**$_2$ in 10 mL of water was irradiated ($\lambda$ > 540 nm) for 1 h at 15 °C, the regiospecific [2+2]-type cycloaddition was occurred to give **10** as a sole product in 36% yield. Similarly, upon irradiation ($\lambda$ > 540 nm) of a water suspension of oOMeST•**1** for 1 h at 15 °C, the cycloaddition reaction proceeded, but more efficiently, resulting in the formation of adduct **9** in good yield (60%). Nevertheless these reaction efficiencies were apparently lower than that of oDV•**1**, prolonged irradiation increased the products yields (Table 5). The [2+2]-cycloadduct **8** was also obtained in 32 % yield by the photolysis ($\lambda$ > 450 nm) of oMeST•**1**

(Table 5). However, further investigations on this system seemed to be inaccessible because the CT crystal was unstable to readily dissociate into the each components under usual conditions.

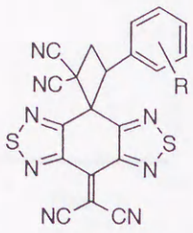


**8**: R=Me
**9**: R = OMe

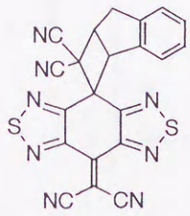


**10**

**Table 5**. CT Excitation Reaction of CT Crystals at 15 °C [a]

| CT crystal | Wavelength / nm | Time / h | Product yield / % |
|---|---|---|---|
| oMeST•**1** | $\lambda > 450$ | 1.5 | **8**: 32[b] |
| oOMeST•**1** | $\lambda > 540$ | 5 | **9**: 77[b] |
| $Ind_3$•$\mathbf{1}_2$ | $\lambda > 540$ | 10 | **10**: 80[c,d] |

[a] A 10 mL water suspension was irradiated by a 2 kW Xe lamp. [b] Isolated yields. [c] Determined on the basis of $^1$H NMR spectra. [d] Based on consumed Ind.

Inspection of the time-course of the reaction can be helpful to understand the reaction sequences. Figure 5 shows the time-dependences of the product yields in the photoreaction of oOMe•**1** and $Ind_3$•$\mathbf{1}_2$ determined on the basis of $^1$H NMR analyses of as-prepared samples. The yields of adduct **9** reached the maximum value (*ca* 80%) after 5 h irradiation. By contrast, much longer irradiation time was needed for obtaining the maximum yield (*ca* 80%). These differences may not arise from the electronic properties of the electron donors but the molecular packing in crystal. That is, the arrangement of reactive double bonds and/or mobility of reactants. Moreover, the observed incomplete conversion in both cases is indicative of crystal-to-amorphous transformation as described in the photoreaction of mDV•**1** (Figure 6). In fact, upon irradiation ($\lambda > 540$ nm, at 15 °C) of the single crystals of oOMe•**1** or $Ind_3$•$\mathbf{1}_2$ causes disintegration of the single crystal form. In order to elucidate the structure-reactivity relationship on above two CT crystals, X-ray analyses were carried out.

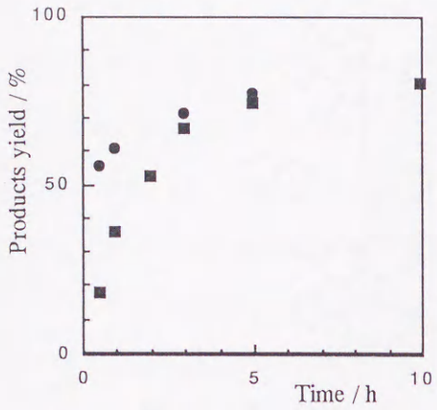


**Figure 5**. The time-course of the solid-state reactions of oOMeST•**1** and $Ind_3$•$\mathbf{1}_2$. The yield of **9** (filled circle) and **10** (filled square) are plotted as a function of irradiation time.

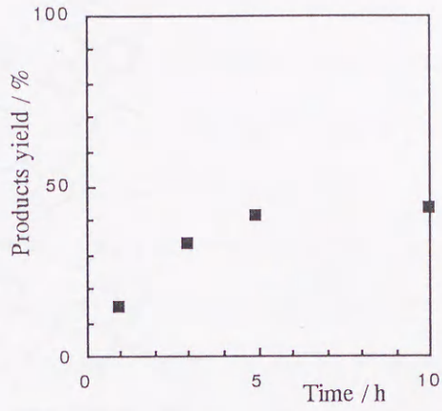


**Figure 6**. The time-course of the solid-state reaction of mDV•**1**. The yield of **2m** are plotted as a function of irradiation time.

**Molecular Arrangement and Structure-Reactivity Relationships in oOMeST•1**

A deep red needle of oOMeST•**1** was successfully obtained by the vapor diffusion method from MeCN/*n*-hexane. Unfortunately, owing to the adoption of achiral space group ($P2_1/c$), solid-state asymmetric induction is impossible to take place. Figure 7 shows the molecular arrangement viewed along the molecular plane, in which there exists positionary disorder at the methoxy moieties in oOMeST. In crystal, molecule **1** are connected by short S•••N≡C interactions (3.07 Å) as well as another S•••N contacts (3.39 Å) between thiadiazole rings, resulting in the formation of zigzag-type ribbon-like networks of **1**. In addition, tunnel-like inclusion cavities are formed between two ribbons as expected. These structural features are in accord with the type b arrangement in Scheme 3. However, considering the fact that only one S•••N≡C interaction participates in the connection of **1** and the large dihedral angle (14.1°) between **1** is observed, the inclusion cavity would be less at work than those in oDV•**1**, which may be relevant to the disorder in oOMeST molecule.

Perpendicularly to this molecular arrangement, one-dimensional columnar stacks are formed along the *b* axis (Figure 8), where is found the dyad formation by the short S•••N≡C interactions (3.26 Å). In the stacks, two different types of molecular overlaps between **1** and oOMeST (*Type 1* and *Type 2*) are repeated infinitely. The molecular overlaps viewed along the molecular planes are shown in Figure 9.

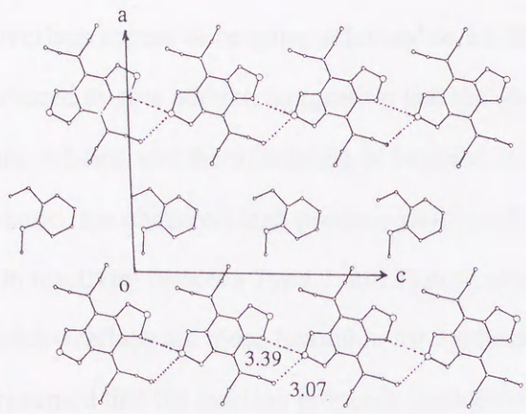


**Figure 7.** Molecular arrangement in oOMeST•**1**. The interatomic distances of S•••N≡C are shown by broken lines.

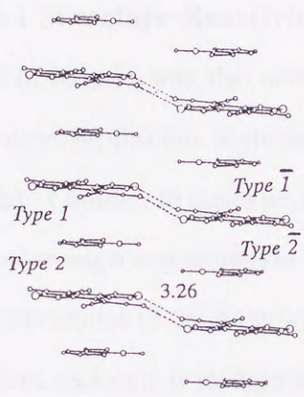


**Figure 8.** One-dimensional columnar stacks in oOMeST•**1**.

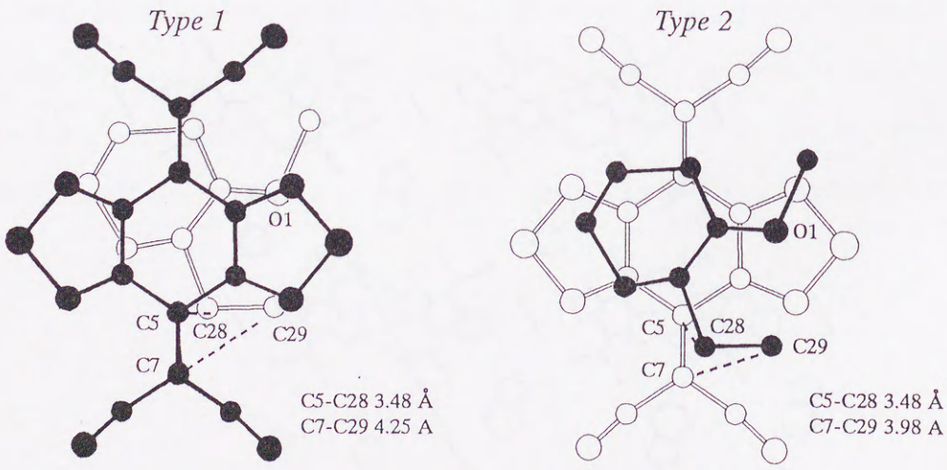


**Figure 9.** Two types of molecular overlaps in oOMeST•**1** (*Type 1* and *Type 2*). The interplanar distances and dihedral angles are 3.37 Å and 1.6° in *Type 1*, and 3.44 Å and 1.6° in *Type 2*, respectively.

Both molecular overlaps appear to be quite unfavorable for the cycloaddition, however, the reaction actually occurred to give adduct, suggesting that the loose inclusion cavities can readily allow the in-plane rotation and the translation of benzene nucleus for the progress of reaction. On the other hand, the observed high product yield (ca 80 %) indicates the significant differences in reactivity between *Type 1* and *Type 2* overlap. Although it is difficult to elucidate which overlaps are more favorable for cycloaddition due to the existence of disorder, one can presumed that the reaction proceeds predominantly via *Type 2* on the basis of distance criteria [*Type 1*: 3.48 and 4.25 Å for C(5) - C(28) and C(7) - C(29), respectively; *Type 2*: 3.48 and 3.98 Å for C(5) - C(28) and C(7) - C(29), respectively].

**Molecular Arrangement and Structure-Reactivity Relationships in Ind$_3$•1$_2$**

A reddish rod-like crystal of Ind$_3$•**1**$_2$ was also obtained by the vapor diffusion method from MeCN/*n*-hexane. In this case, an absolute asymmetric synthesis is unable to realize due to the achiral space group (C2/c). Contrary to the expectation, no ribbon-like networks of **1** was found in coplanar molecular arrangement shown in Figure 10. Instead, the dyad of **1** is formed by the short S•••N≡C interactions (3.19 Å) as well as another S•••N contacts (3.37 Å). Between the dyads, an indene molecule is incorporated nearly perpendicularly to this plane. These structural features are similar to those in mDV$_5$•**1**$_3$.

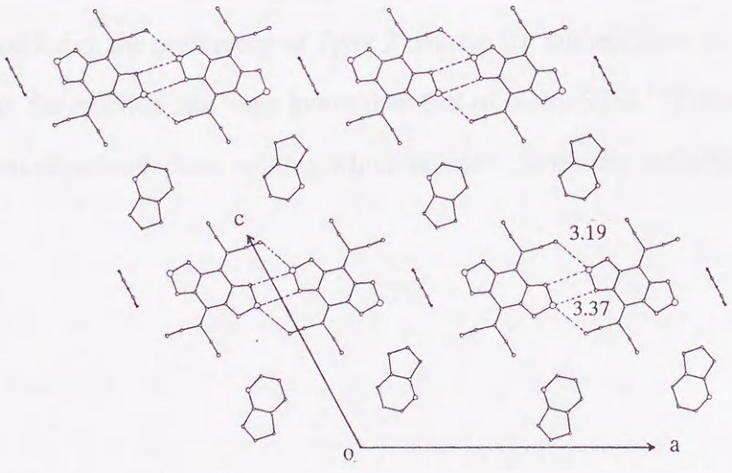


**Figure 10.** Molecular arrangement in Ind$_3$•**1**$_2$.

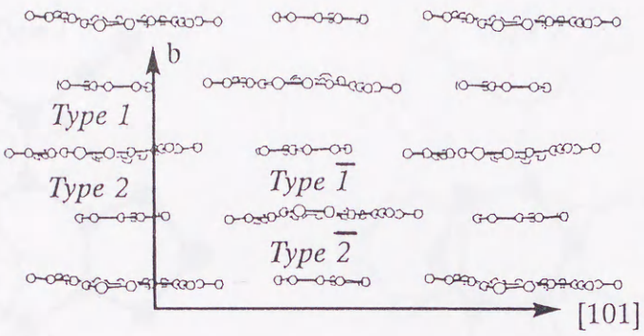


**Figure 11.** One-dimensional columnar stacks in Ind$_3$•**1**$_2$.

Perpendicularly to this molecular arrangement, one-dimensional columnar mixed stacks are formed along the *b* axis (Figure 11), where two different types of molecular overlaps between **1** and Indene (*Type 1* and *Type 2*) are repeated alternately. Figure 12 shows the molecular overlaps viewed along the molecular planes. In terms of MO coefficients, *Type 2* overlaps are more favorable for the interaction between HOMO of mDV and LUMO of **1**. Moreover, according to the geometrical argument of the reactive site [*Type 1*: 3.58 and 3.93 Å for C(6) - C(22) and C(8) - C(21), respectively; *Type 2*: 3.75 and 3.47 Å for C(5) - C(22) and C(7) - C(21), respectively], it can be deduced that the atomic and molecular movements accompanied with the reaction are less in *Type 2*. The observed high product yield is well described by considering the preference of *Type 2* overlap for the reaction. In contrast to the favorable overlap, the reaction rate were lower than that of oOMeST•**1**. This is presumably due to the coplanar close molecular packing which restricts the drastic molecular movements in crystal.

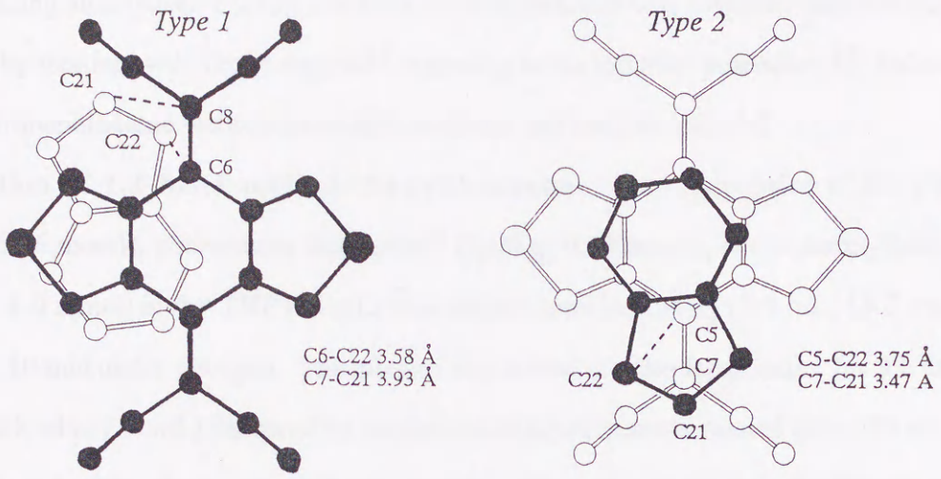


**Figure 12.** Two types of molecular overlaps in $Ind_3$•**1**$_2$ (*Type 1* and *Type 2*). The interplanar distances and dihedral angles are 3.40 Å and 3.20° in *Type 1*, and 3.39 Å and 1.93° in *Type 2*, respectively.

## 2-5. Conclusion

The CT excitation reaction of oDV•**1** proceeds via the single crystal-to-single crystal transformation, which clarified the reaction sequences. Furthermore, the chiral adduct **2o** was obtained nearly quantitative optical yield from achiral components by absolute asymmetric synthesis. The value of enantiomeric excess exihibited significant temperature dependence. In order to explore the generality of the intriguing reaction, several related systems were investigated on the basis of structural arguments, and the difficulty in fully understanding of the crystal structures was suggested. Although only [2+2]-type cycloaddition reaction is the sole reaction mode in this work, it is expected that the further investigations will provide various intriguing reactions via radical ions included in the highly organized crystal lattices.

## Experimental Section

**Materials.** All styrene derivatives were obtained by Wittig reactions[16] of the corresponding aldehydes. 1,2-bis(1-methoxyethenyl)benzene was prepared from dimethyl phthalate by treating with Tebbe reagent[17] according to the reported procedure.[18] Indene and 1,2-dihydronaphthalene were commercially available and used as recieved.

**Preparation of 1,2-bis(1-methylethenyl)benzene.** To a suspension of zinc powder (4.16 g, 63.6 mmol), zirconocene dichloride[19] (2.80 g, 9.59 mmol), and *o*-diacetylbenzene (648 mg, 4.0 mmol) in dry THF (15 mL) was added dropwise $CH_2I_2$ (1.5 mL, 18.6 mmol) at 0 °C over 10 min under nitrogen. The mixture was stirred at room temperature for 9 h and diluted with ether (10 mL) followed by cautious addition of water-saturated ether (20 mL) and water (10 mL). After the reaction mixture was filtered by using Celite pad, the filtrate was washed with water and brine, and the organic layer was dried over $Na_2SO_4$. Removal of solvent followed by chromatographic separation (basic alumina, pentane) gave 41 mg (6%) of 1,2-bis(1-methylethenyl)benzene as a colorless oil: IR (neat) 3070, 3010, 2965, 2910, 1632 $cm^{-1}$; $^1H$ NMR (90 MHz, $CCl_4$) δ 7.10 (4 H, s), 5.06 (2 H, s), 4.93 (2 H, s), 2.03 (6 H, s); MS *m/z* (relative intensity) 158 ($M^+$, 31), 143 ($M^+ - CH_3$, 100), 128 ($M^+ - 2CH_3$, 70). Anal. Calcd for $C_{12}H_{14}$: C, 91.08; H, 8.92. Found: C, 90.22; H, 9.29.

**Preparation of CT Crystals.**

**oMeST•1.** Finely powdered **1** (160 mg, 0.50 mmol) and oMeST (148 mg, 1.25 mmol) were mixed at room temperature. The color of the solid gradually changed from yellow to red. After allowing to stand for 12 h at -40 °C, the red powder of oMeST•**1** (219 mg, yield 100%) was obtained by removal of excess oMeST in vacuo for 30 min at room temperature: mp 93-96 °C dec; IR (KBr) 2218 $cm^{-1}$. Anal. Calcd for $C_{21}H_{10}N_8S_2$ (1:1): C, 55.52; H, 2.30; N, 25.56. Found: C, 56.87; H, 2.47; N, 25.44.

**oOMeST•1.** Finely powdered **1** (32 mg, 0.10 mmol) and oMeST (26.8 mg, 0.10 mmol) were mixed at room temperature. The color of the solid gradually changed from yellow to deep red-purple. After allowing to stand for 12 h at -40 °C, the deep red-purple powder of oOMeST•**1** (47 mg, yield 100%) was obtained by removal of excess oOMeST in vacuo for 45

min at room temperature: mp 103-113 °C dec; IR (KBr) 2222 $cm^{-1}$. Anal. Calcd for $C_{21}H_{10}N_8OS_2$ (1:1): C, 55.50; H, 2.20; N, 24.67. Found: C, 55.03; H, 2.54; N, 25.03.

**$Ind_3$•$1_2$.** Finely powdered **1** (160 mg, 0.50 mmol) and Ind (153 mg, 1.32 mmol) were mixed at room temperature. The color of the solid gradually changed from yellow to deep red-purple. After allowing to stand for overnight at 4 °C, the reddish powder of Ind•**1** (244 mg, yield 99%) was obtained by removal of excess Ind in vacuo for 30 min at room temperature: mp 73-79 °C dec; IR (KBr) 2224 $cm^{-1}$. Anal. Calcd for $C_{51}H_{24}N_{16}S_4$ (3:2): C, 61.06; H, 2.68; N, 22.70. Found: C, 61.93; H, 2.45; N, 22.66.

**1,2-Dihydronaphthalene•1.** Finely powdered **1** (32 mg, 0.10 mmol) and oMeST (35 mg, 0.27 mmol) were mixed at room temperature. The color of the solid gradually changed from yellow to deep red-purple. After allowing to stand for 2 weeks at 4 °C, the dark brown powder (45 mg, yield 100%) was obtained by removal of excess 1,2-dihydronaphthalene in vacuo at room temperature: mp 96-98 °C dec; Anal. Calcd for $C_{22}H_{10}N_8S_2$ (1:1): C, 58.66; H, 2.24; N, 24.87. Found: C, 58.37; H, 2.21; N, 24.76.

**Measurement of Redox Potentials.** All the oxidation potentials ($E^{ox}$) were measured under argon atomosphere by CV method in dry MeCN containing 0.1 mol $dm^{-3}$ $Et_4NClO_4$ as a supporting electrolyte. All the value are in *E*/V vs SCE, and Pt wire was used as the working electrode. In the case of irreversible waves, half-wave potentials were estimated from the peak potentials as $E^{ox} = E^{pa} - 0.03$ V.

**CT Excitation Reactions of CT Crystals**

**oMeST•1.** A water suspension (10 mL) of oMeST•**1** (88 mg, 0.20 mmol) was irradiated by using a 2 kW xenon lamp through a Y-47 glass cutoff filter ($\lambda > 450$ nm) for 1.5 h at 15 °C. The reddish powder gradually turned to yellow. Filtration of the resulting precipitates followed by the TLC separation ($CH_2Cl_2$) afforded 29 mg of **8** as a pale yellow powder in 32% yield.

**8**: pale yellow powder, mp 124-132 °C dec; IR (KBr) 2223 $cm^{-1}$; $^1H$ NMR (400 MHz, $CDCl_3$) δ 7.19-6.84 (4 H, m), 5.26 (1 H, dd, $J$ = 12.0, 8.8 Hz), 4.36 (1 H, dd, $J$ = 12.0, 12.0 Hz), 3.29 (1 H, dd, $J$ = 8.8, 8.8 Hz), 1.37 (3 H, s) Anal. Calcd for $C_{21}H_{10}N_8S_2$• $0.5H_2O$: C, 56.37; H, 2.48; N, 25.04. Found: C, 56.13; H, 2.79; N, 24.03.

**oOMeST•1.** A water suspension (10 mL) of oOMeST•**1** (45 mg, 0.1 mmol) was irradiated by using a 2 kW xenon lamp through an O-57 glass cutoff filter ($\lambda > 540$ nm) for 5 h at 15 °C. The reddish purple powder gradually turned to yellow. Filtration of the resulting precipitate followed by the TLC separation ($CH_2Cl_2$) afforded 36 mg of **9** as a yellow powder in 91% yield. After the similar photolysis for 0.5, 1, 3 h, **9** was obtained after the TLC separation in 55, 60, 71% yields.

**9**: yellow powder, mp 102-112 °C dec; IR (KBr) 2215 $cm^{-1}$; $^1H$ NMR (400 MHz, $CDCl_3$) δ 7.16-6.43 (4 H, m), 5.14 (1 H, dd, J = 12.0, 9.0 Hz), 4.20 (1 H, dd, J = 12.0, 12.0 Hz), 3.46 (1 H, dd, J = 9.0, 12.0 Hz), 2.96 (3 H, s); EI-MS *m/z* (relative intensity) 376 ($M^+$ - $CH_2=C(CN)_2$, 13), 345 ($M^+$ - $CH_2=C(CN)_2$ - OMe, 100). Anal. Calcd for $C_{21}H_{10}N_8OS_2 \cdot CH_2Cl_2$: C, 48.99; H, 2.24; N, 20.77. Found: C, 48.67; H, 2.30; N, 20.67.

**$Ind_3$•$1_2$.** A water suspension (10 mL) of $Ind_3$•$1_2$ (44 mg, 0.044 mmol) was irradiated by using a 2 kW xenon lamp through an O-57 glass cutoff filter ($\lambda > 540$ nm) for 5 h at 15 °C. The reddish powder gradually turned to yellow. The precipitate was filtered and dried. The resulting brownish powder then treated with in 2 mL of $CH_2Cl_2$, and unreacted **1** was separated by filtration. Removal of solvent followed by trituration with ether afforded crude **10** in 79% yield based on consumed Ind. Adduct **10** was so unstable that rapid chromatographic separation through $SiO_2$ column was employed for further purification. However significant decomposition of **10** occured to lower the yield (47%).

**10**: yellow powder, mp 88.5-90 °C dec; IR (KBr) 2224 $cm^{-1}$; $^1H$ NMR (400 MHz, $CDCl_3$) δ 7.49 (1H, d, 7.5 Hz), 7.41 (1H, dd, *J* = 7.5, 7.5 Hz), 7.15 (1H, ddd, *J* = 1.7, 8.0, 8.3 Hz), 3.75 (1H, br-dd, *J* = 1.7, 18.0 Hz), 3.63 (1H, dd, *J* = 8.3, 18.0 Hz); FD-MS *m/z* (relative intensity) 436 ($M^+$, 100), HRMS *m/z* 436.031 ($M^+$; calcd for $C_{21}H_8N_8S_2$, 436.031).

**The Time-Course of the CT Excitation Reaction of $Ind_3$•$1_2$.** Water suspensions (5 mL) of $Ind_3$•$1_2$ (17-18 mg, 0.017- 0.018 mmol) were irradiated ($\lambda > 540$ nm) separetely for 0.5, 1, 2, 3, 4, 5, 7, and 10 h at 15 °C. After filtration, the resulted precipitates were

analyzed by 200 MHz $^1$H NMR spectroscopy ($CDCl_3$) with 1,1,2,2-tetrachloroethane (4 μL, 0.0378 mmol) as an internal standard.

**CT Excitation Reaction of oDV•1 Single Crystals.**

Single crystals oDV•**1** were obtained as red rods by the vapor diffusion method from MeCN/*n*-hexane. Other methods such as recrystallization of **1** from oDV and the vapor diffusion method from $CH_2Cl_2$/*n*-hexane failed to afford the single crystals with an enough size for the photolysis.

For the purpose of the absolute asymmetric synthesis, single crystals of oDV•**1** were sealed piece by piece in glass capillaries. These samples were irradiated until the color of crystals changed completely from red to yellow (3-5 h) by using a 2 kW xenon lamp through an O-57 glass cutoff filter ($\lambda > 540$ nm) in the thermostat bath at four different temperatures (40 °C, 15 °C, -40 °C, and -70 °C). After the photolyses, the resulting crystals were analyzed by HPLC equipped with a SUMICHIRAL OA-2000S column. The typical retention times for (+)-**2o** and (-)-**2o** were 250 min and 260 min, respectively, with *n*-hexane/$CH_2Cl_2$/EtOH (100:10: 1) as an eluent. The values of enantiomeric excess (*ee*) are summarized in Figure 4.

Chiral-**2o** crystals having the same chirality (longer retention time in HPLC) were combined (71% *ee*) and the polarimetric measurement was carried out. The value of $[\alpha]_D^{20}$ was -117 ° in $CHCl_3$ (c = 0.1) at 20 °C.

**Entrainment of oDV•1 CT Crystal by Seeding.** To a saturated solution of **1** (15 mg, 0.05 mmol) in *ca.* 2 mL of oDV was added a seed single crystal of oDV•**1** at 80 °C, and the mixture was allowed to stand at room temperature and then cooled to -40 °C. The resulting oDV•**1** was collected and irradiated ($\lambda > 540$ nm) for 20 min giving 4 mg of chiral-**2o** with 11% *ee* [(-)-**2o**, HPLC]. According to the McBride's procedure,[14] to a saturated solution of **1** (15 mg) in *ca.* 2 mL of oDV was added a seed with vigorous stirring at 80 °C. The oDV•**1** precipitated within 20 s. Similar photolysis as described above gave 5 mg of chiral-**2o** with 9% *ee* [(+)-**2o**, HPLC].

**X-ray Structural Analysis of oDV•1.** The absolute configuration was determined by measuring 19 Bijvoet pairs with CuKα radiation, for which the values of ΔFc are expected to

be larger than 13%. As shown in Table 6, the differences in the magnitude of Fo for the Bijvoet pairs were all consistent with those expected from the differences of Fc, thus confirming the present absolute configuration of this crystal.

$$\Delta Fc = \frac{| \, | Fc(k>0) | - | Fc(k<0) | \, |}{1/2 \, [ \, | Fc(k>0) | + | Fc(k<0) | \, ]}$$

**Table 6.** Comparisons of Averaged Fo for Bijvoet Pairs

| h | k | l | \|Fo(hkl)\| | \|Fo($\bar{h}k\bar{l}$)\| | av. | \|Fc(k>0)\| vs \|Fc(k<0)\| | av. | \|Fo($\bar{h}\bar{k}\bar{l}$)\| | \|Fo($h\bar{k}l$)\| |
|---|---|---|---|---|---|---|---|---|---|
| 0 | 3 | -4 | 146 | 111 | 129 | > | 110 | 119 | 102 |
| 2 | 1 | -4 | 125 | 110 | 118 | < | 152 | 155 | 48 |
| 4 | 2 | -4 | 109 | 107 | 108 | < | 129 | 132 | 126 |
| 5 | 5 | -4 | 119 | 106 | 113 | < | 138 | 141 | 136 |
| 7 | 2 | -4 | 108 | 104 | 106 | < | 126 | 124 | 128 |
| 3 | 11 | -3 | 97 | 84 | 91 | < | 118 | 118 | 117 |
| 3 | 8 | -3 | 105 | 91 | 98 | > | 87 | 94 | 80 |
| 2 | 8 | -2 | 162 | 145 | 154 | > | 141 | 143 | 138 |
| 2 | 4 | -2 | 233 | 177 | 205 | > | 169 | 177 | 161 |
| 4 | 3 | -2 | 142 | 139 | 141 | < | 164 | 168 | 159 |
| 6 | 5 | -1 | 128 | 130 | 129 | > | 109 | 111 | 106 |
| 0 | 5 | 0 | 253 | - | 235 | < | 337 | 337 | - |
| 1 | 10 | 0 | 130 | 135 | 135 | < | 167 | 169 | 164 |
| 3 | 2 | 0 | 161 | 168 | 164 | < | 193 | 196 | 190 |
| 4 | 8 | 0 | 128 | 128 | 128 | > | 119 | 120 | 117 |
| 1 | 5 | 2 | 236 | 274 | 255 | > | 221 | 213 | 228 |
| 3 | 5 | 2 | 96 | 106 | 101 | > | 84 | 87 | 80 |
| 3 | 4 | 2 | 89 | 101 | 95 | < | 123 | 126 | 119 |
| 3 | 7 | 3 | 88 | 102 | 95 | < | 120 | 116 | 123 |

**X-ray Structural Analysis of *dl*-2o.** A pale yellow rod-like crystal with a dimension of 0.20 x 0.20 x 0.15 mm was obtained by recrystallization from $CH_2Cl_2$/*n*-hexane, and used for the data collection on an AFC-5R automated four-circle diffractometer with a rotating anode (120 mA, 50 kV) at 23 °C. The $\omega$ - $2\theta$ scan mode with a scan speed of 8° $min^{-1}$ was employed with the $\omega$ scan range of $(1.10 + 0.5 \tan \theta)°$. A total of 4945 reflections was collected by using graphite monochromated MoK$\alpha$ radiation within $2\theta = 55°$. Crystal data are as follows: MF $C_{22}H_{10}N_8S_2$, MW 450.50, monoclinic, space group $P2_1/n$, a = 14.759(1) Å, b = 9.659 (1) Å, c = 15.120(1) Å, $\beta$ = 106.00(1)°, V = 2071.9(5) $Å^3$, Z = 4, and $D_{calcd}$ = 1.444 g $cm^{-3}$. The structure was solved by the direct method using RANTAN 81 program with some modification, and was refined by the block-diagonal least-squares method with anisotropic temperature factors. All the hydrogen atoms were located in the difference Fourier map and included in the refinement with isotropic temperature factors. The final R value is 7.72% for 4315 non-zero reflections.

**X-ray Structural Analysis of chiral-2o.** The single crystal of chiral-**2o** was obtained as follows. Single rod-like crystals of oDV•**1** were sealed separately in glass capillaries and were irradiated by using a 2 kW xenon lamp with an O-57 glass cutoff filter ($\lambda$ > 540 nm) for 4 h at 40 °C. Although several samples cracked into tiny pieces, one sample still kept the enough size suitable for X-ray crystal structural analysis. As-prepared chiral-**2o** thus obtained was a pale yellow rod-like crystal with a dimension of 0.20 x 0.15 x 0.05 mm. It was used for the data collection on an AFC-5R automated four-circle diffractometer with a rotating anode (200 mA, 45 kV) at 13 °C. The $\omega$ - $2\theta$ scan mode with a scan speed of 3° $min^{-1}$ was employed with the $\omega$ scan range of $(1.10 + 0.3 \tan \theta)°$. A total of 1886 reflections was collected by using graphite monochromated MoK$\alpha$ radiation within $2\theta = 50°$. Crystal data are as follows: MF $C_{22}H_{10}N_8S_2$, MW 450.50, monoclinic, space group $P2_1$, a = 9.120(1) Å, b = 16.394(2) Å, c = 7.181(1) Å, $\beta$ = 106.27(1)°, V = 1030.7(3) $Å^3$, Z = 2, and $D_{calcd}$ = 1.452 g $cm^{-3}$. The structure was solved by the direct method using RANTAN 81 program with some modification, and was refined by the block-diagonal least-squares method with anisotropic temperature factors. Hydrogen atoms were not included in the refinement . The final R value is 8.21% for 1214 reflections with $|Fo| > 3\sigma|Fo|$.

**X-ray Structural Analysis of oOMeST•1.** A reddish needle-like crystal with a dimension of 0.25 x 0.20 x 0.15 mm was obtained by the vapor diffusion method from MeCN/*n*-hexane. It was sealed in a glass capillary with oOMeST and used for the data collection on an AFC-5R automated four-circle diffractometer with a rotating anode (200 mA, 45 kV) at 13 °C. The $\omega$ - $2\theta$ scan mode with a scan speed of 4° $min^{-1}$ was employed. A total of 4332 independent reflections was collected by using graphite monochromated MoK$\alpha$ radiation within $2\theta$ = 52°. Crystal data are as follows: MF $C_{21}H_{10}N_8OS_2$, MW 454.48, monoclinic, space group $P2_1/c$, a = 16.995(3) Å, b = 6.854(1) Å, c = 17.954(2) Å, $\beta$ = 92.99(1)°, V = 2088.5(5) $Å^3$, Z = 4, and $D_{calcd}$ = 1.445 g $cm^{-3}$, $\mu_{MoK\alpha}$ = 2.744 $cm^{-1}$. The structure was solved by the direct method using RANTAN 81 program with some modification, and was refined by the block-diagonal least-squares method with anisotropic temperature factors. The final R value is 11.06% for 2294 reflections with $|Fo| > 3\sigma|Fo|$. Hydrogen atoms were not included in the refinement.

**X-ray Structural Analysis of $Ind_3$•$1_2$.** A reddish needle-like crystal with a dimension of 0.20 x 0.30 x 0.30 mm was obtained by the vapor diffusion method from MeCN/*n*-hexane. It was sealed in a glass capillary with Ind and used for the data collection. All measurement were made on an AFC-5R diffractometer with graphite monochromated MoK$\alpha$ radiation and a 12 kW rotating anode generator. The $\omega$ - $2\theta$ scan mode with a scan speed of 4° $min^{-1}$ was employed with the $\omega$ scan range of $(1.10 + 0.3 \tan\theta)°$. A total of 4891 independent reflections was collected by using graphite monochromated MoK$\alpha$ radiation within $2\theta$ = 52.5°. Crystal data are as follows: MF $C_{51}H_{24}N_{16}S_4$, MW 454.48, monoclinic, space group C2/c, a = 21.944(5) Å, b = 13.422(5) Å, c = 17.660(5) Å, $\beta$ = 118.57(1)°, V = 4567(2) $Å^3$, Z = 4, and $D_{calcd}$ = 1.438 g $cm^{-3}$, $\mu_{MoK\alpha}$ = 2.54 $cm^{-1}$. The structure was solved by the direct method using SAPI91 program and expanded using Fourier techniqes. The non-hydrogen atoms were refined anisotropically. The final R value is 7.1% for 2326 reflections with $|Fo| > 3\sigma|Fo|$. Hydrogen atoms were not included in the refinement.

**References and Notes**

(1) (a) Perrin, R.; Lamartine, R. In *Structure and Properties of Molecular Crystals: Organic Reactions in the Solid State*; Pierrot, M. Ed; Elsevier: Amsterdam, 1990; p 107-159. (b) Addadi, L.; van Mil, J.; Lahav, M. J. *J. Am. Chem. Soc.* **1982**, *104*, 3422. (c) Evans, S. V.; Garcia-Garibay, M.; Omkaram, N.; Scheffer, J. R.; Trotter, J.; Wireko, F. *J. Am. Chem. Soc.* **1986**, *108*, 5648. (d) Hasegawa, M.; Chung, C. -M.; Muro, N.; Maekawa, Y. *J. Am. Chem. Soc.* **1990**, *112*, 5676. (e) Sakamoto, M.; Hokari, N.; Takahashi, M.; Fujita, T.; Watanabe, S.; Iida, I.; Nishio, T. *J. Am. Chem. Soc.* **1993**, *115*, 818. (f) Koshima, H.; Ding, K.; Chisaka, Y.; Matsuura, T. *J. Am. Chem. Soc.* **1996**, *118*, 12059.

(2) For recent review on absolute asymmetric synthesis, Sakamoto, M. *Chem. Eur. J.* **1997**, *3*, 684.

(3) Enkelmann, V. *Adv. Polym. Sci.* **1984**, *63*, 92, and references cited therein.

(4) (a) Nakanishi, H.; Hasegawa, M.; Sasada, Y. *J. Polym. Sci., Polym. Phys. Ed.* **1977**, *15*, 173. (b) Braun, H. G.; Wegner, G. *Makromol. Chem.* **1983**, *184*, 1103.

(5) Nakanishi, H.; Jones, W.; Thomas, J. M.; Hursthouse, M. B.; Motevalli, M. *J. Phys. Chem.* **1981**, *85*, 3636.

(6) Miller, E. J.; Brill, T. B.; Rheingold, A. L.; Fultz, W. C. *J. Am. Chem. Soc.* **1983**, *105*, 7580.

(7) Tieke, B. *J. Polym. Sci., Polym. Chem. Ed.* **1984**, *22*, 2895.

(8) Chang, H. C.; Popovitz-Biro, R.; Lahav, M.; Leiserowitz, L. *J. Am. Chem. Soc.* **1987**, *109*, 3883.

(9) Wang, W-.N.; Jones, W. *Tetrahedron* **1987**, *43*, 1273.

(10) Ohashi, Y. *Acc. Chem. Res.* **1988**, *21*, 268, and references cited therein.

(11) Enkelmann, V.; Wegner, G. *J. Am. Chem. Soc.* **1993**, *115*, 10390.

(12) Novak, K.; Enkelmann, V.; Wegner, G.; Wagener, K. B. *Angew. Chem., Int. Ed. Engl.* **1993**, *32*, 1614.

(13) The absolute configuration of **2o** was successfully determined as follows: the absolute configuration of a selected single crystal of oDV•**1** for crystallography was determined as shown in the Figures by using the anomalous scattering of sulfur atom with CuKα radiation

($\Delta f'' = 0.557$).[20] Then, photoirradiation of this sample followed by HPLC analysis revealed that the resulting **2o** was rich in (+)-**2o**. According to Scheme 2, this sample affords (*R*)-**2o**, therefore, the absolute configuration of **2o** was found to be (*R*)-(+)-**2o**.

(14) McBride, J. M.; Carter, R. L. *Angew. Chem. Int. Ed. Engl.* **1991**, *30*, 293.

(15) After admixing **1** (6 mg, 0.0188 mmol) and neat 1,2-bis(1-methoxyethenyl)benzene (10 mg, 0.0526 mmol), the greenish yellow the mixture was subject to TLC separation ($CH_2Cl_2$), giving a benzofulvene derivative **28** (5 mg) in 60% yield. **28**: pale yellow oil; $^1H$ NMR (500 MHz, $CDCl_3$) d 7.59-7.34 (2 H, m), 7.32-7.27 (2 H, m), 5.81 (1H, s), 5.59 (1 H, s), 5.47 (1 H, s), 3.93 (1 H, s); $^{13}C$ NMR (125 MHz, $CDCl_3$), d 163.21, 144.27, 137.51, 136.08, 127.57, 126.32, 119.23, 117.64, 108.02, 97.88, 57.19; MS *m/z* (relative intensity) 158 ($M^+$, 100). A possible reaction mechanism is as follows.

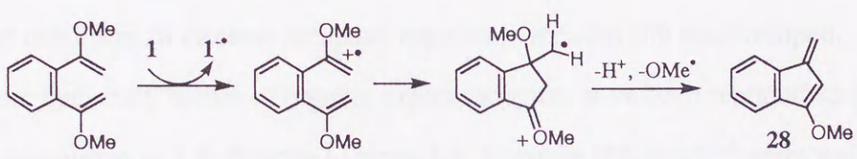


(16) Wittig, G.; Eggera, H.; Duffner, P. *Liebigs Ann. Chem.* **1958**, *619*, 10.

(17) Tebbe, F. N.; Parshall, G. W.; Reddy, G. S. *J. Am. Chem. Soc.* **1978**, *100*, 3611.

(18) Pine, S. H.; Pettit, R. J.; Geib, G. D.; Cruz, S. G.; Gallego, C. H.; Tijerina, T.; Pine, R. D. *J. Org. Chem.* **1985**, *50*, 1212.

(19) Tour, J. M.; Bedworth, P. V.; Wu, R. *Tetrahedron Lett.* **1989**, *30* 3, 927.

(20) *International Tables for X-ray Crystallography, vol IV*; Kynoch Press: Birmingham, 1974, 149.

# Chapter 3

## Structure and Properties of Bi{4*H*,8*H*-4-(dicyanomethylene)benzo-[1,2,5]thiadiazol-7-ylidene}

### 3-1. Introduction

Since the discovery of metallic behavior in CT crystal of tetrathiafulvalene (TTF) and tetracyanoquinodimethane (TCNQ),[1] much attention has been focused on highly conductive organic materials and a variety of electron donors and acceptors have been designed and prepared.[2] The fruition of these efforts, involving the discovery of organic super-conductors,[3] has been mainly brought about by extensive studies on electron donors. However the chemistry of electron acceptors apparently remains still undeveloped. In fact, although more than sixty entries of organic superconductors have been reported so far, only some metal complexes of 1,3-dithiole-2-thione-4,5-dithiolate $[M(dmit)_2]$[4] and $C_{60}$[5] are established as acceptor-based components.

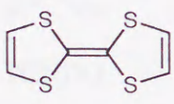

TTF

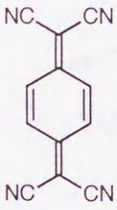

TCNQ

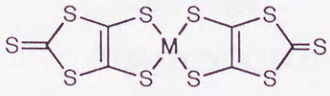

$M(dmit)_2$

In view of the proposed requirements for organic metals,[6] 13,13,14,14-tetracyano-diphenoquinodimethane (TCNDQ) derivatives are among the promising acceptors for such a purpose. However, few examples have so far appeared in the literature,[7] because of the difficulty incurred in thorough investigation of their properties owing to the lack of stability in the neutral state. The instability may come from the twisting about the central double bond due to the repulsion between the biphenylic ortho hydrogens. In order to remove the steric interaction, Agranat *et al.* clamped the biphenyl skeleton by two ethylene bridges.[8] Although

the resulting tetrahydropyrene derivative (TCNTP) could be isolated, their structural details were not given.

Alternatively, a nonbonding interatomic interaction such as a hydrogen bonding seems also useful to fix in a planar geometry. From this point of view, a novel approachand was adopted in this work a novel approach by fusing extra rings to induce the attractive interaction between the ortho hydrogen and the fused ring. Thus, bi{4*H*,8*H*-4-(dicyanomethylene)-benzo[1,2-c:4,5-c´]bis[1,2,5]thiadiazolo-7-ylidene} (TDA-TCNDQ, **11**) was newly designed as a component of highly conductive materials. The preparation, structure, and redox properties of **11** as well as its formation of highly conductive CT complexes will be described herein.

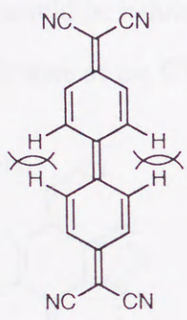


TCNDQ

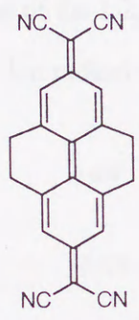


TCNTP

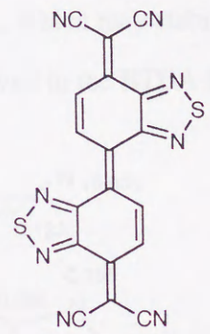


TDA-TCNDQ (**11**)

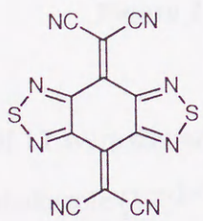


BTDA (**1**)

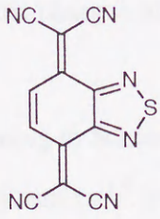


TDA (**10**)

### 3-2. Molecular Design and Preparation

In connection with the present strategy to stabilize the TCNDQ skeleton, 1,2,5-thiadiazole ring is of interest because the negatively polarized N atom on this heterocycle would be available for the C-H•••N hydrogen bonding with the ortho hydrogen. Furthermore, it was reported that, in some cases, introduction of 1,2,5-thiadiazole rings stabilize the inherently unstable skeletons.[9] From these points of view, the novel electron acceptor **11** seems to be a suitable compound to test the validity of the molecular design: first, according to the PM3 calculation (Figure 1), the negative atomic charge is largest at N2 (-0.198) in **11**, leading to considerable stabilization by the electrostatic C-H•••N hydrogen bonding[10,11] between N2 and the ortho hydrogen; secondly, annelation of the 1,2,5-chalcogenadizole ring[12] dose not induce deformation of the TCNQ skeleton but stabilizes the anionic species by delocalization; thirdly, the intermolecular S•••N≡C interaction in the crystal of **11** would be induced by annelation of the 1,2,5-thiadiazole, which may stabilize the metallic state of the CT complexes or ion radical salts as observed in the BTDA (**1**).[13]

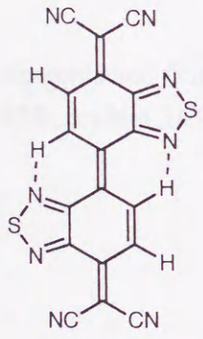


**11**

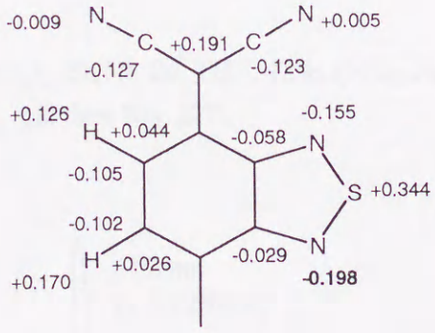


**Figure 1.** Net atomic charges of **11** calculated by the PM3.

The preparation of **11** were carried out according to Scheme 1. Reductive coupling of 4-bromobenzo[1,2,5]thiadiazole (**12**)[14] with Ni(0) catalyst[15] gave **13** in 42% yield, which was converted into the 7,7'-diiodo derivative **14** in 85% yield by treating with $I_2$ and $Ag_2SO_4$ in conc. $H_2SO_4$ at 110 °C. Pd(0)-catalyzed reaction[16] of **14** with $NaCH(CN)_2$ followed by direct oxidation of the resulting dianion with $Br_2$ gave **11** in 22% yield as a sparingly soluble deep violet solid. UV/VIS spectrum in $CH_2Cl_2$ shows no significant absorption except very

strong ones at 522 (log ε = 5.11) and 488 (4.77) nm (Figure 2), suggesting its conformational rigidity in solution. This new electron acceptor is quite stable as the neutral species both in solution and in the solid state and the single crystals could have grown from PhCN solution over several months.

**Scheme 1**

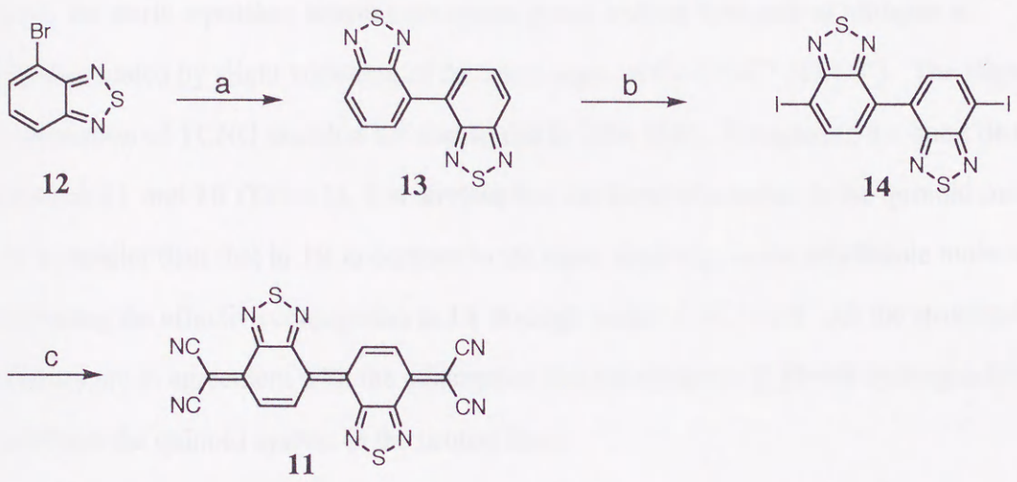


Reagents and Conditions: (a) $NiBr_2(PPh_3)_2$, $Et_4NI$, Zn, THF, 42%; (b) $I_2$, $Ag_2SO_4$, $H_2SO_4$, 85%; (c) $NaCH(CN)_2$, $Pd(PPh_3)_4$, THF, and then $Br_2$, 22%

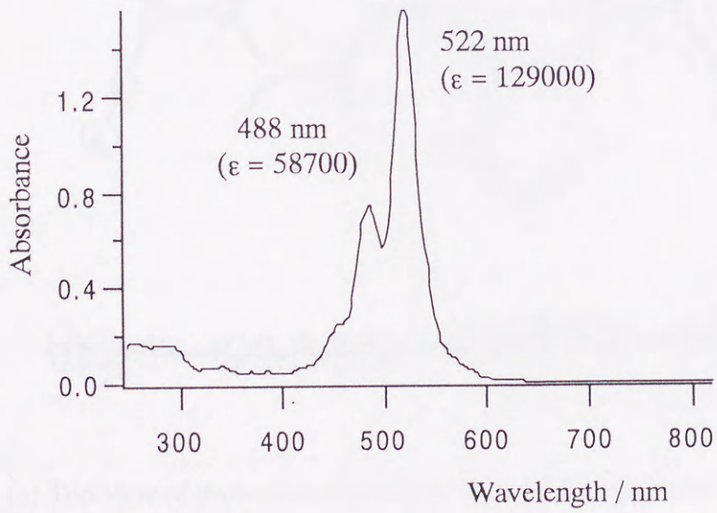


**Figure 2.** UV-vis spectrum of **11** in $CH_2Cl_2$.

### 3-3. Molecular and Crystal Structure

X-ray analysis clearly shows that **11** adopts a planar structure (within 0.19 Å deviation) with *trans*-configuration (Figure 3). It is evident that the two short N•••H contacts (2.14 Å; ∠N2•••H2-C4, 129.8°)[11] connect the biphenyl skeleton, and the twisting angle of the central ethylene bond is 0 degree. Furthermore, there is no indication of repulsive force, and the bond lengths and angles around the molecular center fall into the normal values. On the other hand, the steric repulsion between the cyano group and the lone pair of nitrogen is accommodated by slight widening of the bond angle of C1-C6-C7 (124.3°). The slight deformation of TCNQ skeleton are also found in TDA (**10**). Comparing the bond distances between **11** and **10** (Table 1), it is obvious that the bond alternation in the quinoid moiety of **11** is smaller than that in **10** in contrast to the close similarity in the thiadiazole moieties, indicating the effective conjugation in **11** through central C=C bond. All the structural features are in agreement with the assumption that the attractive C-H•••N hydrogen bond stabilizes the quinoid system in the neutral form.

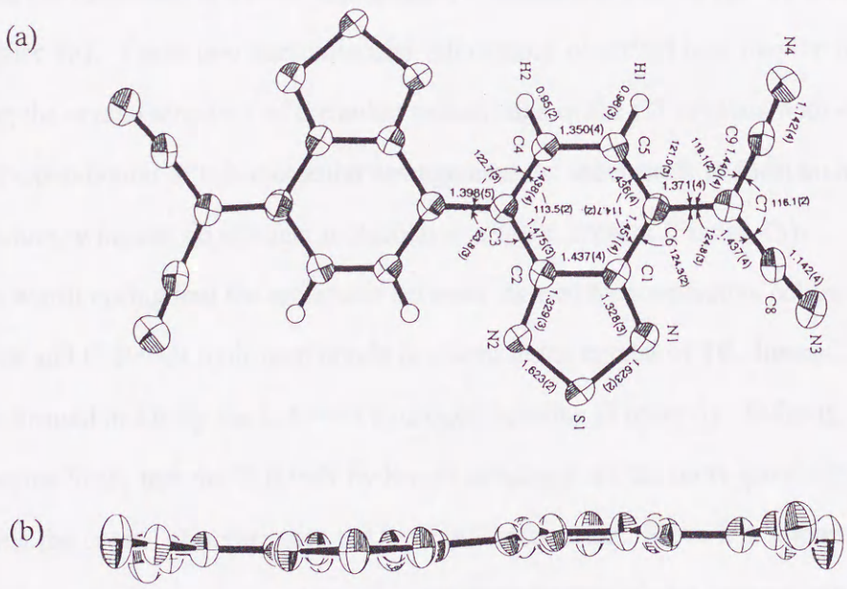


**Figure 3**. (a) Top view of molecular structure of **11** with the bond distances and selected bond angles. The two molecular halves are related by an inversion center. (b) side view.

**Table 1.** Comparisons of Bond Distances.

| | **10** | **11** |
|---|---|---|
| a | 1.622(3) | 1.623(2) |
| b | 1.328(4) | 1.328(3) |
| c | 1.418(4) | 1.437(4) |
| d | 1.453(4) | 1.451(4) |
| e | 1.356(4) | 1.371(4) |
| f | 1.435(4) | 1.437(4) |
| g | 1.132(4) | 1.142(4) |
| h | 1.442(4) | 1.436(4) |
| i | 1.336(4) | 1.350(4) |

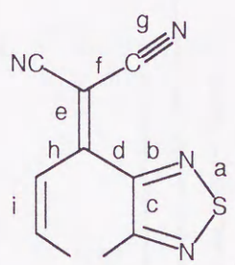


In the crystal, molecules are connected with four neighbors by another C-H•••N hydrogen bond (2.76 Å; ∠N4•••H2-C4, 138.7°) together with two kinds of S•••N contacts (S1•••N3, 3.35 Å; ∠S1•••N3≡C8, 117.5°: S1•••N1, 3.33 Å; ∠S1•••N1=C1, 159.8°) resulting in the formation of a two-dimensional, coplanar sheet-like structure on the (1 0 -1) plane (Figure 4a). These two intermolecular interactions observed here may be helpful in controlling the crystal structure of the anion radical salts or the CT crystals with electron donors. Perpendicular to this molecular arrangement the sheet stack to form an infinite multi-layer structure, whereas no efficient molecular overlap is present (Figure 4b).

It is worth noting that the molecular network formed by cooperative action of S•••N≡C interactions and C-H•••N hydrogen bonds is absent in the crystal of **10**. Instead, only the dyads are formed in **10** by the C-H•••N hydrogen bonding (Figure 5). Judging from these facts, it seems likely that the C-H•••N hydrogen bondings are the more governing factor in determining the crystal structure than the S•••N≡C interaction. Since it is important for crystal engineering to reveal the energy relationship between intermolecular interactions, the energy of S•••N interactions in the supramolecular synthon I and II was estimated by using ab initio calculation.[17]

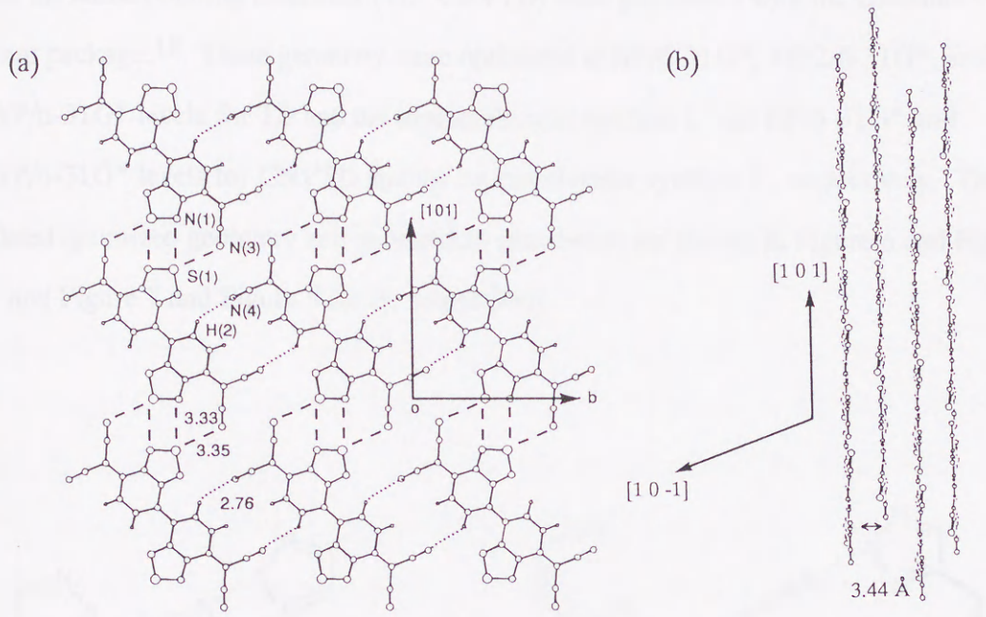


**Figure 4.** (a) Two dimensional coplanar sheet-like molecular arrangement in **11**. Short interatom contacts of C-H•••N (2.76 Å) and S•••N (3.33, 3.35 Å) are indicated by dotted lines and broken lines, respectively. (b) The infinite layer structure in **11**.

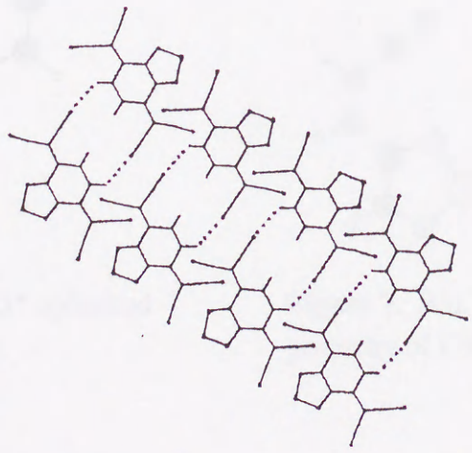

**Figure 5.** Molecular arrangement in TDA (**10**).

### 3-4. Estimation of the Energy of S•••N Interactions

Ab initio molecular orbital and DFT calculations on the supramolecular synthons I, II as well as the corresponding monomer (TD, CNVTD) were performed with the Gaussian 94 program package.[18] These geometry were optimized at HF/6-31G*, MP2/6-31G*, and B3LYP/6-31G* levels for TD and the supramolecular synthon I, and HF/6-31G* and B3LYP/6-31G* levels for CNVTD and the supramolecular synthon II, respectively. The calculated optimized geometry and geometrical parameters are shown in Figure 6 and Figure 8 for I, and Figure 7 and Figure 9 for II, respectively.

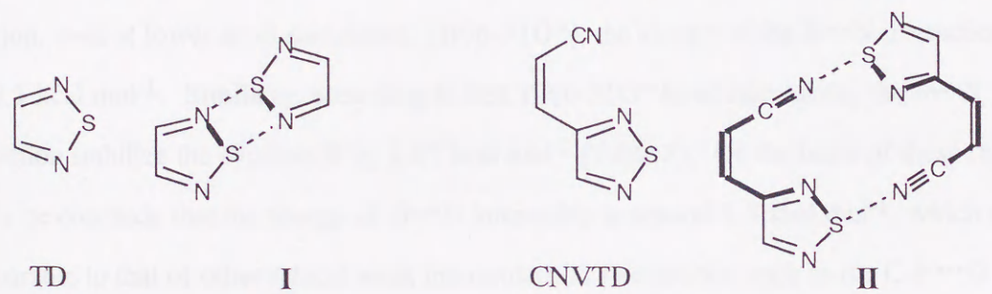


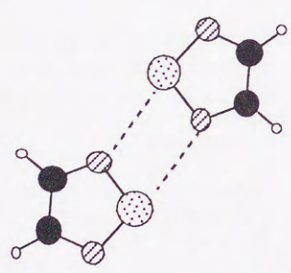

**Figure 6.** MP2/6-31G* optimized geometry of TD dimer.

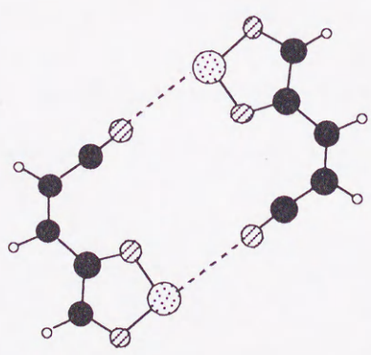

**Figure 7.** B3LYP/6-31G* optimized geometry of CNVTD dimer.

Introduction of the cyanovinyl group into 1,2,5-thiadiazole ring causes larger polarization of =N-S-N= linkage, resulting in an increase of both the total atomic charge on sulfur atom with the apparent bond alternation. Upon dimerization the total atomic charges on sulfur and nitrogen atoms at the interactive sites becomes slightly larger, yet the negligible variation are found in the extent of bond alternation. In accord with the previous observation in **1**,[17] these results strongly suggest the electrostatic nature of the S•••N interaction.

All the calculations on these synthons give coplanar arrangements (Figure 6, 7), in which is observed a decrease of the calculated S•••N separation at higher levels of theory including MP2 and B3LYP. As shown in Table 2, for example, the energy gain upon dimerization of TD by two S•••N interactions is estimated to be 3 kcal $mol^{-1}$ at B3LYP/6-31G* calculation. The total energy of the S•••N interaction is thus calculated to be 1.5 kcal $mol^{-1}$. In addition, even at lower level calculation (HF/6-31G*), the energy of the S•••N interaction is at about 1 kcal $mol^{-1}$. Similarly, according to B3LYP/6-31G* level calculation, the S•••N interaction stabilize the synthon II by 1.85 kcal $mol^{-1}$ (Table 3). On the basis of these results, it may be conclude that the energy of S•••N interaction is around 1.5 kcal $mol^{-1}$, which can be comparable to that of other typical weak intermolecular interactions such as the C-H•••O hydrogen bonding (< 2 kcal $mol^{-1}$).[19]

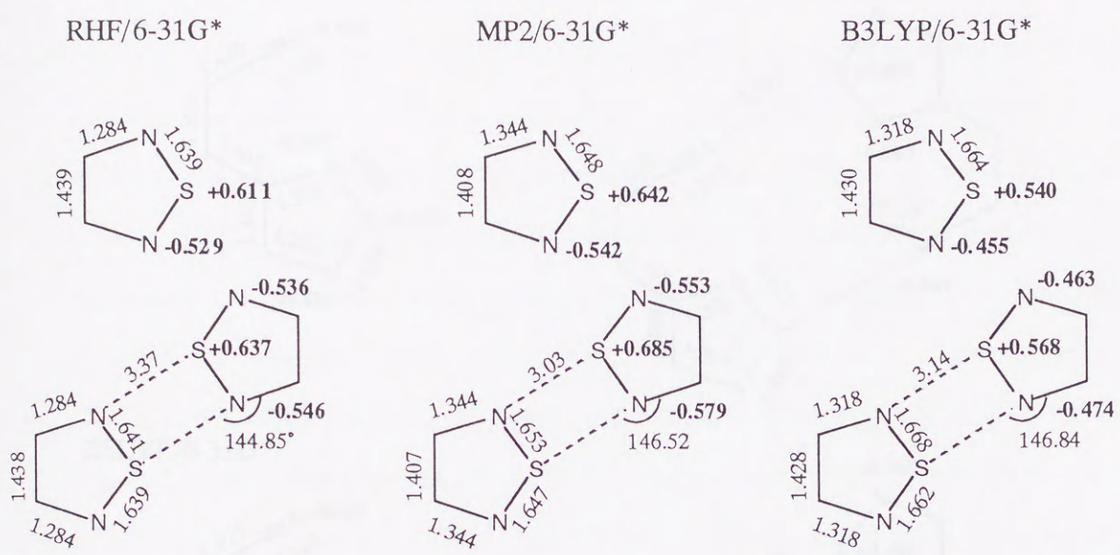


**Figure 8**. Bond distances (Å), a selected angle (degree), and total atomic charges on S and N atoms estimated by *ab initio* calculation.

**Table 2**. Total Energy of TD and TD dimer, and Energy of S••N Interaction ($E_{SN}$) in Supramolecular Synthon I estimated by *ab initio* Calculation.

| | RHF/6-31G* | | MP2/6-31G* | | B3LYP/6-31G* | |
|---|---|---|---|---|---|---|
| | TD | TD dimer | TD | TD dimer | TD | TD dimer |
| Total energy / hartree | -583.2713156 | -1166.5455286 | -583.9830648 | -1167.9756985 | -585.0794478 | -1170.1636977 |
| $\Delta E^a$ / kcal mol$^{-1}$ | | -1.82 | | -6.00 | | -3.01 |
| $E_{SN}$ / kcal mol$^{-1}$ | | 0.91 | | 3.00 | | 1.51 |

[a] total energy of TD x 2 - total energy of TD dimer

RHF/6-31G*

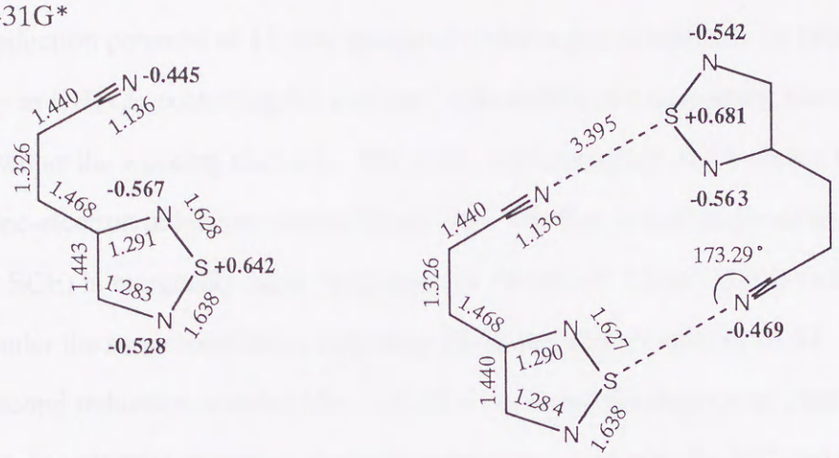


B3LYP/6-31G*

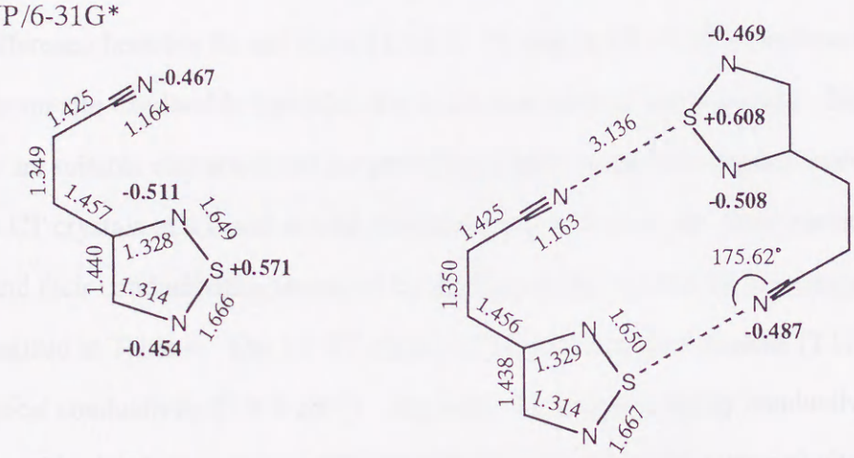


**Figure 9**. Bond distances (Å), a selected angle (degree), and total atomic charges on S and N atoms estimated by *ab initio* calculation.

**Table 3**. Total Energy of CNVTD and CNVTD dimer, and Energy of S ••• N Interaction ($E_{SN}$) in Supramolecular Synthon II estimated by *ab initio* Calculation.

| | RHF/6-31G* | | B3LYP/6-31G* | |
|---|---|---|---|---|
| | CNTD | CNVTD dimer | CNTD | CNVTD dimer |
| Total energy / hartree | -751.8871243 | -1503.7775773 | -754.7216649 | -1509.4492248 |
| $\Delta E^a$ / kcal mol$^{-1}$ | -2.09 | | -3.70 | |
| $E_{SN}$ / kcal mol$^{-1}$ | 1.05 | | 1.85 | |

[a] total energy of CNVTD x 2 - total energy of CNVTD dimer

### 3-5. Redox Properties and Electrical Conductivities of Charge-Transfer Crystals and Anion Radical Salts.

The reduction potential of **11** was measured under argon atmosphere by cyclic voltammetry in $CH_2Cl_2$ containing 0.1 mol $dm^{-3}$ $n$Bu$_4$NBF$_4$ as a supporting electrolyte and Pt wire was used as the working electrode. The cyclic voltammogram of **11** shows two reversible one-electron reduction waves (Figure 10). The first reduction potential of **11** ($E_1$ = +0.33 V *vs* SCE) is marginally higher than those of **10** (+0.29 V) and TCNQ (+0.31 V) measured under the same conditions, indicating the strong electron affinity of **11**. The well-separated second reduction potential ($E_2$ = +0.12 V) indicates the absence of drastic structural change upon one-electron reduction, suggesting the planar geometry for $\mathbf{11}^{-\bullet}$ and $\mathbf{11}^{2+}$. The smaller difference between $E_1$ and $E_2$ in **11** (0.21 V) than in **10** (0.56 V) indicates the large decrease in on-site Coulombic repulsion due to the extension of the π-system. Such redox properties are suitable characteristics for providing highly conductive organic materials.

The CT crystals of **11** and several donors were prepared by the direct method in $CH_2Cl_2$ and their conductivities measured by the four-probe method on the compressed pellets are summarized in Table 4. The 1:1 CT crystal of **11** with tetrathiafulvalene (TTF) exhibits high electrical conductivity (7.9 S $cm^{-1}$). Similarly, **11** afforded highly conductive 1:1 complexes with bis(ethylenedithio)-TTF (BEDT-TTF) (9.8 S $cm^{-1}$), tetramethyltetraselena-fulvalene (TMTSF) (18 S $cm^{-1}$), and tetrathiatetracene (TTT) (9.9 S $cm^{-1}$). Moreover, all the CT crystals showed fairly broad absorption with the characteristic intrastack CT band around 3000 $cm^{-1}$. In conjunction this observation with the high values of electrical conductivity, one can expect that these CT crystals show metallic behavior.

On the other hand, in accord with the reversible redox properties of **11**, the anion radical salt ($n$Bu$_4$N$^+$)$_2$($\mathbf{11}^{-\bullet}$)$_3$ could be isolated upon chemical reduction with $n$Bu$_4$NI, which shows good conductivity (1.9 S $cm^{-1}$). In addition, a good conductivity (1.8 x $10^{-2}$ S $cm^{-1}$) of the 1:1 salt of **11** with *N*-methylquinolinium (NMQ$^+$) which might be in complete CT state is noteworthy. These results indicate that conduction columns of **11** are formed both in the CT crystals and the anion radical salts. It is of interest to clarify the conducting behavior of CT

crystals or anion radical salts. Although the single crystals are necessary for such a purpose, unfortunately many attempts gave rise to affording only microcrystalline samples.

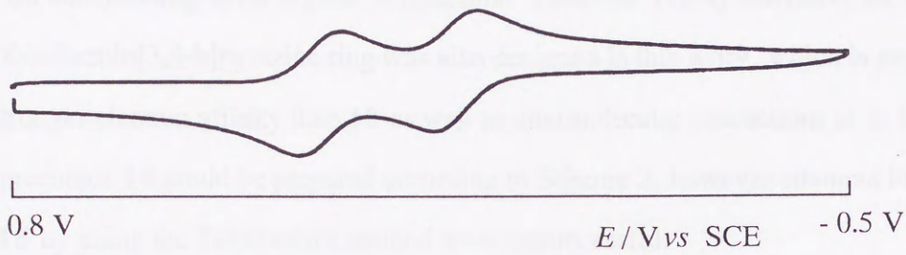


**Figure 10**. Cyclic voltammogram of **11** in $CH_2Cl_2$.

**Table 4**. Room Temperature Conductivities[a] of CT Complexes and Anion-radical Salts

| Donor or Cation (D) | Ratio (D : **11**)[b] | $\sigma_{r.t.}$ / S cm$^{-1}$ |
|---|---|---|
| TTF | 1:1 | 7.9 |
| BEDT-TTF | 1:1 | 9.8 |
| TMTSF | 1:1 | 18.0 |
| TTT | 1:1 | 9.9 |
| $NMQ^+$ | 1:1 | 0.018 |
| $nBu_4N^+$ | 2:3 | 1.7 |

### 3-6. Attempted Preparation of Thiadiazolopyrazino-TCNQ

As described above, TCNDQ derivative **11** which is regard as the π-extended type of TCNQ derivative **10** afforded quite highly conductive CT crystals and anion radical salts. Alternatively, π-extension along the molecular short axis of **10** seems another promising acceptor for constructing novel organic conductors. Thus, the TCNQ derivative **15** fused with the thiadiazolo[3,4-b]pyrazine ring was also designed in this work, which is expected to exhibit stronger electron affinity than **10** as well as intermolecular interactions as in **10** and **11**. Its precursor **18** could be prepared according to Scheme 2, however attempts to convert **18** into **15** by using the Takahashi's method were unsuccessful.

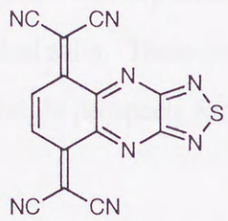

**15**

**Scheme 2**

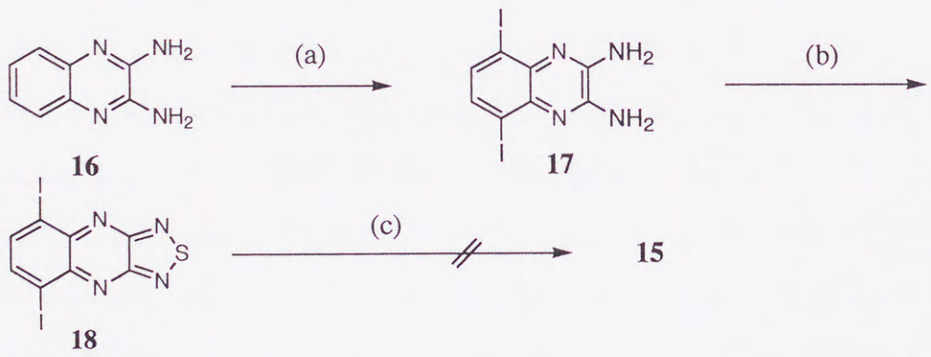


Reagents and Conditions: (a) $I_2$, $Ag_2SO_4$, $H_2SO_4$, 52%; (b) $SOCl_2$, pyridine, $CH_2Cl_2$, 46% ; (c) $NaCH(CN)_2$, $Pd(PPh_3)_4$, THF, and then oxidizing agents

## 3-7. Conclusion

The novel TCNDQ derivative was designed and prepared as a component for highly conductive organic materials. Introduction of the 1,2,5-thiadiazole rings into the TCNDQ skeleton leads to large stabilization in the neutral state. X-ray analysis revealed their structural details which suggest that interatomic interactions (C-H•••N, S•••N) play an important role in determining the molecular and crystal structure. In this connection, the energies of the S•••N interactions in the supramolecular synyhons I and II were estimated by means of ab initio calculation at several level of theory, where the energies of S•••N was proven to be comparable to that of C-H•••O hydrogen bond.

The novel electron acceptor **11** shows strong electron affinity and gives highly conductive CT crystals and anion radical salts. These results indicate the validity of the molecular designing, and **11** shows bright prospects for the development of new organic conductors.

## Experimental Section

**General.** All the melting points are reported uncorrected. Elemental analyses were performed at the Instrumental Analysis Center for Chemistry, Faculty of Science, Tohoku University. MS spectra were obtained in the EI mode at 70 eV. $^1$H NMR spectra were recorded at 200 MHz and 270 MHz. $^{13}$C NMR spectra were recorded at 100 MHz.

**Materials.** All the electron donors were commercially available and used as received. Dry $CH_2Cl_2$, THF, and MeCN were dried over $CaH_2$ and distilled before use.

**4,4'-Bis{benzo[1,2,5]thiadiazole} (13).** A mixture of $NiBr_2(PPh_3)_2$ (8.8 g, 11.8 mmol), $Et_4NI$ (30.8 g, 120 mmol) and Zn powder (11.4 g, 180 mmol) in 180 mL of dry THF was heated at 50 °C for 30 min under $N_2$ atmosphere. To the resulting mixture was added 4-bromobenzo[1,2,5]thiadiazole (**12**)[14] in 120 mL of dry THF and the whole mixture heated at 50 °C for 36 h. After filtration by using Celite pad, the residue was extracted with $CH_2Cl_2$ (Soxhlet). The extract was combined with the filtrate and evaporated. The resulting black tarry material was washed well with MeOH. Recrystallization of insoluble yellowish powder from benzene gave **13** (6.78 g) as yellow needles in 42% yield. mp 240-241 °C; IR (KBr) $\nu_{max}$ 3062, 1530, 1486, 1312, 1145, 869, 856, 815, 804, 758 cm$^{-1}$; $^1$H NMR (400 MHz, $CDCl_3$) $\delta$ 8.26 (2H, dd, $J$ = 6.8, 1.2 Hz), 8.11 (2H, dd, $J$ = 8.8, 1.2 Hz), 7.80 (2H, dd, $J$ = 8.8, 6.8 Hz); $^{13}$C NMR (100 MHz, $CDCl_3$), $\delta$ 155.48, 153.59, 130.77, 129.98, 129.43, 121.63; EI-MS (*m/z*, %) 270 ($M^+$, 100); Anal. Calcd for $C_{12}H_6N_4S_2$: C, 53.32; H, 2.24; N, 20.73; S, 23.72. Found: C, 53.57; H, 2.43; N, 20.73; S, 23.87.

**4,4'-Bis{7-iodobenzo[1,2,5]thiadiazolyl} (14).** To a solution of **13** (3.80 g, 14.1 mmol) in 80 mL of conc. $H_2SO_4$ was added $Ag_2SO_4$ (8.80 g, 28.2 mmol) and iodine (17.9 g, 70.5 mmol), and the whole mixture was heated at 110 °C for 6.5 h. After cooling, the resulting precipitates were filtered and washed with conc. $H_2SO_4$. The filtrate was then poured onto 1 kg of ice and yellow powder was collected by suction. The crude product was washed with water and 2 M $NH_3$aq, and purified by sublimation (4 x 10$^{-2}$ Torr, 280-300 °C), giving yellow crystals of **14** (5.95 g) in 81% yield. mp 311-312 °C; IR (KBr) $\nu_{max}$ 3076, 1560, 1516, 1470, 1315, 1284, 1182, 928, 890, 867, 848, 839, 830, 757 cm$^{-1}$; $^1$H NMR (270 MHz, $CDCl_3$) $\delta$ 8.30 (2H, d, $J$ = 7.4 Hz), 8.06 (2H, d, $J$ = 7.4 Hz); EI-MS (*m/z*, %)

522 ($M^+$, 100); Anal. Calcd for $C_{12}H_4I_2N_4S_2$: C, 27.61; H, 0.77; N, 10.73; I, 48.61. Found: C, 27.54; H, 0.97; N, 10.52; I, 48.68.

**Bi{4*H*,8*H*-4-(dicyanomethylene)benzo[1,2-c:4,5-c´]bis[1,2,5]thiadiazolo-7-ylidene} (TDA-TCNDQ, 11)** A suspension of **14** (522 mg, 1.0 mmol), NaH (60% oil suspension, 530 mg, 10 mmol), Pd(PPh3)4 (210 mg, 0.2 mmol), and malononitrile (280 mg, 5 mmol) in 100 mL of dry THF was heated at 50 °C for 4 h under $N_2$ atmosphere. After cooling in ice-water bath, $Br_2$ (0.5 mL, 9.7 mmol) was slowly added to the resulting mixture and stirred at 0 °C for 30 min. The whole mixture was poured into EtOH and filtered. The residue was washed with *n*-hexane and $CH_2Cl_2$. Recrystallization of insoluble deep violet material from $CH_2Cl_2$ gave **13** (86 mg) as deep violet needles in 22% yield. mp 417 °C (decomp.); IR (KBr) $\nu_{max}$ 3113, 2219, 1633, 1563, 1514, 1429, 1316, 1280, 1255, 830 $cm^{-1}$; $^1H$ NMR (270 MHz, $CDCl_3$) $\delta$ 9.84 (2H, d, $J$ = 10 Hz), 7.75 (2H, d, $J$ = 10 Hz) EI-MS (*m/z*, %) 396 ($M^+$, 100); HRMS (*m/z*) 396.0011 ($M^+$; calcd for $C_{18}H_4N_8S_2$, 396.0000); Anal. Calcd for $C_{18}H_4N_8S_2$: C, 54.54; H, 1.02; N, 28.27; S, 16.18. Found: C, 54.65; H, 1.52; N, 28.21; S, 15.64.

**2,3-Diamino-5,8-diiodoquinoxaline (17).** To a solution of 2,3-diaminoquinoxaline **16**[20] (1.08 g, 6.75 mmol) in 10 mL of conc. $H_2SO_4$ was added $Ag_2SO_4$ (4.21 g, 13.5 mmol) and iodine (8.57 g, 33.8 mmol), and the whole mixture was heated at 110 °C for 12 h. After cooling, the resulting precipitates were filtered and washed with conc. $H_2SO_4$. The filtrate was then poured onto 120 g of ice and yellow powder was collected by suction. The crude product was washed with water and 2 M $NH_3$aq, and purified by sublimation (4 x $10^{-2}$ Torr, 240 °C), giving yellow crystals of **17** (1.29 g) in 46% yield. mp 310-313 °C (decomp.); IR (KBr) $\nu_{max}$ 3520-2920 ($NH_2$), 1656, 1496, 1456 $cm^{-1}$; EI-MS (*m/z*, %) 412 ($M^+$, 100), 158 (20); Anal. Calcd for $C_8H_6N_4I_2$: C, 23.32; H, 1.47; N, 13.60. Found: C, 23.15; H, 1.60; N, 13.35.

**5,8-Diiodo[1,2,5]thiadiazolo[3,4-b]quinoxaline (18).** To a suspension of 17 in 60 mL of dry $CH_2Cl_2$ and 11.5 mL of dry pyridine was added $SOCl_2$ (6.47 g, 56.6 mmol) over 20 min at 0 °C under $N_2$ atmosphere. After stirring at room temperature for 45 h, the volatile materials was completely removed under reduced pressure, and residue was dried *in*

*vacuo* for 24 h. The remaining solid was triturated with 60 mL of MeOH and the reddish precipitates were filtered and washed well with MeOH. Sublimation of this crude product afforded **18** (1.86 g) as deep red crystals in 75% yield. mp 253-255 °C (decomp.); IR (KBr) $\nu_{max}$ 1397 1339, 1305, 922, 893, 896, 548 $cm^{-1}$; EI-MS (*m/z*, %) 440 ($M^+$, 100), 313 (32), 186 (11); Anal. Calcd for $C_8H_2N_4SI_2$: C, 21.84; H, 0.46; N, 12.73. Found: C, 21.69; H, 0.78; N, 12.43.

**Preparation of CT Crystals.** To a hot solution of **11** (10 mg, .0.025 mmol) in 150 mL of $CH_2Cl_2$ was added a solution of TTF (10 mg, 0.049 mmol) in 5 mL of $CH_2Cl_2$, and the mixture was allowed to stand. After cooling, TTF•**11**•$CH_2Cl_2$ crystals (10 mg) was filtered and dried. TTF•**11**•$CH_2Cl_2$: dark purple powder; mp 281-285 °C (decomp.). Anal. Calcd for $C_{25}H_{10}N_8S_6Cl_2$: C, 43.79; H, 1.47; N, 16.34. Found: C, 44.44; H, 1.89; N, 16.00. Similarly, other CT crystals were prepared by direct method in $CH_2Cl_2$.

TMTSF•**11**•$(H_2O)_{1.5}$: dark lustrous purple powder; mp > 350 °C. Anal. Calcd for $C_{56}H_{38}N_{16}O_3S_4Se_8$: C, 38.59; H, 2.20; N, 12.73. Found: C, 38.77; H, 1.96; N, 12.73.

BEDT-TTF•**11**•$(CH_2Cl_2)_{0.33}$: dark brown powder; mp 282-285 °C (decomp.). Anal. Calcd for $C_{85}H_{38}N_{24}S_{30}Cl_2$: C, 42.04; H, 1.58; N, 13.84. Found: C, 42.21; H, 1.73; N, 13.98.

TTT•**11**•$(CH_2Cl_2)_{0.66}$: dark brown powder; mp 320-323 °C (decomp.). Anal. Calcd for $C_{110}H_{40}N_{24}S_{18}Cl_4$: C, 54.67; H, 1.67; N, 13.91. Found: C, 54.19; H, 2.17; N, 13.87. Although these observed analytical values of above CT crystals do not completely agree with the calculated values, they suggest the 1:1 ratio.

**Preparation of Anion Radical Salts.** To a saturated solution of **11** in 200 mL of $CH_2Cl_2$ was added a solution of $NMQ^+I^-$ (12 mg) in 4 mL of $CH_2Cl_2$, and the mixture was allowed to stand. After cooling, $NMQ^+$•**11**•$(CH_2Cl_2)_{0.2}$ crystals (12 mg) was filtered and dried. $NMQ^+$•**11**•$(CH_2Cl_2)_{0.2}$ : brown powder; mp 261-265 °C (decomp.); IR (KBr) $\nu_{max}$ 2200, 1550, 1530, 1475, 1415, 1450, 1420, 1370, 1205, 1130, 835, 810 $cm^{-1}$. Anal. Calcd for $C_{141}H_{72}N_{45}S_{10}Cl_2$: C, 60.75; H, 2.60; N, 22.61. Found: C, 61.00; H, 2.63; N, 22.52. Similarly, other CT crystals were prepared by direct method in $CH_2Cl_2$. Similarly, $(n\text{Bu}N_4^+)_2$•$\mathbf{11}_3$•$(H_2O)_3$ was obtained by direct method. $(n\text{Bu}N_4^+)_2$•$\mathbf{11}_3$•$(H_2O)_3$: green powder ; mp 314-320 °C (decomp.); IR (KBr) $\nu_{max}$ 2150, 1490, 1435, 1160 $cm^{-1}$. Anal.

Calcd for $C_{86}H_{72}N_{25}O_3S_6$: C, 60.75; H, 2.60; N, 22.61. Found: C, 61.00; H, 2.63; N, 22.52.

**Electrical Resistivity Measurements.** All the electrical resistivity of CT crystals and anion radical salts were measured by four probe method on compressed pellets. Gold wires were attached to the pellet with carbon paste. Direct current was generated by YOKOGAWA 7651 programmable DC source and the potential difference was measured on KEITHLEY 2001 digital multimeter.

**X-Ray Structural Analysis of TDA-TCNDQ (11).** A deep violet cube with a dimension of 0.15 x 0.15 x 0.07 nm was obtained by the recrystallization from PhCN. Crystal data for **11**: $C_{18}H_4N_8S_2$, $M$ = 396.40, monoclinic $P2_1/c$, $a$ = 7.336 (3), $b$ = 10.601 (1), $c$ = 10.515 (1) Å, $\beta$ = 101.77 (1)°, $V$ = 800.6 (3) Å$^3$, $D_C$ ($Z$ = 2) = 1.644 g cm$^{-1}$, $\mu$ (MoK$\alpha$) = 3.57 cm$^{-1}$. A total of 1661 unique data ($2\theta_{max}$ = 52°) was collected on a Rigaku AFC-5R diffractometer with graphite monochromated Mo-K$\alpha$ radiation ($\lambda$ = 0.71069 Å) at 13 °C using the $\omega$-$2\theta$ scan technique. After absorption correction, the structure was solved by the direct method (SIR92) and expanded using Fourier techniques. The non-hydrogen atoms were refined anisotropically. Hydrogen atoms were located in the D-map and refined isotropically. The final cycle of full-matrix least-squares refinement was based on 1084 observed reflections [$I > 3\sigma(I)$] and 135 parameters and converged with the $R$ value of 0.034. Residual electron density is 0.15 e Å$^{-3}$.

**References and Notes**

(1) Ferraris, J. P.; Cowan, D. O.; Walatka Jr, V.; Perlstein, J. H. *J. Am. Chem. Soc.* **1973**, *95*, 948.

(2) (a) Bechgaard, K. in *Structure and Properties of Molecular Crystals*, ed. M. Pierrot, Elsevier, Amsterdam, 1990, p. 235. (b) Bryce, M. R.; Murphy, L. C. *Nature* **1984**, *309*, 119.

(3) J. M. Williams, J. R. Ferraro, R. J. Thorn, K. D. Carlson, U. Geiser, H. H. Wang, A. M. Kini and M.-H. Whangbo, *Organic Superconductors* Prentice Hall, New Jersey, 1992.

(4) Brossard, L.; Ribault, M.; Valade, L.; Cassoux, P. *Phisica*. **1986**, *143B*, 378.

(5) (a) Hebard, A. F.; Rsseinsky, M. J.; Haddon, R. C.; Murphy, D. W.; Glarum, S. H.; Palstra, T. T. M.; Ramirez, A. P.; Kortan, A. R.; *Nature* **1991**, *350*, 600. (b) Tanigaki, J.; Ebbesen, T. W.; Saito, S.; Mizuki, J.; Tsai, J. S.; Kubo, Y.; Kuroshima, S. *Nature* **1991**, *352*, 222.

(6) Saito, G.; Ferraris, J. P. *Bull. Chem. Soc. Jpn.* **1980**, *53*, 2141.

(7) (a) Wheland, R. C.; Martin, E. L. *J. Org. Chem*. **1975**, *40*, 3101. (b) Addison, A. W.; Dalal, N. S.; Hoyano, Y.; Huizinga, S.; Weiler, L. *Can. J. Chem*. **1977**, *55*, 4191. A pyrene analogue was also reported in (c) Maxfield, M.; Willi, S. M.; Cowan, D. O.; Bloch, A. N.; Poehler,T. O. *J. Chem. Soc., Chem. Commun*. **1980**, 947. (d) Acton, N.; Hou, D.; Schwarz, J.; Katz, T. J. *J. Org. Chem.* **1982**, *47*, 1011. (e) Maxfield, M.; Bloch, A. N.; Cowan, D. O. *J. Org. Chem*. **1985**, *50*, 1789.

(8) Aharon-Shalom, E.; Becker, J. Y.; Agranat, I. *Nouv. J. Chim*. **1979**, *3*, 643.

(9) (a) Yamashita, Y.; Tanaka, S.; Imaeda, K.; Inokuchi, H.; Sano, M. *Chem. Lett.* **1992**, 419. (b) Yamashita, Y.; Tanaka, S. *Chem. Lett.* **1993**, 73. (c) Yamashita, Y.; Ono, K.; Tomura, M.; Imaeda, K. *Chem. Commun.* **1997**, 1851.

(10) See for example: (a) Taylor, R.; Kennard, O. *J. Am. Chem. Soc*. **1982**, ***104***, 5063. (b) Berkovitch-Yellin, Z.; Leiserowitz, L. *Acta Crystallogr. Sect. B*, **1984**, *40*, 159. (c) Desiraju, G. R. *Angew. Chem. Int. Ed. Engl*. **1995**, *34*, 2311. (d) Cotton, F. A.; Daniels, L. M.; Jordan IV, G. T.; Murillo, C. A. *J. Chem. Soc., Chem. Commun*. **1997**, 1673.

(11) The C-H•••N contacts with H•••N < 2.721 Å and – C-H•••N > 124.6 ° are indicative of weak hydrogen bonding. See ref. 10a.

(12) Suzuki, T.; Yamashita, Y.; Kabuto, C.; Miyashi, T. *J. Chem. Soc., Chem. Commun.*, **1989**, 1102.

(13) Ugawa, A.; Iwasaki, K.; Kawamoto, A.; Yakushi, K.; Yamashita, Y.; Suzuki, T. *Phys. Rev. B* **1991**, *43*, 14718.

(14) Pilgram, K.; Zupan, M.; Skiles, R. *J. Heterocycl. Chem.* **1970**, *7*, 629.

(15) Iyoda, M.; Otsuka, H.; Sato, K.; Nisato, N.; Oda, M. *Bull. Chem. Soc. Jpn.* **1990**, *63*, 80.

(16) Uno, M.; Seto, K.; Masuda, M.; Ueda W.; Takahashi, S. *Tetrahedron Lett.* **1985**, *26*, 1553.

(17) The electrostatic nature of S•••N≡C interaction were suggested previously on the basis of ab initio calculation on **1** at relatively low level of theory (RHF/STO-3G). However the energy of S•••N interaction still remains unclear. Suzuki, T.; Fujii, H.; Yamashita, Y.; Kabuto, C.; Tanaka, S.; Harasawa, M.; Mukai, T.; Miyashi. T. *J. Am. Chem. Soc.* **1992**, *114*, 3034.

(18) Gaussian 94, Revision E.2, Frisch, M. J.; Trucks, G. W.; Schlegel, H. B.; Gill, P. M. W.; Johnson, B. G.; Robb, M. A.; Cheeseman, J. R.; Keith, T.; Petersson, G. A.; Montgomery, J. A.; Raghavachari, K.; Al-Laham, M. A.; Zakrzewski, V. G.; Ortiz, J. V.; Foresman, J. B.; Cioslowski, J.; Stefanov, B. B.; Nanayakkara, A.; Challacombe, M.; Peng, C. Y.; Ayala, P. Y.; Chen, W.; Wong, M. W.; Andres, J. L.; Replogle, E. S.; Gomperts, R.; Martin, R. L.; Fox, D. J.; Binkley, J. S.; Defrees, D. J.; Baker, J.; Stewart, J. P.; Head-Gordon, M.; Gonzalez, C.; Pople, J. A.; Gaussian, Inc., Pittsburgh PA, 1995

(19) See for example: Novoa, J. J.; Constans, P.; Whangbo, M.-H. *Angew. Chem. Int. Ed. Engl.* **1993**, *32*, 588.

(20) Weidingger, H.; Kranz, J. *Chem. Ber.* **1964**, *97*, 1599.

# Chapter 4

## New Entry into Overcrowded Ethylene with High Electron Affinity: Structure and Properties of Bi{4*H*,8*H*-4-(dicyanomethylene)benzo-[1,2-*c*:4,5-*c*′]bis[1,2,5]thiadiazol-8-ylidene}

### 4-1. Introduction

One of the main goals of this work is directed toward the understanding on intermolecular interactions, especially the S•••N interaction, in the context of dynamic behavior in crystal. For such a purpose, it seems reasonable to explore molecules that crystallize into a particular structural pattern with the aid of intermolecular interactions and undergo subsequent chemical reactions. In such a case, to gain deeper insight into the intrinsic role of intermolecular interactions, it is desirable to reduce other governing factors in determining the crystal structure and/or the chemical reactivities.[1] From this point of view, the single-component molecular crystal of an overcrowded ethylene having intermolecular interactive sites is envisaged to provide the intriguing motif because a very simple conformational isomerism would be feasible. As a novel class of overcrowded ethylenes, the π-extended molecule of BTDA (**1**), bi{4*H*,8*H*-4-(dicyanomethylene)benzo[1,2-*c*:4,5-*c*′]bis[1,2,5]thiadiazol-8-ylidene} (**20**) was designed and prepared in this work in anticipation of unique conformational behavior induced by the S•••N interaction in crystal.

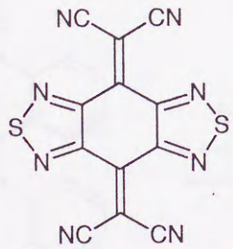


BTDA (**1**)

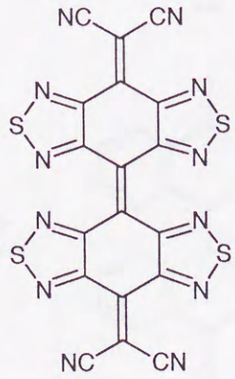


**20**

Overcrowded ethylenes have long attracted much attention in terms of the unusual structure and properties due to the steric congestion about the central C=C bond.[2] Bis(tricyclic) aromatic olefins rank among the most widely studied systems because they exhibit the conformational isomerism associated with the characteristic color change. In recent years, there has been renewal of interest in such molecules as the possible switch units in molecular devices.[3] The leading compound in this family is bianthrone (**21**),[4] which adopts the doubly folded conformation (**21f**) in the ground state to reduce the steric repulsion in the fjord region.[5] Triggered by heating, photoexcitation, or pressure, this yellow conformer partly transforms into green-colored metastable form.[6] Although the geometry in the green-colored form has not so far been characterized crystallographically, the twisted conformation (**21t**) has been widely accepted.[7] It is also known that molecules with central six-membered ring behave in the same way,[8] while molecules with five-membered ring adopts twisted conformation in the ground state. Bifluorenylidene (**22**) is a representative compound in the latter category. The X-ray analysis on **22** reveals that its central C=C bond is twisted by 39°.[9]

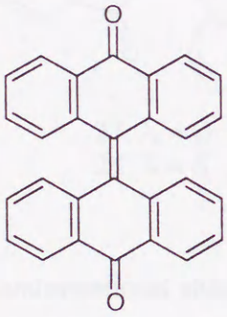

**21**

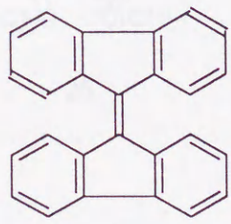

**22**

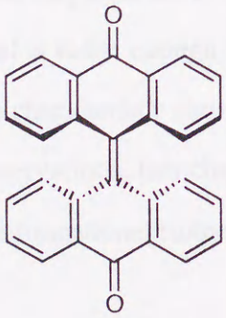

**21f**

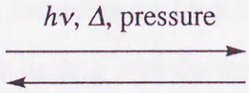


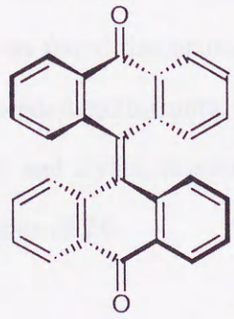

**21t**

Twisted or folded-twisted conformers were isolated in some kinds of overcrowded ethylenes, yet they does not belong to a bis(tricyclic) olefins. 2-(Xanthen-9-ylidene)indane-1,3-dione (**23**) was proven to adopt twisted conformation in deep red crystals.[10] In contrast, closely related 2-(thioxanthen-9-ylidene)indane-1,3-dione (**24**) afforded interconvertible three forms; yellow (folded), deep red (twisted) and orange (folded-twisted) crystals and the structure of the folded and folded-twisted isomers were determined by X-ray analyses, whereas the twisted one is missing.[11] In addition, X-ray analyses were successfully performed on two conformers of bi[1,3-bis(dicyanomethylene)indan-2-ylidene] (**25**) which undergoes one-way isomerization from the folded conformer to the severely twisted one.[12] These results strongly suggest that the twisted conformer is relevant to the characteristic chromic behavior, even so, the structure of deeply colored species in interconvertible bis(tricyclic) aromatic olefins has been somewhat obscure.

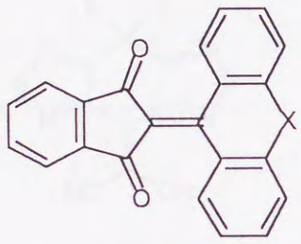

**23**: X = O
**24**: X = S

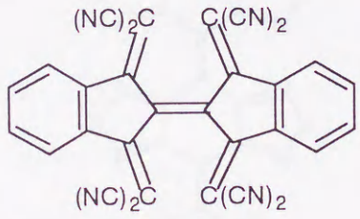


**25**

The conformational change can be also induced electrochemically,[13] yet none of the overcrowded ethylenes so far have afforded stable ion radical salts. In this connection, the title overcrowded ethylenes **20** is outstanding because it possesses high electron affinity and its anion radical is stable enough to be isolated. Furthermore, it was found that neutral **20** exhibits the characteristic chromism involving the folded and twisted conformers. On the basis of these observations, this chapter is dealing with the molecular and crystal structure associated with the conformational isomerism as well as the redox properties of **20**.

## 4-2. Preparation and Isolation of Two Conformers

Tricyclic compound **26** was prepared from BTDA (**1**) according to the reported procedure.[14] Bis(tricyclic) ethylene **20** was obtained in 50% yield upon oxidation of **26** with $SeO_2$ in refluxing EtOH and successive purification by recrystallization (Scheme 1). Interestingly, the appearance of crystalline **26** varies in color with the recrystallization solvents; yellow plates [mp 351-357 °C (decomp.)] were obtained from 1,2-dichloroethane whereas deep violet needles [mp 110-112 °C (decomp.)] or cubes [mp 84-86 °C (decomp.)] were formed in $CH_2Cl_2$ or PhCN solution. Combustion analyses indicated that the latter two crystals contain crystallization solvents (**20**•$CH_2Cl_2$ or **20**•$(PhCN)_2$, respectively).

**Scheme 1**

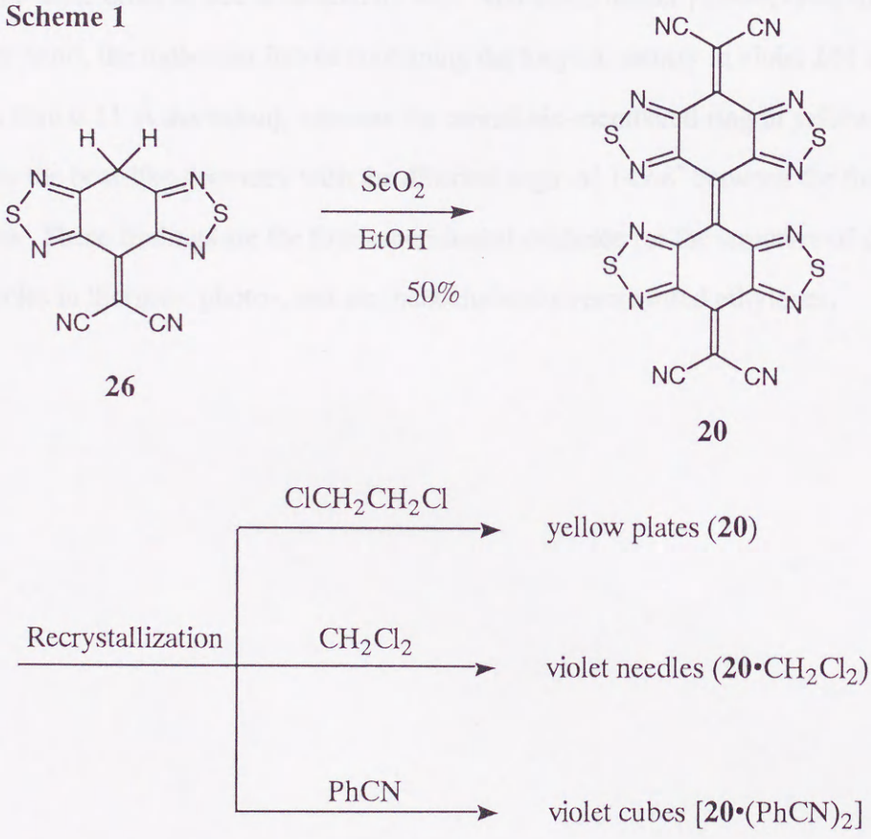

## 4-3. X-Ray Analyses of Two Conformers

In order to elucidate the structural details of the two different forms, X-ray analyses were performed on a yellow crystal and a violet PhCN-solvated crystal. As displayed in Figure 1, molecule in the unsolvated yellow crystal adopts doubly folded geometry (**20f**) which is closely relate to the structure of conventional bis(tricyclic) aromatic olefins in the ground state. On the other hand, Figure 2 clearly shows that **20** exists as the twisted conformer (**20t**) in the violet PhCN-solvated crystal. Both types of deformations arise as a consequence of the repulsive interaction through the short N•••N contacts (2.67 Å in **20f**; 2.74 and 2.81 Å in **20t**) less than the sum of vdW radii (3.0 Å). The central ethylene bond in **20f** [1.362(4) Å] is completely planar within only 0.01 Å deviation of six carbon atoms from the least-square plane, yet the same bond in **20t** is twisted by 48.1° and much longer [1.388(7) Å] than in **20f**. On the other hand, the molecular halves containing the tricyclic moiety in violet **20t** are nearly planar (less than 0.11 Å deviation), whereas the central six-membered ring in yellow **20f** deforms into the boat-like geometry with the dihedral angle of 149.8° between the fused heterocycles. These findings are the first experimental evidence for the structure of deep colored species in thermo-, photo-, and mechanochromic overcrowded ethylenes.

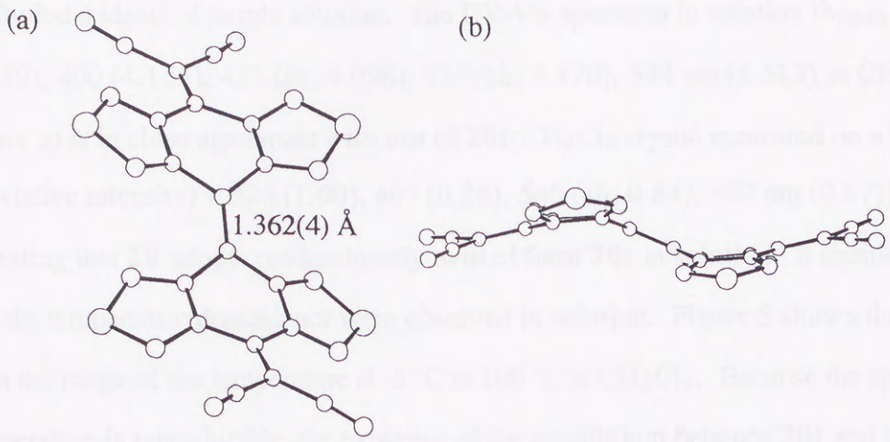


**Figure 1**. (a) Molecular structure of **20f** in yellow crystals. (b) Side view.

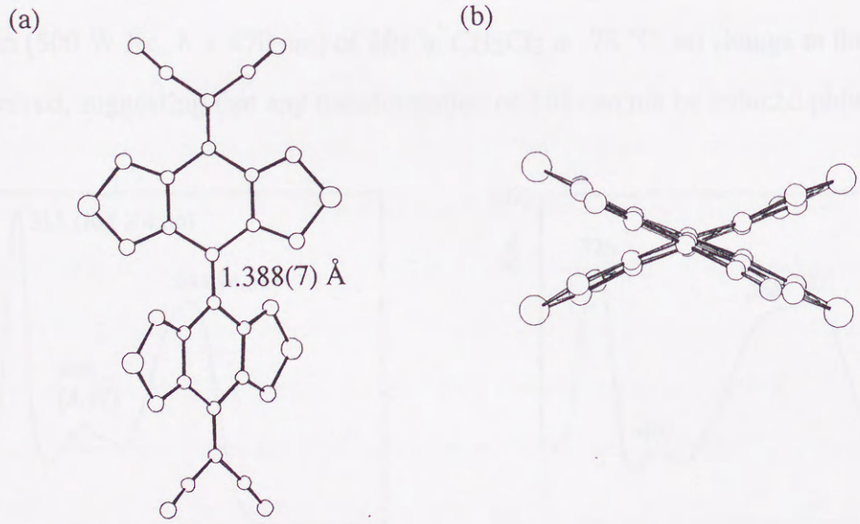


**Figure 2**. (a) Molecular structure of **20t** in **20**•$(PhCN)_2$. (b) Side view.

## 4-4. Conformational Behavior in Solution

Upon dissolution in any organic solvents, both yellow plates and solvated violet crystals of **20** afforded a identical purple solution. The UV-Vis spectrum in solution [$\lambda_{max}$ (log $\varepsilon$) = 313 (4.659), 400 (4.165), 433 (sh, 4.096), 515 (sh, 4.470), 544 nm (4.513) in $CH_2Cl_2$ at 25 °C] (Figure 3) is in close agreement with that of **20t**•$CH_2Cl_2$ crystal measured on a KBr disk [$\lambda_{max}$ (relative intensity) = 326 (1.00), 407 (0.28), 568 (sh, 0.84), 607 nm (0.87)] (Figure 4), suggesting that **20** adopts predominantly twisted form **20t** in solution. It should be noted here that the temperature dependence were observed in solution. Figure 5 shows the UV-Vis spectra in the range of the temperature at -5 °C to 100 °C in $CH_2Cl_2$. Because the spectrum at each temperature is reproducible, the existence of the equilibrium between **20t** and another conformer is expected. Judging from the fact that the crystals of doubly-folded **20f** are actually grown from the solution, **20f** seems one of the possible conformers for the reversible isomerization. However, the presence of isosbestic point at *ca* 500 nm can not be accounted for by the contribution of yellow **20f** which would absorb light at shorter wavelength. Although the actual geometry is still unclear, the conformer with only slight deformation from the **20t** skeleton, such as folding of the planar tricyclic moiety and/or decreasing in the twist angle, might be responsible for the observed spectral change. On the other hand, upon irradiation (500 W Xe, $\lambda$ > 470 nm) of **20t** in $CH_2Cl_2$ at -78 °C, no change in the spectrum was observed, suggesting that any transformation of **20t** can not be induced photochemically.

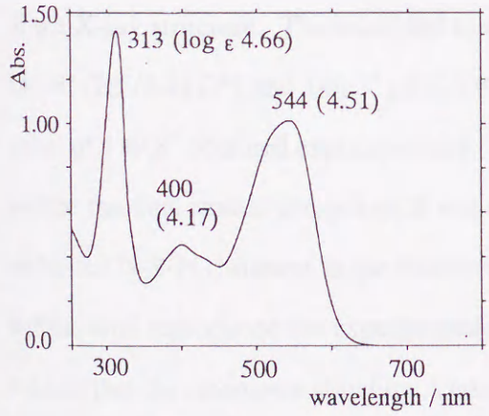


**Figure 3.** UV-VIS spectrum of **20** in $CH_2Cl_2$ at r.t..

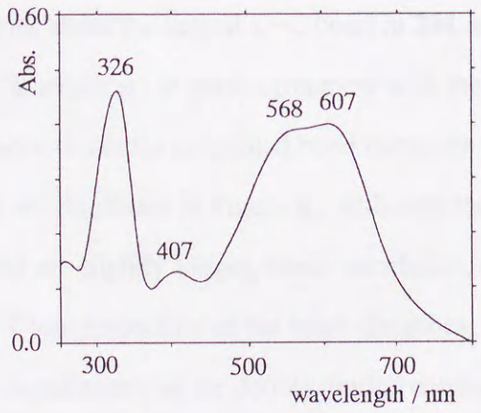


**Figure 4.** UV-VIS spectrum of **20**•$CH_2Cl_2$ in KBr disk.

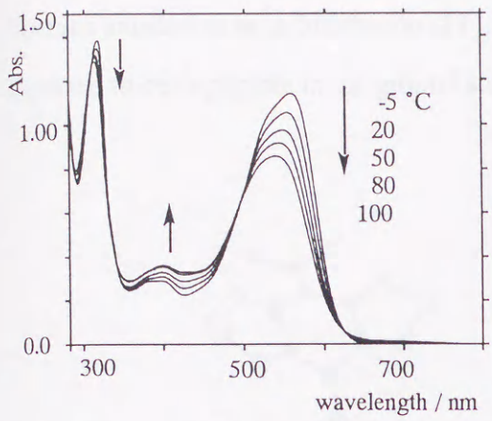


**20t** ⇌ Conformers other than **20t** and **20f** ?

**Figure 5.** UV-VIS spectra of **20** in $CH_2Cl_2$ at various temperatures.

It seems somewhat curious that the heterocyclic overcrowded ethylene **20** adopts twisted conformation as the stable form in solution because other bis(tricyclic) aromatic olefins with central six membered ring are known to be doubly-folded conformer both in solution and in the solid state. To gain further insight into the conformational behavior in **20**, ab initio calculations were performed on two conformers of **20** with the Gaussian 94 program package.[15]

The geometry of **20f** and **20t** were initially optimized at HF/3-21G* level by using the atomic parameters obtained by the X-ray analyses. The DFT calculation at the B3LYP/6-31G* level is also employed. Figure 6 and Figure 7 show the optimized geometry of **20f** and **20t** at the B3LYP/6-31G* level, respectively. These optimized structures are closely related to those of the X-ray structure. The calculated torsion angles about the central C=C bond in **20t** are 143.5° (HF/3-21G*) and 140.3° (B3LYP/6-31G*), which are in good agreement with the value of 139.8° obtained experimentally. The observed and the calculated bond distances as well as the total atomic charges on S and N atoms are illustrated in Figure 8. Although the estimated N-S-N distances in the thiadiazole moiety are slightly longer, these calculation, as a whole, well reproduced the experimental values. Close inspection of the bond distances, it is evident that the resonance structure A contributes significantly in the doubly-folded conformer **20f** (Scheme 2). By contrast, it is likely that the magnitude of more polarized resonance structure B is larger in **20t**, which leads to stabilize the twisted conformation. In the case of

benzene annelation as in bianthrone (**21**), the contribution of the resonance structure B is expected to be negligible in the ground state.

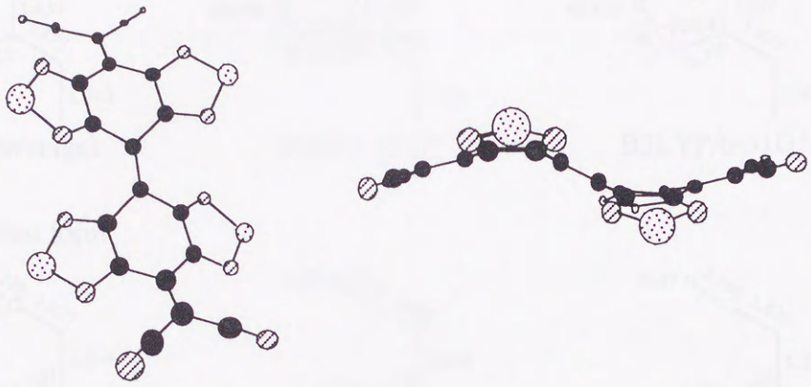

**Figure 6.** B3LYP/6-31G* optimized geometry of **20f**.

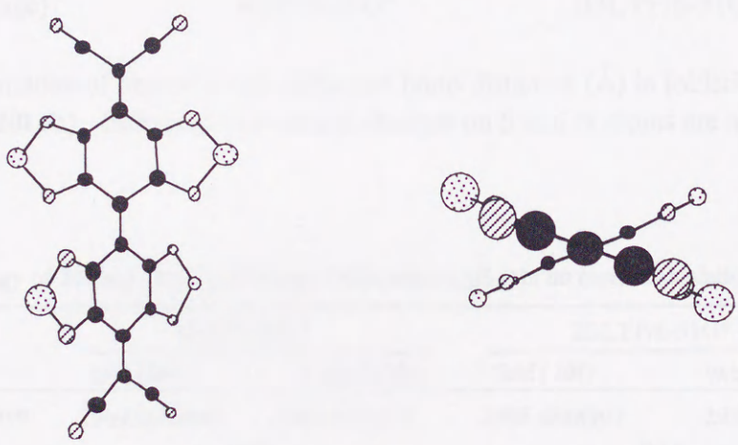

**Figure 7.** B3LYP/6-31G* optimized geometry of **20t**.

**Scheme 2**

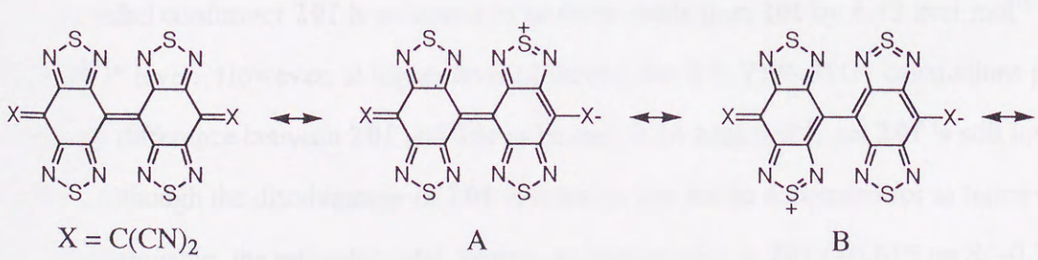

(a) Folded form

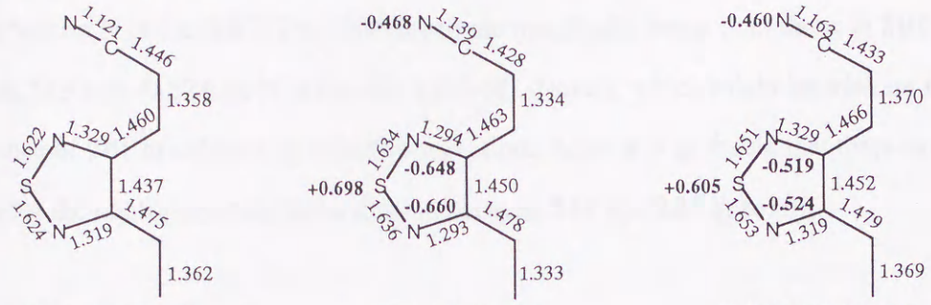


X-Ray (average) RHF/3-21G* B3LYP/6-31G*

(b) Twisted form

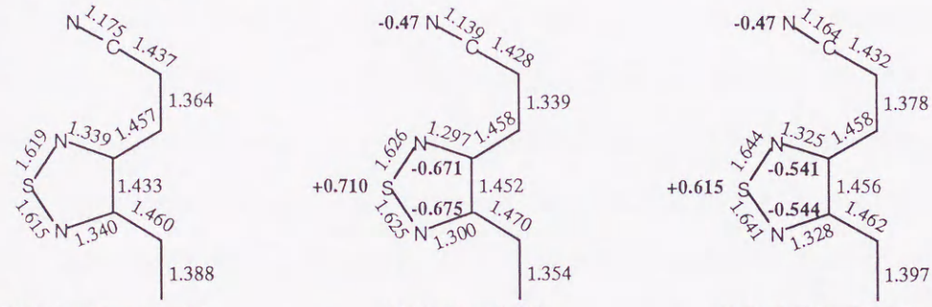


X-Ray (average) RHF/3-21G* B3LYP/6-31G*

**Figure 8**. Comparisons of observed and calculated bond distances (Å) in folded form **20f** (a) and twisted form **20t** (b). Estimated total atomic charges on S and N atoms are also shown.

**Table 1**. Total Energy of **20f** and **20t** in and Energy Differences ($\Delta E_{f\text{-}t}$) in *ab initio* Calculation.

| | RHF/3-21G* | | B3LYP/6-31G* | |
|---|---|---|---|---|
| | fold (**20f**) | twisted (**20t**) | fold (**20f**) | twisted (**20t**) |
| Total energy / hartree | -2909.9652640 | -2909.9582271 | -2935.4848993 | -2935.4846811 |
| $\Delta E_{f\text{-}t}$ / kcal mol$^{-1}$ | -4.42 | | -0.14 | |

The calculated total energy to the two conformers of **20** are summarized in Table 1. The doubly-folded conformer **20f** is estimated to be more stable than **20t** by 4.42 kcal mol$^{-1}$ at the HF/3-21G* level. However, at higher level of theory, the B3LYP/6-31G* calculations predict the energy difference between **20f** and **20t** to be only 0.14 kcal mol$^{-1}$, yet **20f** is still lower in energy. Although the disadvantage of **20f** in solution can not be accounted for in terms of the energy relationship, the estimated total charges on heterocycles in **20t** (+0.615 on S; -0.541

energy relationship, the estimated total charges on heterocycles in **20t** (+0.615 on S; -0.541 and -0.544 on N at the B3LYP/6-31G* level) are marginally larger than those in **20f** (+0.605 on S; -0.519 and -0.524 on N at the B3LYP/6-31G*level), which might be relevant to the preference of **20t** in solution by effective solvation. Also, it is probable that there exist large barrier for the conformational isomerization between **20t** and **20f** in solution.

## 4-5. Conformational Behavior in the Solid State

It is of interest that the stable conformer of **20** in the solid state is different from that in solution. Removal of the solvent from the purple solution of **20** gave a yellow solid. In addition, the solvated violet crystals turned yellow with losing volatile $CH_2Cl_2$ or PhCN at elevated temperature. The resulting yellow solids as well as the yellow plates exhibited no change up to the decomposition point. These results indicate the higher stability of yellow **20f** in the solid state at high temperatures. On the other hand, yellow plates of **20f** were transformed to a purple powder by grinding, exhibiting the mechanochromic behavior. Upon heating the resulting violet solid, yellow color was reproduced. Thus, the interconversion between **20f** and **20t** associated with the color change exists apparently in the solid state.

The FT-IR spectrum is a useful tool for obtaining the direct information about the sequences of the solid-state conformational isomerism. Microscope FT-IR instrument was employed on the yellow single crystal of **20**. In Figure 9a, a band at 1581 $cm^{-1}$ is assigned to the C=C stretching of dicyanomethylene groups. After grinding, this band still remained at 1580 $cm^{-1}$ in the spectrum (KBr disk) but a new and larger one appeared at 1553 $cm^{-1}$ (Figure 9b), whose frequency is quite similar to those of **20t**•$(PhCN)_2$ (1550 $cm^{-1}$) (Figure 9d) crystals.[16] The new band disappeared upon heating the KBr pellet at 220 °C for 5 h with developing the original band and concomitant fading of violet color (Figure 9c). Such a phenomenon is best interpreted as reversible mechano- and thermochromism involving the two conformers, **20f** and **20t**. The reasons for the higher stability of **20f** compared to **20t** in the solid state were well accounted for in terms of the crystal structure.

**Scheme 3**

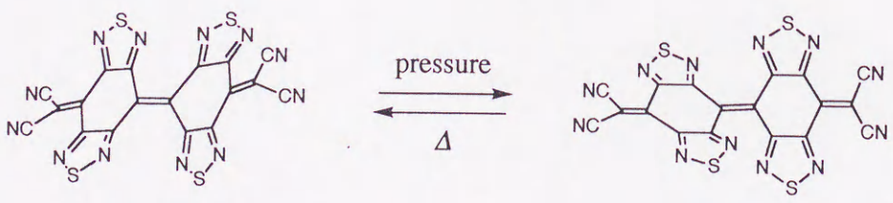


yellow (**20f**) violet (**20t**)

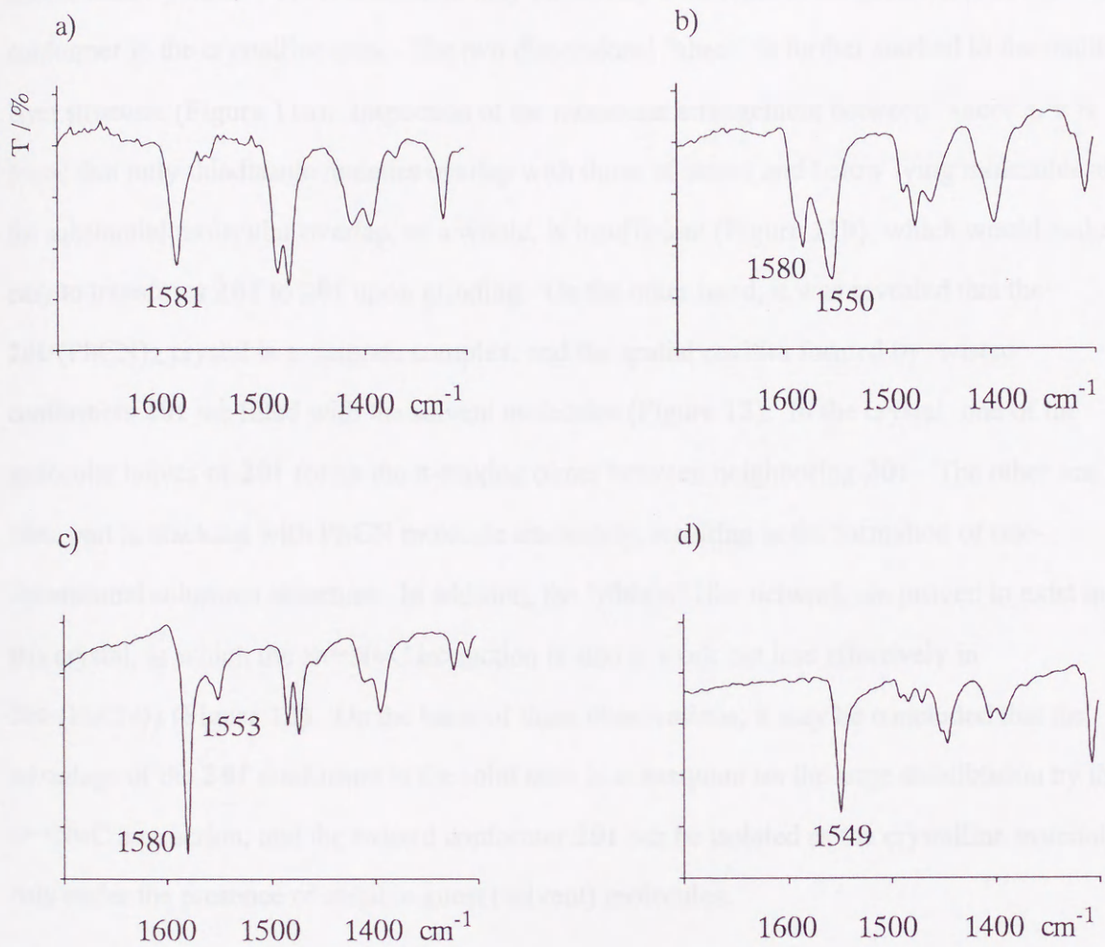


**Figure 9**. IR spectral changes in the range of 1650-1300 $cm^{-1}$ upon solid-state comformational isomerism. a) single crystal IR spectrum of yellow **20**. b) ground **20** (KBr disk). c) after heating at 200 °C for 3 h (KBr disk). d) IR spectrum of **20**•$(PhCN)_2$ for comparisons.

As shown in Figure 10, molecules are connected with four neighbors by the S•••N≡C interaction in the lateral direction to form an infinite "sheet-like" network. Thus, the stabilization by the S•••N≡C interaction may effectively contribute to the preference of the **20f** conformer in the crystalline state. The two dimensional "sheet" is further stacked to the multi-layer structure (Figure 11a). Inspection of the molecular arrangement between "sheet"s, it is found that only thiadiazole moieties overlap with those of above and below lying molecules and the substantial molecular overlap, as a whole, is insufficient (Figure 11b), which would make easy to transform **20f** to **20t** upon grinding. On the other hand, it was revealed that the **20t**•$(PhCN)_2$ crystal is a clathrate complex, and the spatial cavities formed by twisted conformers **20t** are filled with the solvent molecules (Figure 12). In the crystal, one of the molecular halves of **20t** forms the π-staking dimer between neighboring **20t**. The other one takes part in stacking with PhCN molecule alternately, resulting in the formation of one-dimensional columnar structure. In addition, the "ribbon"-like network are proven to exist in this crystal, in which the S•••N≡C interaction is also at work but less effectively in **20t**•$(PhCN)_2$ (Figure 13). On the basis of these observations, it may be concluded that the advantage of the **20f** conformer in the solid state is consequent on the large stabilization by the S•••N≡C interaction, and the twisted conformer **20t** can be isolated as the crystalline material only under the presence of suitable guest (solvent) molecules.

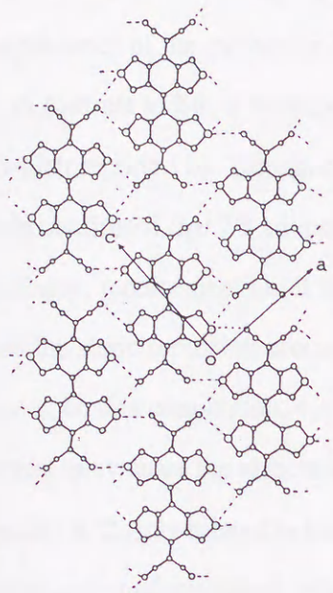


**Figure 10**. Molecular arrangement viewed along the *b* axis. Short S ••• N≡C contacts of 3.30, 3.32, 3.36 Å are indicated by dotted lines.

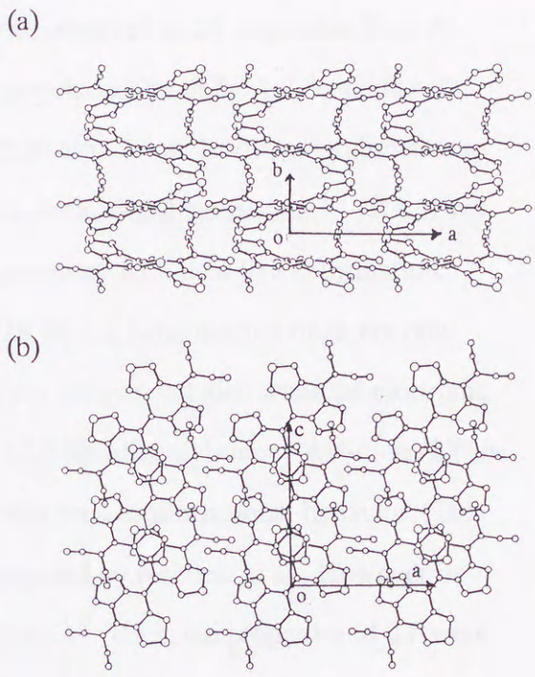


**Figure 11**. (a) Molecular arrangement viewed along the *c* axis. (b) Molecular overlaps between multi-layer structures.

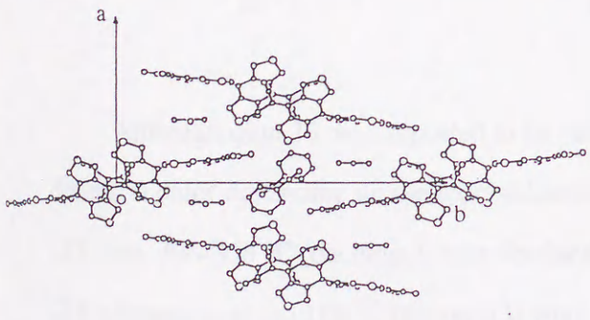


**Figure 12**. Molecular arrangement in **20**•$(PhCN)_2$. PhCN molecules are omitted for clarity.

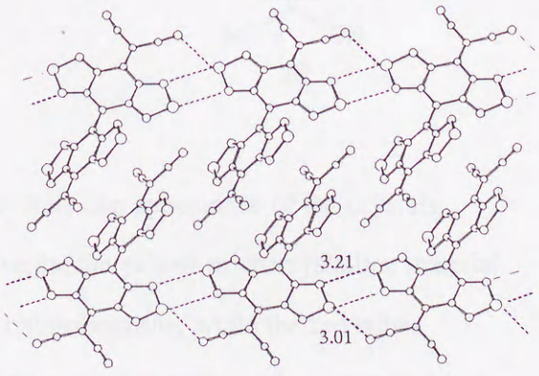


**Figure 13**. Ribbon-like networks by S ••• N contacts along the *c* axis. Short S ••• N contacts of 3.01, 3.21 Å are indicated by dotted lines.

## 4-6. Related Overcrowded Ethylene Fused with 1,2,5-Thiadiazole Rings.

It is likely that the unique conformational behavior observed in **20** originates from the higher planarity of the molecular halves as well as large polarization of the 1,2,5-thiadiazole ring. In contrast to **20**, a benzene analogue, 29,29,30,30-tetracyanobianthraquinodimethane (**28**) which reported by Yamaguchi *et al.*, shows no conformational isomerism.[17] The X-ray analysis confirmed that **28** adopts the doubly-folded geometry with boat-like deformation. Accordingly, replacement of all the benzene rings of **28** by 1,2,5-thiadiazole rings not only reduces the steric repulsion around the dicyanomethylene groups, but also alters the electronic structure. In this connection, 4,4'-binaphtho[2,3-c][1,2,5]thiadiazolylidene]-9,9'-dion (**27**) is of interest to evaluate the effects of 1,2,5-thiadiazole ring on a conformational behavior. This compound is closely related to bianthrone (**21**) and prepared by Neidlein et al. However its structural and conformational information were not given.[18] Thus, the properties of **27** were investigated in this work.

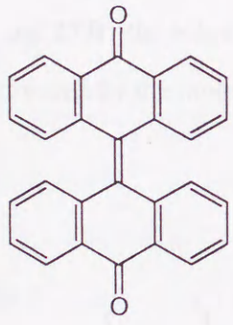


**21**

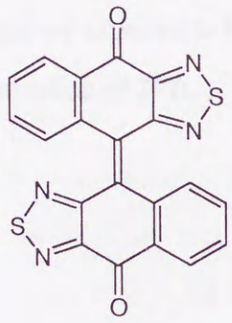


**27**

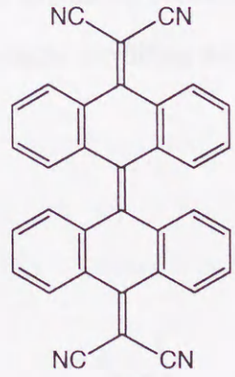


**28**

Although dion **27** was reported to be yellow crystals, the appearance of the crystals differs in color depending on the recrystallization solvents; the yellow microcrystalline material [**27**; mp. 306-308 °C (decomp.)] was obtained from chlorobenzene, while the red cubes [**27**•(dioxane)$_{0.5}$; mp 180 °C (decomp.)] were formed from 1,4-dioxane. Upon grinding in a mortar, the yellow solid turned purple, indicating the mechanochromic behavior. The resulting purple powder changed back to yellow upon heating at 180 °C. Furthermore, both yellow and

red crystals show a identical reddish color solution in organic solvents. These phenomena are quite similar to **20** and absent in **21**.[19]

Many attempts to prepare a single crystal of the yellow form were failed. However X-ray analysis on the **27**•(dioxane)$_{0.5}$ crystal was successfully carried out. As shown in Figure 14, it was found that **27** adopts folded-twisted structure (**27ft**) with weak pyramidalization of the carbon atoms at the central C=C bond. The central six-membered ring slightly deforms into the boat-like geometry with the dihedral angles of 16.1° and 16.8°. The twist angles around the central C=C bond (133.1° for C2-C3-C13-C12; -36.4° for C2-C3-C13-C14; 37.7° for C4-C3-C13-C12; 152.8° for C4-C3-C13-C12) in **27ft** are smaller than those in **21t**, whereas the distance is almost identical (1.387 Å for **27ft**; 1.388 Å for **21t**). Figure 15 represents the packing arrangement in **27**•(dioxane)$_{0.5}$. In the crystal, the C-H•••O hydrogen bonding between oxygen atom at the carbonyl group and aromatic hydrogen is operative, resulting in the dyad formation. In addition, the dyads are connected each other by the S•••N contacts between thiadiazole rings. Because of the absence of any attractive interaction between the solvent and **27ft**, the solvent molecules are expected to be only available for filling the spatial cavities formed by the molecular deformation of **27ft**.

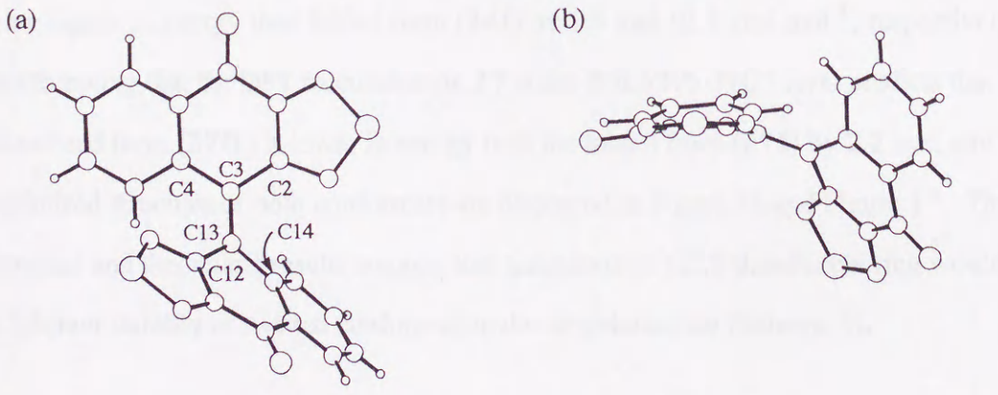


**Figure 14**. (a) Molecular structure of **27**•dioxane$_{0.5}$ (top view). (b) Side view.

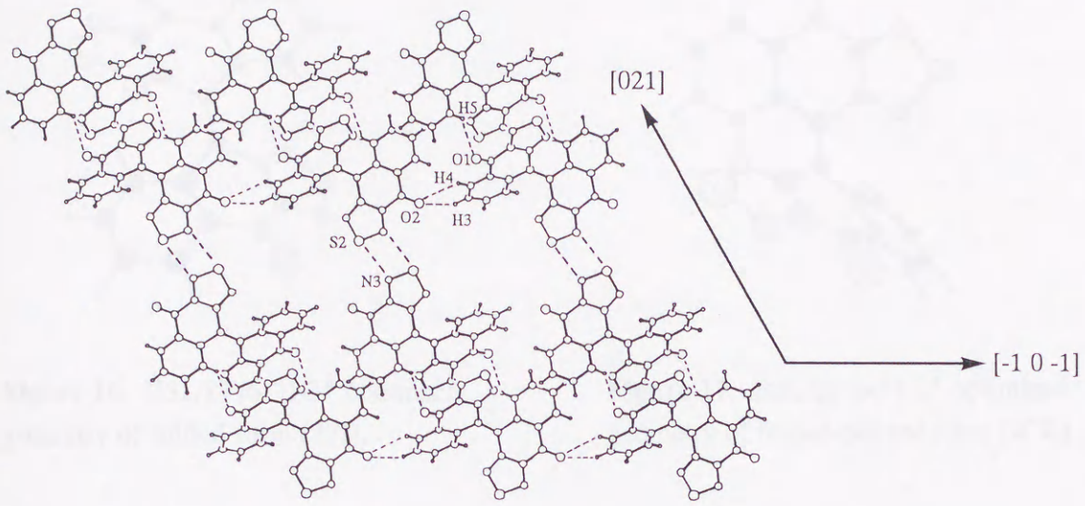


**Figure 15**. Molecular arrangement on the (12$\bar{1}$) plane. Dioxane molecules are omitted for clarity. Short S ••• N contacts of 3.04 Å (S2-N3) and C-H ••• O contacts of 2.59 (O1-H5), 2.68 (O2-H3), and 2.77 Å (O2-H4) are indicated by dotted lines. Another C-H ••• O contacts of 2.66 Å (O1-H7) are also present in crystal.

The folded-twisted conformer of bis(tricyclic) olefin has not been isolated so far, however, the donor-acceptor substituted olefin **24** give the same kind of conformer.[11] Semi-empirical calculation on **24** suggests that the folded-twisted form (**24ft**) and the twisted form (**24t**) are higher in energy than folded form (**24f**) by 1.9 and 12.3 kcal mol$^{-1}$, respectively.[11] It is worth noting that the DFT calculation on **27** at the B3LYP/6-31G* level predicts that the folded-twisted form (**27ft**) is lower in energy than the folded form (**27f**) by 2.2 kcal mol$^{-1}$. The optimized structure of both conformers are displayed in Figure 16 and Figure 17. These experimental and theoretical results suggest that annelation of 1,2,5-thiadiazole ring would lead to the inherent stability of twisted conformation due to polarization (Scheme 4).

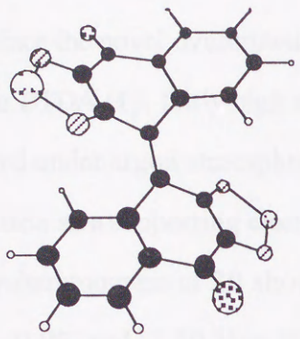

**Figure 16**. B3LYP/6-31G* optimized geometry of folded form (**27f**).

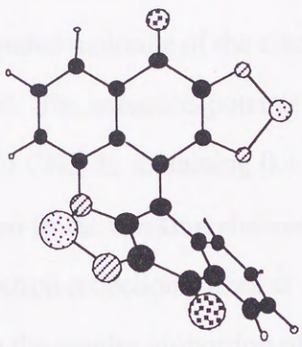

**Figure 17**. B3LYP/6-31G* optimized geometry of folded-twisted form (**27ft**).

**Scheme 4**

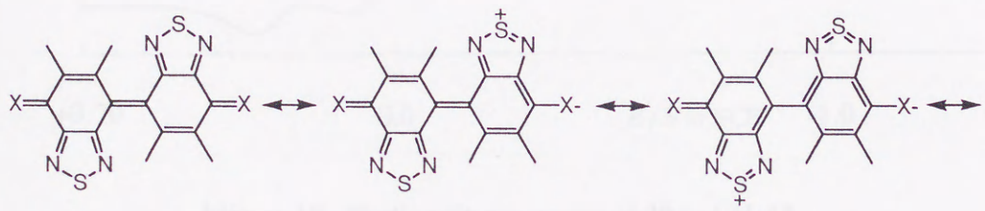

## 4-7. Redox Properties of 20

Since the novel overcrowded ethylene **20** is a π-extended molecule of the electron acceptor BTDA (**1**), fairly high electron affinity is expected. The reduction potential of **20** was measured under argon atmosphere by cyclic voltammetry in $CH_2Cl_2$ containing 0.1 mol $dm^{-3}$ $n$Bu$_4$NBF$_4$ as a supporting electrolyte and Pt wire was used as the working electrode. The cyclic voltammogram of **20** shows four reversible one-electron reduction waves at +0.28, +0.06, -0.95, and -1.10 V vs SCE (Figure 18). Although the precise proportion of **20f/20t** in solution is not known, the cyclic voltammogram of **20** can be explained by the presence of only one conformer (**20t**) (Scheme 5).

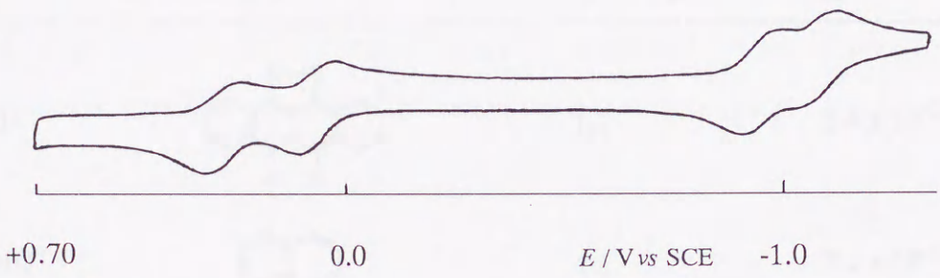


**Figure 18.** Cyclic voltammogram of **20** in $CH_2Cl_2$.

**Scheme 5**

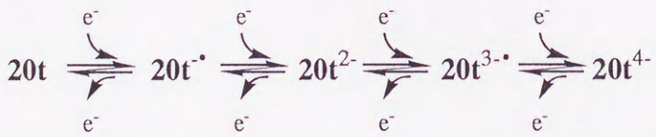


The electron affinity of **20** is similar to that of TCNQ ($E_1^{red}$ = +0.30 V) and much higher than those of **1** or its bis(dicyanomethylene) derivative ($E_p^{red}$ = -1.16 and -0.77 V, under the same conditions). Hence, **20** was readily reduced by the reaction with iodide ion, leading to the formation of stable anion radical salts with *N*-methylquinolinium ($NMQ^+$) and *N*-methylacridinium ($NMAc^+$) as the counter cations. In contrast, when relatively smaller counter cations ($Na^+$, $n$Bu$_4$N$^+$, Et$_4$N$^+$, and *N*-methylpyridinium) were used, no anion radical salt was

formed. Also, attempts to prepare CT crystals with some TTF derivatives were failed.[20] Interestingly, despite its severely deformed geometry, **20** gave the CT complex with tetrathiatetracene (TTT). Their electrical conductivities of **20**•TTT as well as two anion radical salts are summarized in Table 2. It remains still unknown what kind of guest molecules are preferable for the complexation with **20t**, apparent shape dependence of counter molecules was found both in the neutral and in the ionic state during the crystallization.

**Table 2.** Room Temperature Conductivities[a] of CT Complexes and Anion-radical Salts

| Donor or Cation (D) | Ratio (D : **20**)[b] | $\sigma_{r.t.}$ / S cm$^{-1}$ |
|---|---|---|
| TTT 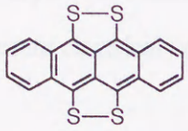 | 1:1 | $3.4 \times 10^{-2}$ |
| $NMQ^+$ 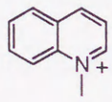 | 1:1 | $3.2 \times 10^{-3}$ |
| $NMAc^+$ 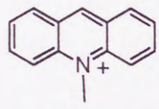 | 1:1 | $6.2 \times 10^{-4}$ |

[a] Measured by a four-probe method on compaction samples. [b] Determined on the basis of elemental analyses.

## 4-8. Conclusion

The newly prepared bis(tricyclic) olefin **20** showed reversible mechano- and thermochromic behavior based on the interconvertible folded and twisted conformers. This is the first interconvertible overcrowded ethylene of which both conformers can be isolated and their geometry unambiguously determined by X-ray analyses. X-ray analyses reveal that **20** adopts folded geometry in the thermally stable yellow crystal and twisted geometry in the violet solvated crystal, respectively. The stabilization by S•••N≡C interaction may be responsible for the preference of the folded conformer in the solid state. On the other hand, UV-Vis and CV measurement suggest that only the twisted conformer exists in solution. In addition, **20** possesses high electron affinity among other overcrowded ethylenes, resulting in the formation of stable charge-transfer crystal and anion radical salts. In spite of severely deformed structure of **20**, they exhibit moderate electrical conductivities.

## Experimental Section

**Bi{4*H*,8*H*-4-(dicyanomethylene)benzo[1,2-*c*:4,5-*c*']bis[1,2,5]thiadiazol-8-ylidene} (20).** A mixture of **26**[14] (330 mg, 1.28 mmol) and $SeO_2$ (630 mg, 5.68 mmol) in 30 mL of EtOH was heated under reflux for 18 h. After filtration, the precipitate was washed with EtOH and ether. The resulting brown solid was extracted with benzene in a Soxhlet apparatus to give deep purple solution. After removal of solvent, recrystallization from PhCN afforded 229 mg of **20t**•$(PhCN)_2$ (50%) as deep violet lustrous cubes: mp 84-86 °C dec; IR (KBr) 2220 $cm^{-1}$. Anal. Calcd for $C_{32}H_{10}N_{14}S_4$: C, 53.47; H, 1.40; N, 27.28. Found: C, 53.35; H, 1.56; N, 27.42. Upon heating at 150 °C *in vacuo*, the solvent molecules in **20t**•$(PhCN)_2$ was removed to give pure **20** as yellow powder: mp 351-357 °C dec; IR (KBr) 2220 $cm^{-1}$; FD-MS *m/z* 512 ($M^+$, 100). Anal. Calcd for $C_{18}N_{12}S_4$: C, 42.18; N, 32.79; S, 25.02. Found: C, 42.25; H, 32.99; S, 24.82. Recrystallization from 1,2-dichloroethane afforded yellow plates of **20f**. Alternatively, $CH_2Cl_2$ was used for recrystallization solvent, the violet fine needles of **20t**•$(CH_2Cl_2)$ were obtained: mp 110-112 °C dec, Anal. Calcd for $C_{19}H_2N_{12}S_4Cl_2$: C, 38.20; N, 0.34; N, 28.13. Found: C, 38.80; H, 0.66; S, 28.26.

**Preparation of a CT Crystal and Anion Radical Salts.**

**TTT•20.** To a hot solution of **20** (11 mg, .0.0215 mmol) in 45 mL of 1,2-dichloroethane was added a saturated solution of TTT (8 mg, 0.0227 mmol) of 1,2-dichloroethane, and the mixture was allowed to stand. After cooling, TTT•**20** (16 mg) was filtered and dried: black powder; IR (KBr) 2220 $cm^{-1}$. Anal. Calcd for $C_{36}H_{10}N_{12}OS_4$: C, 48.97 H, 1.14; N, 19.03. Found: C, 49.25; H, 1.51; N, 18.94.

**DBTTF•20.** To a hot solution of **20** (29 mg, .0.0403 mmol) in 40 mL of 1,2-dichloroethane was added a solution of DBTTF (31 mg, 0.102 mmol) in 4 mL of 1,2-dichloroethane, and the mixture was allowed to stand. After cooling, DBTTF•**20** (16 mg) was filtered and dried: deep violet fiber; IR (KBr) 2222 $cm^{-1}$. Anal. Calcd for $C_{32}H_8N_{12}S_8$: C, 47.04 H, 0.99; N, 20.57. Found: C, 46.99; H, 1.27; N, 20.43.

**$NMQ^+$•20.** To a hot solution of **20** (26 mg, .0.051 mmol) in 40 mL of 1,2-dichloroethane was added a solution of $NMQ^+I^-$ (83 mg, 0.306 mmol) in 5 mL of 1,2-

dichloroethane, and the mixture was allowed to stand. After cooling, $NMQ^{+}$•**20** (29 mg) was filtered and dried: dark violet powder; IR (KBr) 2188, 1436, 1266 $cm^{-1}$. Anal. Calcd for $C_{28}H_{10}N_{13}S_4$: C, 51.21 H, 1.53; N, 27.73. Found: C, 50.99; H, 1.78; N, 27.06.

**$NMAc^{+}$•20.** To a hot solution of **20** (26 mg, .0.051 mmol) in 40 mL of 1,2-dichloroethane was added a solution of $NMAc^{+}I^{-}$ (93 mg, 0.305 mmol) in 5 mL of 1,2-dichloroethane, and the mixture was allowed to stand. After cooling, $NMAc^{+}$•**20** (24 mg) was filtered and dried: dark violet powder; IR (KBr) 2188, 1476, 1392, 1162 $cm^{-1}$. Anal. Calcd for $C_{32}H_{12}N_{13}S_4$: C, 514.38 H, 1.71; N, 25.76. Found: C, 53.60; H, 1.94; N, 24.90.

**Electrical Resistivity Measurements.** All the electrical resistivity of CT crystals and anion radical salts were measured by four probe method on compressed pellets. Gold wires were attached to the pellet with Au paste. Direct current was generated by YOKOGAWA 7651 programmable DC source and the potential difference was measured on KEITHLEY 2001 digital multimeter.

**X-Ray Structural Analysis of 20f.** A yellow plate-like crystal with dimensions of 0.35 x 0.35 x 0.15 mm was obtained upon recrystallization of **20** from 1,2-dichloroethane. Intensity data collection was performed on a Rigaku AFC-7R rotating anode diffractometer by using graphite monochromated Mo-K$\alpha$ radiation ($\lambda$ = 0.71073 Å). A total of 2672 unique data was collected within $2\theta$ = 58° at 295 K with a scan speed of 4° $min^{-1}$. Crystal data are as follows: $C_{18}N_{12}S_4$, *M* 512.52, monoclinic, $P2_1/c$, *a* = 10.226(2), *b* = 7.820(1), *c* = 11.725(1) Å, $\beta$ = 91.03(1)°, *V* = 937.5(3) $Å^3$, *Dc* (Z = 2) = 1.816 g $cm^{-1}$, $\mu$ = 5.48 $cm^{-1}$. The structure was solved by Patterson methods. Refinement by full-matrix least-squares method on *F* (anisotropic temperature factors) gave the final *R* value of 0.039 for 2017 reflections with $I > 3\sigma I$ and 154 parameters. Residual electron density was 0.40 e $Å^{-3}$.

**X-Ray Structural Analysis of 20t•(PhCN)$_2$.** A violet cube-like crystal with dimensions of 0.45 x 0.50 x 0.35 mm was obtained upon recrystallization of 2 from PhCN. Intensity data collection was performed on a Mac Science MXC18 rotating anode diffractometer by using graphite monochromated Mo-K$\alpha$ radiation ($\lambda$ = 0.71073 Å). A total of 6137 unique data was collected within $2\theta$ = 55° at 296 K with a scan speed of 6° $min^{-1}$. Crystal data are as follows: $C_{32}H_{10}N_{14}S_4$, *M* 718.77, monoclinic, $P2_1/n$, *a* = 13.554(2), *b* =

26.348(5), $c$ = 8.929(1) Å, $\beta$ = 97.56(1)°, $V$ = 3161.2(9) Å$^3$, $Dc$ (Z = 4) = 1.511 g cm$^{-1}$, $\mu$ = 4.68 cm$^{-1}$. The structure was solved by the direct method by using the CRYSTAN program. Hydrogen atoms were located at the calculated positions. Refinement by full-matrix least-squares method on $F$ (anisotropic temperature factors for non-H atoms) gave the final $R$ value of 0.061 for 5042 reflections with $|F| > 3\sigma|F|$ and 553 parameters. Residual electron density was 0.36 e Å$^{-3}$.

**X-Ray Structural Analysis of 27•(dioxane)$_{0.5}$.** A reddish plate with a dimension of 0.15 x 0.20 x 0.30 nm was obtained upon recrystallization from 1,4-dioxane. Intensity data collection was performed on a a Rigaku AFC-5R rotating anode diffractometer by using graphite monochromated Mo-K$\alpha$ radiation ($\lambda$ = 0.71069 Å). A total of 4137 unique data was collected within $2\theta$ = 55° at 150 K with a scan speed of 8° min$^{-1}$. Crystal data are as follows: $C_{22}H_{12}N_4O_3S_2$, $M$ 444.48, triclinic, $P\bar{1}$, $a$ = 10.9362(9), $b$ = 12.331(2), $c$ = 7.1455(8) Å, $\alpha$ = 97.01(1)°, $\beta$ = 100.475(8)°, $\gamma$ = 72.338(8)°, $V$ = 900.5(2) Å$^3$, $Dc$ (Z = 2) = 1.639 g cm$^{-1}$, $\mu$ = 3.33 cm$^{-1}$. The structure was solved by the direct method (SIR92) and expanded using Fourier techniques (DIRDIF94). Hydrogen atoms were located in the D-map and refined isotropically. The final cycle of full-matrix least-squares refinement was based on 3262 observed reflections [$I > 3\sigma(I)$] and 328 parameters and converged with the $R$ value of 0.033. Residual electron density is 0.29 e Å$^{-3}$.

## References and Notes

(1) The solid-state photoreaction of two-component molecular crystals described in chapter 1 also seems promising candidates, however, in that case, other factors such as charge-transfer interaction would be operative significantly both in determining the crystal structure and the chemical reactivities.

(2) Tidwell, T. T. *Tetrahedron*, **1978**, *34*, 1855.

(3) (a) Feringa, B. L.; Jager, W. F.; de Lange, B.; Meijer, E. W. *J. Am. Chem. Soc.* **1991**, *113*, 5468. (b) de Lange, B.; Jager, W. F.; Feringa, B. L. *Mol. Cryst. Liq. Cryst.* **1992**, *217*, 129; *idem., ibid.* **1992**, *217*, 133. (c) Feringa, B. L.; Jager, W. F.; de Lange, B. *Tetrahedron* **1993**, *49*, 8267. (d) Jørgensen, M; Lerstrup, K.; Frederiksen, P.; Bjørnholm, T.; Sommer-Larsen, P.; Schaumburg, K.; Brunfeldt, K.; Bechgaard, K. *J. Org. Chem.* **1993**, *58*, 2785.

(4) Bercovici, T.; Korenstein, R.; Muszkat, K. A.; Fisher, E. *Pure Appl. Chem.* **1970**, *24*, 531.

(5) (a) Harnik, E.; Schmidt, G. M. J. *J. Chem. Soc.* **1954**, 3295. (b) Agranat, I.; Tapuhi, Y. *J. Org. Chem.* **1979**, *44*, 1941.

(6) (a) Meyer, H. *Monatsh. Chem.* **1909**, *30*, 165. (b) Y. Hirshberg, E. Fisher, *J. Chem. Soc.* **1953**, 629; D. L. Fanselow, H. G. Drickamer, *J. Chem. Phy.* **1974**, *61*, 4567.

(7) Korenstein, R.; Muszkat, K. A.; Sharafy-Ozeri, S. *J. Am. Chem. Soc.* **1973**, *95*, 6177.

(8) Mills, J. F. D.; Nyburg, S. C. *J. Chem. Soc.* **1963**, 308.

(9) Lee, J.-S.; Nyburg, S. C. *Acta Crystallogr. Sect C* **1985**, *41*, 560.

(10) Schönberg, A.; Singer, E.; Stephan, W.; Sheldric, W. S. *Tetrahedron*, **1983**, *39*, 2429.

(11) Stezowski,J. J.; Biedermann, P. U.; Hildenbrand, T.; Dorsch, J. A.; Eckhardt, C. J. ; Agranat, I. *J. Chem. Soc., Chem. Commun.* **1993**, 213.

(12) Beck, A.; Gompper, R.; Polborn, K.; Wagner, H. -U. *Angew. Chem.* **1993**, *105*, 1424; *Angew. Chem. Int. Ed. Engl.* **1993**, *32*, 1352.

(13) (a) Evans, D. H.; Xie, N. *J. Am. Chem. Soc.* **1983**, *105*, 315. (b) Evans, D. H.; Busch, R. W. *ibid.* **1982**, *104*, 5057. (c) Neta, P.; sEvans, D. H. *ibid.* **1981**, *103*, 7041. (d) Olsen, B. A.; Evans, D. H. *ibid.* **1981**, *103*, 839.

(14) Suzuki, T.; Fujii, H.; Yamashita, Y.; Kabuto, C.; Tanaka, S.; Harasawa, M.; Mukai, T.; Miyashi, T. *J. Am. Chem. Soc.* **1992**, *114*, 3034.

(15) Gaussian 94, Revision E.2, Frisch, M. J.; Trucks, G. W.; Schlegel, H. B.; Gill, P. M. W.; Johnson, B. G.; Robb, M. A.; Cheeseman, J. R.; Keith, T.; Petersson, G. A.; Montgomery, J. A.; Raghavachari, K.; Al-Laham, M. A.; Zakrzewski, V. G.; Ortiz, J. V.; Foresman, J. B.; Cioslowski, J.; Stefanov, B. B.; Nanayakkara, A.; Challacombe, M.; Peng, C. Y.; Ayala, P. Y.; Chen, W.; Wong, M. W.; Andres, J. L.; Replogle, E. S.; Gomperts, R.; Martin, R. L.; Fox, D. J.; Binkley, J. S.; Defrees, D. J.; Baker, J.; Stewart, J. P.; Head-Gordon, M.; Gonzalez, C.; Pople, J. A.; Gaussian, Inc., Pittsburgh PA, 1995

(16) The C=C stretching band was also observed at 1551 $cm^{-1}$ in **20t**•$CH_2Cl_2$

(17) Yamaguchi, S.; Hanafusa, T.; Tanaka, T.; Sawada, M.; Kondo, K.; Irie, M.; Tatemitsu, H.; Sakata, Y.; Misumi, S. *Tetrahedron Lett.* **1986**, *27*, 2411.

(18) Neidlein, R.; Droste-Tran-Viet, D.; Gieren, A.; Kokkinidis, M.; Wilckens, R.; Geserich, H.-P.; Ruppel, W. *Helv. Chim. Acta* **1984**, *67*, 574.

(19) The preparation of yellow and red crystals of **27** and the spectroscopic detection of the interconversion are described in detail: Chiba, B. S. Thesis, Tohoku University, 1999.

(20) Only dibenzo-TTF (DBTTF) afforded the CT crystal with **20** but it was found to be insulator.

# *Acknowledgment*

The present work has been carried out under the supervision of Professor Tsutomu Miyashi at the Department of Chemistry, Graduate School of Science, Tohoku University. The author would like to express his sincere gratitude to Professor Miyashi for his helpful suggestions and comments.

The work described in the Chapter 4 was conducted in collaboration with Professor Takashi Tsuji at the Division of Chemistry, Graduate School of Science, Hokkaido University. The author is deeply grateful to Professor Tsuji for his valuable suggestions and advice.

The author would like to express his sincere gratitude to Professor Takanori Suzuki, Division of Chemistry, Graduate School of Science, Hokkaido University, for his continuous interest in this work and fruitful discussions. The author owes this work much to thoughtful and helpful comments of Professor Suzuki. The author wishes to express his thanks Ms. Ritsuko Suzuki for encouragement.

The author wishes to thank Professor Tsutomu Kumagai, Tohoku University, for his kind suggestions and instructive advice for ab initio calculations. The author is indebted to Professor Yasutake Takahashi, Chemistry Department for Materials, Faculty of Engineering, Mie University, and Dr. Hiroshi Ikeda, Tohoku University, for valuable comments. The author would like to express his thanks to Professor Yoshiro Yamashita, Institute for Molecular Science, for his kind advice and help in the X-ray measurements.

The author wishes to thank Dr. Chizuko Kabuto, Tohoku University, for her help in X-ray analyses. The author is grateful to Professor Kuninobu Kabuto, Tohoku University, for his help in the polarimetric measurements. The author is also indebted to Professor Tamotsu Inabe, Division of Chemistry, Graduate School of Science, Hokkaido University, for the use of the X-ray analysis system and FT-IR instrument. The author gratefully acknowledges all the staffs in the Instrumental Analysis Center for Chemistry, Graduate School of Science, Tohoku University, for their technical assistance.

The author thanks Dr. Masatoshi Ando, Dr. Shinji Tarutani, and Dr. Masahiro Okuyama for their encouragement. The author is thankful to all the members in the Miyashi laboratory for their kind assistance and encouragement.

Finally, the author would like to express his sincere gratitude to his family and Ms. Rieko Fukushima for all their help and encouragement.

Department of Chemistry

Graduate School of Science

Tohoku University

Takanori Fukushima

August 1999

*Appendix X-ray Diffraction Data*

## Chapter 1

### Charge-Transfer Crystal of *o*-Divinylbenzene and BTDA (oDV•1)

**Table 1.** Positional parameters and Equivalent Temperature Factors ($Å^2$)

| ATOM | X | Y | Z | Beq |
|---|---|---|---|---|
| S 1 | 0.8153(1) | 0(0) | 0.7294(2) | 4.6 |
| S 2 | 1.5419(1) | -0.1689(1) | 0.8278(2) | 4.2 |
| N 1 | 0.8646(4) | -0.0915(2) | 0.7042(6) | 3.7 |
| N 2 | 1.4907(4) | -0.0762(2) | 0.8522(6) | 3.8 |
| N 3 | 0.9816(5) | 0.0412(2) | 0.7838(6) | 4.1 |
| N 4 | 1.3752(5) | -0.2095(2) | 0.7732(6) | 3.9 |
| N 5 | 1.1690(7) | 0.1982(3) | 0.9421(9) | 7.1 |
| N 6 | 1.1876(5) | -0.3673(3) | 0.6238(9) | 6.9 |
| N 7 | 1.5961(5) | 0.1079(3) | 0.9279(8) | 5.7 |
| N 8 | 0.7604(6) | -0.2651(4) | 0.5396(9) | 6.9 |
| C 1 | 1.0190(5) | -0.0929(3) | 0.7392(6) | 3.1 |
| C 2 | 1.3404(5) | -0.0752(3) | 0.8173(6) | 3.0 |
| C 3 | 1.0844(5) | -0.0170(3) | 0.7858(6) | 3.1 |
| C 4 | 1.2735(5) | -0.1523(3) | 0.7736(6) | 3.0 |
| C 5 | 1.2497(5) | -0.0027(3) | 0.8293(6) | 3.0 |
| C 6 | 1.1081(5) | -0.1653(3) | 0.7232(6) | 3.0 |
| C 7 | 1.3109(5) | 0. 0693(3) | 0.8785(7) | 3.3 |
| C 8 | 1.0453(5) | -0.2369(3) | 0.6625(7) | 3.6 |
| C 9 | 1.2237(6) | 0.1401(3) | 0.9082(8) | 4.5 |
| C 10 | 1.1319(6) | -0.3073(3) | 0.6466(8) | 4.4 |
| C 11 | 1.4725(6) | 0.0870(3) | 0.9069(7) | 4.0 |
| C 12 | 0.8824(6) | -0.2491(3) | 0.5976(8) | 4.5 |
| C 21 | 0.1458(6) | -0.0882(3) | 0.2614(7) | 4.0 |
| C 22 | 0.2904(6) | -0.0569(3) | 0.3170(6) | 4.0 |
| C 23 | 0.4190(7) | -0.1097(4) | 0.3301(8) | 5.4 |
| C 24 | 0.3975(8) | -0.1885(4) | 0.2886(8) | 6.3 |
| C 25 | 0.2538(8) | -0.2192(4) | 0.2296(9) | 6.0 |
| C 26 | 0.1290(6) | -0.1710(4) | 0.2178(7) | 4.9 |
| C 27 | 0.0049(6) | -0.0378(3) | 0.2444(8) | 4.8 |
| C 28 | -0.1368(7) | -0.0626(5) | 0.2203(9) | 6.1 |
| C 29 | 0.3195(6) | 0.0283(4) | 0.3669(7) | 4.7 |
| C 30 | 0.4491(8) | 0.0675(5) | 0.3836(9) | 6.6 |

**Table 1.** (Continued).

| ATOM | X | Y | Z | Beq |
|---|---|---|---|---|
| H 23 | 0.523(7) | -0.075(4) | 0.418(8) | 7.7(1.6) |
| H 24 | 0.477(7) | -0.237(4) | 0.322(8) | 7.5(1.6) |
| H 25 | 0.244(7) | -0.284(4) | 0.207(8) | 7.2(1.6) |
| H 26 | 0.034(7) | -0.194(4) | 0.212(8) | 8.4(1.7) |
| H 27 | 0.035(7) | 0.032(4) | 0.229(8) | 9.0(1.8) |
| H281 | -0.230(6) | -0.027(3) | 0.170(8) | 7.8(1.7) |
| H282 | -0.158(7) | -0.126(4) | 0.165(9) | 8.9(1.8) |
| H 29 | 0.230(6) | 0.062(3) | 0.403(7) | 6.0(1.4) |
| H301 | 0.548(7) | 0.043(4) | 0.374(8) | 8.4(1.8) |
| H302 | 0.420(8) | 0.136(5) | 0.384(9) | 11.0(2.1) |

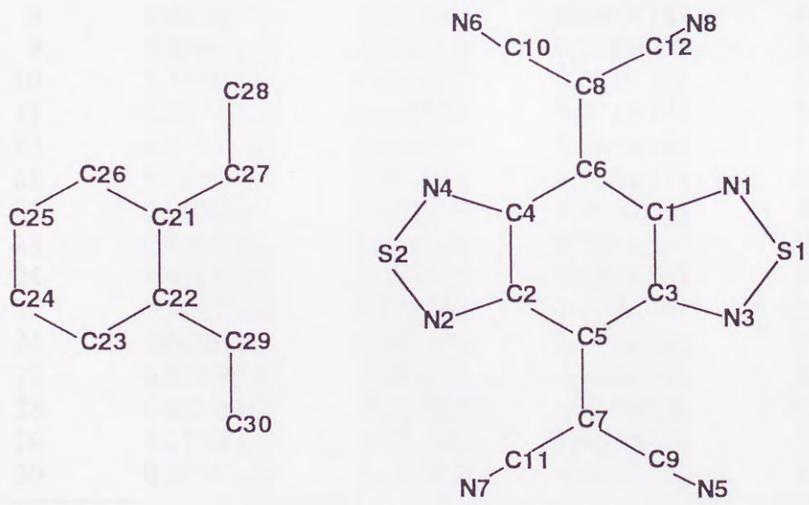


**Figure 1.** Atomic numbering system.

**Table 2.** Positional parameters and Equivalent Temperature Factors ($Å^2$)

| ATOM | X | Y | Z | Beq |
|---|---|---|---|---|
| S 1 | 0.8910(3) | 0.1448(1) | 0.4921(4) | 6.0 |
| S 2 | 0.2902(3) | 0.3234(1) | 0.4879(4) | 5.1 |
| N 1 | 0.8956(8) | 0.2356(4) | 0.5668(10) | 4.8 |
| N 2 | 0.2833(7) | 0.2312(4) | 0.4137(9) | 4.2 |
| N 3 | 0.7050(8) | 0.1075(4) | 0.4136(11) | 5.0 |
| N 4 | 0.4746(8) | 0.3620(4) | 0.5585(9) | 4.3 |
| N 5 | 0.4211(11) | -0.0491(5) | 0.1980(14) | 8.1 |
| N 6 | 0.7613(11) | 0.5220(4) | 0.7391(14) | 7.6 |
| N 7 | 0.705(10) | 0.0491(5) | 0.2555(16) | 8.4 |
| N 8 | 0.11084(9) | 0.4182(5) | 0.7178(15) | 8.3 |
| C 1 | 0.7498(9) | 0.2406(4) | 0.5307(10) | 3.7 |
| C 2 | 0.4290(8) | 0.2273(4) | 0.4478(10) | 3.4 |
| C 3 | 0.6392(9) | 0.1661(4) | 0.4419(11) | 4.1 |
| C 4 | 0.5400(9) | 0.3029(4) | 0.5303(10) | 3.4 |
| C 5 | 0.4730(9) | 0.1544(4) | 0.3951(11) | 3.8 |
| C 6 | 0.7084(8) | 0.3143(4) | 0.5736(10) | 3.5 |
| C 7 | 0.3665(10) | 0.0824(5) | 0.3159(12) | 4.5 |
| C 8 | 0.8130(9) | 0.3872(5) | 0.6463(11) | 4.2 |
| C 9 | 0.4044(11) | 0.0111(5) | 0.2582(13) | 5.3 |
| C 10 | 0.7745(10) | 0.4606(5) | 0.6929(13) | 5.2 |
| C 11 | 0.2017(10) | 0.0685(5) | 0.2833(14) | 5.3 |
| C 12 | 0.9753(10) | 0.3989(5) | 0.6848(14) | 5.4 |
| C 21 | 0.6979(12) | 0.3067(5) | 1.0656(11) | 5.9 |
| C 22 | 0.5610(9) | 0.2455(5) | 0.9920(11) | 4.4 |
| C 23 | 0.4166(10) | 0.2597(6) | 0.9711(12) | 5.0 |
| C 24 | 0.4118(15) | 0.3394(7) | 1.0289(15) | 8.5 |
| C 25 | 0.5487(19) | 0.3996(6) | 1.1021(16) | 10.1 |
| C 26 | 0.6879(16) | 0.3836(6) | 1.1219(14) | 8.4 |
| C 27 | 0.8549(12) | 0.2952(8) | 1.0964(15) | 8.1 |
| C 28 | 0.8853(14) | 0.2274(10) | 1.0549(20) | 10.9 |
| C 29 | 0.2736(11) | 0.1954(8) | 0.8966(15) | 7.8 |
| C 30 | 0.2554(12) | 0.1210(7) | 0.8325(17) | 8.6 |

**Table 2.** (Continued).

| ATOM | X | Y | Z | Beq |
|---|---|---|---|---|
| H 23 | 0.564(5) | 0.185(12) | 0.946(12) | 7.4(2.3) |
| H 24 | 0.305(6) | 1.009(15) | 1.009(15) | 10.9(3.0) |
| H 25 | 0.550(6) | 1.144(14) | 1.144(14) | 10.7(3.0) |
| H 26 | 0.800(6) | 1.184(14) | 1.184(14) | 10.2(2.9) |
| H 27 | 0.970(5) | 1.173(13) | 1.173(13) | 8.6(2.6) |
| H 29 | 0.171(5) | 0.882(15) | 0.882(13) | 7.9(2.4) |
| H281 | 1.005(6) | 1.093(15) | 1.093(15) | 11.1(3.1) |
| H282 | 0.787(7) | 0.990(16) | 0.990(16) | 12.6(3.4) |
| H301 | 0.144(6) | 0.778(14) | 0.778(14) | 9.6(2.8) |
| H302 | 0.361(6) | 0.828(15) | 0.828(15) | 10.7(3.0) |

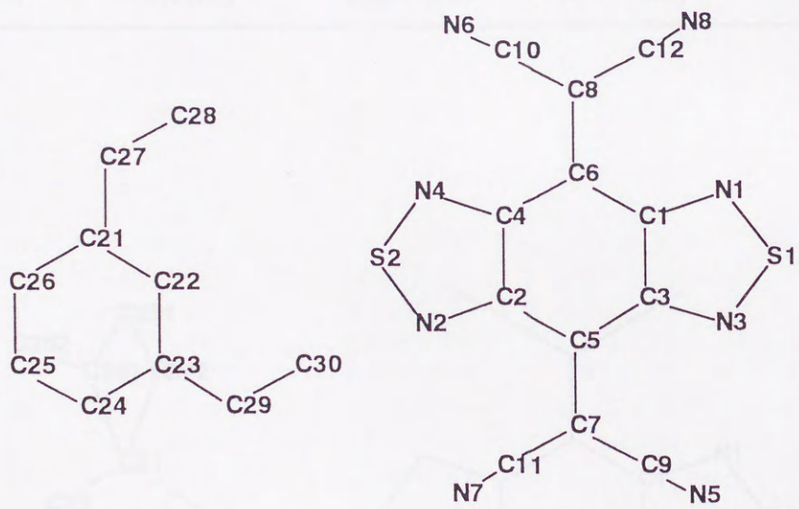


**Figure 2.** Atomic numbering system.

**Table 3.** Positional parameters and Equivalent Temperature Factors ($Å^2$)

| ATOM | X | Y | Z | Beq |
|---|---|---|---|---|
| S 1 | 0.4093(2) | 0.1741(2) | -0.0453(2) | 4.8 |
| N 1 | 0.2892(5) | 0.2626(5) | 0.0338(6) | 4.4 |
| N 3 | 0.2847(5) | -0.0166(5) | -0.1011(6) | 4.4 |
| N 5 | 0.2078(7) | -0.4041(7) | -0.3265(9) | 6.8 |
| N 7 | -0.2306(6) | -0.5965(6) | -0.1623(8) | 6.3 |
| C 1 | 0.1443(6) | 0.1416(6) | 0.0182(7) | 3.6 |
| C 3 | 0.1393(6) | -0.0203(6) | -0.0602(7) | 3.7 |
| C 5 | -0.0032(5) | -0.1710(6) | -0.0836(7) | 3.5 |
| C 7 | -0.0081(6) | -0.3253(6) | -0.1598(7) | 4.0 |
| C 9 | 0.1195(7) | -0.3600(7) | -0.2478(8) | 4.6 |
| C 11 | -0.1390(7) | -0.4723(6) | -0.1610(8) | 4.5 |
| C 21 | 0.1613(8) | 0.0618(10) | 0.4737(9) | 6.5 |
| C 22 | 0.0914(9) | 0.1693(8) | 0.5533(9) | 6.3 |
| C 23 | -0.0702(9) | 0.1069(9) | 0.5780(9) | 6.7 |
| C241 | 0.3443(13) | 0.1672(14) | 0.4657(14) | 6.8 |
| C242 | 0.3196(19) | 0.0403(24) | 0.4019(24) | 5.4 |
| C251 | 0.4407(15) | 0.1346(21) | 0.4143(17) | 10.9 |
| C252 | 4262(28) | 0.3047(36) | 0.5036(36) | 10.3 |

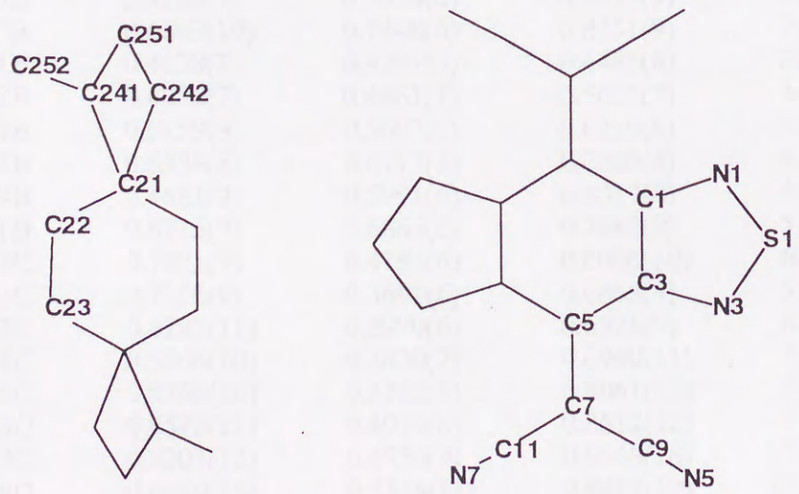


**Figure 3.** Atomic numbering system.

**Table 4.** Positional parameters and Equivalent Temperature Factors ($Å^2$)

| ATOM | X | Y | Z | Beq |
|---|---|---|---|---|
| S 1A | 0.9984(2) | 0.2738(2) | 0.8630(3) | 5.2 |
| S 2A | 0.5689(3) | -0.0298(2) | 0.8176(3) | 6.9 |
| N 1A | 0.9335(7) | 0.2705(5) | 0.9508(7) | 4.7 |
| N 2A | 0.6252(7) | -0.0227(5) | 0.7250(8) | 5.5 |
| N 3A | 0.9273(7) | 0.1919(5) | 0.7516(7) | 4.7 |
| N 4A | 0.6293(7) | 0.0568(5) | 0.9211(8) | 5.3 |
| N 5A | 0.8841(9) | 0.0842(6) | 0.4818(9) | 7.5 |
| N 6A | 0.6464(12) | 0.1790(7) | 1.1641(11) | 10.1 |
| N 7A | 0.6273(12) | -0.0903(8) | 0.4529(10) | 10.9 |
| N 8A | 0.8977(10) | 0.3613(6) | 1.1929(10) | 8.3 |
| C 1A | 0.8515(8) | 0.2021(5) | 0.8998(8) | 3.7 |
| C 2A | 0.6999(7) | 0.0508(5) | 0.7687(8) | 4.0 |
| C 3A | 0.8502(7) | 0.1584(5) | 0.7860(7) | 3.4 |
| C 4A | 0.7010(7) | 0.0966(5) | 0.8852(8) | 3.7 |
| C 5A | 0.7703(7) | 0.0795(5) | 0.7098(8) | 3.5 |
| C 6A | 0.7747(7) | 0.1773(5) | 0.9561(8) | 3.5 |
| C 7A | 0.7658(8) | 0.0418(6) | 0.5988(8) | 4.3 |
| C 8A | 0.7750(9) | 0.2201(5) | 0.10598(9) | 4.4 |
| C 9A | 0.8354(9) | 0.0684(6) | 0.5375(9) | 5.1 |
| C10A | 0.6959(10) | 0.1950(6) | 1.1159(10) | 5.7 |
| C11A | 0.6858(10) | -0.0348(7) | 0.5204(10) | 6.4 |
| C12A | 0.8482(10) | 0.2998(6) | 1.1343(9) | 5.6 |
| S 1B | 0.2745(3) | 0.3789(2) | 0.5149(3) | 5.8 |
| N 1B | 0.3286(7) | 0.3659(5) | 0.4168(7) | 4.8 |
| N 3B | 0.3561(7) | 0.4651(5) | 0.6089(7) | 4.5 |
| N 5B | 0.4266(9) | 0.5958(6) | 0.8693(9) | 7.0 |
| N 7B | 0.6843(10) | 0.7448(6) | 0.8451(9) | 7.7 |
| C 1B | 0.4138(7) | 0.4291(5) | 0.4485(8) | 3.7 |
| C 3B | 0.4276(7) | 0.4861(5) | 0.5621(7) | 3.5 |
| C 5B | 0.5159(8) | 0.5607(5) | 0.6210(8) | 4.0 |
| C 7B | 0.5338(8) | 0.6117(5) | 0.7309(8) | 4.0 |
| C 9B | 0.4681(9) | 0.5991(6) | 0.8017(8) | 4.6 |
| C11B | 0.6215(9) | 0.6865(6) | 0.7883(9) | 5.1 |
| C21C | 0.7271(9) | 0.4197(6) | 0.8026(10) | 6.2 |
| C22C | 0.7150(9) | 0.3691(6) | 0.6868(9) | 5.2 |
| C23C | 0.6282(11) | 0.2990(6) | 0.6326(9) | 6.8 |
| C24C | 0.5566(10) | 0.2820(7) | 0.6960(11) | 7.5 |
| C25C | 0.5768(10) | 0.3322(8) | 0.8061(12) | 7.3 |
| C26C | 0.6573(11) | 0.4019(8) | 0.8612(12) | 7.3 |
| C27C | 0.8201(12) | 0.4956(9) | 0.8668(18) | 11.5 |
| C28C | 0.8849(15) | 0.5316(11) | 0.8467(19) | 12.5 |
| C29C | 0.6148(19) | 0.2476(9) | 0.5123(12) | 14.1 |
| C30C | 0.5913(19) | 0.2065(10) | 0.4336(14) | 13.6 |

**Table 4.** (Continued).

| ATOM | X | Y | Z | Beq |
|---|---|---|---|---|
| C21E | 0.2187(11) | 0.2309(7) | 0.7544(11) | 6.5 |
| C22E | 0.1161(10) | 0.2594(8) | 0.6603(10) | 6.3 |
| C23E | 0.0898(12) | 0.3520(10) | 0.6574(12) | 8.7 |
| C24E | 0.1811(13) | 0.4154(8) | 0.7591(14) | 8.9 |
| C25E | 0.2818(12) | 0.3814(9) | 0.8474(13) | 8.3 |
| C26E | 0.3027(11) | 0.2934(8) | 0.8497(11) | 7.5 |
| C27E | 0.2348(15) | 0.1315(10) | 0.7513(16) | 10.8 |
| C28E | 0.3153(18) | 0.0887(12) | 0.8271(21) | 14.3 |
| C29E | -0.0224(17) | 0.3947(14) | 0.5653(16) | 13.6 |
| C30E | -0.0940(17) | 0.3567(15) | 0.4763(16) | 14.7 |
| C21D | 0.9570(26) | -0.0371(18) | 0.9991(29) | 8.9 |
| C22D | 0.9848(12) | -0.0478(9) | 0.8985(13) | 8.8 |
| C23D | 1.0621(23) | -0.0009(17) | 0.8774(25) | 8.1 |
| C24D | 1.1209(21) | 0.0762(18) | 0.9780(21) | 6.3 |
| C25D | 1.0879(23) | 0.0921(18) | 1.0665(24) | 7.7 |
| C27D | 0.9150(30) | -0.1368(21) | 0.8019(31) | 11.7 |
| C28D | 1.0239(28) | -0.0581(20) | 0.7906(27) | 9.7 |
| C29D | 0.9504(19) | -0.1421(12) | 0.7000(17) | 13.8 |

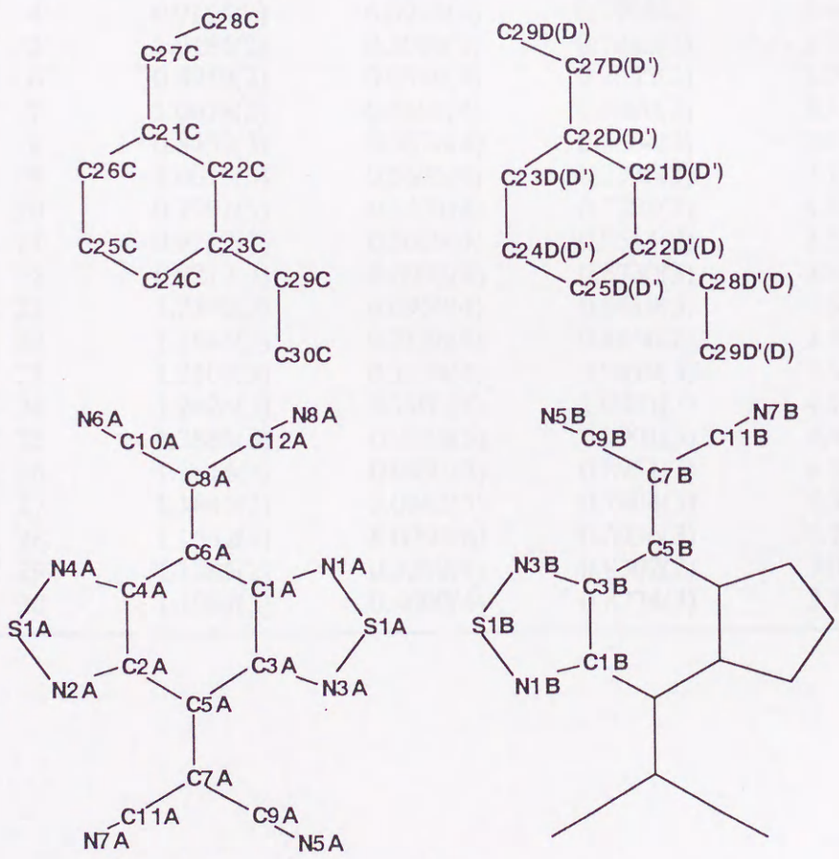


**Figure 4.** Atomic numbering system.

*dl*-2o

**Table 5.** Positional parameters and Equivalent Temperature Factors ($Å^2$)

| ATOM | X | Y | Z | Beq |
|---|---|---|---|---|
| S 1 | 0.9857(1) | 0.2515(1) | 0.5270(1) | 4.6 |
| S 2 | 0.9123(1) | 0.1195(1) | 0.9550(1) | 4.1 |
| N 1 | 0.9297(2) | 0.1274(4) | 0.5597(2) | 3.9 |
| N 2 | 0.9762(2) | 0.2374(3) | 0.9246(2) | 3.4 |
| N 3 | 1.0228(2) | 0.3345(4) | 0.6240(2) | 3.8 |
| N 4 | 0.8790(2) | 0.0339(3) | 0.8595(2) | 3.7 |
| N 5 | 0.9959(4) | 0.6528(5) | 0.6809(3) | 6.6 |
| N 6 | 0.7596(3) | -0.2218(5) | 0.7542(3) | 6.3 |
| N 7 | 0.8755(3) | 0.5342(4) | 0.8859(3) | 5.1 |
| N 8 | 0.7995(3) | -0.1425(4) | 0.5005(3) | 5.3 |
| C 1 | 0.9374(2) | 0.1481(4) | 0.6488(2) | 2.9 |
| C 2 | 0.9709(2) | 0.2160(4) | 0.8368(2) | 2.8 |
| C 3 | 0.9911(2) | 0.2667(4) | 0.6852(2) | 2.9 |
| C 4 | 0.9155(2) | 0.0978(4) | 0.7995(2) | 2.9 |
| C 5 | 1.0184(2) | 0.3099(3) | 0.7842(2) | 2.7 |
| C 6 | 0.8959(2) | 0.0549(4) | 0.7033(2) | 2.9 |
| C 7 | 1.0078(3) | 0.4691(4) | 0.8090(2) | 3.1 |
| C 8 | 0.8432(3) | -0.0576(4) | 0.6684(3) | 3.4 |
| C 9 | 1.0013(3) | 0.5685(4) | 0.7336(3) | 4.1 |
| C 10 | 0.7991(3) | -0.1471(4) | 0.7203(3) | 4.3 |
| C 11 | 0.9317(3) | 0.5039(4) | 0.8514(2) | 3.5 |
| C 12 | 0.8217(3) | -0.0995(4) | 0.5730(3) | 3.9 |
| C 21 | 1.2102(3) | 0.0959(4) | 0.8419(3) | 3.6 |
| C 22 | 1.1845(2) | 0.2128(4) | 0.8856(2) | 2.9 |
| C 23 | 1.2107(3) | 0.2176(4) | 0.9819(3) | 3.5 |
| C 24 | 1.2626(3) | 0.1101(5) | 1.0331(3) | 4.1 |
| C 25 | 1.2886(3) | -0.0019(5) | 0.9901(3) | 4.6 |
| C 26 | 1.2616(3) | -0.0091(5) | 0.8951(3) | 4.5 |
| C 27 | 1.1845(3) | 0.0842(5) | 0.7404(3) | 4.3 |
| C 28 | 1.1552(4) | -0.0298(6) | 0.6936(3) | 5.7 |
| C 29 | 1.1285(2) | 0.3290(4) | 0.8302(2) | 3.0 |
| C 30 | 1.1087(3) | 0.4609(4) | 0.8774(3) | 3.7 |

**Table 5.** (Continued).

| ATOM | X | Y | Z | Beq |
|---|---|---|---|---|
| H 23 | 1.195(3) | 0.309(4) | 1.020(3) | 4.3 |
| H 24 | 1.285(3) | 0.116(4) | 1.104(3) | 4.3 |
| H 25 | 1.322(3) | -0.067(4) | 1.030(3) | 4.9 |
| H 26 | 1.278(3) | -0.086(4) | 0.858(3) | 4.8 |
| H 27 | 1.187(3) | 0.174(4) | 0.704(3) | 4.4 |
| H281 | 1.137(3) | -0.114(4) | 0.722(3) | 4.6 |
| H282 | 1.153(3) | -0.028(5) | 0.635(3) | 5.2 |
| H 29 | 1.159(3) | 0.363(4) | 0.781(3) | 4.2 |
| H301 | 1.146(3) | 0.551(4) | 0.871(3) | 4.9 |
| H302 | 1.110(3) | 0.464(5) | 0.942(3) | 5.2 |

**Table 6.** Bond lengths (Å)

| atom | length | atom | length |
|---|---|---|---|
| S1-N1 | 1.609(4) | C7-C30 | 1.564(6) |
| S1-N3 | 1.628(4) | C8-C10 | 1.440(6) |
| S2-N2 | 1.624(3) | C8-C12 | 1.446(6) |
| S2-N4 | 1.619(4) | C21-C22 | 1.412(5) |
| N1-C1 | 1.335(5) | C21-C26 | 1.384(6) |
| N2-C2 | 1.324(5) | C21-C27 | 1.480(6) |
| N3-C3 | 1.320(5) | C22-C23 | 1.401(5) |
| N4-C4 | 1.327(5) | C22-C29 | 1.504(5) |
| N5-C9 | 1.127(7) | C23-C24 | 1.391(6) |
| N6-C10 | 1.134(7) | C24-C25 | 1.370(7) |
| N7-C11 | 1.133(6) | C25-C26 | 1.384(7) |
| N8-C12 | 1.133(6) | C27-C28 | 1.316(7) |
| C1-C3 | 1.416(5) | C29-C30 | 1.527(5) |
| C1-C6 | 1.465(5) | C23-H23 | 1.11(4) |
| C2-C4 | 1.427(5) | C24-H24 | 1.03(4) |
| C2-C5 | 1.501(5) | C25-H25 | 0.91(4) |
| C3-C5 | 1.499(5) | C26-H26 | 1.00(4) |
| C4-C6 | 1.463(5) | C27-H27 | 1.03(4) |
| C5-C7 | 1.601(5) | C28-H281 | 0.99(4) |
| C5-C29 | 1.592(5) | C28-H282 | 0.87(4) |
| C6-C8 | 1.355(5) | C29-H29 | 1.02(4) |
| C7-C9 | 1.473(6) | C30-H301 | 1.04(4) |
| C7-C11 | 1.477(6) | C30-H302 | 0.96(4) |

**Table 7.** Bond angles (degree)

| atom | angle | atom | angle |
|---|---|---|---|
| N1-S1-N3 | 99.4(1) | N7-C11-C7 | 177.4(4) |
| N2-S2-N4 | 99.3(1) | N8-C12-C8 | 173.1(4) |
| S1-N1-C1 | 106.8(2) | C22-C21-C26 | 119.3(3) |
| S2-N2-C2 | 107.2(2) | C22-C21-C27 | 121.4(3) |
| S1-N3-C3 | 106.9(2) | C26-C21-C27 | 119.2(3) |
| S2-N4-C4 | 106.9(2) | C21-C22-C23 | 118.6(3) |
| N1-C1-C3 | 113.3(3) | C21-C22-C29 | 120.9(3) |
| N1-C1-C6 | 122.9(3) | C23-C22-C29 | 120.3(3) |
| C3-C1-C6 | 123.7(3) | C22-C23-C24 | 120.3(3) |
| N2-C2-C4 | 112.9(3) | C23-C24-C25 | 120.6(4) |
| N2-C2-C5 | 121.9(3) | C24-C25-C26 | 119.5(4) |
| C4-C2-C5 | 125.0(3) | C21-C26-C25 | 121.4(4) |
| N3-C3-C1 | 113.4(3) | C21-C27-C28 | 125.0(4) |
| N3-C3-C5 | 120.8(3) | C5-C29-C22 | 119.6(2) |
| C1-C3-C5 | 125.5(3) | C5-C29-C30 | 89.8(2) |
| N4-C4-C2 | 113.4(3) | C22-C29-C30 | 120.5(3) |
| N4-C4-C6 | 122.7(3) | C7-C30-C29 | 90.1(2) |
| C2-C4-C6 | 123.6(3) | C22-C23-H23 | 122.0(21) |
| C2-C5-C3 | 108.9(2) | C24-C23-H23 | 117.4(21) |
| C2-C5-C7 | 111.4(2) | C23-C24-H24 | 120.5(23) |
| C2-C5-C29 | 114.0(2) | C25-C24-H24 | 118.7(23) |
| C3-C5-C7 | 119.0(2) | C24-C25-H25 | 113.4(27) |
| C3-C5-C29 | 115.4(2) | C26-C25-H25 | 126.9(27) |
| C7-C5-C29 | 86.5(2) | C21-C26-H26 | 113.4(25) |
| C1-C6-C4 | 112.7(3) | C25-C26-H26 | 125.0(25) |
| C1-C6-C8 | 123.8(3) | C21-C27-H27 | 116.9(23) |
| C4-C6-C8 | 123.3(3) | C28-C27-H27 | 117.9(23) |
| C5-C7-C9 | 115.7(3) | C27-C28-H281 | 122.4(25) |
| C5-C7-C11 | 117.1(3) | C27-C28-H282 | 116.1(29) |
| C5-C7-C30 | 88.2(2) | H281-C28-H282 | 121.4(38) |
| C9-C7-C11 | 107.0(3) | C5-C29-H29 | 109.1(23) |
| C9-C7-C30 | 113.0(3) | C22-C29-H29 | 110.5(23) |
| C11-C7-C30 | 115.1(3) | C30-C29-H29 | 104.6(23) |
| C6-C8-C10 | 124.4(3) | C7-C30-H301 | 108.9(23) |
| C6-C8-C12 | 123.9(3) | C7-C30-H302 | 114.7(26) |
| C10-C8-C12 | 111.5(3) | C29-C30-H301 | 118.6(23) |
| N5-C9-C7 | 174.2(5) | C29-C30-H302 | 122.5(26) |
| N6-C10-C8 | 174.0(5) | H301-C30-H302 | 101.6(35) |

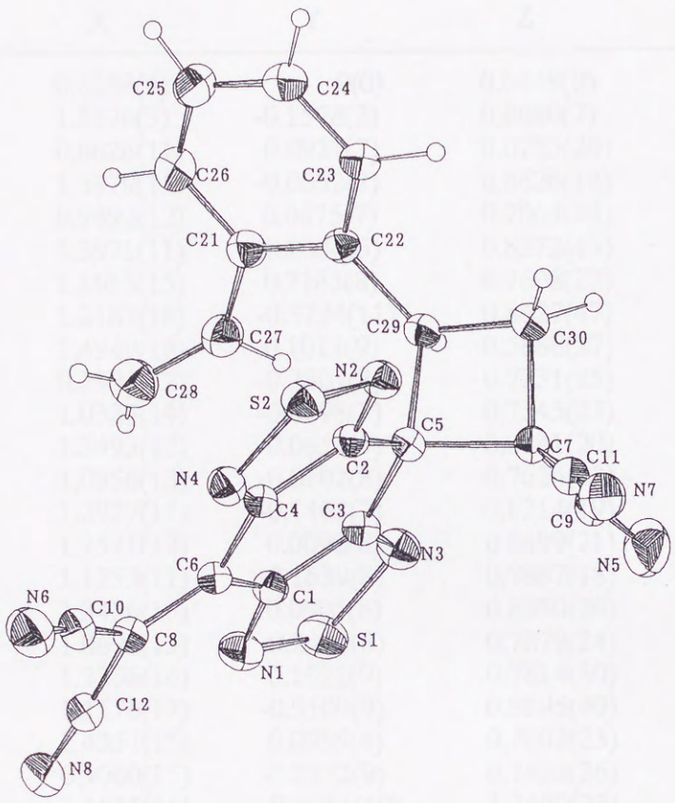


**Figure 5.** Molecular structure with of *dl*-**2o** with atomic numbering system.

**Table 8.** Positional parameters and Equivalent Temperature Factors ($Å^2$)

| ATOM | X | Y | Z | Beq |
|---|---|---|---|---|
| S 1 | 0.8238(4) | 0(0) | 0.6449(9) | 9.2 |
| S 2 | 1.5576(3) | -0.1578(2) | 0.8640(7) | 6.6 |
| N 1 | 0.8826(11) | -0.0921(7) | 0.6755(20) | 7.0 |
| N 2 | 1.4979(11) | -0.0632(7) | 0.8626(18) | 6.1 |
| N 3 | 0.9892(12) | 0.0475(7) | 0.7064(24) | 8.0 |
| N 4 | 1.3971(11) | -0.2034(6) | 0.8372(18) | 5.4 |
| N 5 | 1.1615(15) | 0.2183(8) | 0.7608(27) | 9.9 |
| N 6 | 1.2183(18) | -0.3734(11) | 0.8627(47) | 19.1 |
| N 7 | 1.4949(18) | 0.1011(9) | 0.5880(27) | 10.3 |
| N 8 | 0.7903(12) | -0.2807(8) | 0.7331(25) | 8.9 |
| C 1 | 1.0325(14) | -0.0898(7) | 0.7345(23) | 5.9 |
| C 2 | 1.3493(12) | -0.0655(7) | 0.8341(20) | 4.9 |
| C 3 | 1.0956(13) | -0.0102(8) | 0.7626(22) | 5.4 |
| C 4 | 1.2927(11) | -0.1463(7) | 0.8214(19) | 4.7 |
| C 5 | 1.2571(12) | 0.0092(8) | 0.8499(21) | 5.1 |
| C 6 | 1.1253(11) | -0.1639(8) | 0.7887(18) | 4.4 |
| C 7 | 1.3426(16) | 0.0905(8) | 0.8350(26) | 6.9 |
| C 8 | 1.0698(13) | -0.2421(8) | 0.7879(24) | 6.0 |
| C 9 | 1.2308(16) | 0.1621(9) | 0.7814(30) | 7.8 |
| C 10 | 1.1576(17) | -0.3109(9) | 0.8195(40) | 11.9 |
| C 11 | 1.4351(15) | 0.0955(8) | 0.7102(23) | 5.8 |
| C 12 | 0.9060(15) | -0.2572(9) | 0.7432(26) | 6.6 |
| C 21 | 1.1835(16) | -0.0783(10) | 1.2490(23) | 6.0 |
| C 22 | 1.3180(17) | -0.0408(9) | 1.2171(24) | 6.8 |
| C 23 | 1.4647(16) | -0.0797(9) | 1.2853(25) | 7.2 |
| C 24 | 1.4752(18) | -0.1553(12) | 1.3595(25) | 8.3 |
| C 25 | 1.3460(23) | -0.1599(11) | 1.3769(28) | 9.2 |
| C 26 | 1.1950(18) | -0.1727(11) | 1.3251(25) | 7.8 |
| C 27 | 1.0364(16) | -0.0347(10) | 1.2050(27) | 7.5 |
| C 28 | 0.9017(21) | -0.0727(11) | 1.1742(31) | 9.2 |
| C 29 | 1.2909(14) | 0.0315(8) | 1.0837(21) | 5.4 |
| C 30 | 1.4222(16) | 0.0895(9) | 1.0576(25) | 7.0 |

**Table 9.** Bond lengths (Å)

| atom | length | atom | length |
|---|---|---|---|
| S1-N1 | 1.59(1) | C5-C7 | 1.56(2) |
| S1-N3 | 1.64(1) | C5-C29 | 1.66(2) |
| S2-N2 | 1.64(1) | C6-C8 | 1.37(2) |
| S2-N4 | 1.60(1) | C7-C9 | 1.53(2) |
| N1-C1 | 1.31(2) | C7-C11 | 1.39(2) |
| N2-C2 | 1.31(2) | C7-C30 | 1.55(2) |
| N3-C3 | 1.33(2) | C8-C10 | 1.36(3) |
| N4-C4 | 1.31(1) | C8-C12 | 1.45(2) |
| N5-C9 | 1.10(2) | C21-C22 | 1.44(2) |
| N6-C10 | 1.16(4) | C21-C26 | 1.43(2) |
| N7-C11 | 1.16(2) | C21-C27 | 1.47(2) |
| N8-C12 | 1.10(2) | C22-C23 | 1.43(2) |
| C1-C3 | 1.41(2) | C22-C29 | 1.50(2) |
| C1-C6 | 1.47(2) | C23-C24 | 1.34(2) |
| C2-C4 | 1.41(2) | C24-C25 | 1.41(2) |
| C2-C5 | 1.50(2) | C25-C26 | 1.46(2) |
| C3-C5 | 1.46(2) | C27-C28 | 1.33(3) |
| C4-C6 | 1.50(1) | C29-C30 | 1.58(2) |

**Table 10.** Bond angles (degree)

| atom | angle | atom | angle |
|---|---|---|---|
| N1-S1-N3 | 99(8) | C5-C7-C11 | 119(1) |
| N2-S2-N4 | 98(7) | C5-C7-C30 | 91(1) |
| S1-N1-C1 | 107(1) | C9-C7-C11 | 105(1) |
| S2-N2-C2 | 107(1) | C9-C7-C30 | 110(1) |
| S1-N3-C3 | 106(1) | C11-C7-C30 | 117(1) |
| S2-N4-C4 | 106(1) | C6-C8-C10 | 124(1) |
| N1-C1-C3 | 114(1) | C6-C8-C12 | 120(1) |
| N1-C1-C6 | 122(1) | C10-C8-C12 | 114(1) |
| C3-C1-C6 | 122(1) | N5-C9-C7 | 171(1) |
| N2-C2-C4 | 112(1) | N6-C10-C8 | 169(1) |
| N2-C2-C5 | 122(1) | N7-C11-C7 | 171(1) |
| C4-C2-C5 | 124(1) | N8-C12-C8 | 166(1) |
| N3-C3-C1 | 112(1) | C22-C21-C26 | 118(1) |
| N3-C3-C5 | 122(1) | C22-C21-C27 | 121(1) |
| C1-C3-C5 | 125(1) | C26-C21-C27 | 119(1) |
| N4-C4-C2 | 114(1) | C21-C22-C23 | 120(1) |
| N4-C4-C6 | 123(1) | C21-C22-C29 | 116(1) |
| C2-C4-C6 | 121(1) | C23-C22-C29 | 122(1) |

**Table 10.** (Continued).

| atom | angle | atom | angle |
|---|---|---|---|
| C2-C5-C3 | 107(1) | C22-C23-C24 | 120(1) |
| C2-C5-C7 | 112(1) | C23-C24-C25 | 122(1) |
| C2-C5-C29 | 107(1) | C24-C25-C26 | 120(1) |
| C3-C5-C7 | 128(1) | C21-C26-C25 | 117(1) |
| C3-C5-C29 | 111(1) | C21-C27-C28 | 123(1) |
| C7-C5-C29 | 85(1) | C5-C29-C22 | 114(1) |
| C1-C6-C4 | 111(1) | C5-C29-C30 | 86(1) |
| C1-C6-C8 | 125(1) | C22-C29-C30 | 123(1) |
| C4-C6-C8 | 122(1) | C7-C30-C29 | 88(1) |
| C5-C7-C9 | 111(1) | | |

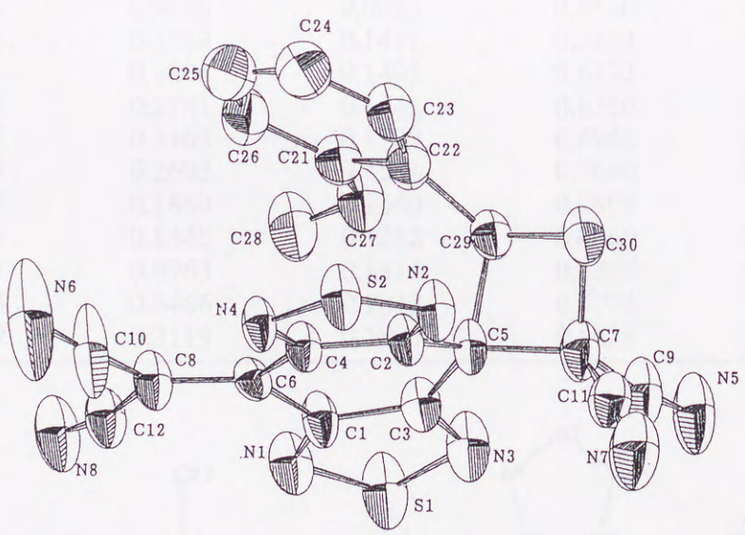


**Figure 6.** Molecular structure with of chiral-**2o** with atomic numbering system.

**Table 11.** Positional parameters and Equivalent Temperature Factors ($Å^2$)

| ATOM | X | Y | Z | Beq |
|---|---|---|---|---|
| S 1 | 0.8187 | 0.1553 | 1.0430 | 5.48 |
| S 2 | 0.6613 | 0.1789 | 0.6769 | 6.81 |
| N 1 | 0.8615 | 0.1369 | 0.9658 | 4.89 |
| N 2 | 0.6184 | 0.1934 | 0.7561 | 5.56 |
| N 3 | 0.7282 | 0.1774 | 1.0112 | 4.85 |
| N 4 | 0.7513 | 0.1542 | 0.7084 | 5.43 |
| N 5 | 0.5433 | 0.2150 | 1.0476 | 10.69 |
| N 6 | 0.9317 | 0.0737 | 0.6709 | 8.64 |
| N 7 | 0.4555 | 0.2402 | 0.8346 | 10.25 |
| N 8 | 1.0252 | 0.0641 | 0.8846 | 8.22 |
| C 1 | 0.8045 | 0.1467 | 0.9107 | 3.93 |
| C 2 | 0.6740 | 0.1783 | 0.8084 | 4.35 |
| C 3 | 0.7284 | 0.1708 | 0.9377 | 3.89 |
| C 4 | 0.7500 | 0.1554 | 0.7823 | 3.96 |
| C 5 | 0.6565 | 0.1842 | 0.8879 | 3.96 |
| C 6 | 0.8213 | 0.1339 | 0.8315 | 4.04 |
| C 7 | 0.5849 | 0.2038 | 0.9126 | 5.15 |
| C 8 | 0.8951 | 0.1078 | 0.8063 | 4.59 |
| C 9 | 0.5668 | 0.2098 | 0.9882 | 7.10 |
| C10 | 0.9103 | 0.0912 | 0.7294 | 6.12 |
| C11 | 0.5130 | 0.2197 | 0.8639 | 6.88 |
| C12 | 0.9646 | 0.0825 | 0.8540 | 5.71 |
| C 1 | 0.1759 | 0.1411 | 0.5444 | 16.41 |
| C21 | 0.2008 | 0.1495 | 0.6123 | 7.70 |
| C22 | 0.2781 | 0.1642 | 0.6350 | 10.18 |
| C23 | 0.3163 | 0.1739 | 0.6942 | 12.25 |
| C24 | 0.2603 | 0.1584 | 0.7640 | 11.87 |
| C25 | 0.1860 | 0.1360 | 0.7498 | 9.04 |
| C26 | 0.1445 | 0.1262 | 0.6669 | 14.96 |
| C27 | 0.0763 | 0.1314 | 0.5375 | 10.48 |
| C28 | 0.3466 | 0.1842 | 0.5774 | 9.14 |
| C29 | 0.3119 | 0.1805 | 0.5018 | 11.45 |

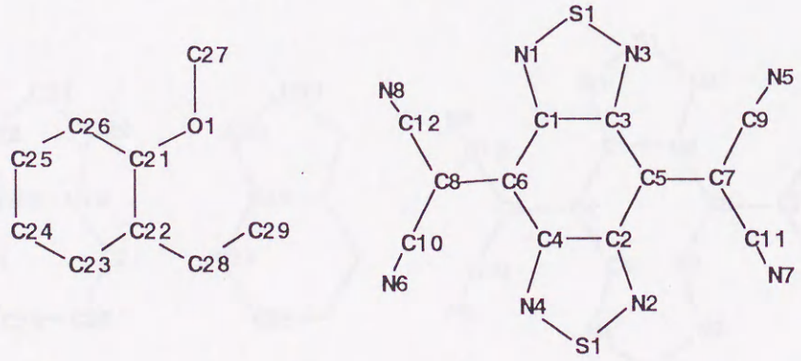


**Figure 7.** Atomic numbering system.

**Table 12.** Positional parameters and Equivalent Temperature Factors ($Å^2$)

| ATOM | X | Y | Z | Beq |
|---|---|---|---|---|
| S(1) | 0.32920(9) | 0.1029(2) | 0.6776(1) | 5.23(5) |
| S(2) | 0.09282(9) | 0.1181(2) | 0.8341(1) | 6.67(6) |
| N(1) | 0.2452(2) | 0.1083(4) | 0.6253(3) | 4.4(1) |
| N(2) | 0.1763(2) | 0.1182(4) | 0.8845(3) | 5.0(1) |
| N(3) | 0.3422(2) | 0.1102(4) | 0.7756(3) | 4.2(1) |
| N(4) | 0.0794(2) | 0.1211(5) | 0.7358(3) | 5.7(2) |
| N(5) | 0.4536(3) | 0.1387(6) | 0.9757(4) | 7.5(2) |
| N(6) | 0.1083(3) | 0.1117(5) | 0.4422(3) | 7.4(2) |
| N(7) | 0.3136(3) | 0.1388(6) | 1.0678(3) | 8.0(2) |
| N(8) | -0.0326(3) | 0.1168(6) | 0.5333(3) | 7.5(2) |
| C(1) | 0.2245(3) | 0.1152(5) | 0.6845(4) | 3.7(2) |
| C(2) | 0.1968(3) | 0.1208(5) | 0.8252(4) | 3.8(2) |
| C(3) | 0.2797(3) | 0.1166(5) | 0.7706(4) | 3.8(2) |
| C(4) | 0.1417(3) | 0.1217(5) | 0.7406(4) | 3.8(2) |
| C(5) | 0.2695(3) | 0.1224(5) | 0.8468(3) | 3.5(2) |
| C(6) | 0.1516(3) | 0.1189(5) | 0.6635(4) | 3.6(2) |
| C(7) | 0.3224(3) | 0.1288(5) | 0.9276(4) | 4.2(2) |
| C(8) | 0.0986(3) | 0.1173(5) | 0.5825(4) | 4.4(2) |
| C(9) | 0.3949(4) | 0.1338(6) | 0.9495(4) | 5.3(2) |
| C(10) | 0.1077(3) | 0.1138(6) | 0.5065(4) | 5.1(2) |
| C(11) | 0.3146(3) | 0.1344(6) | 1.0037(4) | 5.3(2) |
| C(12) | 0.0258(3) | 0.1175(6) | 0.5582(4) | 5.1(2) |
| C(21) | 0.6579(5) | 0.1255(6) | 0.0337(5) | 7.3(3) |
| C(22) | 0.6411(3) | 0.1257(5) | 0.1003(5) | 6.3(2) |
| C(23) | 0.7090(4) | 0.1297(5) | 0.1832(5) | 5.6(2) |
| C(24) | 0.7233(5) | 0.1309(5) | 0.2691(6) | 7.0(3) |
| C(25) | 0.7939(5) | 0.1321(6) | 0.3338(5) | 7.2(3) |
| C(26) | 0.8476(5) | 0.1333(6) | 0.3134(4) | 6.8(2) |
| C(27) | 0.8340(4) | 0.1328(5) | 0.2241(5) | 6.1(2) |
| C(28) | 0.7631(4) | 0.1311(5) | 0.1614(4) | 4.7(2) |
| C(29) | 0.7343(4) | 0.1284(6) | 0.0649(4) | 6.2(2) |
| C(31) | 1.0000 | 0.257(1) | 1/4 | 7.5(4) |
| C(32) | 0.9984(4) | 0.3123(7) | 0.1795(5) | 6.8(3) |
| C(33) | 1.0001(4) | 0.4169(8) | 0.2074(5) | 7.8(3) |
| C(34) | 0.9990(4) | 0.5008(8) | 0.1665(6) | 8.8(3) |
| C(35) | 1.0001(5) | 0.5976(7) | 0.2091(5)) | 9.5(3) |

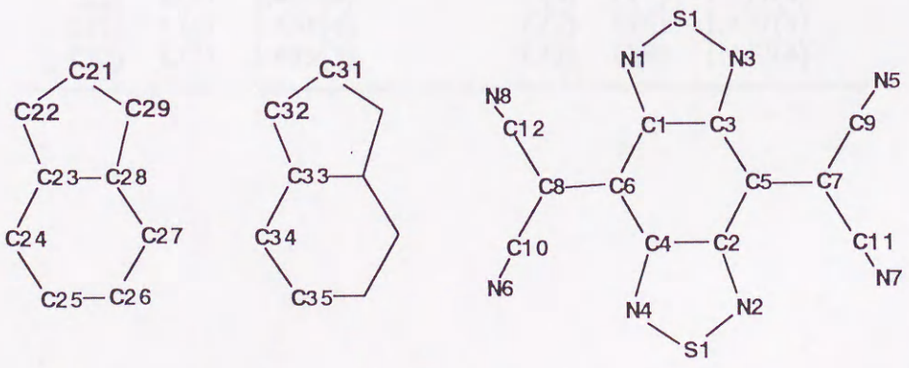


**Figure 8.** Atomic numbering system.

## Bi{4*H*,8*H*-4-(dicyanomethylene)benzo[1,2,5]thiadiazol-7-ylidene} (11)

**Table 13.** Positional parameters and Equivalent Temperature Factors ($Å^2$)

| ATOM | X | Y | Z | Beq |
|---|---|---|---|---|
| S(1) | 0.1812(1) | -0.06513(7) | 0.62789(7) | 3.68(2) |
| N(1) | 0.1641(3) | 0.0874(2) | 0.6309(2) | 3.33(5) |
| N(2) | 0.3091(3) | -0.0882(2) | 0.7712(2) | 3.24(5) |
| N(3) | -0.0251(4) | 0.3457(3) | 0.4935(3) | 5.26(7) |
| N(4) | 0.2865(4) | 0.5794(3) | 0.8071(3) | 4.96(7) |
| C(1) | 0.2598(4) | 0.1253(3) | 0.7456(2) | 2.70(6) |
| C(2) | 0.3443(4) | 0.0238(2) | 0.8275(2) | 2.68(5) |
| C(3) | 0.4613(4) | 0.0477(2) | 0.9569(2) | 2.68(5) |
| C(4) | 0.4899(4) | 0.1795(3) | 0.9866(3) | 3.02(6) |
| C(5) | 0.4078(4) | 0.2744(3) | 0.9102(3) | 3.05(6) |
| C(6) | 0.2851(4) | 0.2559(3) | 0.7866(2) | 2.77(6) |
| C(7) | 0.2026(4) | 0.3564(3) | 0.7151(3) | 3.06(6) |
| C(8) | 0.0757(4) | 0.3465(3) | 0.5919(3) | 3.54(7) |
| C(9) | 0.2448(4) | 0.4823(3) | 0.7636(3) | 3.47(7) |
| H(1) | 0.432(4) | 0.361(2) | 0.941(2) | 2.7(5) |
| H(2) | 0.568(3) | 0.204(2) | 1.067(2) | 2.6(5) |

**Table 14.** Bond lengths (Å)

| atom | atom | distance | atom | atom | distance |
|---|---|---|---|---|---|
| S(1) | N(1) | 1.623(2) | C(3) | C(3) | 1.398(5) |
| S(1) | N(2) | 1.623(2) | C(3) | C(4) | 1.438(4) |
| N(1) | C(1) | 1.328(3) | C(4) | C(5) | 1.350(4) |
| N(2) | C(2) | 1.329(3) | C(4) | H(2) | 0.95(2) |
| N(3) | C(8) | 1.142(4) | C(5) | C(6) | 1.436(4) |
| N(4) | C(9) | 1.142(4) | C(5) | H(1) | 0.98(3) |
| C(1) | C(2) | 1.437(4) | C(6) | C(7) | 1.371(4) |
| C(1) | C(6) | 1.451(4) | C(7) | C(8) | 1.437(4) |
| C(2) | C(3) | 1.475(3) | C(7) | C(9) | 1.440(4) |

**Table 15.** Bond angles (degree)

| atom | atom | atom | angle | atom | atom | atom | angle |
|---|---|---|---|---|---|---|---|
| N(1) | S(1) | N(2) | 99.5(1) | C(3) | C(4) | H(2) | 119(2) |
| S(1) | N(1) | C(1) | 106.9(2) | C(5) | C(4) | H(2) | 116(2) |
| S(1) | N(2) | C(2) | 107.6(2) | C(4) | C(5) | C(6) | 123.9(3) |
| N(1) | C(1) | C(2) | 113.7(2) | C(4) | C(5) | H(1) | 119(1) |
| N(1) | C(1) | C(6) | 124.8(2) | C(6) | C(5) | H(1) | 118(1) |
| C(2) | C(1) | C(6) | 121.5(2) | C(1) | C(6) | C(5) | 114.7(2) |
| N(2) | C(2) | C(1) | 112.4(2) | C(1) | C(6) | C(7) | 124.3(2) |
| N(2) | C(2) | C(3) | 126.0(2) | C(5) | C(6) | C(7) | 121.0(3) |
| C(1) | C(2) | C(3) | 121.5(2) | C(6) | C(7) | C(8) | 124.8(3) |
| C(2) | C(3) | C(3) | 123.8(3) | C(6) | C(7) | C(9) | 119.1(2) |
| C(2) | C(3) | C(4) | 113.5(2) | C(8) | C(7) | C(9) | 116.1(2) |
| C(3) | C(3) | C(4) | 122.7(3) | N(3) | C(8) | C(7) | 176.3(3) |
| C(3) | C(4) | C(5) | 124.6(2) | N(4) | C(9) | C(7) | 176.1(3) |

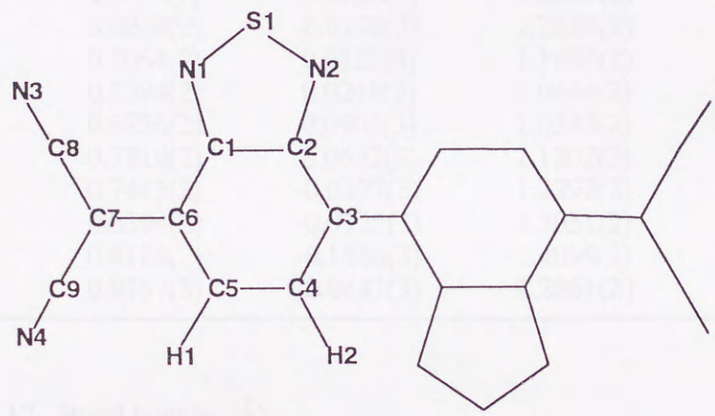


**Figure 9.** Atomic numbering system.

## Chapter 4

**Bi{4*H*,8*H*-4-(dicyanomethylene)benzo[1,2-*c*:4,5-*c*']bis[1,2,5]thiadiazol-8-ylidene} (folded form, 20f)**

**Table 16.** Positional parameters and Equivalent Temperature Factors ($Å^2$)

| ATOM | X | Y | Z | Beq |
|---|---|---|---|---|
| S11 | 0.40075(6) | 0.0061(1) | 1.34538(5) | 3.13(1) |
| S14 | 0.87237(7) | 0.2119(1) | 0.96930(6) | 3.41(1) |
| N11 | 0.5568(2) | -0.0298(3) | 1.3575(2) | 2.78(4) |
| N12 | 0.3889(2) | 0.0333(3) | 1.2081(2) | 2.93(4) |
| N14 | 0.7177(2) | 0.1789(3) | 0.9459(2) | 2.86(4) |
| N15 | 0.8887(2) | 0.1226(3) | 1.0933(2) | 2.94(4) |
| N18 | 0.8031(2) | -0.2257(3) | 1.4934(2) | 3.92(6) |
| N19 | 1.0853(2) | -0.0216(5) | 1.2841(2) | 4.99(7) |
| C11 | 0.6048(2) | -0.0198(3) | 1.2529(2) | 2.18(4) |
| C12 | 0.5064(2) | 0.0121(3) | 1.1662(2) | 2.27(4) |
| C13 | 0.5394(2) | 0.0248(3) | 1.0444(2) | 2.26(4) |
| C14 | 0.6736(2) | 0.0908(3) | 1.0332(2) | 2.28(4) |
| C15 | 0.7719(2) | 0.0632(3) | 1.1202(2) | 2.23(4) |
| C16 | 0.7445(2) | -0.0177(3) | 1.2292(2) | 2.20(4) |
| C17 | 0.8394(2) | -0.0725(3) | 1.3031(2) | 2.49(5) |
| C18 | 0.8124(2) | -0.1586(3) | 1.4099(2) | 2.70(5) |
| C19 | 0.9767(3) | -0.0442(3) | 1.2861(2) | 3.27(6) |

**Table 17.** Bond lengths (Å)

| atom | length | atom | length |
|---|---|---|---|
| S11-N11 | 1.624(2) | C11-C12 | 1.439(3) |
| S11-N12 | 1.626(2) | C11-C16 | 1.461(3) |
| S14-N14 | 1.621(2) | C12-C13 | 1.476(3) |
| S14-N15 | 1.619(2) | C13-C13 | 1.362(4) |
| N11-C11 | 1.332(3) | C13-C14 | 1.474(3) |
| N12-C12 | 1.317(3) | C14-C15 | 1.435(3) |
| N14-C14 | 1.320(3) | C15-C16 | 1.458(3) |
| N15-C15 | 1.325(3) | C16-C17 | 1.358(3) |
| N18-C18 | 1.116(3) | C17-C18 | 1.453(3) |
| N19-C19 | 1.125(3) | C17-C19 | 1.439(3) |

**Table 18.** Bond angles (degree)

| atom | angle | atom | angle |
|---|---|---|---|
| N11-S11-N12 | 99.5(1) | N14-C14-C13 | 125.7(2) |
| N14-S14-N15 | 99.7(1) | N14-C14-C15 | 112.6(2) |
| S11-N11-C11 | 106.7(2) | C13-C14-C15 | 121.7(2) |
| S11-N12-C12 | 107.5(2) | N15-C15-C14 | 113.7(2) |
| S14-N14-C14 | 107.3(2) | N15-C15-C16 | 123.2(2) |
| S14-N15-C15 | 106.6(2) | C14-C15-C16 | 123.1(2) |
| N11-C11-C12 | 113.4(2) | C11-C16-C15 | 112.1(2) |
| N11-C11-C16 | 123.7(2) | C11-C16-C17 | 124.4(2) |
| C12-C11-C16 | 122.5(2) | C15-C16-C17 | 123.4(2) |
| N12-C12-C11 | 112.9(2) | C16-H17-C18 | 123.5(2) |
| N12-C12-C13 | 125.3(2) | C16-H17-C19 | 123.4(2) |
| C11-C12-C13 | 121.8(2) | C18-H17-C19 | 113.0(2) |
| C12-C13-C13 | 125.3(3) | N18-C18-C17 | 173.9(3) |
| C12-C13-C14 | 109.8(2) | N19-C19-C17 | 173.2(3) |
| C13-C13-C14 | 124.8(3) | | |

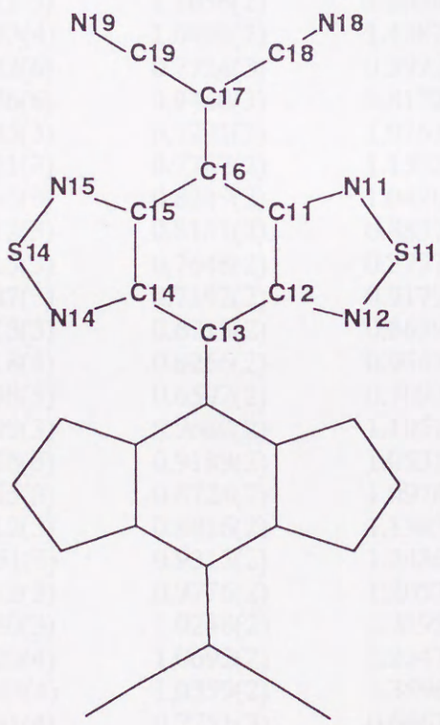


**Figure 10.** Atomic numbering system.

**Bi{4*H*,8*H*-4-(dicyanomethylene)benzo[1,2-*c*:4,5-*c*′]bis[1,2,5]thiadiazol-8-ylidene} (twisted form, 20t)**

**Table 19.** Fractional atomic coordinates and U(iso)

| ATOM | X | Y | Z | U(iso) |
|---|---|---|---|---|
| S11 | 0.12911(13) | 0.72059(6) | 1.34016(14) | 0.056 |
| S14 | 0.11525(10) | 0.82321(5) | 0.61922(13) | 0.040 |
| S21 | 0.24476(10) | 0.97793(5) | 0.96297(15) | 0.046 |
| S24 | -0.12878(11) | 0.87377(6) | 1.33238(16) | 0.052 |
| N11 | 0.1413(3) | 0.6927(2) | 1.1823(4) | 0.045 |
| N12 | 0.1123(4) | 0.7782(2) | 1.2842((4) | 0.048 |
| N14 | 0.1100(3) | 0.8509(2) | 0.7796(4) | 0.036 |
| N15 | 0.1303(3) | 0.7650(2) | 0.6756(4) | 0.035 |
| N18 | 0.1733(5) | 0.5895(2) | 1.0192(6) | 0.072 |
| N19 | 0.1636(6) | 0.6438(2) | 0.5916(6) | 0.087 |
| N21 | 0.1664(3) | 1.0052(2) | 1.0591(5) | 0.041 |
| N22 | 0.2103(3) | 0.9193(2) | 0.9738(5) | 0.042 |
| N24 | -0.0490(3) | 0.8457(2) | 1.2407(5) | 0.042 |
| N25 | -0.0932(3) | 0.9322(2) | 1.3207(5) | 0.046 |
| N28 | 0.1111(5) | 1.1058(2) | 1.2038(8) | 0.088 |
| N29 | -0.1073(4) | 1.0496(2) | 1.4387(5) | 0.054 |
| N37 | 0.3702(6) | 0.7724(3) | 0.3972(8) | 0.101 |
| N47 | 0.4276(6) | 0.9440(3) | 0.8172(10) | 0.121 |
| C11 | 0.1305(3) | 0.7291(2) | 1.0763(5) | 0.032 |
| C12 | 0.1121(3) | 0.7787(2) | 1.1332(5) | 0.034 |
| C13 | 0.1065(3) | 0.8249(2) | 1.0426(5) | 0.032 |
| C14 | 0.1212(3) | 0.8151(2) | 0.8857(5) | 0.030 |
| C15 | 0.1315(3) | 0.7648(2) | 0.8257(5) | 0.030 |
| C16 | 0.1387(3) | 0.7192(2) | 0.9179(5) | 0.030 |
| C17 | 0.1513(3) | 0.6715(2) | 0.8639(5) | 0.035 |
| C18 | 0.1618(4) | 0.6266(2) | 0.9563(6) | 0.046 |
| C19 | 0.1578(5) | 0.6597(2) | 0.7093(6) | 0.053 |
| C21 | 0.1099(3) | 0.9680(2) | 1.1051(5) | 0.033 |
| C22 | 0.1326(3) | 0.9189(2) | 1.0531(5) | 0.032 |
| C23 | 0.0855(3) | 0.8724(2) | 1.0976(5) | 0.031 |
| C24 | 0.0112(3) | 0.8816(2) | 1.1983(5) | 0.033 |
| C25 | -0.0151(3) | 0.9313(2) | 1.2436(5) | 0.034 |
| C26 | 0.0352(3) | 0.9776(2) | 1.2057(5) | 0.031 |
| C27 | 0.0180(3) | 1.0248(2) | 1.2595(5) | 0.035 |
| C28 | 0.0723(4) | 1.0692(2) | 1.2247(7) | 0.050 |
| C29 | -0.0543(4) | 1.0359(2) | 1.3596(5) | 0.039 |
| C31 | 0.3791(4) | 0.7751(3) | 0.6867(7) | 0.052 |
| C32 | 0.3788(5) | 0.8215(3) | 0.7603(8) | 0.061 |
| C33 | 0.3806(5) | 0.8222(3) | 0.9150(9) | 0.070 |
| C34 | 0.3823(5) | 0.7770(3) | 0.9956(8) | 0.069 |
| C35 | 0.3830(4) | 0.7311(3) | 0.9196(9) | 0.068 |
| C36 | 0.3808(4) | 0.7301(2) | 0.7660(8) | 0.056 |
| C37 | 0.3759(5) | 0.7734(3) | 0.5259(9) | 0.071 |

**Table 19.** (Continued).

| ATOM | X | Y | Z | U(iso) |
|---|---|---|---|---|
| C41 | 0.5417(5) | 1.0116(3) | 0.7196(7) | 0.064 |
| C42 | 0.5250(7) | 1.0627(3) | 0.7393(10) | 0.091 |
| C43 | 0.5888(9) | 1.0963(4) | 0.6881(12) | 0.113 |
| C44 | 0.6672(8) | 1.0813(5) | 0.6190(12) | 0.112 |
| C45 | 0.6809(6) | 1.0313(5) | 0.5983(10) | 0.104 |
| C46 | 0.6197(6) | 0.9950(3) | 0.6478(9) | 0.082 |
| C47 | 0.4778(6) | 0.9742(3) | 0.7739(9) | 0.077 |
| H32 | 0.37688 | 0.85271 | 0.70447 | 0.050 |
| H33 | 0.38087 | 0.85401 | 0.96742 | 0.050 |
| H34 | 0.38438 | 0.77730 | 1.10346 | 0.050 |
| H35 | 0.38432 | 0.69975 | 0.97436 | 0.050 |
| H36 | 0.37974 | 0.69825 | 0.71335 | 0.050 |
| H42 | 0.47081 | 1.07442 | 0.78943 | 0.050 |
| H43 | 0.57837 | 1.13211 | 0.69876 | 0.050 |
| H44 | 0.71358 | 1.10512 | 0.58630 | 0.050 |
| H45 | 0.73479 | 1.02021 | 0.54665 | 0.050 |
| H46 | 0.63278 | 0.95982 | 0.63127 | 0.050 |

**Table 20.** Bond lengths (Å)

| atom | length | atom | length |
|---|---|---|---|
| S11-N11 | 1.617(5) | S11-N12 | 1.604(5) |
| S14-N14 | 1.617(4) | S14-N15 | 1.619(5) |
| S21-N21 | 1.620(5) | S21-N22 | 1.620(5) |
| S24-N24 | 1.619(5) | S24-N25 | 1.620(5) |
| N11-C11 | 1.341(7) | N12-C12 | 1.348(6) |
| N14-C14 | 1.331(6) | N15-C15 | 1.338(6) |
| N18-C18 | 1.128(8) | N19-C19 | 1.143(8) |
| N21-C21 | 1.342(7) | N22-C22 | 1.344(6) |
| N24-C24 | 1.338(7) | N25-C25 | 1.336(7) |
| N28-C28 | 1.127(9) | N29-C29 | 1.130(7) |
| N37-C37 | 1.141(11) | N47-C47 | 1.147(12) |
| C11-C12 | 1.437(7) | C11-C16 | 1.456(6) |
| C12-C13 | 1.457(7) | C13-C14 | 1.464(6) |
| C13-C23 | 1.388(7) | C14-C15 | 1.442(7) |
| C15-C16 | 1.454(7) | C16-C17 | 1.364(7) |
| C17-C18 | 1.438(8) | C17-C19 | 1.429(7) |
| C21-C22 | 1.422(7) | C21-C26 | 1.460(7) |
| C22-C23 | 1.461(7) | C23-C24 | 1.456(7) |
| C24-C25 | 1.430(7) | C25-C26 | 1.458(7) |
| C26-C27 | 1.364(7) | C27-C28 | 1.437(8) |
| C27-C29 | 1.442(7) | C31-C32 | 1.389(10) |

**Table 20.** (Continued).

| atom | length | atom | length |
|---|---|---|---|
| C31-C36 | 1.381(10) | C31-C37 | 1.432(10) |
| C32-C33 | 1.379(11) | C33-C34 | 1.390(12) |
| C34-C35 | 1.386(12) | C35-C36 | 1.367(11) |
| C41-C42 | 1.382(12) | C41-C46 | 1.377(11) |
| C41-C47 | 1.437(11) | C42-C43 | 1.358(15) |
| C43-C44 | 1.356(16) | C44-C45 | 1.347(19) |
| C45-C46 | 1.376(14) | C32-H32 | 0.960(7) |
| C33-H33 | 0.959(8) | C34-H34 | 0.960(7) |
| C35-H35 | 0.960(8) | C36-H36 | 0.960(7) |
| C42-H42 | 0.960(9) | C43-H43 | 0.960(10) |
| C44-H44 | 0.960(12) | C45-H45 | 0.960(9) |
| C46-H46 | 0.959(9) | | |

**Table 21.** Bond angles (degree)

| atom | angle | atom | angle |
|---|---|---|---|
| N11-S11-N12 | 100.6(3) | N14-S14-N15 | 99.8(2) |
| S21-S21-N22 | 100.2(3) | N24-S24-N25 | 100.2(3) |
| S11-N11-C11 | 106.1(4) | S11-N12-C12 | 107.7(4) |
| S14-N14-C14 | 107.3(4) | S14-N15-C15 | 107.4(4) |
| S21-N21-C21 | 106.2(4) | S21-N22-C22 | 106.9(4) |
| S24-N24-C24 | 107.0(4) | S24-N25-C25 | 106.3(4) |
| N11-C11-C12 | 114.1(4) | N11-C11-C16 | 122.8(5) |
| C12-C11-C16 | 123.1(5) | N12-C12-C11 | 111.5(5) |
| N12-C12-C13 | 123.9(5) | C11-C12-C13 | 124.2(4) |
| C12-C13-C14 | 112.4(4) | C12-C13-C23 | 123.7(4) |
| C14-C13-C23 | 123.9(5) | N14-C14-C13 | 122.7(5) |
| N14-C14-C15 | 113.2(4) | C13-C14-C15 | 123.3(4) |
| N15-C15-C14 | 112.4(4) | N15-C15-C16 | 124.1(4) |
| C14-C15-C16 | 123.5(4) | C11-C16-C15 | 113.2(4) |
| C11-C16-C17 | 122.6(5) | C15-C16-C17 | 124.3(4) |
| C16-C17-C18 | 124.1(5) | C16-C17-C19 | 124.7(5) |
| C18-C17-C19 | 111.2(5) | N18-C18-C17 | 174.2(6) |
| N19-C19-C17 | 171.1(7) | N21-C21-C22 | 114.1(4) |
| N21-C21-C26 | 122.1(5) | C22-C21-C26 | 123.7(5) |
| N22-C22-C21 | 112.5(5) | N22-C22-C23 | 123.4(4) |
| C21-C22-C23 | 123.6(4) | C13-C23-C22 | 122.9(4) |
| C13-C23-C24 | 124.0(5) | C22-C23-C24 | 113.0(4) |
| N24-C24-C23 | 123.7(5) | N24-C24-C25 | 112.6(4) |
| C23-C24-C25 | 123.1(5) | N25-C25-C24 | 113.9(5) |
| N25-C25-C26 | 122.2(5) | C24-C25-C26 | 123.9(4) |
| C21-C26-C25 | 112.4(4) | C21-C26-C27 | 122.6(5) |
| C25-C26-C27 | 125.0(5) | C26-C27-C28 | 123.4(5) |

**Table 21.** (Continued).

| atom | angle | atom | angle |
|---|---|---|---|
| C26-C27-C29 | 124.5(5) | C28-C27-C29 | 112.2(5) |
| N28-C28-C27 | 175.2(7) | N29-C29-C27 | 173.0(6) |
| C32-C31-C36 | 121.0(6) | C32-C31-C37 | 120.0(7) |
| C36-C31-C37 | 119.0(7) | C31-C32-C33 | 119.0(7) |
| C32-C33-C34 | 120.3(8) | C33-C34-C35 | 119.6(7) |
| C34-C35-C36 | 120.6(7) | C31-C36-C35 | 119.5(7) |
| N37-C37-C31 | 177.8(8) | C42-C41-C46 | 121.1(8) |
| C42-C41-C47 | 120.5(7) | C46-C41-C47 | 118.3(8) |
| C41-C42-C43 | 118.1(9) | C42-C43-C44 | 122.4(10) |
| C43-C44-C45 | 118.5(11) | C44-C45-C46 | 122.4(9) |
| C41-C46-C45 | 117.5(9) | N47-C47-C41 | 179.2(9) |
| C31-C32-H32 | 120.7(7) | C33-C32-H32 | 120.3(7) |
| C32-C33-H33 | 119.9(8) | C34-C33-H33 | 119.8(8) |
| C33-C34-H34 | 120.6(9) | C35-C34-H34 | 119.8(9) |
| C34-C35-H35 | 120.1(8) | C36-C35-H35 | 119.3(8) |
| C31-C36-H36 | 120.0(7) | C35-C36-H36 | 120.4(7) |
| C41-C42-H42 | 121.4(9) | C43-C42-H42 | 120.5(10) |
| C42-C43-H43 | 119.9(12) | C44-C43-H43 | 117.7(12) |
| C43-C44-H44 | 122.1(13) | C45-C44-H44 | 119.3(11) |
| C44-C45-H45 | 119.4(11) | C46-C45-H45 | 118.1(12) |
| C41-C46-H46 | 123.1(8) | C45-C46-H46 | 119.4(9) |

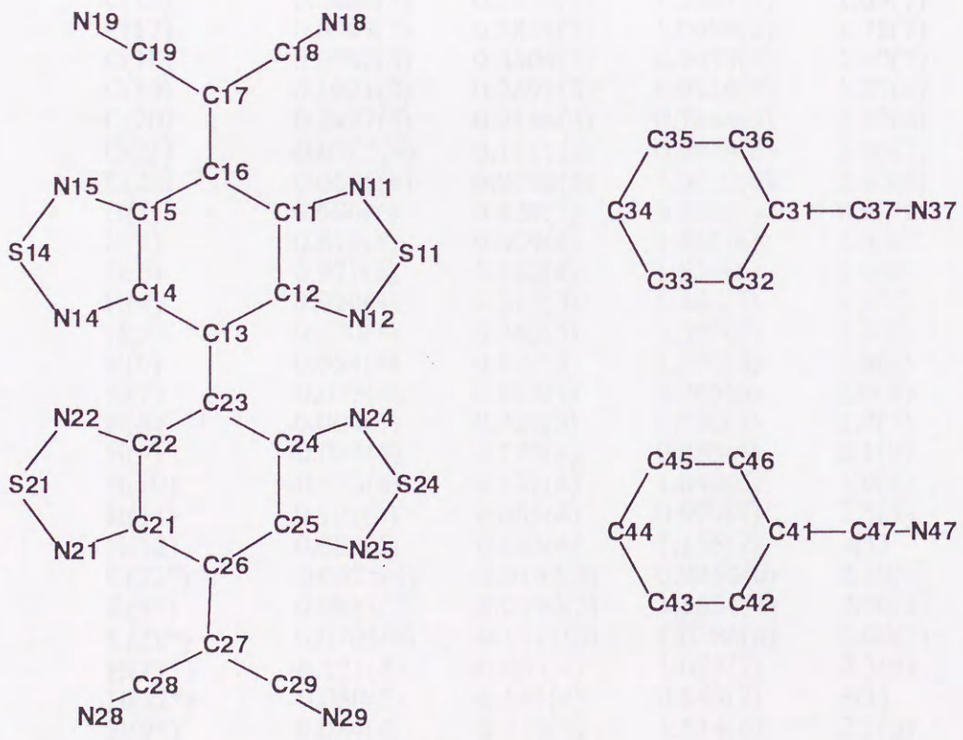


**Figure 11.** Atomic numbering system.

**4,4'-Binaphtho[2,3-*c*][1,2,5]thiadiazolylidene]-9,9'-dion (27)**

**Table 22.** Positional parameters and Equivalent Temperature Factors ($Å^2$)

| ATOM | X | Y | Z | Beq |
|---|---|---|---|---|
| S(1) | 0.35383(9) | 0.65360(7) | 1.2141(1) | 1.76(2) |
| S(2) | 0.59481(8) | 0.03522(8) | 0.7455(1) | 1.70(2) |
| O(1) | 0.7781(2) | 0.5067(2) | 1.3361(4) | 1.98(5) |
| O(2) | 0.1754(2) | 0.2059(2) | 0.5928(4) | 2.18(5) |
| O(3) | -0.0951(3) | 0.0190(2) | 0.8346(4) | 2.00(5) |
| N(1) | 0.5102(3) | 0.6255(3) | 1.2710(4) | 1.69(6) |
| N(2) | 0.3393(3) | 0.5251(2) | 1.1903(4) | 1.62(6) |
| N(3) | 0.4420(3) | 0.0802(2) | 0.6535(4) | 1.48(6) |
| N(4) | 0.5907(3) | 0.1106(3) | 0.9493(4) | 1.64(6) |
| C(1) | 0.5563(3) | 0.5126(3) | 1.2743(4) | 1.34(6) |
| C(2) | 0.4589(3) | 0.4536(3) | 1.2295(4) | 1.25(6) |
| C(3) | 0.4977(3) | 0.3281(3) | 1.2057(4) | 1.24(6) |
| C(4) | 0.6334(3) | 0.2725(3) | 1.2881(4) | 1.21(6) |
| C(5) | 0.6662(3) | 0.1605(3) | 1.3416(5) | 1.42(6) |
| C(6) | 0.7897(3) | 0.1057(3) | 1.4280(5) | 1.67(7) |
| C(7) | 0.8853(3) | 0.1617(3) | 1.4633(5) | 1.76(7) |
| C(8) | 0.8553(3) | 0.2734(3) | 1.4187(5) | 1.58(7) |
| C(9) | 0.7294(3) | 0.3307(3) | 1.3353(4) | 1.29(6) |
| C(10) | 0.6976(3) | 0.4544(3) | 1.3141(4) | 1.36(6) |
| C(11) | 0.3834(3) | 0.1563(3) | 0.7818(5) | 1.25(6) |
| C(12) | 0.4677(3) | 0.1739(3) | 0.9529(5) | 1.23(6) |
| C(13) | 0.4187(3) | 0.2686(3) | 1.0926(4) | 1.19(6) |
| C(14) | 0.2764(3) | 0.3072(3) | 1.0795(5) | 1.25(6) |
| C(15) | 0.2219(3) | 0.3566(3) | 1.2439(5) | 1.49(7) |
| C(16) | 0.0888(3) | 0.3936(3) | 1.2391(5) | 1.69(7) |
| C(17) | 0.0069(3) | 0.3831(3) | 1.0698(5) | 1.78(7) |
| C(18) | 0.0582(3) | 0.3304(3) | 0.9079(5) | 1.60(7) |
| C(19) | 0.1921(3) | 0.2891(3) | 0.9119(5) | 1.27(6) |
| C(20) | 0.2427(3) | 0.2186(3) | 0.7444(5) | 1.40(6) |
| C(21) | -0.0705(4) | 0.1111(3) | 0.9614(6) | 2.00(7) |
| C(22) | 0.0675(4) | 0.0798(3) | 1.0632(6) | 2.10(8) |
| H(1) | 0.606(4) | 0.124(3) | 1.322(5) | 0.9(7) |
| H(2) | 0.815(4) | 0.029(4) | 1.465(6) | 1.9(8) |
| H(3) | 0.971(4) | 0.122(4) | 1.524(6) | 2.0(8) |
| H(4) | 0.920(4) | 0.315(3) | 1.448(5) | 1.3(7) |
| H(5) | 0.270(4) | 0.363(3) | 1.357(6) | 1.8(8) |
| H(6) | 0.054(4) | 0.427(3) | 1.352(6) | 1.8(8) |
| H(7) | -0.078(4) | 0.410(4) | 1.065(6) | 2.0(8) |
| H(8) | 0.004(4) | 0.321(3) | 0.792(5) | 1.0(7) |
| H(9) | -0.084(4) | 0.175(4) | 0.886(6) | 2.1(8) |
| H(10) | -0.123(4) | 0.132(4) | 1.049(6) | 1.9(8) |
| H(11) | 0.121(4) | 0.065(4) | 0.977(7) | 2.5(9) |
| H(12) | 0.080(5) | 0.143(4) | 1.155(7) | 3(1) |
| C(22*) | -0.0675(4) | -0.0798(3) | 0.9368(6) | 2.10(8) |
| O(3*) | 0.0951(3) | -0.0190(2) | 1.1654(4) | 2.00(5) |
| C(21*) | 0.0705(4) | -0.1111(3) | 1.0386(6) | 2.00(7) |
| H(11*) | -0.121(4) | -0.065(4) | 1.023(7) | 2.5(9) |
| H(12*) | -0.080(5) | -0.143(4) | 0.845(7) | 3(1) |
| H(9*) | 0.084(4) | -0.175(4) | 1.114(6) | 2.1(8) |
| H(10*) | 0.123(4) | -0.132(4) | 0.951(6) | 1.9(8) |

**Table 23.** Bond lengths (Å)

| atom | atom | distance | atom | atom | distance |
|---|---|---|---|---|---|
| S(1) | N(1) | 1.623(3) | C(7) | H(3) | 0.97(4) |
| S(1) | N(2) | 1.626(3) | C(8) | C(9) | 1.401(5) |
| S(2) | N(3) | 1.630(3) | C(8) | H(4) | 0.97(4) |
| S(2) | N(4) | 1.629(3) | C(9) | C(10) | 1.478(5) |
| O(1) | C(10) | 1.219(4) | C(11) | C(12) | 1.428(4) |
| O(2) | C(20) | 1.216(4) | C(11) | C(20) | 1.488(5) |
| O(3) | C(21) | 1.424(4) | C(12) | C(13) | 1.476(4) |
| O(3) | C(22) | 1.423(5) | C(13) | C(14) | 1.472(4) |
| N(1) | C(1) | 1.331(4) | C(14) | C(15) | 1.402(4) |
| N(2) | C(2) | 1.340(4) | C(14) | C(19) | 1.411(4) |
| N(3) | C(11) | 1.331(4) | C(15) | C(16) | 1.383(5) |
| N(4) | C(12) | 1.337(4) | C(15) | H(5) | 0.89(4) |
| C(1) | C(2) | 1.433(5) | C(16) | C(17) | 1.385(5) |
| C(1) | C(10) | 1.484(5) | C(16) | H(6) | 0.95(4) |
| C(2) | C(3) | 1.473(5) | C(17) | C(18) | 1.381(5) |
| C(3) | C(4) | 1.477(4) | C(17) | H(7) | 0.88(4) |
| C(3) | C(13) | 1.387(4) | C(18) | C(19) | 1.393(5) |
| C(4) | C(5) | 1.400(5) | C(18) | H(8) | 0.94(4) |
| C(4) | C(9) | 1.415(4) | C(19) | C(20) | 1.480(4) |
| C(5) | C(6) | 1.381(5) | C(21) | C(22) | 1.508(5) |
| C(5) | H(1) | 0.89(4) | C(21) | H(9) | 0.97(4) |
| C(6) | C(7) | 1.391(5) | C(21) | H(10) | 0.89(4) |
| C(6) | H(2) | 0.96(4) | C(22) | H(11) | 0.89(5) |
| C(7) | C(8) | 1.379(5) | C(22) | H(12) | 0.98(5) |

**Table 24.** Bond angles (degree)

| atom | atom | atom | angle | atom | atom | atom | angle |
|---|---|---|---|---|---|---|---|
| N(1) | S(1) | N(2) | 100.1(2) | C(6) | C(7) | H(3) | 119(2) |
| N(3) | S(2) | N(4) | 99.3(1) | C(8) | C(7) | H(3) | 121(2) |
| C(21) | O(3) | C(22) | 109.9(3) | C(7) | C(8) | C(9) | 120.5(3) |
| S(1) | N(1) | C(1) | 106.2(2) | C(7) | C(8) | H(4) | 121(2) |
| S(1) | N(2) | C(2) | 107.0(2) | C(9) | C(8) | H(4) | 119(2) |
| S(2) | N(3) | C(11) | 106.6(2) | C(4) | C(9) | C(8) | 120.0(3) |
| S(2) | N(4) | C(12) | 107.3(2) | C(4) | C(9) | C(10) | 121.4(3) |
| N(1) | C(1) | C(2) | 114.5(3) | C(8) | C(9) | C(10) | 118.4(3) |
| N(1) | C(1) | C(10) | 121.7(3) | O(1) | C(10) | C(1) | 121.9(3) |
| C(2) | C(1) | C(10) | 123.8(3) | O(1) | C(10) | C(9) | 124.1(3) |
| N(2) | C(2) | C(1) | 112.2(3) | C(1) | C(10) | C(9) | 113.9(3) |
| N(2) | C(2) | C(3) | 127.3(3) | N(3) | C(11) | C(12) | 114.2(3) |
| C(1) | C(2) | C(3) | 119.9(3) | N(3) | C(11) | C(20) | 121.9(3) |
| C(2) | C(3) | C(4) | 114.5(3) | C(12) | C(11) | C(20) | 123.9(3) |
| C(2) | C(3) | C(13) | 122.1(3) | N(4) | C(12) | C(11) | 112.5(3) |
| C(4) | C(3) | C(13) | 122.8(3) | N(4) | C(12) | C(13) | 127.6(3) |
| C(3) | C(4) | C(5) | 118.8(3) | C(11) | C(12) | C(13) | 119.0(3) |
| C(3) | C(4) | C(9) | 123.2(3) | C(3) | C(13) | C(12) | 122.7(3) |
| C(5) | C(4) | C(9) | 117.6(3) | C(3) | C(13) | C(14) | 122.2(3) |
| C(4) | C(5) | C(6) | 121.7(3) | C(12) | C(13) | C(14) | 114.4(3) |
| C(4) | C(5) | H(1) | 120(2) | C(13) | C(14) | C(15) | 118.8(3) |

**Table 24.** (Continued).

| atom | atom | atom | angle | atom | atom | atom | angle |
|---|---|---|---|---|---|---|---|
| C(6) | C(5) | H(1) | 119(2) | C(13) | C(14) | C(19) | 122.8(3) |
| C(5) | C(6) | C(7) | 119.9(3) | C(15) | C(14) | C(19) | 118.2(3) |
| C(5) | C(6) | H(2) | 124(2) | C(14) | C(15) | C(16) | 121.0(3) |
| C(7) | C(6) | H(2) | 116(2) | C(14) | C(15) | H(5) | 122(3) |
| C(6) | C(7) | C(8) | 119.9(3) | C(16) | C(15) | H(5) | 117(3) |
| C(15) | C(16) | C(17) | 120.1(3) | C(15) | C(16) | H(6) | 120(2) |
| C(17) | C(16) | H(6) | 120(2) | C(16) | C(17) | C(18) | 120.0(3) |
| C(16) | C(17) | H(7) | 120(3) | C(18) | C(17) | H(7) | 120(3) |
| C(17) | C(18) | C(19) | 120.6(3) | C(17) | C(18) | H(8) | 121(2) |
| C(19) | C(18) | H(8) | 118(2) | C(14) | C(19) | C(18) | 119.8(3) |
| C(14) | C(19) | C(20) | 121.2(3) | C(18) | C(19) | C(20) | 118.7(3) |
| O(2) | C(20) | C(11) | 122.1(3) | O(2) | C(20) | C(19) | 124.0(3) |
| C(11) | C(20) | C(19) | 113.8(3) | O(3) | C(21) | C(22) | 111.1(3) |
| O(3) | C(21) | H(9) | 108(2) | O(3) | C(21) | H(10) | 112(3) |
| C(22) | C(21) | H(9) | 109(2) | C(22) | C(21) | H(10) | 108(3) |
| H(9) | C(21) | H(10) | 109(4) | O(3) | C(22) | C(21) | 110.9(3) |
| O(3) | C(22) | H(11) | 109(3) | O(3) | C(22) | H(12) | 108(3) |
| C(21) | C(22) | H(11) | 109(3) | C(21) | C(22) | H(12) | 109(3) |
| H(11) | C(22) | H(12) | 111(4) | | | | |

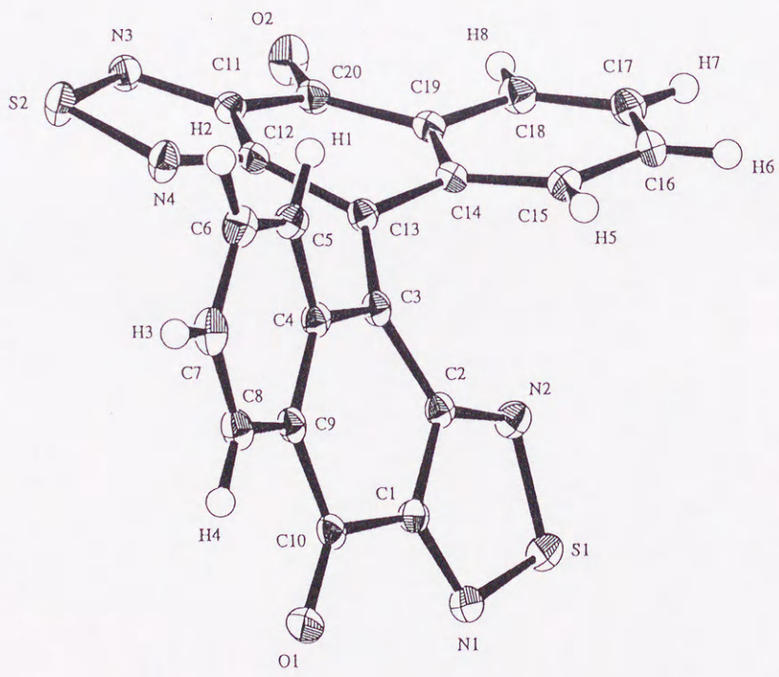


**Figure 12.** Molecular structure of **27** with atomic numbering system.

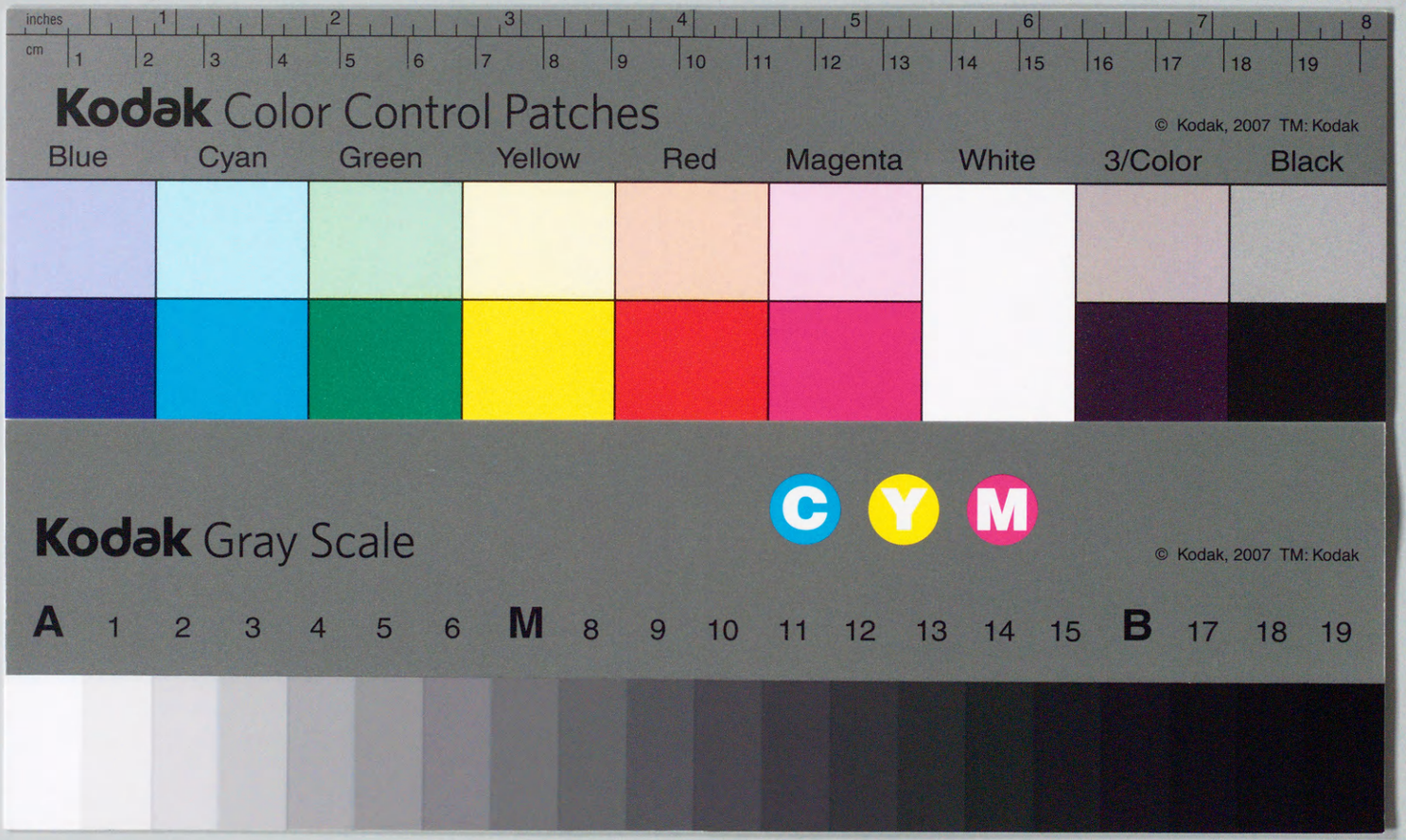
inches
cm
Kodak Color Control Patches
© Kodak, 2007 TM: Kodak
Blue
Cyan
Green
Yellow
Red
Magenta
White
3/Color
Black
Kodak Gray Scale
C
Y
M
© Kodak, 2007 TM: Kodak
A 1 2 3 4 5 6 M 8 9 10 11 12 13 14 15 B 17 18 19